Alternative Tests of Quarkonium Production Theory Using Jets

by

Yiannis Makris

Department of Physics
Duke University

Date: _____

Approved:

_____
Thomas C. Mehen, Supervisor

_____
Harold U. Baranger

_____
Shailesh Chandrasekharan

_____
Alfred T. Goshaw

_____
Ronen Plesser

Dissertation submitted in partial fulfillment of the requirements for the degree of
Doctor of Philosophy in the Department of Physics
in the Graduate School of Duke University
2017

Abstract

Alternative Tests of Quarkonium Production Theory Using Jets

by

Yiannis Makris

Department of Physics
Duke University

Date: _____

Approved:

_____
Thomas C. Mehen, Supervisor

_____
Harold U. Baranger

_____
Shailesh Chandrasekharan

_____
Alfred T. Goshaw

_____
Ronen Plesser

An abstract of a dissertation submitted in partial fulfillment of the requirements for the degree of Doctor of Philosophy in the Department of Physics in the Graduate School of Duke University
2017

Abstract

In this thesis I discuss an alternative approach for investigating quarkonium production in hadron colliders. I present a complete framework for developing observables for studies of charmonium states produced within a jet. My work is based on the use of effective field theories of quantum chromodynamics that allow for the approximate factorization of jet cross sections in perturbative calculable terms and universal non-perturbative functions that are extracted from data. Particularly in this thesis I explore the factorization approach of non-relativistic quantum chromodynamics and soft-collinear effective theory. The fragmenting jet functions play central role in factorization theorems for cross sections for identified hadrons within jets. These cross sections can depend on the hadron-jet energy ratio and possibly on other jet observables. I expand this concept to jet-shape observables known as angularities and introduce the transverse momentum dependent fragmenting jet functions. Applications of these advanced methods to J/ψ production from gluon fragmentation in electron-positron annihilation are presented and I develop the tools for expanding this work in hadron colliders. Additionally, I compare predictions for J/ψ production in jets, based on the framework of fragmenting jet functions, against recent experimental data from the LHCb collaboration.

I would like to dedicate this work to my parents Fiona and Demetres Makris and my sister Miranda Makri, who supported me during my graduate studies.

Contents

Abstract **iv**

List of Tables **x**

List of Figures **xii**

List of Abbreviations and Symbols **xv**

Acknowledgements **xvi**

1 Introduction **1**

1.1 Basics of Quarkonium 1

1.2 Quarkonium production at hadron colliders 4

1.2.1 The color evaporation model 7

1.2.2 The color singlet model 8

1.3 The NRQCD framework 9

1.3.1 Quarkonium production in fixed order NRQCD calculations . 12

1.4 J/ψ production 13

1.4.1 NRQCD fragmentation functions 16

1.5 Quarkonium polarization 19

2 Soft Collinear Effective Theory **23**

2.1 Lightcone coordinates 24

2.2 The SCET Lagrangian 26

2.3 Wilson lines 29

2.4 Gauge Invariance and operators in SCET 31
2.5 Factorization in SCET 33

3 Analytic and Monte Carlo Studies of Jets with Heavy Mesons and Quarkonia 38

3.1 Outline 38
3.2 Definition of fragmenting jet functions 39
3.3 Fragmenting Jet Functions with Angularities 42
3.4 $e^+e^- \to 2$ Jets with a B Meson 45
3.5 $e^+e^- \to 3$ Jets with the Gluon Jet Fragmenting to J/ψ 52
3.6 Semi-analytic calculations for $pp \to jet(J/\psi) + X$ 60
3.7 Conclusion 64

4 Transverse Momentum Dependent Fragmenting Jet Functions with Applications to Quarkonium Production 67

4.1 Outline 67
4.2 Transverse momentum dependent fragmenting jet function 68
4.2.1 Definition and factorization 69
4.2.2 Perturbative results 73
4.3 Numerical Results 77
4.3.1 Renormalization Group (RG) and Rapidity Renormalization Group (RRG) 77
4.3.2 Applications to quarkonium production 81
4.4 Conclusions 86

5 Jet Shapes in Dijet Events at the LHC in SCET 88

5.1 Outline 88
5.2 Jet Algorithms and Shapes at Hadron Colliders 93
5.3 Factorized Dijet Cross Section 95

5.4 Fixed-Order $\mathcal{O}(\alpha_s)$ Calculation of Factorized Components 97
5.4.1 Jet Functions 97
5.4.2 Unmeasured Beam Functions 99
5.4.3 Soft Function 100
5.5 RG Evolution and the Total NLL' Cross Section 107
5.5.1 Hard Function 107
5.5.2 Jet Functions and Unmeasured Beam Functions 109
5.5.3 Soft Function 111
5.5.4 Total NLL' Resummed Cross Section 117
5.5.5 A Simple Example 120
5.6 Conclusion 128
6 Conclusions **130**
A Renormalization Group and Resummation **132**
A.1 Evolution of Measured and Unmeasured Functions 132
A.1.1 Plus-distribution identities 134
A.2 Reorganization of logarithms of $(1-z)$ 136
A.3 Profile Functions 137
A.4 Rapidity RG Evolution 139
B FJFs matching Coefficients and Consistency Checks **141**
B.1 Evaluation of matching coefficients 141
B.2 Sum Rules 146
C TMDFJFs in Factorization Theorems **148**
C.1 Definition and relation to jet functions 148
C.2 Matching calculation 150

D Calculations of Soft Function Components **153**

D.1 Beam-Beam Interference Terms 154

D.2 Beam-Jet Interference Terms 154

D.3 Jet-Jet Interference Terms 156

Bibliography **159**

Biography **172**

List of Tables

1.1 Table from [1] showing the velocity scaling rules for elementary operators in NRQCD. 11

1.2 LDMEs for NRQCD production mechanisms. Central values taken from global fits in Refs. [2,3]. The values are in units of GeV^3. The v scaling is also shown. 14

1.3 Contributions to the J/ψ charm quark and gluon fragmentation function. 18

2.1 The collinear and soft gauge transformations of the SCET fields . . . 32

3.1 Characteristic scales of the different functions in the factorization theorem of Eq. (3.23). 51

3.2 NRQCD LDMEs for J/ψ production mechanisms used in this paper in units of GeV^3. 63

4.1 Characteristic scales of the different functions in the factorization theorem. 81

4.2 Results of fits of $\ln(f_\omega(z))$ shown in Fig. 4.7 to the function $C_0 \exp(-z\, C_1)$. 86

5.1 A summary of results for the "unmeasured" part of the soft function, S^{unmeas}, up to $\mathcal{O}(e^{-y_{\text{cut}}}, \mathcal{R}^2)$. Here, the subscript J refers to the two jets, $J = 1, 2$, and B and $\bar{B}$ refer to the two beams, and $\Delta y = y_1 - y_2$. Each component is explicitly boost invariant about the beam direction (with $2y_{\text{cut}}$ in the B-$\bar{B}$ interference terms in general given by the rapidity difference of the forward and backward beam cuts). . . . 104

5.2 Ingredients for anomalous dimensions of the color-trivial parts components to the factorization formula and the corresponding canonical scale choices μ_F, which take the form of Eq.(A.2) and (A.13). The hard and (unmeasured) soft components require an additional color-nontrivial factor derived explicitly in the text. Here, C_i is the quadratic Casimir (C_F or C_A for quarks and gluons, respectively), γ_i is given in Eq. (5.21), $\Gamma \equiv \Gamma_c(\alpha_s)$ is the cusp (given in Eq.(A.3)), x_i are the momentum fractions of the partons in the beams (fixed via Eq. (5.13)), and $\Delta\gamma_{ss}$ is given in Eq. (5.49) (and m_i is an arbitrary parameter that cancels both within $\mathbf{\Gamma}_H$ and within $\mathbf{\Gamma}_S$ and can for example be chosen based on the partonic channel to coincide with the conventions of Ref. [4] as described in the text). For refactorizing the soft function as in [5], the last two rows are used in place of $\gamma_S^{\rm unmeas}$. 117

A.1 Values of the cusp and non-cup parts of the anomalous dimensions for the collinear and collinear-soft functions. 140

List of Figures

1.1 Charmonium spectrum from [6]. 5

1.2 Bottomonium spectrum from [6]. 6

1.3 J/ψ transevse momentum spectrum from ATLAS at $\sqrt{s} = 7$ TeV from CEM (green) and CSM (red/grey). These resutls were published in Ref. [7]. 9

1.4 J/ψ transevse momentum spectrum from experiments at LHC (ALICE, CMS, ATLAS, LHCb) at $\sqrt{s} = 7$ TeV compared against predictions from NRQCD framework where the LDMEs are extracted from global fits to the world's data. Figure from Ref. [2, 3]. 15

1.5 J/ψ pollarization spectrum in the HX frame, from LHCb at $\sqrt{s} = 7$ TeV, compared against predictions from NRQCD and CSM [8]. The LDMEs for the NRQCD predictions are extracted from three different fits (blue [8], red [9], green [10]). These resutls were published in Ref. [11]. 16

1.6 Standard reference frames for measuring quarkonium pollarization. Picture taken from Ref. [12]. 21

1.7 Measured normalized $z(J/\psi)$ distributions for J/ψ mesons produced promptly compared to predictions obtained from Pythia 8. This figure was published in Ref. [13] 22

2.1 Example of multiple collinear directions in a single event. In this particular case we have a di-jet event in pp or $p\bar{p}$ collision. 24

3.1 The z distributions for $d\sigma(\tau_0, z)$ at $\tau_0 = (1.5,\ 2.0,\ 2.5) \times 10^{-3}$ for analytic calculations with theoretical uncertainty are shown in green. Monte carlo simulations using Madgraph + PYTHIA and Madgraph + Herwig are shown in black and red, respectively. 49

3.2 Analytic results for the z distributions of $d\sigma(\tau_0, z)$ at $\tau_0 = (1.5,\ 2.0,\ 2.5)\times 10^{-3}$. The orange curve is calculated with a measured jet scale that does not depend on z whereas the green curve uses a scale that does depend on z (as in Fig. 3.1). 50

3.3 Angularity distributions of $d\sigma(\tau_a, z)$ for $a = 0$ at $z = 0.4,\ 0.6,\ 0.8$. Analytic results are shown as green bands. Monte carlo results are shown as black lines for Madgraph + PYTHIA and red lines for Madgraph + HERWIG. 52

3.4 Angularity distributions of $d\sigma(\tau_a, z)$ for $a = 0$ at $z = 0, 1,\ 0.3,\ 0.5,\ 0.7$. Analytic calculations are shown as red (green) bands for the ${}^3S_1^{(8)}$ (${}^1S_0^{(8)}$) production mechanisms. Results from Madgraph + PYTHIA are shown as red (green) dashed lines for the same mechanisms. . . . 57

3.5 Angularity distributions of $d\sigma(\tau_a, z)$ for $a = +1/2,\ 0,\ -1/2,\ -1$ at $z = 0.5$. Analytic calculations are shown as red (green) solid lines for the ${}^3S_1^{(8)}$ (${}^1S_0^{(8)}$) production mechanisms. Results from Madgraph + PYTHIA are shown as red (green) dashed lines for the same mechanisms. 58

3.6 z distributions of $d\sigma(\tau_a, z)$ for NLL' analytic calculations (bands), PYTHIA (dashed lines), and GFIP (solid lines) for fixed values of $\tau_0 = (4,\ 5,\ 6) \times 10^{-3}$. 59

3.7 PYTHIA predictions for c and g z distributions (where z is the fraction of the energy of the parton initiating the jet) after showering to the scale $2m_c$. 61

3.8 Predicted $z(J/\psi)$ distribution using GFIP (gray) and FJF (red) for the three choices of LDME in Table 1 and the LHCb measurements of $z(J/\psi)$. 62

4.1 Feynman diagrams that give non-scaleless contributions to the gluon TMDFJF at NLO in α_s. Diagram (b) also has a mirror image that is not explicitly shown. 73

4.2 Associated non-scaleless diagrams that contribute to the quark TMDFJF at NLO. Again, Diagram (b) has a mirror image that is not explicitely drawn above. 74

4.3 Real gloun emission diagrams that contribute to the collinear-soft function $S_C^i(\mathbf{p}_\perp, z, \mu, \nu)$ at $\mathcal{O}(\alpha_s)$. The gluons passing through the shaded oval indicate they are contained within the phase-space of the jet. 76

4.4 The TMDFJF as a function of the $p_\perp$ of the J/ψ for the ${}^3S_1^{[1]}, {}^3S_1^{[8]}, {}^1S_0^{[8]}, {}^3P_J^{[8]}$ production mechanisms where the for jet energies $E_J = 100$ GeV. Theoretical uncertainties are calculated by varying the renormalization scales by factors of 1/2 and 2. 82

4.5 The TMDFJF as a function of the $p_\perp$ of the J/ψ for the ${}^3S_1^{[1]}, {}^3S_1^{[8]}, {}^1S_0^{[8]}, {}^3P_J^{[8]}$ production mechanisms where the for jet energies $E_J = 500\,\text{GeV}$. Theoretical uncertainties are calculated by varying the renormalization scales by factors of 1/2 and 2. 83

4.6 The TMDFJF as a function of the z of the J/ψ for the ${}^3S_1^{[1]}, {}^3S_1^{[8]}, {}^1S_0^{[8]}, {}^3P_J^{[8]}$ production mechanisms, with $p_\perp = 10$ GeV for $E_J = 100$ and 500 GeV. Theoretical uncertainties are calculated by varying the renormalization scales by factors of 1/2 and 2. 84

4.7 The function $f_\omega^{J/\psi}(z)$ (as defined in the text) as a function of z relative to the jet axis for each NRQCD production mechanism where the jet has $E_J = \omega/2 = 100$ GeV(left) and $500\,\text{GeV}$ (right). The J/ψ is restricted to have $p_\perp \in [5, 20]$ GeV in the 100 GeV jet and $p_\perp \in [5, 60]$ GeV in the 500 GeV jet. 86

5.1 Profile functions for μ_S and μ_J. These functions are defined in Eq. (5.119) and below. 123

5.2 Differential cross section for four different values of R with soft function refactorized (blue) and without (red). Central values are dotted lines and band includes scale variation. 124

5.3 Differential cross sections for three different values of p_T^{cut}. 125

5.4 Differential cross sections for four different values of a. 127

A.1 Profile functions for $\mu_S^{PF}(\tau_0)$ and $\mu_J^{PF}(\tau_0)$, the τ_0-dependent renormalization scales that we use in the scale variations of our measured soft function and measured jet function. Also shown are traditional scale variations done by varying μ by $\pm 50\%$. 137

List of Abbreviations and Symbols

Symbols

In this manuscript we use greek letters for the four-vector notation and Einsteins convention where for repeated indices (greek or latin) a summation over that index is implied unless otherwise stated.

A^{μ}	Greek letter indexing for four-vector notation.
$\eta^{\mu\nu}$	Minkowski metric.
$f_{i/h}$	Parton distribution functions.
$D_{i/h}$	Fragmentation functions.
$\mathcal{G}_{i/h}$	Fragmenting jet functions.
$\mathcal{J}_{i/j}$	Short distance matching coefficients.

Abbreviations

SCET	Soft-Collinear Effective Theory.
QCD	Quantum Chromodynamics
NRQCD	Non-Relativistic Quantum Chromodynamics
LDME	Long Distance Matrix Elements
PDF	Parton Distribution Functions
FJF	Fragmenting Jet Functions
TMD	Transverse Momentum Dependent
HQET	Heavy Quark Effective Theory

Acknowledgements

I would first like to thank my graduate advisor, Dr. Thomas Mehen, who provided mentorship and considerable resources during my graduate studies at Duke University. The work in this thesis would not be possible without his guidance and supervision. I would also like to express gratitude to my collaborator Dr. Andrew Hornig, whose help was essential for the completion of the research presented in this thesis and who taught me important concepts of physics throughout my graduate studies. A major part of my research was in collaboration with Dr. Adam K. Leibovich, Lin Dai (U. Pitt.) and Reggie Bain (Duke U.), who I would like to acknowledge for their help and support during the completion of my degree. I would like to express my appreciation to Dr. Christopher Lee for his hospitality and support during my visit to Los Alamos National Laboratory in the summer of 2015. The research performed at Duke University was supported in part by the Director, Office of Science, Office of Nuclear Physics, of the U.S. Department of Energy. During my graduate studies, travel expenses were covered in part by the A.G. Leventis Foundation.

1

Introduction

1.1 Basics of Quarkonium

Quantum Chromodynamics (QCD) is the sector of Standard Model (SM) that describes the strong nuclear interactions between quarks through the exchange of gauge bosons known as gluons. According to QCD, the six flavors of quarks (up (u), down (d), strange (s), charm (c), bottom (b), and top (t)) come in three possible strong charges referred to as color. Since QCD is a non-abelian theory (in contrast to quantum electrodynamics (QED)) gluons also carry color and have self-interactions. This property of gluons gives QCD very interesting properties. For example the β-function of QCD, which describes the evolution of the strong coupling constant, is negative, as a consequence the strong coupling constant decreases logarithmically with increasing momentum scales, thus at sufficiently high momenta one may use perturbative methods for making predictions. This phenomenon is also known as asymptotic freedom. The scales at which QCD becomes non-perturbative are described by a scheme dependent parameter $\Lambda_{\mathrm{QCD}} \sim 0.3 - 0.5$ GeV. Λ_{QCD} is called the QCD scale and is defined such that at this scale the strong coupling constant α_s be-

comes non perturbative (i.e. $\alpha_s(\Lambda_{\rm QCD}) \gtrsim 1$). Additionally, color confinement which appears at lower energies and therefore cannot be studied perturbatively, requires that colored particles cluster to form colorless combinations and only those may be observed experimentally. Such states are called hadrons and are classified according to their quark content. Quark-antiquark bound states are refered to as mesons and three-quark hadrons are called baryons.

The interactions of quarks and gluons in QCD are described through the corresponding Lagrangian:

$$\mathcal{L}_{\rm QCD} = \sum_{flavor(f)} \bar{\psi}_f \left(i \not{D} - m_f \right) \psi_f - \frac{1}{4} G^a_{\mu\nu} G^{\mu\nu}_a, \tag{1.1}$$

where ψ and A^a_μ are the quark and gluon fields respectively, $\not{D} = \gamma^\mu (i\partial_\mu + g_s A^a_\mu T_a)$, and $G^a_{\mu\nu} = \partial_\mu A^a_\nu - \partial_\nu A^a_\mu + g_s f^{abc} A^b_\mu A^c_\nu$. Here γ_μ are the Dirac matrices, T^a and f^{abc} are the generators in the fundamental representation and the structure constants of SU(3), respectively. The Lagrangian parameter m_f corresponds to the mass of the quarks and based on that parameter we classify quarks as light quarks where $m_f < \Lambda_{\rm QCD}$ ($f = u$, d, or s) and heavy quarks where $m_f > \Lambda_{\rm QCD}$ ($f = c$, b, or t).

Quarkonium is the bound state of a heavy quark, Q, and its antiquark, $\overline{Q}$, due to strong nuclear interactions. The $Q\overline{Q}$ bound states can be formed either from charm quark, c, or bottom quark, b, pairs and we refer to those states as charmonium ($c\bar{c}$) and bottomonium ($b\bar{b}$) respectively. Charmonium was first discovered by groups at SLAC [14] and BNL [15] in November of 1974. The first charmonium state discovered has mass of 3.1 GeV and is now known as the J/ψ particle. At the time only the three light quarks were experimentally observed. A fourth quark was theorized in Ref. [16] and later in Ref. [17] a complete theoretical model (Glashow - Iliopoulos - Maiani (GIM) mechanism) was introduced but, until 1974 no hadrons were discovered containing such a quark. After the discovery of the charm quark started a

period with series of discoveries of other hadrons with charm content, known as the November Revolution. The discovery of the charm quark along with the GIM mechanism set the foundation for the construction of the Standard Model as we know it today. Bottomonium was first observed by a group at Ferimlab [18] in 1977 with the discovery of Υ.

The lighter quarkonia have an approximate lifetime of 10^{-20} seconds which is particularly long relative to other strongly decaying particles with typical lifetime of 10^{-23} seconds. This is attributed to the fact that while the decays to pions are suppressed by the OZI rule [19,20], the open flavor decays are forbidden kinematically since the open flavor threshold (for charmonium this is the $D\bar{D}$ threshold $\sim$ 3.74 GeV, for bottomonium this is the $B\bar{B}$ threshold $\sim$ 10.56 GeV) is higher than the mass of the quarkonium states. Excited states can have masses above the open flavor threshold and therefore shorter lifetimes. There are eight charmonium states below the $D\bar{D}$ threshold and fourteen experimentally observed[1] bottomonium states below the $B\bar{B}$ threshold.

Due to their large mass, heavy quarks have non-relativistic velocities in the rest frame of the quarkonium. If we denote with v the relative velocity of quark and antiquark in the the rest frame of quarkonium, from lattice calculations we have that $v^2 \sim 0.1$ for bottomonium and $v^2 \sim 0.3$ for charmonia (see for example Ref. [21]). This implies that one could use a potential model for the quark-antiquark interactions and solve the Shrödinger equation to find the spectrum of quarkonium. Indeed potential models have been applied with great success in predicting the quarkonium spectrum. Unfortunately the exact potential cannot be calculated due to the non-perturbative aspects of QCD but reasonable approximations can be made. At short distances (large momentum scales compared to Λ_{QCD}) where $\alpha_s \ll 1$, the form of the potential could be evaluated at leading order in perturbation theory with the single

[1] The states $\eta_b(2S)$ and $\eta_b(3S)$ are expected to exist but not yet experimentally observed.

gluon exchange interaction. This results in a Coulomb-like potential, $V_C = -C\alpha_s/r$, where for a color singlet configuration, $C = 4/3$, and for a color octet, $C = -1/8$. On the other hand, at long distances (scales similar to Λ_{QCD}) the qualitative features of QCD suggest a distance independent force which translates to a linear potential of the form $V_L = Kr$ and the value of K is fixed from experimental data. A common potential model that has been used in the past with great success is simply $V(r) = V_L + V_C$

$$V(r) = -\frac{4}{3}\frac{\alpha_s}{r} + Kr + \mathcal{O}(\alpha_s^2). \tag{1.2}$$

which correctly reproduces the behavior at the long and short distances. Additional relativistic and spin-orbit coupling terms can be added to this potential for better accuracy [22–24]. Such corrections are essential for explaining the splitting between the χ_{cJ} states. Furthermore the splitting between $^3S_1$ and $^1S_0$ states can be explained due to the hyperfine structure from spin-spin interactions. In Figs. 1.1 and 1.2 we show the charmonium and bottomonium spectrum where by convention we use the standard spectroscopic notation $n^{(2S+1)}L_J$ to describe the quarkonium states.

1.2 Quarkonium production at hadron colliders

Quarkonium production in hadron colliders is usually studied within the framework of QCD factorization. The idea of the QCD factorization is based on the fact that the two characteristic scales of the process, the QCD confinement scale $\Lambda_{QCD} \sim 0.3$ GeV, and the hard scale, q^2, are widely separated, allowing us to factorize the underlying physics. In this framework a generic cross section (or differential cross section) is factorized into parton distribution functions (PDFs), denoted by $f_{i/h}$ and the partonic cross section, $\hat{\sigma}_{ij}$,

$$\sigma(h_1(P_1), h_2(P_2)) = \sum_{ij} \int dx_1 dx_2 f_{i/h_1}(x_1, \mu^2) f_{j/h_2}(x_2, \mu^2) \hat{\sigma}_{ij}(\hat{s} = x_1 x_2 s, \mu^2, q^2) \tag{1.3}$$

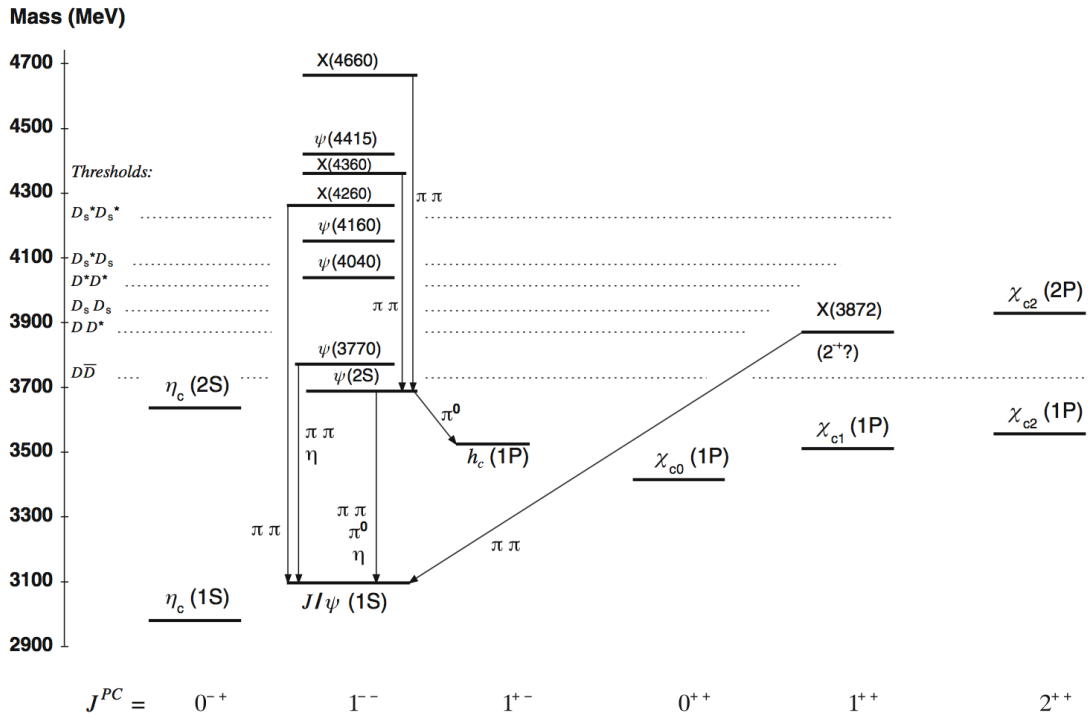

FIGURE 1.1: Charmonium spectrum from [6].

where x_i is the fraction of the hadron's energy carried by the parton i, q^2 is the square of the transferred momentum in the hard process, and μ the factorization scale. Intuitively[2] we could interpret PDFs, $f_{i/h}(x, \mu^2)$, as the probability to find a parton i within the region of size $A \sim r^3 \sim (1/\mu)^3$ inside the hadron, carrying x fraction of the hadron's energy. In hard scattering with transferred momentum q^μ the exchanged gluon (or photon) can travel distance $r \sim 1/|q|$ before getting reabsorbed. Thus a common choice of the factorization scale in Eq.(1.3) is $\mu^2 = q^2$.

While the hard partonic cross section can be calculated systematically in perturbation theory, PDFs are non-perturbative objects that must be extracted from experimental data. The predictive power of PDFs rely on their universality which ensures that the same distributions can be used for multiple processes. Thus PDFs

[2] This simplified picture of PDFs can only be used for intuitive purposes. More details regarding the matter can be found in Ref. [25].

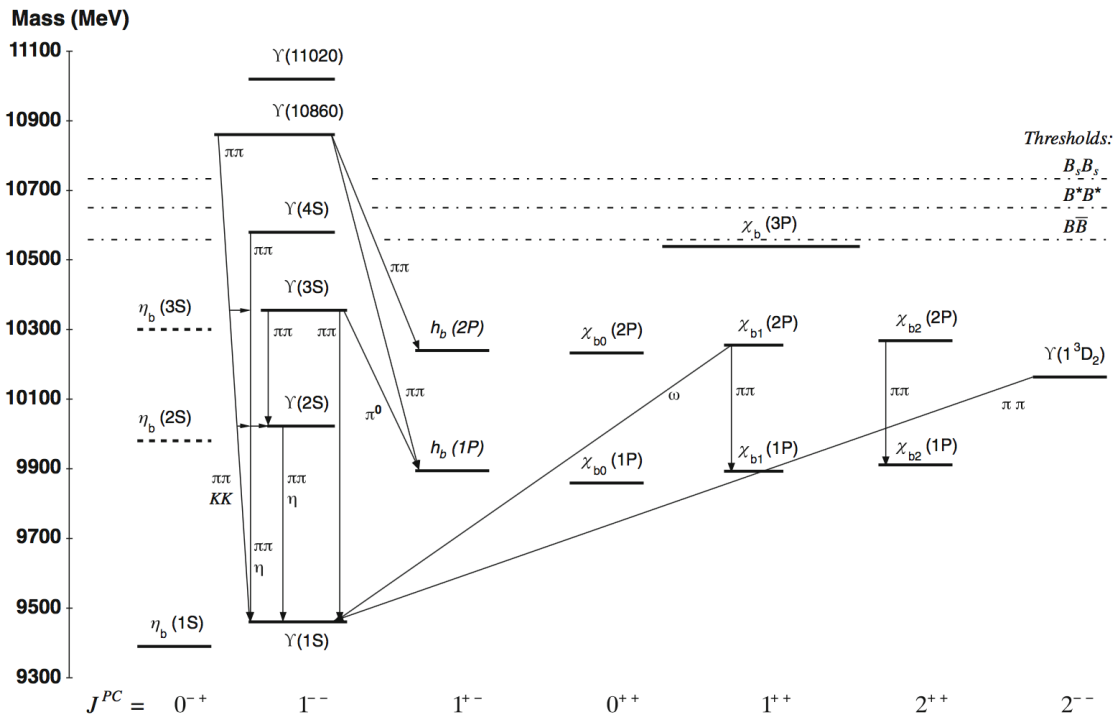

FIGURE 1.2: Bottomonium spectrum from [6].

are extracted from some processes (e.g., neutrino Deep Inelastic Scattering (DIS)) and used to make predictions for others (e.g., quarkonium production). Though the extraction of PDFs happen at a particular scale, usually calculations require knowing these distributions at other scales. For this reason PDFs are evaluated at different scales using renormalization group evolution via the Dokshitzer-Gribov-Lipatov-Altarelli-Parisi (DGLAP) equations [26–28].

$$\mu \frac{d}{d\mu} f_{i/h}(x,\mu) = \frac{\alpha_s(\mu)}{2\pi} \sum_j \int_x^1 \frac{dz}{z} P_{ij}\left(\frac{x}{z}\right) f_{j/h}(z,\mu), \tag{1.4}$$

where $P_{ij}(x)$ are the QCD splitting kernels and can be evaluated in perturbation theory.

Up to this point we discussed the form of a generic cross section in QCD factorization framework. To extend this discussion on quarkonium production we need to establish a model on how the form of the partonic cross section, σ_{ij}, is modified

in order to describe the production of quarkonium state $\mathcal{Q}$. We are going to briefly mention two partly successful models used in early studies and discuss why they failed to give a complete description.

1.2.1 The color evaporation model

In the color evaporation model (CEM) [29–31] the quarkonium state is produced from the evolution of a heavy quark-antiquark pair ($Q\overline{Q}$) with invariant mass below the open flavor threshold. The evolution is assumed independent of the polarization and the color configuration of the pair. Therefore in the CEM framework the probability of a $Q\overline{Q}$ configuration with invariant mass $\hat{s}$ to evolve in quarkonium state $\mathcal{Q}$ is given by

$$P_{CEM}(Q\overline{Q}(\hat{s}) \to \mathcal{Q}) = F_{\mathcal{Q}}\, \Theta(4m_Q^2 < \hat{s} < 4M_Q^2)\ , \tag{1.5}$$

where M_Q is the mass of the lightest meson containing Q and $F_{\mathcal{Q}}$ is a parameter unique for each state $\mathcal{Q}$ and is assumed to be universal, which needs to be extracted from experimental data. Applying Eq.(1.5) to the QCD factorization at leading order we have

$$\sigma_{CEM}(h_1(P_1), h_2(P_2) \to \mathcal{Q}) = F_{\mathcal{Q}} \sum_{ij} \int dx_1 dx_2 f_{j/h_1}(x_1, \mu^2) f_{i/h_2}(x_2, \mu^2)$$
$$\times\, \hat{\sigma}_{ij\to Q\overline{Q}(\hat{s})}(\hat{s}, \mu^2, q^2)\Theta(4m_Q^2 < \hat{s} < 4M_Q^2)\Big|_{\hat{s}=x_1x_2s}\ . \tag{1.6}$$

Despite its early success predicting various features of quarkonium, CEM failed to give a complete description of the quarkonium production. For example, the universality of the CEM parameters $F_{\mathcal{Q}}$ suggest that the ratio $F_{J/\psi}/F_{\chi_c}$ should be independent of the production process, in contrast to experimental results that give different values for hadro-production compared to photo-production processes [32].

1.2.2 The color singlet model

In contrast to CEM, the color singlet model (CSM) requires that a quarkonium state $\mathcal{Q}(n^{(2S+1)}L_J)$ can only be produced from the evolution of a heavy quark-antiquark pair in a color singlet configuration and with the same quantum numbers as the quarkonium state. The probability of the pair[3] $Q\overline{Q}(n^{(2S+1)}L_J^{(1)})$ to evolve into the corresponding quarkonium state is given by the wave function of $Q\overline{Q}$ pair at the origin,

$$P_{CSM}\left(Q\overline{Q}(n^{(2S+1)}L_J^{(1)}) \to \mathcal{Q}(n'^{(2S'+1)}L'_{J'})\right) = |\Psi(0)|^2\delta_{nn'}\delta_{SS'}\delta_{LL'}\delta_{JJ'} \ . \qquad (1.7)$$

Though the probability in equation Eq.(1.7) is true only for S-wave states ($L = 0$) similar relations for higher angular momentum states do exist and involve the derivatives of the wave function at the origin. Unfortunately calculations for $L > 0$ suffer from infrared divergences that require the inclusion of color-octet contribution for their cancelation (see below). The value of $|\psi(0)|$ can be evaluated in the quark potential model by solving Shrödinger equation for the wave function or can be extracted from quarkonium di-lepton decay rates ($\Gamma(\mathcal{Q} \to \ell\bar{\ell})$). The cross section at hadron colliders in CSM is given by

$$\sigma_{CSM}(h_1(P_1), h_2(P_2) \to \mathcal{Q}(n^{(2S+1)}L_J)) = |\Psi(0)|^2 \sum_{ij} \int dx_1 dx_2 f_{i/h_1}(x_1, \mu^2)$$
$$\times f_{i/h_2}(x_2, \mu^2)\hat{\sigma}_{ij\to Q\overline{Q}(n^{(2S+1)}L_J^{(1)})}(\hat{s}, \mu^2, q^2)\Big|_{\hat{s}=x_1x_2s} \ . \quad (1.8)$$

The CSM was used extensively for various calculations such as the η_c and χ_c production from gluon fusion [33–36] as well as the J/ψ and η_c production from B meson decays [37,38]. The CSM approach was abandoned in 1995 after the dramatic failure to predict the direct J/ψ production from Tevatron in $p\bar{p}$ collisions.

[3] The superscript (1) indicates that the $Q\bar{Q}$ pair are in a color singlet configuration.

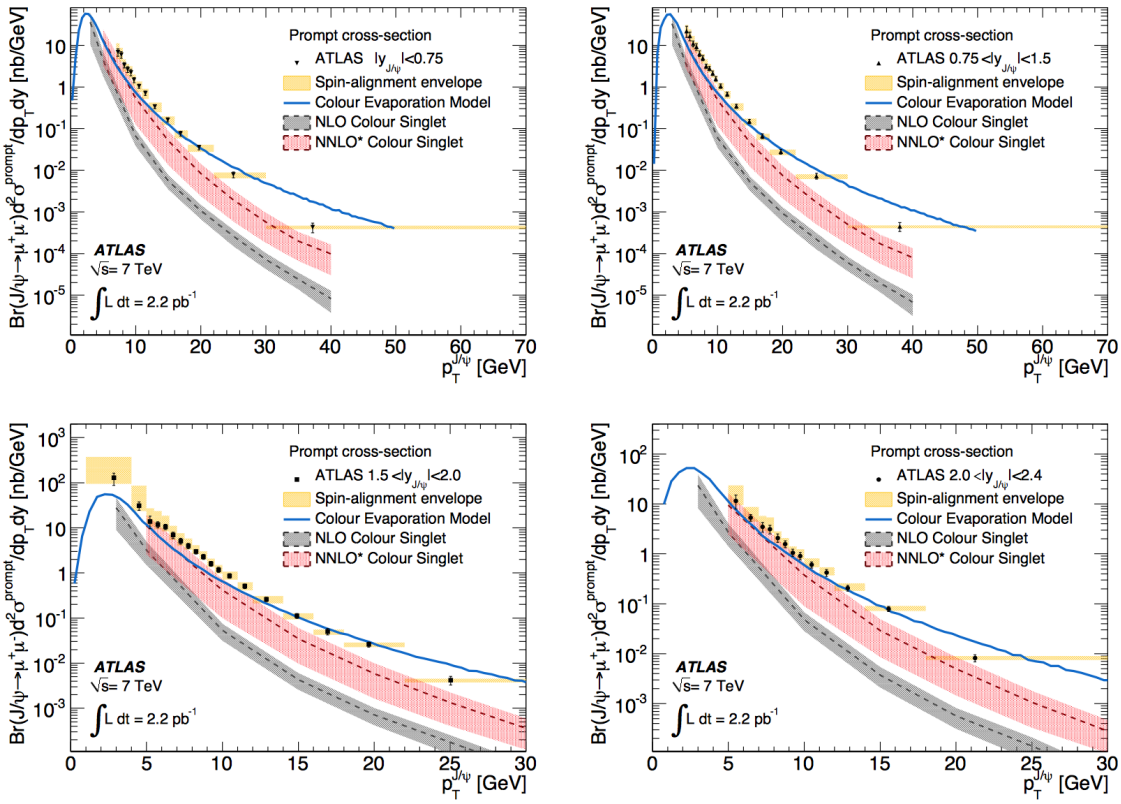

FIGURE 1.3: J/ψ transevse momentum spectrum from ATLAS at $\sqrt{s} = 7$ TeV from CEM (green) and CSM (red/grey). These resutls were published in Ref. [7].

Fig.1.3 from Ref. [7] shows how predictions for J/ψ production from the CSM and CEM framework compare against data from ATLAS experiment at LHC. We note that the NLO CSM predictions have significant disagreement with the data and NNLO CSM predictions suffer from large theoretical uncertainties.

1.3 The NRQCD framework

Inside the quarkonium, the heavy quark and antiquark have small relative velocity, ($v^2 \sim 0.1$ for $b\bar{b}$ and $v^2 \sim 0.3$ for $c\bar{c}$), therefore NRQCD [39]−which is an effective field theory that describes Quantum Chromodynamics in the non-relativistic limit−provides the correct theoretical framework for studying their interactions. There are three important scales that appear when studying the dynamics of non-

relativistic heavy quarks: m_Q, which is the mass of the heavy quark, $m_Q v$, is the size of their momentum in the rest frame of quarkonium, and $m_Q v^2$, which characterizes their kinetic energy in the same reference frame. The distance $r \sim 1/(m_Q v)$ gives an estimate of the size of the quarkonium state and the separation between the heavy quark-antiquark pair and the energy $\Delta E \sim m_Q v^2$ is of order of the energy splittings of radial excitations.

For bound states such as quarkonium we should expect that kinetic energy balance the Coulomb like potential energy, i.e., $m_Q v^2 \sim \alpha_s(1/r)/r$. The typical distance r between quark and antiquark is $1/Mv$ and since $\alpha_s(p)$ decreases with the increase of momentum scale (due to asymptotic freedom of QCD) we have

$$v \sim \alpha_s(m_Q v) \Rightarrow v \gtrsim \alpha_s(m_Q). \tag{1.9}$$

This scaling relation has an important implication: relativistic corrections of order v^{2n} are expected to be more important than perturbative corrections of order $(\alpha_s(m_Q))^{2n}$. Therefore when performing higher order calculation in the strong coupling, relativistic corrections must properly taken into consideration. For this reason we need a simultaneous expansion in the strong coupling and the relative velocity. The NRQCD framework allows us to do exactly that.

In NRQCD the heavy quark and antiquark are described by two separate spin 1/2 non-relativistic Schrödinger fields. Thus the Lagrangian that describes the heavy quark ψ and antiquark χ is

$$\mathcal{L}_{\text{heavy}} = \psi^\dagger \left(iD_t + \frac{\mathbf{D}^2}{2M} \right) \psi + \chi^\dagger \left(iD_t - \frac{\mathbf{D}^2}{2M} \right) \chi. \tag{1.10}$$

Light quarks are described in the NRQCD Lagrangian by the four-component Dirac spinor and their mass is set to zero. Also the gluon propagation and interactions are added to the Lagrangian through the standard gauge-invariant combination of the

Table 1.1: Table from [1] showing the velocity scaling rules for elementary operators in NRQCD.

Operators	Estimate	Description
ψ	$(Mv)^{3/2}$	Quark (annihilation) field
χ	$(Mv)^{3/2}$	Antiquark (creation) field
D_t	Mv^2	Gauge covariant time derivative
$\mathbf{D}$	Mv	Gauge covariant space derivative
$g\phi$	Mv^2	Scalar potential (Coulomb gauge)
$g\mathbf{A}$	Mv^3	Vector potential (Coulomb gauge)
$g\mathbf{E}$	M^2v^3	Chromoelectric field
$g\mathbf{B}$	M^2v^4	Chromomagnetic field

gluonic field tensor $G_{\mu\nu}$ as in Eq.(1.1). The corresponding term reads

$$\mathcal{L}_{\text{light}} = -\frac{1}{4}G^a{}_{\mu\nu}G^{a\mu\nu} + \sum_{n_f}\bar{q}i\not{D}q, \tag{1.11}$$

and the full Lagrangian is

$$\mathcal{L}_{\text{NRQCD}} = \mathcal{L}_{\text{heavy}} + \mathcal{L}_{\text{light}} + \delta\mathcal{L}. \tag{1.12}$$

where $\delta\mathcal{L}$ includes all the relativistic corrections up to the desired accuracy. Such terms are

$$\delta\mathcal{L} = \frac{c_1}{8M^3}[\psi^\dagger\left(D^2\right)^2\psi - \chi^\dagger\left(D^2\right)^2\chi] + \frac{c_2}{2M}[\psi^\dagger(g\mathbf{B}\cdot\boldsymbol{\sigma})^2\psi - \chi^\dagger(g\mathbf{B}\cdot\boldsymbol{\sigma})^2\chi] + \dots \tag{1.13}$$

Other important contributions to $\delta\mathcal{L}$ come from the four-fermion interactions that are associated with the quarkonium annihilation but not relevant to the work presented here. The relative importance of the operators in $\delta\mathcal{L}$ is determined by the NRQCD power counting. For evaluating the velocity scaling rules of the different

operators we start with the number operator of the quark field which equals 1, i.e.,

$$\int d^3x \psi^\dagger(x)\psi(x) = 1, \tag{1.14}$$

and since the integral has support only over of the quarkonium size

$$\int d^3x \sim V_3(\text{quarkonium}) \sim \frac{1}{p^3} \sim \frac{1}{(Mv)^3} \quad \Rightarrow \quad \psi \sim (Mv)^{3/2}. \tag{1.15}$$

Similarly we can find the estimated size of other elementary operators. A summary of these results is shown in Table 1.1 [1].

1.3.1 Quarkonium production in fixed order NRQCD calculations

In NRQCD framework the quarkonium production cross section is factorized into the perturbatively calculable short distance coefficients (SDC) and long distance matrix elements (LDME) that need to be extracted from data:

$$d\sigma_{NRQCD}(a + b \to \mathcal{Q} + X) = \sum_n d\sigma(a + b \to Q\bar{Q}[n] + X)\langle \mathcal{O}_n \rangle, \tag{1.16}$$

where

$$\mathcal{O}^n_{\mathcal{Q}} = \mathcal{O}^{n\dagger}_2 \left(\sum_J \sum_{m_J} |\mathcal{Q} + X\rangle\langle\mathcal{Q} + X| \right) \mathcal{O}^n_2 \quad \text{and} \quad \mathcal{O}^n_2 = \psi^\dagger \mathcal{K}_n \chi, \tag{1.17}$$

where $\mathcal{K}_n$ is a tensor in the Dirac and color algebra. Therefore the index n runs over all possible color and angular momentum configurations. While the short distance coefficients $d\sigma(a + b \to Q\bar{Q}[n] + X)$ in Eq.(1.16) have an expansion in the strong coupling, α_s, the LDMEs scale based on the NRQCD scaling rules. Thus truncating the sum can give us the desirable accuracy from a simultaneous expansion in the α_s and v. In this approach for calculating quarkonium production cross sections, SDCs appearing in Eq.(1.16) are calculated up to a specific order in perturbation theory. For this reason we refer to these calculations as fixed order calculations.

We note that including in the sum in Eq.(1.22) only the case where n matches the quantum numbers of the quarkonium state, then the NRQCD framework recovers the results from CSM. Though, for S-wave quarkonia the singlet LDME dominates in the relative velocity expansion, for P-wave quarkonia the singlet LDME scales the same as the leading color-octet LDMEs. This explains the necessity for inclusion of octet states for complete cancelation of infrared divergences that appear in CSM calculations for the P-wave quarkonia.

NRQCD has been the most successful model for the description of quarkonium production in hadron colliders. The values of the singlet matrix element are extracted either from quark potential model calculations and from quarkonium di-lepton decay rates. The rest of the relevant values included in the expansion are fitted to results from experimental data.

1.4 J/ψ production

Experimentally the most studied charmonium state is J/ψ. With quantum numbers 1^3S_1, J/ψ has clean experimental signal through di-lepton decays as we will describe later in this chapter. In the work presented here we focus on the production of J/ψ but the methodology and the framework we develop can be applied to any quarkonium state and more generally to any hadron.

In hadron colliders the major production processes of J/ψ are:

- Through b-hadron decays (i.e., $h_b \to J/\psi + X$) which we refer to as non-prompt production.
- Direct production from energetic partons.
- Feed-down decays of excited charmonium states.

The main contribution to feed-down production are radiative decays of P-wave states

Table 1.2: LDMEs for NRQCD production mechanisms. Central values taken from global fits in Refs. [2,3]. The values are in units of GeV^3. The v scaling is also shown.

$\langle \mathcal{O}^{J/\psi}(^3S_1^{(1)}) \rangle$	$\langle \mathcal{O}^{J/\psi}(^3S_1^{(8)}) \rangle$	$\langle \mathcal{O}^{J/\psi}(^1S_0^{(8)}) \rangle$	$\langle \mathcal{O}^{J/\psi}(^3P_J^{(8)}) \rangle / m_c^2$
1.32 ± 0.2	$(2.24 \pm 0.59) \times 10^{-3}$	$(4.97 \pm 0.44) \times 10^{-2}$	$(-7.16 \pm 0.9) \times 10^{-3}$
$\sim v^3$	$\sim v^7$	$\sim v^7$	$\sim v^7$

($\chi_c \to J/\psi\gamma$) which approximately consists of 71% of the feed-down contribution and hadronic decays of other excited vector states ($\psi(2S) \to J/\psi + hadrons$) [40,41] with approximately 23% contribution to the feed-down production of J/ψ. Additionally, any production process that does not involve b-hadron decays is refer to as prompt production, that includes the direct production and feed-down decays.

The NRQCD framework has been applied extensively in predicting transverse momentum of the J/ψ in excellent agreement with experimental data. These results are demonstrated in Fig. 1.4, which shows how the predictions agree with various experiments in hadron colliders for a large range of the transverse momentum and rapidity. The values of the LDMEs that are used in the demonstrated calculations are extracted in Refs. [3, 42] from global fits to the world data and are summarized in Table. 1.2. In Fig. 1.4 only two of the thirty-two data-sets used are presented. We note that these values are in agreement with the NRQCD velocity scaling rules in the second line of Table. 1.2.

Despite the great success of NRQCD in describing the transverse momentum spectrum of J/ψ, NRQCD fails to correctly predict the J/ψ polarization. Fig. 1.5 shows that measurements [11] of J/ψ polarization disagree with NRQCD predictions.In Fig. 1.5 the blue band corresponds to the polarization prediction in NLO calculations using the LDMEs from Table 1.2 [8] and the red band to same order calculations including the effect of feed-down decays [9]. The green band, which

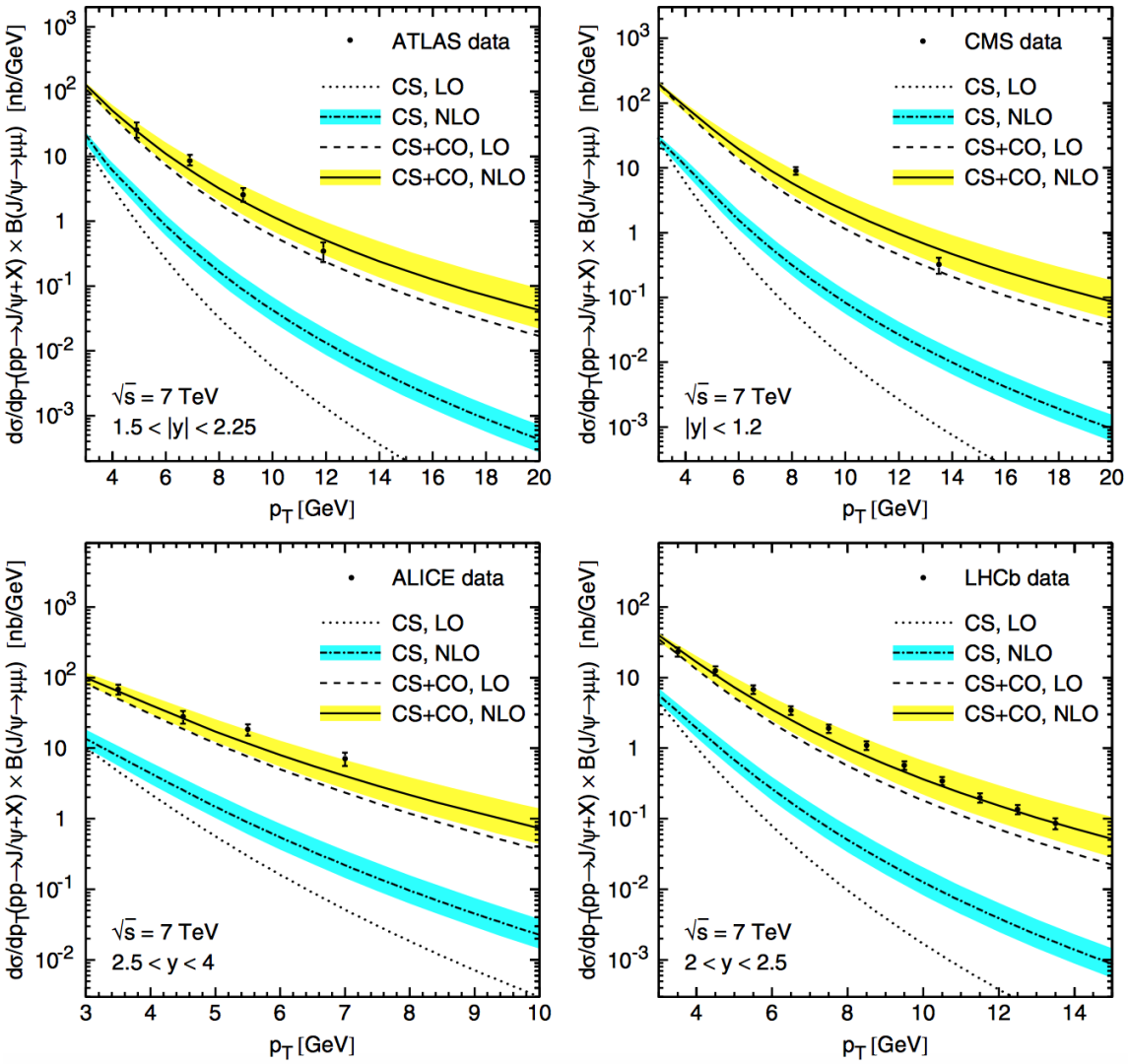

FIGURE 1.4: J/ψ transevse momentum spectrum from experiments at LHC (ALICE, CMS, ATLAS, LHCb) at $\sqrt{s} = 7$ TeV compared against predictions from NRQCD framework where the LDMEs are extracted from global fits to the world's data. Figure from Ref. [2, 3].

shows the best agreement with the data corresponds to LDMEs that are extracted from simultaneous fits to the transverse momentum and polarization spectrum of J/ψ [10] at high $p_\perp$, at hadron colliders only. The magenta curve corresponds to predictions from CSM calculations in $k_\perp$ factorization from Ref. [8]. While the experimental data find that the quarkonium is produced unpolarized (i.e. $\lambda_\theta \sim 0$)

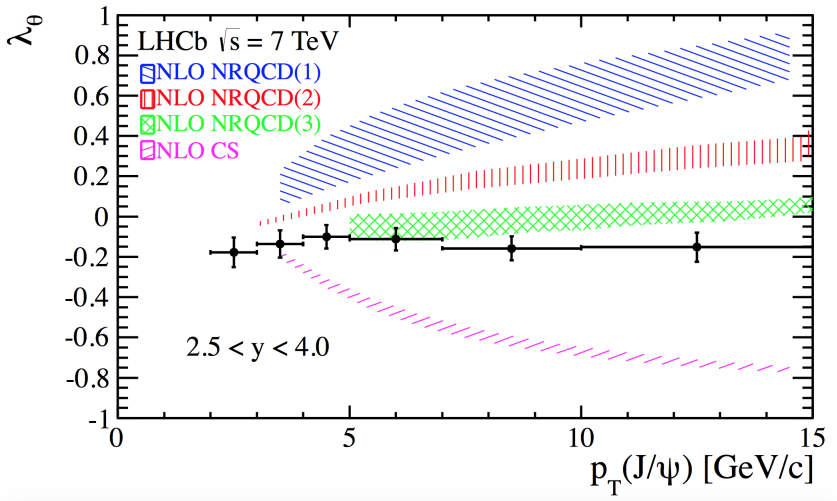

FIGURE 1.5: J/ψ pollarization spectrum in the HX frame, from LHCb at $\sqrt{s} = 7$ TeV, compared against predictions from NRQCD and CSM [8]. The LDMEs for the NRQCD predictions are extracted from three different fits (blue [8], red [9], green [10]). These resutls were published in Ref. [11].

various theoretical studies consistently predict some or full transverse polarization. Measurements from other experiments (e.g. CMS [43], ALICE [44], CDF [45]) find similar results. This discrepancy between theoretical predictions and data is also known as the polarization puzzle of J/ψ.

1.4.1 NRQCD fragmentation functions

There have been recent attempts [46, 47] to resolve the polarization puzzle, by refitting LDMEs from charmonium production transverse momentum spectrum at high p_T including the color-octet dominating mechanisms and resuming logarithms of $p_T/m_{J/\psi}$ using renormalization group evolution techniques. This is achieved by using the leading power (LP) factorization approach which states that at large transverse momenta fragmentation processes dominate the production cross section. For a generic hadron h this is expressed through the following factorization formula:

$$\frac{d\sigma(h+X)}{dx} = \sum_i \int_x^1 \frac{dz}{z} d\sigma^i(z,\mu) D_{i/h}\left(\frac{x}{z},\mu\right) + \mathcal{O}(m_h/p_\perp^h). \tag{1.18}$$

where $d\sigma^i(z,\mu)$ is the partonic cross section and $D_{i/h}(x,\mu)$ the fragmentation function (FF). Similarly to PDFs, fragmentation functions are fundamentally non-perturbative and describe the production of identified hadrons from energetic partons. The factorization scale dependence, at leading order, is the same DGLAP evolution equation (cf. Eq(1.4)) for the FFs as for PDFs. At higher orders the form of the evolution equation remains the same but the splitting kernels, $P_{ij}(x)$, differ starting at two loops (i.e., at $\mathcal{O}(\alpha_s)$). The DGLAP evolution conserves the normalization of fragmentation function which reads

$$\sum_h \int_0^1 dx\ x D_{i/h}(x,\mu) = 1. \tag{1.19}$$

For a parton i fragmenting into a hadron h the operator definition of the corresponding fragmentation function is given by [48]

$$D_{q/h}(z,\mu) = \frac{1}{z}\sum_X \frac{1}{2N_c}\delta(\omega - p_X^- - p_h^-)\ \mathrm{Tr}\left[\frac{\bar{\not{n}}}{2}\langle 0|\psi(0)|Xh\rangle\langle Xh|\bar{\psi}(0)|0\rangle\right]\Big|_{\mathbf{p}_\perp^X = -\mathbf{p}_\perp^h}, \tag{1.20}$$

for quark fragmentation, and

$$D^{\mu\rho}_{g/h}(z,\mu) = -\frac{1}{(d-a)(N_c^2-1)\omega z}\sum_X \delta(\omega - p_X^- - p_h^-)\langle 0|G^a_{\mu\nu}(0)|Xh\rangle\langle Xh|G^{\nu a}_{\rho}(0)|0\rangle, \tag{1.21}$$

for gluon fragmentation, where z is the fraction of the energy of the original parton, $E_i = \omega$, carried by the hadron. The energy conservation delta function is expressed in terms of the light-cone coordinates ($p^- = p^0 + p^3 \approx 2p^0$).

Applying Eq.(1.18) to the NRQCD factorization conjecture in Eq.(1.16) we can extract the quarkonium fragmentation functions [49].

$$D_{i/\mathcal{Q}}(z,\mu) = \sum_n d_i^n(z)\langle \mathcal{O}^n_{\mathcal{Q}}\rangle, \tag{1.22}$$

Table 1.3: Contributions to the J/ψ charm quark and gluon fragmentation function.

Mechanism	LO to $d_i^n(z)$	LDME scaling	Total scaling
$c \to (c\bar{c}[^3S_1^{(1)}])$	$\mathcal{O}(\alpha_s^2)$	$\sim v^3$	$\sim \alpha_s^2 v^3$
$g \to (c\bar{c}[^3S_1^{(1)}])$	$\mathcal{O}(\alpha_s^3)$	$\sim v^3$	$\sim \alpha_s^3 v^3$
$g \to (c\bar{c}[^3S_1^{(8)}])$	$\mathcal{O}(\alpha_s^1)$	$\sim v^7$	$\sim \alpha_s^1 v^7$
$g \to (c\bar{c}[^1S_0^{(8)}])$	$\mathcal{O}(\alpha_s^2)$	$\sim v^7$	$\sim \alpha_s^2 v^7$
$g \to (c\bar{c}[^3P_J^{(8)}])$	$\mathcal{O}(\alpha_s^2)$	$\sim v^7$	$\sim \alpha_s^2 v^7$

where now $d_i^n(z)$ are matching coefficients that can be evaluated in perturbation theory through a matching process from QCD onto NRQCD. Applying Eq.(1.22) in the QCD factorization framework (i.e. Eqs.(1.18) and (1.3)) we have

$$d\sigma^{LP}_{NRQCD}(h_1(P_2 1)h_2(P_2) \to \mathcal{Q}(x) + X) = \sum_n \langle \mathcal{O}^n_{\mathcal{Q}} \rangle \times \sum_i \int_x^1 \frac{dz}{z} d\sigma(h_1(P_2 1)h_2(P_2) \to i(z) + X) d_i^n \left(\frac{x}{z}\right) \quad (1.23)$$

In the NRQCD leading power approximation we consider charm quark and gluon fragmentation separately. In the charm quark fragmentation the dominant production mechanism is through a $c\bar{c}$ bound state in $^3S_1^{(1)}$ configuration. In the strong coupling and relative velocity expansion this mechanism scales as $c \to (c\bar{c}[^3S_1^{(1)}]) + X \sim \alpha_s^2\ v^3$. In the gluon fragmentation process the situation is more complicated since various production mechanisms have comparable contributions to the fragmentations function. The most important mechanisms are $^3S_1^{(1)}$, $^3S_1^{(8)}$, $^1S_0^{(8)}$, and $^3P_J^{(8)}$, and their estimated sizes are summarized in Table 1.3.

The leading power factorization approach yields good fits for the cross section data, however the extracted values of LDMEs are inconsistent with previous fits to

the world's data suggesting that an independent measurement of LDMEs is needed.

1.5 Quarkonium polarization

The vector states, 1^3S_1, with $J^{PC} = 1^{--}$ (i.e. J/ψ and $\Upsilon(1S)$) have very characteristic and experimentally clean di-lepton (e^+e^-, $\mu^+\mu^-$) decays that are used for measuring the polarization of quarkonium, where a state is transversely polarized if $J_z = \pm 1$ and longitudinally polarized if $J_z = 0$, and the direction $\hat{z}$ is chosen along the direction of the motion. This choice of axis is called the helicity reference frame and other common choices are the Gottfried-Jackson frame [50], GJ, and Collins-Soper frame [51], CS, as shown in Fig. 1.6(left). The angular distribution of the dimuons in the quarkonium rest frame gives a direct measurement of the polarization. An observable used widely by all high energy experiments is the coefficient, λ_θ, of the polar cosine from the dimoun angular distribution

$$W(\theta, \phi) = N(1 + \lambda_\theta \cos^2\theta + \lambda_\phi \sin^2\theta \cos 2\phi + \lambda_{\theta\phi} \sin 2\theta \cos\phi), \tag{1.24}$$

where the angle θ and ϕ are the polar and azimuthal angles of the direction of the positive charge lepton as displayed in Fig. 1.6 (right). We can derive Eq.(1.24) by noticing that in the quarkonium rest frame the muons are approximately massless and therefore helicity eigenstates. Also due to helicity conservation in QED the dimuon system must have the same helicity as the decayed photon, i.e. ± 1, therefore the spin of the two muons is parallel and pointing in the direction of their motion. On the other hand the quarkonium state, in the most general case has components

$$|^3S_1\rangle = a_1|m = 1\rangle + a_0|m = 0\rangle + a_{-1}|m = -1\rangle, \tag{1.25}$$

where $J_z|\ m\ \rangle = m|\ m\ \rangle$ (in $\hbar = 1$ units) and $\hat{z}$ is the direction of motion of the quarkonium. Using the three dimensional unitary representation of rotations we can

easily evaluate

$$W \sim \sum_{\ell=\pm 1} \left| \langle \mu^+ \mu^-; \ell | \, \hat{\mathcal{B}} \, |^3 S_1 \rangle \right|^2, \tag{1.26}$$

where the action of the transition operator $\hat{\mathcal{B}}$ on the quarkonium state is uniform among the different eigenstates of J_z, due to the rotational invariance of QED as discussed in Ref. [12],

$$\hat{\mathcal{B}} \, |^3 S_1 \rangle = B \Big[a_1 |m = 1\rangle + a_0 |m = 0\rangle + a_{-1} |m = -1\rangle \Big]. \tag{1.27}$$

After evaluating the transition amplitude $\langle \mu^+ \mu^-; \ell | \, \hat{\mathcal{B}} \, |^3 S_1 \rangle$ and summing the probabilities over the possible polarizations of the dimuon system ($\ell = \pm 1$) we recover Eq.(1.24) with

$$\lambda_\theta = \frac{1 - 3|a_0|^2}{1 + |a_0|^2}. \tag{1.28}$$

We note that the observable λ_θ is useful for measuring the polarization of quarkonium since it has distinct behavior for all three special cases.

$$\begin{aligned} \text{Transverse polarization } (|a_{\pm 1}| = 1, a_0 = 0): &\qquad \lambda_\theta = +1 \,, \\ \text{Longitudinal polarization } (a_{\pm 1} = 0, |a_0| = 1): &\qquad \lambda_\theta = -1 \,, \\ \text{No polarization } (a_1 = a_{-1} = a_0 = \pm 1/\sqrt{3}): &\qquad \lambda_\theta = 0. \end{aligned} \tag{1.29}$$

As we saw earlier in this chapter theoretical predictions fail to reproduce experimental results regarding the polarization of J/ψ. This discrepancy is the well known polarization puzzle. This thesis is focused on developing alternative observables for studying quarkonium production to give further insight into the fragmentation production of J/ψ and therefore shed light on the polarization puzzle.

The work presented here focuses on approaches for extracting charmonium production LDMEs by studying jet observables in semi-inclusive processes. The pro-

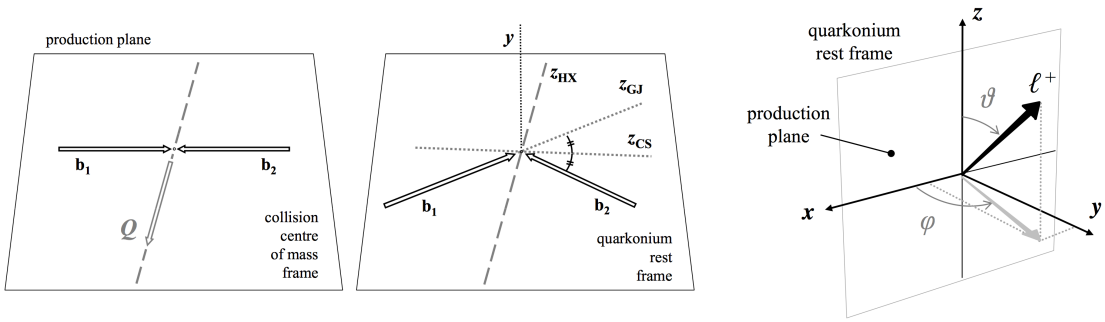

FIGURE 1.6: Standard reference frames for measuring quarkonium pollarization. Picture taken from Ref. [12].

cesses we will consider are quarkonium produced within a jet[4] of particles. The production mechanisms could have great impact on the jet substructure and topology therefore, measurements of jet observables can help discriminate between various production mechanisms. Thus, such measurements could help perform an independent extraction of the LDMEs. We believe that the extracted LDMEs will give us further insight into the polarization puzzle.

Measurements on J/ψ production in jets were performed for the first time recently by the LHCb collaboration [13]. In this measurement the transverse momentum ratio $z = p^{\perp}_{J/\psi}/p^{\perp}_{\text{jet}}$ is measured for jets with cone size $R = 0.5$, within the pseudo-rapidity range $\eta \in (2.5, 4.0)$ and transverse momentum $p^{\perp}_{\text{jet}} > 20$ GeV. For J/ψ produced promptly the observed data are compared against predictions from the simulation package PYTHIA 8 in Fig. 1.7. We discuss the LHCb measurements in the last section of Chapter 3 and we give semi-analytic predictions for three different extractions of LDME, a complete analytic[5] calculation is in development.

Over the past few years there has been a great effort made towards the develop-

[4] A jet of particles is a collimated spray of hadrons initiated by a single energetic parton. Jets are the result of hadronization of gluons and quarks due to confinement.

[5] By complete analytic we refer to calculations that do not involve input from monte-carlo simulations but will include non-perturbative parton distribution functions

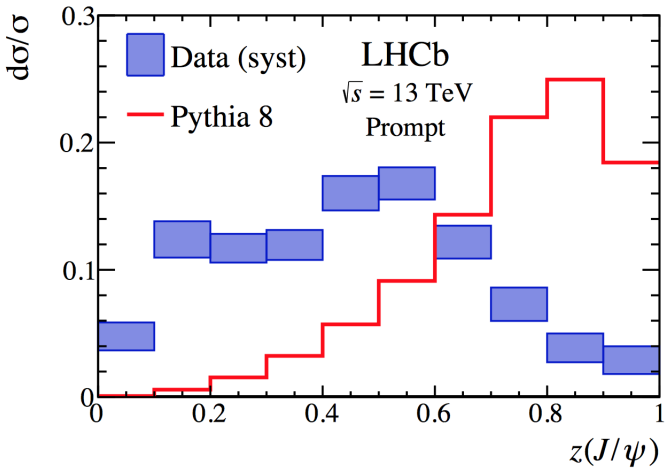

FIGURE 1.7: Measured normalized $z(J/\psi)$ distributions for J/ψ mesons produced promptly compared to predictions obtained from Pythia 8. This figure was published in Ref. [13]

ment of theoretical tools for the study of jets. Particularly, in the framework of SCET (Soft-Collinear Effective Theory) [52–54]−an effective theory of QCD in the soft and collinear limit−jet observables are factorized into pieces calculable in perturbation theory and universal nonperturbative parts. For hadron or quarkonium production inside jets, these pieces include newly-defined fragmenting jet functions (FJFs) [55]. These advanced methods allow us to investigate the effects of the hadron's production mechanism on the observed substructure and topology of the jet. More details on the development of SCET and how FJFs are constructed and enter factorization theorems in SCET are presented in Chapters 2 and 3. In Chapter 4 we present the generalization of FJFs to transverse momentum dependent (TMD) observables where the transverse momentum of the identified hadron is measured with respect to the jet axis. In Chapter 5 we evaluate all the necessary pieces for the factorization theorem in dijet events at hadron colliders and we develop a prescription for implementing the FJF formalism in such events. The work presented in Chapters 3, 4, and 5 was published in [56–58] respectively and the manuscript closely follows the corresponding publications.

2

Soft Collinear Effective Theory

Beyond leading order calculations of jet cross sections in QCD, soft and collinear divergences from the real emission diagrams cancel against infrared divergences from the virtual emissions. The soft and collinear divergences appear from the region of phase-space where the real particles are emitted within the jet boundary or are soft enough such that they do not form a new jet. A characteristic example of fixed order calculations of jet cross sections is given in Ref. [59]. In soft collinear effective theory [52–54] collinear and soft modes are systematically extracted from the full QCD fields. This allows us to isolate these divergences in soft and collinear functions respectively. The infrared divergences from loop corrections to the hard process are included in the hard functions. This way one can establish a renormalization procedure for each function separately and using renormalization group techniques, resum logarithms of widely separated scales that can potentially ruin the perturbative expansion in fixed order calculations.

2.1 Lightcone coordinates

In this section we introduce the notation that will be used in this and the following chapters. Since in SCET we encounter collinear and soft modes of the quark and gluon fields, is convenient to express the corresponding momenta in the lightcone coordinates with respect to the unit vector $\hat{n}$. In the context of jet cross sections $\hat{n}$ is chosen to point in the direction of the corresponding jet or beam axis. In a particular process multiple directions are relevant, e.g. for the process $pp \to 2$ jets four directions are of interest (the two beam and the two jet axis) and thus four unit vectors need to employed ($\hat{n}_B$, $\hat{n}_{\bar{B}}$, $\hat{n}_1$, and $\hat{n}_2$) as shown in Fig. 2.1.

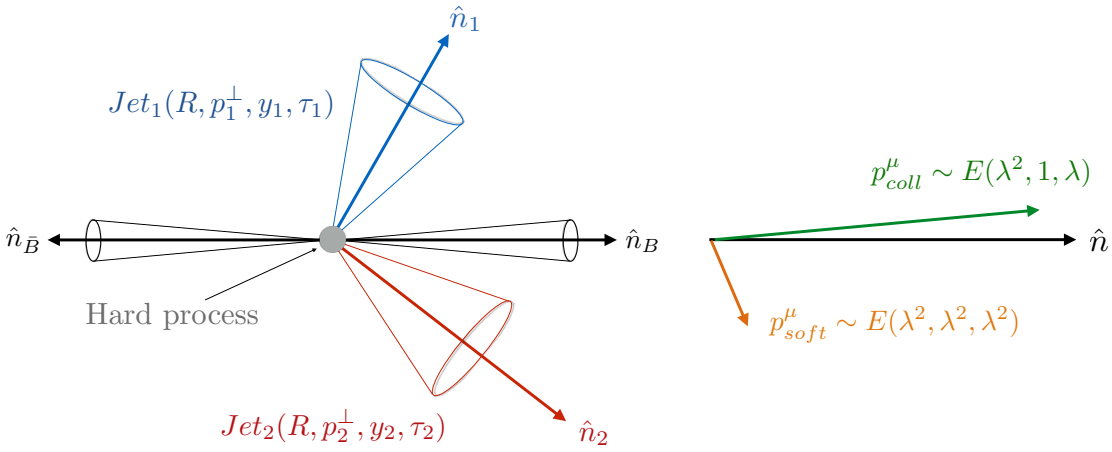

FIGURE 2.1: Example of multiple collinear directions in a single event. In this particular case we have a di-jet event in pp or $p\bar{p}$ collision.

For every direction $\hat{n}_i$ we define the corresponding lightlike four-vectors, $n_i^\mu = (1, \hat{n}_i)$ and $\bar{n}_i^\mu = (1, -\hat{n}_i)$ such that $n^2 = \bar{n}^2 = 0$ and $n \cdot \bar{n} = 2$. Then every four-vector, A^μ can be expanded in the lightcone coordinates in the following way

$$A^\mu = \frac{n^\mu}{2} A^- + \frac{\bar{n}^\mu}{2} A^+ + A_\perp^\mu, \tag{2.1}$$

where $A^+ = n \cdot A$, $A^- = \bar{n} \cdot A$, and $A_\perp^\mu$ are the two spatial components perpendicular to the direction of the unit vector $\hat{n}$ such that $A_\perp \cdot n = A_\perp \cdot \bar{n} = 0$. We represent this

decomposition in component notation as $A^\mu = (A^+, A^-, A^\mu_\perp)$. Furthermore the vector product in Minkowski metric $A \cdot B$ is writen in terms of the lightcone coordinates as

$$A \cdot B = \frac{A^+B^-}{2} + \frac{A^-B^+}{2} + A_\perp \cdot B_\perp = \frac{A^+B^-}{2} + \frac{A^-B^+}{2} - \vec{A}_\perp \cdot \vec{B}_\perp \, . \tag{2.2}$$

The momentum components p^μ of energetic particles emitted in an angle θ with respect to $\hat{n}$ are $p^+ \approx E(1-\cos\theta)$, $p^- \approx E(1+\cos\theta)$, and $|p_\perp| \approx E\sin\theta$. For particles collinear to the $\hat{n}$ direction where $\theta \ll 1$ their four momenta scale as $p^\mu_{coll.} \sim E(\lambda^2, 1, \lambda)$, where $\lambda = E/|p_\perp| \approx \theta$. On the other hand, momenta of soft particles satisfy the following scaling, $p^\mu_{soft} \sim E(\lambda^\alpha, \lambda^\alpha, \lambda^\alpha)$, where for $\alpha = 2$ are called ultra-soft emissions and for $\alpha = 1$ are simply referred to as soft emissions. The version of SCET that is associated with the ultra-soft modes is known as $\mathrm{SCET_I}$ where the soft modes are relevant in $\mathrm{SCET_{II}}$ [52–54]. Extended versions of SCET such as $\mathrm{SCET_+}$ [5,60] and $\mathrm{SCET_G}$ [61] involve additional soft-collinear and Glauber modes. Some of the extended versions of SCET ($\mathrm{SCET_+}$ and $\mathrm{SCET_{++}}$) will be discussed later in Chapters 4 and 5.

The collinear and soft gluon fields are defined by the corresponding momenta that are functions in momentum space, i.e., for the collinear gluon field we have $A^\mu_n(p_{coll})$ and for the soft gluon field $A^\mu_{us}(p_{soft})$. Using the definition of the gluon propagator we can establish a power counting of the four-vector components of the gluon field

$$\int d^4x e^{ik\cdot x} \langle 0|A^\mu_n(x) A^\nu_n(0)|0\rangle = -\frac{i}{k^4}(k^2 g^{\mu\nu} - (1-\xi)k^\mu k^\nu), \tag{2.3}$$

where ξ is the parameter that controls the choice of gauge (e.g. Feynman and 't Hooft gauge, in which $\xi = 1$ and Landau gauge, where $\xi = 0$) and since d^4x has support in a region that scales as the inverse of the corresponding momenta we have $d^4x \sim dx^+dx^-d^2x_\perp \sim \lambda^{-4}$ and it must that $A^\mu_n A^\nu_n \sim (k^2 g^{\mu\nu} - \xi k^\mu k^\nu)$. By taking the perpendicular component in both four-vector indices μ and ν, we have

$(A_{n,\perp})^2 \sim (Q\lambda)^2$ thus $A_{n,\perp} \sim Q\lambda$. The $+-$ combination will give $A_n^+ A_n^- \sim (Q\lambda)^2$ and the $++$ combination $A_n^+ A_n^+ \sim (Q\lambda)^4$. Therefore the collinear gluon field four-vector components has the same scaling as the collinear four-momenta. Similar analysis also shows that the soft gluon field scales the same as soft four-momenta:

$$A_n^\mu \sim p_{coll}^\mu \sim Q(\lambda^2, 1, \lambda) \quad \text{and} \quad A_{us}^\mu \sim p_{u-soft}^\mu \sim Q(\lambda^2, \lambda^2, \lambda^2)\,, \tag{2.4}$$

where here and for the rest of this chapter we work in SCET_I where soft radiation scales as ultra-soft modes (i.e. $p_{soft} \sim E(\lambda^2, \lambda^2, \lambda^2)$).

For developing the SCET Lagrangian for Dirac spinors is useful to introduce the projection operators P_{+-} and P_{-+} defined as

$$P_{+-} = \frac{\gamma^+\gamma^-}{4}, \quad P_{-+} = \frac{\gamma^-\gamma^+}{4}. \tag{2.5}$$

where γ^μ are the Dirac matrices. Directly from their anti-commutation relations (i.e. $\{\gamma^\mu, \gamma^\nu\} = 2\eta^{\mu\nu}$) the projection operators satisfy

$$P_{+-} + P_{-+} = \mathbb{1}. \tag{2.6}$$

Additionally we can show that $\{\gamma^+, \gamma^-\} = 4$ and since $\gamma^+\gamma^+ = \gamma^-\gamma^- = 0$ the following relations are true

$$P_{+-}\gamma^+ = \gamma^+, \quad P_{-+}\gamma^- = \gamma^-, \text{ and } P_{+-}\gamma^- = P_{-+}\gamma^+ = 0\,, \tag{2.7}$$

thus the following projection operator relations are also true

$$(P_{+-})^2 = P_{+-}, \quad (P_{-+})^2 = P_{-+}, \text{ and } P_{+-}P_{-+} = P_{-+}P_{+-} = 0. \tag{2.8}$$

2.2 The SCET Lagrangian

In this section we discuss the derivation of the SCET_I Lagrangian for the collinear quark field[1]. We start the derivation from the massless limit of QCD and expanding

[1] The discussion closely follows the notes from Ref. [62].

by applying Eq.(2.6) to the quark field ψ.

$$\psi = (P_{+-} + P_{-+})\psi = \xi_n + \psi_{\bar{n}} \ , \tag{2.9}$$

thus

$$\mathcal{L}_{\rm QCD} = \bar{\psi}(i\gamma \cdot D)\psi = (\bar{\phi}_{\bar{n}} + \bar{\xi}_n)\left(i\frac{\gamma^+ D^-}{2} + i\frac{\gamma^- D^+}{2} + i\gamma_\perp \cdot D_\perp\right)(\phi_{\bar{n}} + \xi_n) \ , \tag{2.10}$$

where $\xi_n \equiv P_{+-}\psi$ and $\phi_{\bar{n}} \equiv P_{-+}\psi$. To simplify this expression we expand and use the fact that $\gamma^+\xi_n = \bar{\xi}_n\gamma^+ = \gamma^-\phi_{\bar{n}} = \bar{\phi}_{\bar{n}}\gamma^- = 0$ which is directly derived from the relations in Eq. (2.7). Applying these relations gives

$$\begin{aligned}\mathcal{L}_{\rm QCD} = \bar{\xi}_n\left(i\frac{\gamma^- D^+}{2}\right)\xi_n + \bar{\phi}_{\bar{n}}\left(i\frac{\gamma^+ D^-}{2}\right)\phi_{\bar{n}} + \bar{\xi}_n(i\gamma_\perp \cdot D_\perp)\phi_{\bar{n}} + \bar{\phi}_{\bar{n}}(i\gamma_\perp \cdot D_\perp)\xi_n \\ + \bar{\xi}_n(i\gamma_\perp \cdot D_\perp)\xi_n + \bar{\phi}_{\bar{n}}(i\gamma_\perp \cdot D_\perp)\phi_{\bar{n}} \ , \end{aligned} \tag{2.11}$$

The last two terms in the second line also vanish since

$$\bar{\xi}_n(i\gamma_\perp \cdot D_\perp)\xi_n = \bar{\xi}_n(i\gamma_\perp \cdot D_\perp)P_{+-}\xi_n = \bar{\xi}_n P_{+-}(i\gamma_\perp \cdot D_\perp)\xi_n = 0, \tag{2.12}$$

where in the second line we used $\gamma_\perp\gamma^\pm = -\gamma^\pm\gamma_\perp$. Therefore we have

$$\mathcal{L}_{\rm QCD} = \bar{\xi}_n\left(i\frac{\gamma^- D^+}{2}\right)\xi_n + \bar{\phi}_{\bar{n}}\left(i\frac{\gamma^+ D^-}{2}\right)\phi_{\bar{n}} + \bar{\xi}_n(i\gamma_\perp \cdot D_\perp)\phi_{\bar{n}} + \bar{\phi}_{\bar{n}}(i\gamma_\perp \cdot D_\perp)\xi_n. \tag{2.13}$$

Up to this point he have only expanded the QCD Lagrangian in terms of the ξ_n and $\phi_{\bar{n}}$ fields. In the next step we will eliminate the component $\phi_{\bar{n}}$ from the Lagrangian using the equations of motion. This component will give subleading contributions in λ which will not contibute to the leading order SCET Lagrangian. We may see how the $\phi_{\bar{n}}$ component will give contributions of subleading orders by expanding the equation of motion for the Dirac spinor u: $0 = \not{p}u = \not{p}(P_{+-} + P_{-+})u = p^-\frac{\gamma^+}{2}(P_{+-}u) + \mathcal{O}(\lambda)$. The corresponding equation of motion satisfied by $\phi_{\bar{n}}$ is

$$\frac{\partial\mathcal{L}}{\partial\bar{\phi}_{\bar{n}}} = 0 \ , \tag{2.14}$$

which directly leads to

$$\frac{\gamma^+ D^-}{2}\phi_{\bar{n}} + (\gamma_\perp \cdot D_\perp)\xi_n = 0$$

$$D^-\phi_{\bar{n}} - (\gamma_\perp \cdot D_\perp)\frac{\gamma^-}{2}\xi_n = 0 \to \phi_{\bar{n}} = \frac{1}{D^-}(\gamma_\perp \cdot D_\perp)\frac{\gamma^-}{2}\xi_n \,. \tag{2.15}$$

Using this expression for replacing the subleading component $\phi_{\bar{n}}$ in the QCD Lagrangian we get

$$\mathcal{L} = \bar{\xi}_n \left(iD^+ + i\not{D}_\perp \frac{1}{iD^-} i\not{D}_\perp \right) \frac{\gamma^-}{2}\xi_n \,, \tag{2.16}$$

where we used the shorthand notation $\not{D}_\perp \equiv \gamma_\perp \cdot D_\perp$.

We continue by separating the collinear momentum to label and residual into a similar manner as in heavy quark effective theory (HQET) [63] where $p^\mu = p_\ell^\mu + p_r^\mu$. The residual momenta has ultra-soft scaling i.e. $p_r^\mu \sim Q(\lambda^2, \lambda^2, \lambda^2)$ and the label moment scales as $p_\ell^\mu \sim Q(0, 1, \lambda)$. Using this decomposition we may write the $\xi_n(x)$ as $\xi_{n,p_\ell}(x_r)$ where we explicitly show the label momentum and the coordinate variable x_r which is conjugate variable of the residual momentum. Thus the coordinate derivative ∂_x now is separated in a derivative term with respect to x_r and the label momentum operator $\mathcal{P} = (0, \bar{\mathcal{P}}, \mathcal{P}_\perp)$: $i\partial_x \to \mathcal{P} + i\partial_{x_r}$. For simplicity of notation we relabel $x_r \to x$ and ignore the label momentum index such that $\xi_{n,p_\ell}(x_r) \to \xi_n(x)$. Applying these modifications and including only the leading terms after power counting in λ we have the final result for the SCET Lagrangian for the collinear quark fields:

$$\mathcal{L}^0_{n\xi} = \bar{\xi}_n \left(iD^+ + i\not{D}_{n,\perp} \frac{1}{iD_n^-} i\not{D}_{n,\perp} \right) \frac{\gamma^-}{2}\xi_n \,, \tag{2.17}$$

where

$$iD^\mu_{n,\perp} = \mathcal{P}^\mu_\perp + gA^\mu_{n,\perp}, \quad iD^-_n = \bar{\mathcal{P}} + gA^-_n, \quad \text{and} \quad iD^+ = i\partial^+ + g(A^+_n + A^+_s). \tag{2.18}$$

The superscript 0 notation denotes that this is the leading contribution to the

SCET Lagrangian in the power counting parameter λ. The complete SCET Lagrangian also includes the collinear gluon sector, $\mathcal{L}_{ng}$, that describes the propagation and the dynamics of gluon-gluon interactions, as well as the hard sector, $\mathcal{L}_{hard}$, that describes the operator matching from QCD onto SCET,

$$\mathcal{L}^0_{SCET} = \sum_n \left(\mathcal{L}^0_{n\xi} + \mathcal{L}^0_{ng}\right) + \mathcal{L}_{hard} + \mathcal{O}(\lambda). \tag{2.19}$$

In this section we are not going to perform the derivation of the other terms since the gluon interactions sector can be derived in a similar manner as the quark sector by expanding and performing power counting at leading order. The hard sector is evaluated through a matching process and for the work presented here all the relevant parts are going to be extracted from the literature. Also note that in Eq.(2.19) we included a summation over all distinct collinear sectors. Two collinear sectors described by the light-like vectors n_1^μ and n_2^μ are considered distinct if $n_1 \cdot n_2 \gg \lambda^2$.

2.3 Wilson lines

In this section we review some of the properties of Wilson lines that will be used later in this chapter. We start with the definition of Wilson lines in non-Abelian theories.

$$W^R(x_{fin}, x_{init}) = \mathbb{P} \exp\left(ig \int_c dx^\mu A^R_\mu(x)\right), \tag{2.20}$$

where the integration dx^μ is along the contour $c(x_{fin}, x_{init})$, R is the representation of the gluon field, and $\mathbb{P}$ the path ordering operator. We may parametrize the integral with the parameter s that runs over the integration contour and each point on the contour corresponds to unique value of s

$$W^R(x_{fin}, x_{init}) = \mathbb{P} \exp\left(ig \int_{s_{init}}^{s_{fin}} ds \frac{dx^\mu}{ds} A^R_\mu(x(s))\right). \tag{2.21}$$

If the integration contour is a straight line in the collinear direction $\bar{n}^\mu$ and we parametrize coordinates as $x^\mu = \bar{n}^\mu s$ thus $dx^\mu/ds = \bar{n}^\mu$ such that

$$W(x) \equiv W(x, -\infty) = \mathbb{P} \exp\left(ig \int_{-\infty}^{x} ds A^-(x(s)) \right), \tag{2.22}$$

where we removed the representation index for simplicity. We can show that the Wilson line satisfies the following differential equation[2]

$$\begin{aligned} -i\frac{d}{ds} W(s) &= A^-(x(s)) W(s) \\ \left(-i\frac{dx^\mu}{ds}\partial_\mu - A^-(x(s)) \right) W(s(x)) &= 0 \\ D^- W(s(x)) &= 0. \end{aligned} \tag{2.23}$$

Replacing the generic gluon field A^μ with the collinear gluon field A_n^μ and expanding in the SCET power counting parameter, the above relation becomes

$$iD_n^- W_n(s(x)) = 0 \quad \text{where} \quad W(s)_n \equiv W_n(s, -\infty) = \mathbb{P} \exp\left(ig \int_{-\infty}^{s} ds A_n^-(x(s)) \right), \tag{2.24}$$

where the Wilson line $W_n(x)$ can be also written in the following form using the label momentum operator

$$W_n(x) = \sum_{perm.} \exp\left(-\frac{g}{\bar{\mathcal{P}}} A_n^-(x) \right), \tag{2.25}$$

and the sum over all permutations is a result of path ordering operator. Using Eq.(2.24) we can show that the action of $iD_n^- W_n$ on an arbitrary operator $\mathcal{O}$ is

$$\begin{aligned} iD_n^-(W_n \mathcal{O}) &= (\bar{\mathcal{P}} + g A_n^-) W_n \mathcal{O} \\ &= (iD_n^- W_n)\mathcal{O} + W_n \bar{\mathcal{P}} \mathcal{O} \\ &= W_n \bar{\mathcal{P}} \mathcal{O}. \end{aligned} \tag{2.26}$$

[2] It should be noted that this equation is analogous to the differential equation satisfied by the time evolution operator in the Hamiltonian formalism with the transformation: $\mathbb{P} \to \mathbb{T}$, $s \to t$, and $H_I^{int}(t) \to -A_\mu^-(x(s))$.

Then, Eq.(2.26) along with the unitarity condition $W_n W_n^\dagger = 1$, gives $(iD_n^-)^{-1} = W_n^\dagger(\bar{\mathcal{P}})^{-1}W_n$ which allows us to rewrite the Lagrangian for the SCET quark field in Eq.(2.17):

$$\mathcal{L}_{n\xi} = \bar{\xi}_n \left(iD^+ - i\not{D}_{n,\perp} W_n^\dagger \frac{1}{\bar{\mathcal{P}}} W_n \not{D}_{n,\perp} \right) \frac{\gamma^-}{2} \xi_n. \tag{2.27}$$

2.4 Gauge Invariance and operators in SCET

Gauge transformations in SCET are defined in a similar way as in QCD and other non-Abelian gauge theories. Since we now have two distinct gauge fields, the collinear and ultra-soft gluons, a gauge transformation on those fields should respect their scaling, i.e., collinear gluons remain collinear after the transformation (and the same holds for soft gluons). We can achive that by separating collinear and soft gauge transformation such that $\partial_\mu U_{n/s} \sim p^\mu_{n/s} U_{n/s}$ where $U_{n/s}$ is the gauge transformation and $p^\mu_{n/s}$ the corresponding momentum scaling. Additionally, the soft gluons due to their large wavelength are seen as a background field from the collinear radiation. Therefore the collinear gauge transformations do not change the soft gluon fields and the soft gauge transformation is directly analogous to the traditional QCD gauge transformation.

In Table 2.1 the soft covariant derivative is given by

$$iD_s^\mu = \frac{n^\mu}{2}\bar{\mathcal{P}}^\mu + \mathcal{P}_\perp^\mu + i\frac{\bar{n}^\mu}{2}\left(\partial^+ - igA_s^+(x)\right). \tag{2.28}$$

For the collinear gauge transformations of the corresponding Wilson lines in the last entry of Table 2.1 we used the fact that under gauge transformations the Wilson line transforms as $W(x,y) \to U(x)W(x,y)U^\dagger(y)$ and since in the particular case $y \to -\infty$, by convention $U(-\infty) = 1$, so W_n only tranforms on the left. The soft gauge transformation is a direct result of applying the gluon field transformation to Wilson lines in Eq.(2.25).

Table 2.1: The collinear and soft gauge transformations of the SCET fields

SCET fields	Collinear Gauge Trnas.	Soft Gauge Trans.
$\xi_n(x)$	$U_n(x)\xi_n(x)$	$U_s(x)\xi_n(x)$
$A_n^\mu(x)$	$U_n(x)(A_n^\mu(x) + i/gD_s^\mu)U_n^\dagger(x)$	$U_s(x)A_n^\mu(x)U_s^\dagger(x)$
$A_s^\mu(x)$	$A_s^\mu(x)$	$U_s(x)(A_s^\mu(x) + i/g\partial^\mu)U_s^\dagger(x)$
$W_n(x)$	$U_n(x)W_n(x)$	$U_s(x)W_n(x)U_s^\dagger(x)$

We note that the combination $(\bar{\xi}_{n_1}W_{n_1})\gamma^\mu(W_{n_2}^\dagger\xi_{n_2})$ is gauge invariant in contrast to $\bar{\xi}_{n_1}\gamma^\mu\xi_{n_2}$ which at leading order matches onto the dijet QCD current $J^\mu_{\rm QCD} = \bar{\psi}\gamma^\mu\psi$. Indeed higher order matching reveals that the complete set of SCET operators needed to match onto the QCD current are given in the gauge invariant combination. Also we note that the combination $\chi_n \equiv W_n\xi_n$ is independently gauge invariant. For this reason we use the fields χ_n as one of the fundamental building blocks for gauge invariant operators in SCET. For the example of dijet events, the QCD current is matched onto $J^\mu_{\rm SCET} = \bar{\chi}_{n_1}\gamma^\mu\chi_{n_2}$ and the operator χ_n is also known as the quark jet field. Using similar gauge invariance arguments and polarization considerations we derive the gluon jet field

$$\mathcal{B}_n^\perp = \frac{1}{g}W_n^\dagger(\mathcal{P}_\perp + A_n^\perp)W_n. \tag{2.29}$$

It should be noted that we can constrain the SCET Lagrangian using gauge invariance and dimensionality constraints. Although, an additional operator that is not present in the Lagrangian derived in Eq.(2.27) is also allowed by gauge invariance, it can be shown that this term can be eliminated using an additional symmetry of SCET, namely, reparameterization invariance (RPI) [64]. RPI is the remaining Lorentz invariance of the full QCD and describes the freedom we have in the choice of the collinear directions n and $\bar{n}$ such that collinear radiation has the same scaling.

2.5 Factorization in SCET

SCET is a powerful tool for the study of jet cross sections where we usually consider only collinear and ultra-soft (or soft) final state radiation. This is usually done through factorization theorems that are proven within the framework of SCET and hold up to $\mathcal{O}(\lambda)$ corrections. A typical factorization theorem involves the hard function, that describes the hard interaction of energetic partons, the soft function, which encapsulates all the interjet cross-talk and the soft out of jet radiation, and the jet function which includes the collinear radiation within a jet. Usually those terms are universal, meaning that can be used in a variety of processes.

The proof of any factorization theorem in SCET initiates with the BPS field redefinition that allows us to decouple, at the level of the Lagrangian, collinear and soft modes. It should be mentioned that the the BPS redefinition decouples soft and collinear modes only at the leading order part of the Lagrangian that we are considering here. Higher order operators in the Lagrangian involve interactions that couple these modes but since in the work presented here we always consider $\lambda \ll 1$, we may ignore such contributions. Necessary for the BPS field redefinition is the definition of the soft Wilson line in the adjoint representation which is defined as

$$Y_n(x) = \mathbb{P} \exp\left(ig \int_{-\infty}^{0} A_s^+(x + ns) \right). \tag{2.30}$$

Similar to the collinear Wilson line, $W_n(x)$, the soft Wilson lines satisfy relations analogous to those in Eqs.(2.24) and (2.26), specifically:

$$iD_s^+ Y_n = 0, \quad Y_n Y_n^\dagger = 1, \quad \text{and} \quad Y_n^\dagger i D_s^+ [Y_n \mathcal{O}] = i\partial^+ \mathcal{O}, \tag{2.31}$$

here D_s^+ is + component of the soft covariant derivative defined in Eq.(2.28). Also since the soft Wilson line involves the soft gluon field that does not have any label momenta it commutes with the label momentum operator ($[Y_n, \mathcal{P}^\mu] = 0$). In terms

of $Y_n(x)$ the BPS field definition is defined as

$$\xi_n(x) = Y_n(x)\xi_n^{(0)}(x), \qquad A_n^\mu(x) = Y_n(x)A_n^{\mu(0)}(x)Y_n^\dagger(x), \tag{2.32}$$

which from Eq.(2.25) implies

$$W_n(x) = Y_n(x)W_n^{(0)}(x)Y_n^\dagger(x). \tag{2.33}$$

Applying this transformations in the Lagrangian $\mathcal{L}_{n\xi}^{(0)}$ and using the properties of the soft Wilson lines from Eq.(2.31) we find

$$\mathcal{L}_{n\xi} = \bar{\xi}_n^{(0)}\left(i\partial^+ + gA_n(x)^{(0)} - i\not{D}_{n,\perp}^{(0)}W_n^{\dagger(0)}\frac{1}{\bar{\mathcal{P}}}W_n^{(0)}\not{D}_{n,\perp}^{(0)}\right)\frac{\bar{\gamma}^-}{2}\xi_n^{(0)}. \tag{2.34}$$

where $iD_{n\perp}^{(0)} = \mathcal{P}_\perp + gA_{n\perp}^{(0)}(x)$. We note that the only fields appearing in the resulting Lagrangian are $\xi_n^{(0)}(x)$ and $A_n^{\mu(0)}(x)$, meaning the soft gluons are decoupled from the collinear fields at the level of the Lagrangian. It should be mentioned that using the BPS transformed fields as the fundamental fields, when performing calculations in perturbation theory, requires the transformation of the fields in SCET currents as well. For example in the case of the bilinear operator

$$J_{SCET} = \bar{\chi}_{n_1}\gamma^\mu\chi_{n_2} \xrightarrow[\text{BPS}]{} \bar{\chi}_{n_1}^{(0)}Y_{n_1}^\dagger\gamma^\mu Y_{n_2}\chi_{n_2}^{(0)}. \tag{2.35}$$

It is instructive to perform a schematic factorization of a generic process where some jet observable, denoted τ is measured. The differential cross section for this process is

$$\frac{d\sigma}{d\tau} \sim \sum_{X_{fin}}\int d\Pi_{X_{fin}}\ |\langle X_{fin}|\mathcal{O}_{QCD}|0\rangle|^2\ \ \delta(\tau - \tau_{X_{fin}})\ . \tag{2.36}$$

We start with the matching procedure from QCD onto SCET.

$$\mathcal{O}_{QCD} = \mathcal{C}_{\{i\}}\mathcal{O}_{SCET}^{\{i\}}, \tag{2.37}$$

where summation over the set of indices $\{i\}$ is implied. The Wilson matching coefficients $\mathcal{C}_i$ are evaluated in perturbation theory by demanding that both sides of the above equation give the same results for specific matrix elements. Applying this relation to the differential cross section we have

$$\frac{d\sigma}{d\tau} \sim \mathcal{C}_{\{i\}}\mathcal{C}^{\dagger}_{\{j\}} \sum_{X_{fin}} \int d\Pi_{X_{fin}} \langle 0|\mathcal{O}^{\{i\}}_{SCET}|X_{fin}\rangle\langle X_{fin}|\mathcal{O}^{\{j\}\dagger}_{SCET}|0\rangle \ \delta(\tau - \tau_{X_{fin}}). \quad (2.38)$$

Next we use the fact that soft and collinear modes are decoupled at the level of the Lagrangian, after performing the BPS field redefinition. This allow as to factorize the final Hilbert state to soft and collinear final states $|X_{fin}\rangle \to |X_s\rangle|X_n\rangle$. Also the contribution to the observable τ is separated into the contribution from the soft radiation and the collinear radiation inside the jet. Depending on the observable, the contribution from the soft modes may be neglected. For example, if the contribution from a jet constituent k to the observable scales as $\tau_k \sim p_k^+$ then both soft and collinear radiation should be included since $p^+_{coll} \sim p^+_{soft} \sim \lambda^2$. On the other hand, if $\tau_k \sim p_k^-$ then from power counting, only the collinear radiation is contributing to the observable. The SCET operator is next separated into collinear and soft fields such that $\mathcal{O}_{SCET} = \mathcal{O}_n\mathcal{O}_s$:

$$\begin{aligned}\frac{d\sigma}{d\tau} \sim \mathcal{C}_{\{i\}}\mathcal{C}^{\dagger}_{\{j\}} \sum_{X_n} \int d\Pi_{X_n} \langle 0|\mathcal{O}^{\{i\}}_{n}|X_n\rangle\langle X_n|\mathcal{O}^{\{j\}\dagger}_{n}|0\rangle \\ \times \sum_{X_s} \int d\Pi_{X_s} \langle 0|\mathcal{O}^{\{i\}}_{s}|X_s\rangle\langle X_s|\mathcal{O}^{\{j\}\dagger}_{s}|0\rangle \ \delta(\tau - \tau_{X_s} - \tau_{X_n}). \quad (2.39)\end{aligned}$$

To continue with the factorization theorem we introduce the measurement operator $\hat{\tau}$ defined such that when acting on a state in the Hilbert space, $\hat{\tau}$ returns the value of the observable that corresponds to that state (i.e. $\hat{\tau}|X\rangle = \tau_X|X\rangle$). The measurement operator can be defined through the use of the energy-momentum

tensor but the exact definition depends on the observable.

$$\frac{d\sigma}{d\tau} \sim \mathcal{C}_{\{i\}}\mathcal{C}^{\dagger}_{\{j\}} \int d\tau_s d\tau_n \sum_{X_n} \int d\Pi_{X_n} \langle 0|\mathcal{O}_n^{\{i\}}\delta(\tau_n - \hat{\tau})|X_n\rangle\langle X_n|\mathcal{O}_n^{\{j\}\dagger}|0\rangle$$
$$\times \sum_{X_s} \int d\Pi_{X_s} \langle 0|\mathcal{O}_s^{\{i\}}\delta(\tau_s - \hat{\tau})|X_s\rangle\langle X_s|\mathcal{O}_s^{\{j\}\dagger}|0\rangle \;\; \delta(\tau - \tau_s - \tau_n). \quad (2.40)$$

We complete the factorization with the definition of the jet, soft and hard functions

$$J(\tau_n)\mathcal{I}_{\{i,j\}} \equiv \sum_{X_n} \int d\Pi_{X_n} \langle 0|\mathcal{O}_n^{\{i\}}\delta(\tau_n - \hat{\tau})|X_n\rangle\langle X_n|\mathcal{O}_n^{\{j\}\dagger}|0\rangle \,, \quad (2.41)$$

$$S_{\{i,j\}}(\tau_s) \equiv \sum_{X_s} \int d\Pi_{X_s} \langle 0|\mathcal{O}_s^{\{i\}}\delta(\tau_s - \hat{\tau})|X_s\rangle\langle X_s|\mathcal{O}_n^{\{j\}\dagger}|0\rangle \,, \quad (2.42)$$

$$H_{\{i,j\}} \equiv \mathcal{C}_{\{i\}}\mathcal{C}^{\dagger}_{\{j\}}\mathcal{I}_{\{i,j\}} \,, \quad (2.43)$$

where $\mathcal{I}_{\{i,j\}}$ contains all the spinor and color structure of the collinear sector that usually factorizes from the observable dependent term. Finally the result for the factorized cross section is

$$\frac{d\sigma}{d\tau} \sim H_{\{i,j\}} \int d\tau' S_{\{i,j\}}(\tau') J(\tau - \tau') = H_{\{i,j\}} S_{\{i,j\}} \otimes J \,. \quad (2.44)$$

Eq.(2.44) is the major result of this chapter. It demonstrates how for processes described by SCET one may perform a factorization of the cross section into collinear, soft and hard sector. The advantage of this approach is that allows us to evaluate each term separately and establish renormalization group equations for each term that we can use in order to resum large logarithmic enhancements to all orders in perturbation theory.

In multijet events the collinear part from Eq.(2.41) is further factorized in multiple jet functions since the various collinear sectors in the SCET Lagrangian are decoupled. Ref. [65] establishes an elegant formalism for developing factorization

theorems for $n-$jet cross sections in e^+e^- annihilation with multiple collinear sectors when those sectors are widely separated. Examples and applications for cases with up to four collinear functions will be discussed in the following chapters.

3

Analytic and Monte Carlo Studies of Jets with Heavy Mesons and Quarkonia

3.1 Outline

In this chapter we calculate cross sections for e^+e^- to jets, where one of the jets contains a hadron with either open or hidden heavy flavor. In particular, we will derive factorization theorems and perform analytical Next-to-Leading-Log prime (NLL') resummation[1] for these cross sections using renormalization group (RG) techniques. We will also compare our results with monte carlo simulations of the same cross sections.

Recently, there has been considerable interest in cross sections of this type [55,67–75]. Ref. [55] demonstrated that the cross section for producing a jet with an identified hadron can be determined using a distribution function called the fragmenting jet function (FJF). FJFs are in turn related to the more commonly studied fragmentation functions (FFs) by a matching calculation at the jet energy scale. This implies that cross sections for jets with an identified hadron provide a new arena to mea-

[1] NLL' includes NLL resummation for each function in the factorization theorem, where all functions are computed to NLO [66].

sure FFs, which are more commonly extracted from the semi-inclusive cross section $e^+e^- \to H + X$. Especially important is that this provides an opportunity to extract gluon FFs [74, 75], since quark FFs are more readily studied in $e^+e^- \to H + X$. In addition, it was recently shown in Ref. [73] that since the FFs for quarkonia production can be calculated in the Non-Relativistic Quantum Chromodynamics (NRQCD) factorization formalism [49], FJFs can be used to make novel tests of quarkonium production theory.

Part of section 3.2 and sections 3.3-3.5 of this chapter appeared first in Ref. [56] and section 3.6 is taken from Ref. [76].

3.2 Definition of fragmenting jet functions

The FJF was first introduced in Ref. [55] however here we give an alternative derivation constructed from measured jet functions for generic jet observable τ. It is shown in Ref. [65] that the cross-section for the production of two jets in electron-positron annihilation can be written as,

$$\frac{d\sigma}{d\tau} = d\sigma^{(0)} H_2(\mu) \times S_\Lambda(\mu) \times J^{\bar{q}}_{\bar{n}}(\omega, \mu) \times S_{meas}(\tau, \mu) \otimes J^q_n(\tau, \omega, \mu)\,, \tag{3.1}$$

where $d\sigma^{(0)}$ is the Born cross section, $H_2(\mu)$ is the hard function resulting from matching a 2-jet operator in full QCD onto the corresponding SCET operators, $S_\Lambda(\mu)$ is the soft function describes the cross-talk between the jets and the soft out-of-jet radiation is constrained via $E_{\rm out} < \Lambda$. The measured soft and jet functions $S_{meas}(\tau, \mu)$ and $J_n(\tau, \omega, \mu)$ respectively describe the contribution from the soft and collinear radiation to the jet observable τ, and $J_n(\omega, \mu)$ is an unmeasured jet function that describes collinear radiation within a jet in the $\hat{n}$ direction that has energy

$E_J = \omega/2$ (here $\omega = E_{\rm cm}$). The measured jet function is defined in SCET as

$$J_n^q(\tau) = \int \frac{dk^+}{2\pi} \int d^4x \ \exp(ik^+x^-/2) \frac{1}{N_C} \mathrm{Tr}\left[\frac{\bar{n}\!\!\!/}{2} \langle 0|\delta_{\omega,\overline{\mathcal{P}}}\ \delta_{0,\mathcal{P}_\perp} \chi_n(x) \delta(\tau - \hat{\tau}) \bar{\chi}_n(0)|0\rangle\right]. \tag{3.2}$$

where we omitted the jet energy ω and the renormalization scale dependence from the argument of the jet function for simplicity of notation. To study jets with identified hadrons, we insert the following expression for the identity

$$\mathbf{1} = \sum_X |X\rangle\langle X| = \sum_X \sum_{h\in\mathcal{H}_i} \int \frac{dz d^2p_h^\perp}{2(2\pi)^3} |Xh(z,\mathbf{p}_\perp^h)\rangle\langle Xh(z,p_h^\perp h)| \tag{3.3}$$

$$\begin{aligned} J_n^q(\tau) = &\sum_{h\in\mathcal{H}_i} \int \frac{dz d^2p_h^\perp}{2(2\pi)^3} \int \frac{dk^+}{2\pi} \int d^4x \ \exp(ik^+x^-/2) \frac{1}{N_C} \\ &\times \sum_X \mathrm{Tr}\Big[\frac{\bar{n}\!\!\!/}{2} \langle 0|\delta_{\omega,\overline{\mathcal{P}}}\ \delta_{0,\mathcal{P}_\perp} \chi_n(x) \delta(\tau - \hat{\tau}) |Xh(z,p_h^\perp)\rangle\langle Xh(z,p_h^\perp)| \bar{\chi}_n(0)|0\rangle\Big]. \end{aligned} \tag{3.4}$$

where h is an identified hadron within the jet. We may rewrite the above equation in the following form

$$J_n^q(\tau) = \sum_{h\in\mathcal{H}_i} \int \frac{z\ dz}{2(2\pi)^3} \mathcal{G}_{i/h}(\tau, z), \tag{3.5}$$

where

$$\begin{aligned} \mathcal{G}_{i/h}(\tau,z) \equiv &\frac{1}{z} \int d^2p_h^\perp \int \frac{dk^+}{2\pi} \int d^4x \ \exp(ik^+x^-/2) \frac{1}{N_C} \\ &\times \sum_X \mathrm{Tr}\Big[\frac{\bar{n}\!\!\!/}{2} \langle 0|\delta_{\omega,\overline{\mathcal{P}}}\ \delta_{0,\mathcal{P}_\perp} \chi_n(x) \delta(\tau - \hat{\tau}) |Xh(z,p_h^\perp)\rangle\langle Xh(z,p_h^\perp)| \bar{\chi}_n(0)|0\rangle\Big], \end{aligned} \tag{3.6}$$

is the operator definition of the fragmenting jet function (FJF). Inserting this back to Eq.(C.1) we have

$$\frac{d\sigma}{d\tau} = \sum_{h\in\mathcal{H}_i} \int z dz\ d\sigma^{(0)} H_2(\mu) \times S_\Lambda(\mu) \times J_{\bar{n}}^{\bar{q}}(\omega,\mu) \times S_{meas}(\tau,\mu) \otimes \frac{\mathcal{G}_{q/h}(\tau,z,\mu)}{2(2\pi)^3}. \tag{3.7}$$

which directly implies

$$\frac{d\sigma^{i/h}}{d\tau dz} = d\sigma^{(0)} H_2(\mu) \times S_\Lambda(\mu) \times J^{\bar{q}}_{\bar{n}}(\omega, \mu) \times S_{meas}(\tau, \mu) \otimes \frac{\mathcal{G}_{q/h}(\tau, z, \mu)}{2(2\pi)^3} \,. \tag{3.8}$$

This suggests a rather powerful rule: a factorization theorem for a jet with an identified hadron, H, is obtained from the factorization theorem for a jet cross section by the replacement

$$J_i(\tau, \mu) \to \frac{1}{2(2\pi)^3} \mathcal{G}_i^H(\tau, z, \mu) dz, \tag{3.9}$$

where $J_i(\tau, \mu)$ is the measured jet function initiated by parton i, and the renormalization scale is μ. The FJF, denoted $\mathcal{G}_i^H(\tau, z, \mu)$, additionally depends on the fraction z of the jet energy that is carried by the identified hadron. These functions implicitly depend on the jet clustering algorithm and cone size R used to define the jets. It is also possible to define jet functions and FJFs that depend on the total energy of the jet rather than the invariant mass [70].

For $\tau = s$, with s the jet invariant mass, FJFs are related to the well-known FFs, $D_i^H(z, \mu)$, through operator product expansion by the formulae

$$\mathcal{G}_i^H(s, z, \mu) = \sum_j \int_z^1 \frac{dz'}{z'} \mathcal{J}_{ij}(s, z', \mu) D_j^H(z/z', \mu) + \mathcal{O}\left(\Lambda^2_{\rm QCD}/s\right) \,, \tag{3.10}$$

where the coefficients $\mathcal{J}_{ij}(s, z, \mu)$ are perturbatively calculable matching coefficients whose large logs are minimized at the jet scale, s, and are calculated to NLO in Ref. [68]. For heavy quarks the $\mathcal{J}_{ij}(s, z, \mu)$ have been calculated to $O(\alpha_s^2)$ in Ref. [72]. From properties of FFs these matching coefficients obey the sum rule

$$J_i(s, \mu) = \frac{1}{2(2\pi)^3} \sum_j \int_0^1 dz z \mathcal{J}_{ij}(s, z, \mu) \,. \tag{3.11}$$

The properties of FJFs were further studied in Refs. [67–71]. These papers focused on the FJFs for light hadrons such as pions. FJFs for particles with a single

heavy quark were studied in Ref. [72] and FJFs for quarkonia were calculated in Ref. [73].

One important goal of this work is to generalize FJFs to jets in which the angularity is measured. The angularity, denoted τ_a, is defined as [77]

$$\tau_a = \frac{1}{\omega}\sum_i (p_i^+)^{1-a/2}(p_i^-)^{a/2}\,, \tag{3.12}$$

where the sum is over all the particles in the jet, and $\omega = \sum_i p_i^-$ is the large lightlike momentum of the jet. The angularity should be viewed as a generalization of the invariant mass squared of the jet since $s = \omega^2\tau_0$. We calculate the matching coefficients appropriate for jets in which the angularity has been measured, denoted $\mathcal{J}_{ij}(\tau_a, z, \mu)$, and verify the $s \to \tau_a$ generalization of the sum rules in Eq. (3.11) in Appendix B.

3.3 Fragmenting Jet Functions with Angularities

In this section we extend the calculation of Ref. [68] to FJFs with measured angularities. We will follow the terminology of Ref. [65], in which a jet whose angularity is measured is referred to as a "measured" jet, while a jet for whom only the total energy is measured but the angularity is not is called an "unmeasured" jet. Here we consider the case of two particles as this is the most that will appear in a one-loop calculation. In Ref. [68] the measurement operator in the definition of FJFs forces the mass squared of the jet to be s. The measurement operator takes the form

$$\delta(\omega(k^+ - l^+ - p^+)) = \delta(s - \omega(l^+ + p^+)), \tag{3.13}$$

where k^μ is the parent parton's momentum and l^μ and p^μ are the momenta of the partons carrying large lightcone components $l^- = (1-z)k^-$ and $p^- = zk^-$ of the parent's momentum, respectively. The operator definition of the FJF with measured

angularities is given by Eq.(3.6) where at $\mathcal{O}(\alpha_s)$ the operator $\hat{\tau}_a$ takes the form (cf. Eq. (3.12))

$$\delta(\tau_a - ((l^+)^{1-a/2}(l^-)^{a/2} - (p^+)^{1-a/2}(p^-)^{a/2})/\omega)\,. \tag{3.14}$$

Other than replacing Eq. (3.13) with Eq. (3.14), the integrals of all diagrams are the same as in Ref. [68]. However, rather than using the δ-regulator and a gluon mass, we will use pure dimensional regularization to regulate all divergences. In this limit, it is possible to show that the one-loop evaluation of the FF yields

$$D_{i\to j}(z) = \delta_{ij}\delta(1-z) + T_{ij}\frac{\alpha_s}{2\pi}P_{ij}(z)\left(\frac{1}{\epsilon_{UV}} - \frac{1}{\epsilon_{IR}}\right), \tag{3.15}$$

where T_{ij} are the color structures, $T_{qq} = C_F,\ T_{gg} = C_A,\ T_{qg} = C_F,\ T_{gq} = T_R$. Additionally, we have verified that the same $1/\epsilon_{IR}$ poles appear in the calculation of FJFs and appropriately cancel in the matching between the FJFs and FFs for all values of $a < 1$. This justifies the formula

$$\mathcal{G}_i^h(\tau_a, z, \mu) = \sum_j \int_z^1 \frac{dx}{x}\, \mathcal{J}_{ij}(\tau_a, x, \mu) D_{j\to h}\left(\frac{z}{x}, \mu\right), \tag{3.16}$$

which is the analog of Eq. (3.9) for FJFs that depend on the angularities.

Since the matching coefficients $\mathcal{J}_{ij}(\tau_a, z, \mu)$ are free of IR divergences, we can simplify the matching calculation by using pure dimensional regularization, setting all scaleless integrals to zero and interpreting all $1/\epsilon$ poles as UV. A detailed calculation of the renormalized finite terms of $\mathcal{J}_{ij}(\tau_a, z, \mu)$ can be found in Appendix B, the results of which are shown below. We parametrize the matching coefficients $\mathcal{J}_{ij}(\tau_a, z, \mu)$ as

$$\begin{aligned}\frac{\mathcal{J}_{ij}(\tau_a, z, \mu)}{2(2\pi)^3} &= \delta_{ij}\delta(1-z)\delta(\tau_a) \\ &\quad + T_{ij}\frac{\alpha_s}{2\pi}\Big[c_0^{ij}(z,\mu)\delta(\tau_a) + c_1^{ij}(z,\mu)\left(\frac{1}{\tau_a}\right)_+ + c_2\delta_{ij}\delta(1-z)\left(\frac{\ln\tau_a}{\tau_a}\right)_+\Big],\end{aligned} \tag{3.17}$$

where

$$
\begin{aligned}
c_0^{ij}(z,\mu) &= \frac{1-a/2}{1-a}\delta_{ij}\delta(1-z)\Big[\ln^2\frac{\mu^2}{\omega^2} - \frac{\pi^2}{6}\Big] + c^{ij}(z) \\
&\quad - \bar{P}_{ji}\left[\ln\frac{\mu^2}{\omega^2} + \frac{1}{1-a/2}\ln\left(1+\left(\frac{1-z}{z}\right)^{1-a}\right) + (\delta_{ij}-1)\frac{1-a}{1-a/2}\ln(1-z)\right], \\
c_1^{ij}(z,\mu) &= -\frac{2}{1-a}\delta_{ij}\delta(1-z)\ln\frac{\mu^2}{\omega^2} + \frac{1-a}{1-a/2}\bar{P}_{ij}\,, \\
c_2 &= \frac{2}{(1-a)(1-a/2)}\,,
\end{aligned}
\tag{3.18}
$$

with

$$
\begin{aligned}
c^{qq}(z) &= 1 - z + \frac{1-a}{1-a/2}(1+z^2)\left(\frac{\ln(1-z)}{1-z}\right)_+\,, \\
c^{gg}(z) &= \frac{1-a}{1-a/2}\frac{2(1-z+z^2)^2}{z}\left(\frac{\ln(1-z)}{1-z}\right)_+\,, \\
c^{qg}(z) &= z\,, \\
c^{gq}(z) &= 2z(1-z)\,,
\end{aligned}
\tag{3.19}
$$

and where the $\bar{P}_{ij}$ are the splitting functions of Ref. [68] except for the case $i = j = q$,

$$
\begin{aligned}
\bar{P}_{qq} &= P_{qq} - \frac{3}{2}\delta(1-z) = \frac{1+z^2}{(1-z)_+}\,, \\
\bar{P}_{gg} &= P_{gg} = 2\frac{(1-x+x^2)^2}{x(1-x)_+}\,, \\
\bar{P}_{qg} &= P_{qg} = x^2 + (1-x)^2\,, \\
\bar{P}_{gq} &= P_{gq} = \frac{1+(1-x)^2}{x}\,.
\end{aligned}
\tag{3.20}
$$

Notice that our results for the matching coefficients $\mathcal{J}_{ij}(\tau_a, z, \mu)$ are independent of the jet algorithm and the jet size parameter R. To include modifications of the $\mathcal{J}_{ij}(\tau_a, z, \mu)$ that come from these effects, one would have to multiply the measurement operator in Eq. (3.14) by an additional Θ-function that imposes the phase

space constraints required by the jet algorithm. However, for jets with measured angularities, it was shown in Ref. [65] that jet-algorithm dependent terms for cone and k_T-type algorithms are suppressed by powers of τ_a/R^2. Inuitively, this is because as $\tau_a \to 0$ all the particles in the jet lie along the jet axis so the result must be insensitive to which algorithm is used and to the value of R in this limit. For the values of τ_a and R considered here, τ_a/R^2 is negligible and we will drop these corrections.

As a non-trivial check of our results we show in Appendix B that our $\mathcal{J}_{ij}(\tau_a, z, \mu)$ satisfy the following identities and sum rules,

$$\lim_{a\to 0} \mathcal{J}_{ij}(\tau_a, z, \mu) = \omega^2 \mathcal{J}_{ij}(s, z, \mu)\,, \tag{3.21}$$

and

$$J_i(\tau_a, \mu) = \frac{1}{2(2\pi)^3} \sum_j \int_0^1 dz\; z\; \mathcal{J}_{ij}(\tau_a, z, \mu)\,, \tag{3.22}$$

where $\mathcal{J}_{ij}(s, z, \mu)$ are the matching coefficients for measured jet invariant mass found in Ref. [68] and $J_i(\tau_a, \mu)$ are the jet functions for measured jets that can be found in Ref. [65].

3.4 $e^+e^- \to 2$ Jets with a B Meson

In this section we present an analytic calculation of the cross section for e^+e^- to two b jets in which the B meson is identified in a measured jet. Following the analysis of Ref. [65], the factorization theorem for the cross section for one measured b jet and one unmeasured $\bar{b}$ jet is

$$\frac{1}{\sigma_0}\frac{d\sigma}{d\tau_a} = H_2(\mu) \times S^{\rm unmeas}(\mu) \times J_{\bar{n}}^{(\bar{b})}(\mu) \times \Big[S^{\rm meas}(\tau_a, \mu) \otimes J_n^{(b)}(\tau_a, \mu)\Big], \tag{3.23}$$

where $H_2(\mu)$ is the hard function, $S^{\rm unmeas}(\mu)$ and $S^{\rm meas}(\tau_a, \mu)$ are the unmeasured and measured soft functions, $J_{\bar{n}}^{(\bar{b})}(\mu)$ is the unmeasured jet function containing the $\bar{b}$ quark

and $J_n^{(b)}(\tau_a, \mu)$ is the measured jet function containing the b quark. These describe the short-distance process, surrounding soft radiation, and radiation collinear to unmeasured and measured jets, respectively. At NLO the τ_a-independent functions are given by

$$\begin{aligned} H_2(\mu) &= 1 - \frac{\alpha_s(\mu) C_F}{2\pi} \left[8 - \frac{7\pi^2}{6} + \ln^2 \frac{\mu^2}{\omega^2} + 3 \ln \frac{\mu^2}{\omega^2} \right], \\ S^{\text{unmeas}}(\mu) &= 1 + \frac{\alpha_s(\mu) C_F}{2\pi} \left[\ln^2 \frac{\mu^2}{4\Lambda^2} - \ln^2 \frac{\mu^2}{4\Lambda^2 r^2} - \frac{\pi^2}{3} \right], \\ J_{\bar{n}}^{(\bar{b})}(\mu) &= 1 + \frac{\alpha_s(\mu) C_F}{2\pi} J_{\text{alg}}^q(\mu), \end{aligned} \tag{3.24}$$

where Λ is a veto on out-of-jet energy, $r = \tan(R/2)$ and $J_{\text{alg}}^q(\mu)$ is a function that depends on the algorithm used (and we will use the cone algorithm below) and is given in Eq. (A.18) of Ref. [65]. We note that unlike measured jets, algorithm dependent contributions to the unmeasured jet are not power suppressed. We also note that, beginning at $\mathcal{O}(\alpha^2)$, non-global logarithms of the ratio $Q\tau_a/(2\Lambda r^2)$ begin to appear in the cross-section [5]. For the values of the parameters we consider, these ratios are such that we can treat these logarithms as $\mathcal{O}(1)$ and thus these would enter as fixed order corrections needed at NNLL' accuracy, which is beyond the scope of this work.

We suppress the dependence of all these functions on scales other than the renormalization scale μ. Measured functions are convolved according to

$$f(\tau) \otimes g(\tau) = \int d\tau' \, f(\tau - \tau') g(\tau'). \tag{3.25}$$

To calculate the differential cross section for a measured jet with an identified B hadron, we apply the analogous replacement rule in Eq. (3.9) to Eq. (3.23) and use

the expression for the FJF in Eq. (3.16) to obtain

$$\frac{1}{\sigma_0}\frac{d\sigma^{(b)}}{d\tau_a dz} = H_2(\mu)\times S^{\text{unmeas}}(\mu)\times J_{\bar{n}}^{(\bar{b})}(\mu)$$
$$\times\sum_j\Big[\Big(S^{\text{meas}}(\tau_a,\mu)\otimes\frac{\mathcal{J}_{bj}^{(b)}(\tau_a,z,\mu)}{2(2\pi)^3}\Big)\bullet D_{j\to B}(z)\Big], \quad (3.26)$$

where

$$G(z)\bullet F(z) = F(z)\bullet G(z)\equiv\int_z^1\frac{dx}{x}F(x)G\Big(\frac{z}{x}\Big). \quad (3.27)$$

To obtain an NLL' resummed formula for the cross section, we evaluate each function in the factorization theorem in Eq. (3.26) at its "characteristic" scale (where potentially large logarithms are minimized) and, using renormalization group techniques, evolve each function to a common scale, μ, which we will choose to be equal to the hard scale. The details of this evolution are discussed in Appendix A.

The convolutions in Eq. (3.26) must be performed over angularity over S^{meas}, $\mathcal{J}_{ij}$, and factors arising from RG equations. Since such RG factors are distributions (δ or plus-distributions) in the angularity our final answer is written in terms of distributions that can be computed analytically using Eqs. (A.21-A.22). Upon performing convolutions and resummation to NLL' accuracy we find for the cross section

$$d\sigma(\tau_a,z)\equiv\frac{1}{\sigma_0}\frac{d\sigma^{(b)}}{d\tau_a dz} = H_2(\mu_H)\times S^{\text{unmeas}}(\mu_\Lambda)\times J_{\bar{n}}^{(\bar{b})}(\mu_{J_{\bar{n}}})\times \quad (3.28)$$
$$\times\sum_j\Bigg\{\left(\frac{\Theta(\tau_a)}{\tau_a^{1+\Omega}}\right)\Big[\delta_{bj}\delta(1-z)\,(1+f_S(\tau_a,\mu_{S^{\text{meas}}}))+f_{\mathcal{J}}^{bj}(\tau_a,z,\mu_{J_n})\Big]\bullet\frac{D_{j\to B}(z,\mu_{J_n})}{2(2\pi)^3}$$
$$\times\,\Pi(\mu,\mu_H,\mu_\Lambda,\mu_{J_{\bar{n}}},\mu_{J_n},\mu_{S^{\text{meas}}})\Bigg\}_+,$$

where the '+' distribution is defined in Eq. (A.18) (and acts on all τ_a-dependent quantities, including any implicit dependencies arising from the choice of scales μ_F)

and $\Omega(\mu_{J_n}, \mu_{S^{\rm meas}}) = \omega_{J_n}(\mu, \mu_{J_n}) + \omega_{S^{\rm meas}}(\mu, \mu_{S^{\rm meas}})$, the functions ω_{J_n} and $\omega_{S^{\rm meas}}$ are given in Appendix A, the function f_S is given by [65]

$$f_S(\tau,\mu) = -\frac{\alpha_s(\mu) C_F}{\pi} \frac{1}{1-a} \left\{ \left[\ln \frac{\mu \tan^{1-a} \frac{R}{2}}{\omega \tau} + H(-1-\Omega) \right]^2 + \frac{\pi^2}{6} - \psi^{(1)}(-\Omega) \right\}, \tag{3.29}$$

and $f_{\mathcal{J}}^{ij}$ are written in terms of the coefficients c_0^{ij}, c_1^{ij} and c_2 presented in Eq. (3.18) as

$$\begin{aligned} f_{\mathcal{J}}^{ij}(\tau,z,\mu) = T_{ij} \frac{\alpha_s(\mu)}{2\pi} \Bigg(& c_0^{ij}(z,\mu) + c_1^{ij}(z,\mu) \Big(\ln \tau - H(-1-\Omega) \Big) \\ & + c_2 \delta_{ij} \delta(1-z) \Big(\frac{(\ln \tau - H(-1-\Omega))^2 + \pi^2/6 - \psi^{(1)}(-\Omega)}{2} \Big) \Bigg). \end{aligned} \tag{3.30}$$

The evolution kernel Π is given in terms of $K_F(\mu,\mu_0)$ and $\omega_F(\mu,\mu_0)$ (cf. Appendix A),

$$\begin{aligned} \Pi(\mu, \mu_H, \mu_\Lambda, \mu_{J_{\bar{n}}}, \mu_{J_n}, \mu_{S^{\rm meas}}) = & \prod_{F=H,J_{\bar{n}},S^{\rm unmeas}} e^{K_F(\mu,\mu_F)} \left(\frac{\mu_F}{m_F} \right)^{\omega_F(\mu,\mu_F)} \\ & \times \frac{1}{\Gamma(-\Omega(\mu_{J_n}, \mu_{S^{\rm meas}}))} \times \prod_{F=J_n,S^{\rm meas}} e^{(K_F(\mu,\mu_F) + \gamma_E \omega_F(\mu,\mu_F))} \left(\frac{\mu_F}{m_F} \right)^{j_F \omega_F(\mu,\mu_i)}, \end{aligned} \tag{3.31}$$

where μ_F, m_F and j_F are given in Table 4.1. Because they involve FFs (cf. Appendix B), the z convolutions must be evaluated numerically. For the fragmentation of the b quark we use a two-parameter power model FF introduced in Ref. [78], in which $D_{b\to B}(z,\ \mu = m_b = 4.5\ \text{GeV})$ is proportional to $z^\alpha(1-z)^\beta$. Values for the parameters $\alpha = 16.87$ and $\beta = 2.628$ with $\chi^2_{d.o.f.} = 1.495$ were determined using a fit to LEP data in Ref. [79] for the inclusive process $e^+e^- \to B + X$. Errors in these parameters were not quoted in Ref. [79], so we cannot quantify errors associated with the extracted FF in our calculation. Additionally, we neglect the contribution from the fragmentation of other partons for our e^+e^- collider studies as in Ref. [79].

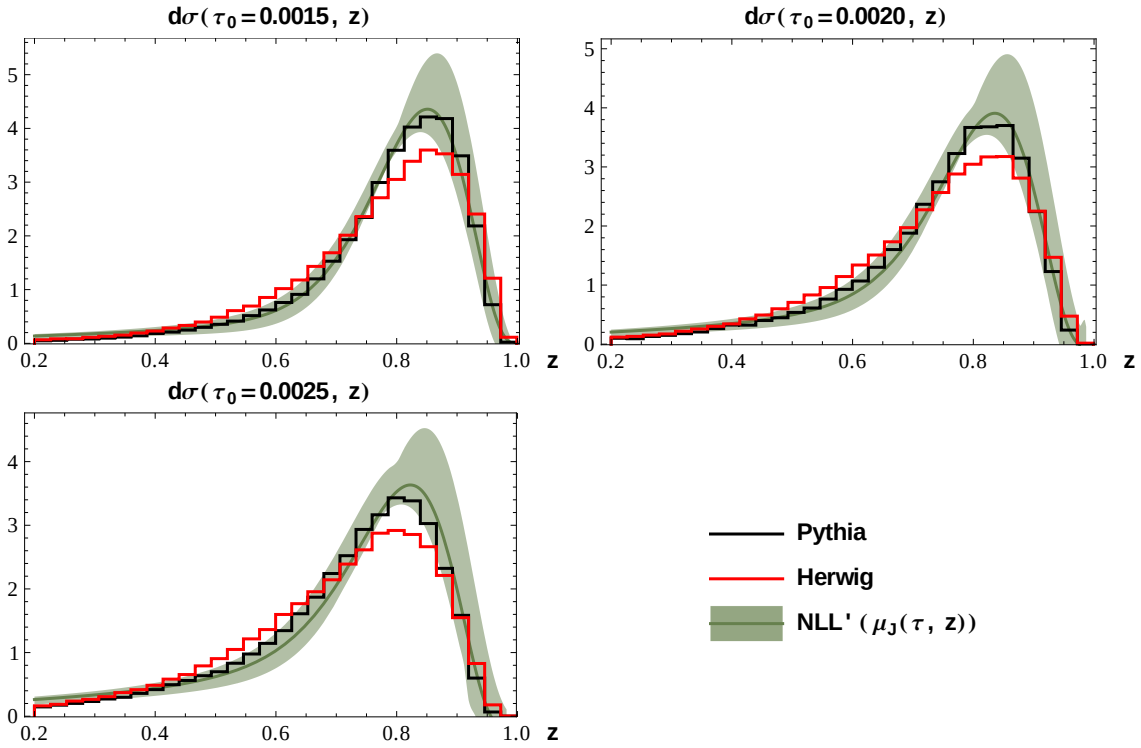

FIGURE 3.1: The z distributions for $d\sigma(\tau_0, z)$ at $\tau_0 = (1.5,\ 2.0,\ 2.5) \times 10^{-3}$ for analytic calculations with theoretical uncertainty are shown in green. Monte carlo simulations using Madgraph + PYTHIA and Madgraph + Herwig are shown in black and red, respectively.

In proton-proton collisions at the LHC, gluon FJFs must also be included since the dijet channel $gg \to gg$ gives a significant contribution to the production of jets with heavy flavor [75]. For the evolution of the FF up to the jet scale we solve the DGLAP equation using an inverse Mellin transformation as done in Ref. [73].

Fig. 3.1 shows the z distributions from $d\sigma(\tau_0, z)$ for $\tau_0 = (1.5,\ 2.0,\ 2.5) \times 10^{-3}$ of our analytic NLL' calculation (green) and monte-carlo simulations using Madgraph + PYTHIA (black) and Madgraph + HERWIG (red). For each monte carlo and for each NLL' calculation, the graphs are independently normalized to unit area. For plots with fixed τ_a we use a z-bin of ± 0.1 and for plots with fixed z we use a τ_a bin of size $\pm 2 \times 10^{-4}$. Jets are reconstructed in PYTHIA using the Seedless-Infared-Safe Cone (SISCONE) algorithm in the FastJets package [80] with $R = 0.6$, which will be

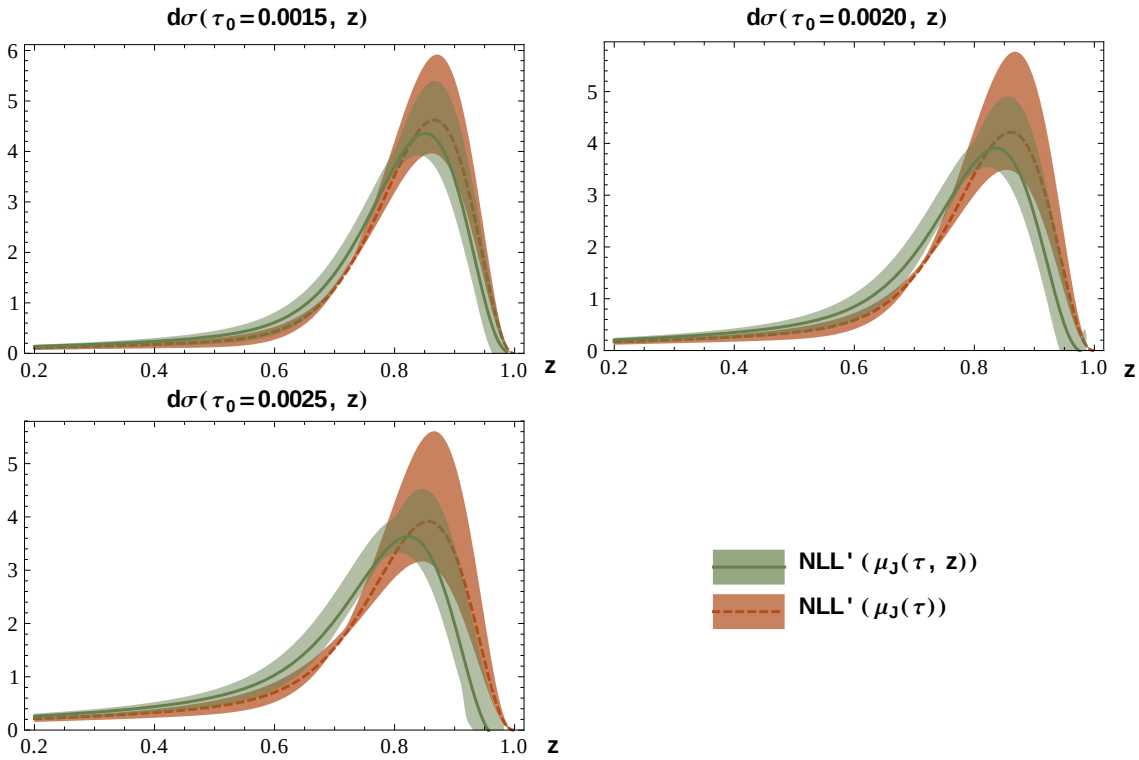

FIGURE 3.2: Analytic results for the z distributions of $d\sigma(\tau_0, z)$ at $\tau_0 = (1.5,\ 2.0,\ 2.5) \times 10^{-3}$. The orange curve is calculated with a measured jet scale that does not depend on z whereas the green curve uses a scale that does depend on z (as in Fig. 3.1).

used throughout this work. We produced simulated dijet events at $E_{cm} = 250$ GeV in which each jet has an energy of at least $(E_{cm} - \Lambda)/2$ where $\Lambda = 30$ GeV.[2] The central green line corresponds to the NLL' calculation with the various functions in the factorization theorem evaluated at their characteristic values shown in Table 4.1, and the green band corresponds to the estimate of theoretical uncertainty obtained by varying the scales of the unmeasured functions by $\pm 50\%$, and using profile functions [58, 81, 82] to estimate the uncertainty of the measured functions. Profile functions allow us to introduce an angularity dependent scale variation that freezes at the characteristic scale for high values of τ_a where the factorization theorem breaks down

[2] This is different than simply placing a cut Λ on energy outside the jets (which is what is assumed in our analytical results), but this difference only appears at $O(\alpha_s^2)$ in the soft function, which is higher order than we work here.

and at a fixed scale for small values of τ_a where we reach the non-perturbative regime. This method for estimating theoretical uncertainties is used throughout this work. Additional details on the profile functions we use can be found in Appendix A.

Table 3.1: Characteristic scales of the different functions in the factorization theorem of Eq. (3.23).

Function (F)	H_2	$J^{\bar{b}}_{\bar{n}}$	S^{unmeas}	$\mathcal{J}(\tau, z)$	$S^{\text{meas}}(\tau)$
Scale (μ_F)	E_{cm}	$\omega_{\bar{n}} r$	$2\Lambda r^{1/2}$	$\omega_n \tau^{1/(2-a)}(1-z)^{(1-a)/(2-a)}$	$\omega_n \tau / r^{1-a}$
m_F	ω	$w_{\bar{n}} r$	$2\Lambda r^{1/2}$	ω_n	ω_n / r^{1-a}
j_F	1	1	1	$2-a$	1

The orange curves in Fig. 3.2 show the differential cross section as a function of z for fixed τ_0 where $\mu_J(\tau) = \mu_J(\tau, z=0) = \omega\tau^{1/(2-a)}$ is chosen as the characteristic scale of the measured jet function, and the error band is obtained the same way as for Fig. 3.1. As in Fig. 3.1, the green curves show the cross section for a measured jet scale $\mu_J(\tau, z) = \omega\tau^{1/(2-a)}(1-z)^{(1-a)/(2-a)}$. The reorganization of logarithms of $(1-z)$ shown in Eq. (A.26) suggests that we can improve the accuracy of our calculations for $z \to 1$ by choosing the characteristic value of the measured jet scale to be $\mu_J(\tau, z)$. This improvement is clearly seen in Fig. 3.2 which shows the scale variation for the choices $\mu_J(\tau)$ and $\mu_J(\tau, z)$, the latter choice gives smaller scale variation near the peak in the z distribution.

In Fig. 3.3 we present the results for the τ_0 distributions of the differential cross section $d\sigma(\tau_a, z)$ for $z = 0.4,\ 0.6,$ and 0.8. The color and normalization schemes match those in Fig. 3.1. We see that for higher values of z the distributions of τ_0 are shifted towards smaller values. This is expected since the majority of the energy of the jet is carried by the B meson which results in narrower jets. Figs. 3.1 and 3.3 show that our results are consistent within the monte carlo uncertainty that is suggested by

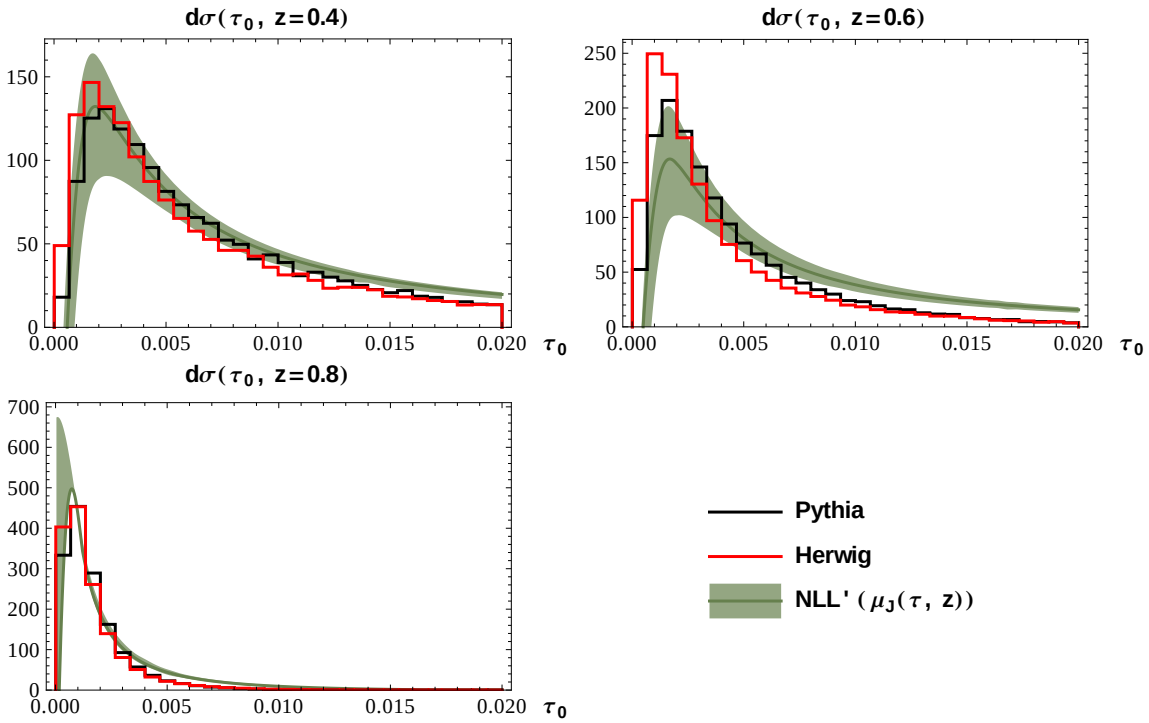

FIGURE 3.3: Angularity distributions of $d\sigma(\tau_a, z)$ for $a = 0$ at $z = 0.4,\ 0.6,\ 0.8$. Analytic results are shown as green bands. Monte carlo results are shown as black lines for Madgraph + PYTHIA and red lines for Madgraph + HERWIG.

the difference between PYTHIA and HERWIG predictions. This gives us confidence that the FJF formalism combined with NLL' resummation can be used to correctly calculate both the substructure and the identified hadron's energy fraction within a jet.

3.5 $e^+e^- \to 3$ Jets with the Gluon Jet Fragmenting to J/ψ

We can also use the FJF formalism to calculate the cross section for $e^+e^- \to 3$ jets with a J/ψ. As we expect gluon fragmentation to be the dominant production channel at the LHC, we focus on the case where J/ψ is found within a gluon jet. In addition, we assume that the angularity of this jet is also measured. To obtain a physical observable, one must also include contributions from all jets fragmenting to J/ψ, however, we expect the contribution from quark jets to be smaller. It is

theoretically possible to isolate the J/ψ coming from gluon jets in experiments by b-tagging the other two jets in the event, so we will focus on the process $e^+e^- \to b\bar{b}g$ followed by gluon fragmentation to J/ψ.

The analytic expression for this cross section is

$$\frac{1}{\sigma_0}\frac{d\sigma^{(g)}}{d\tau_a dz} = H_3(\mu_H) \times S^{\rm unmeas}(\mu_\Lambda) \times J^{(\bar{b})}_{n_1}(\mu_{J_{n_1}}) \times J^{(b)}_{n_2}(\mu_{J_{n_2}})$$

$$\times \sum_i \Bigg\{ \left(\frac{\Theta(\tau_a)}{\tau_a^{1+\Omega}}\right) \Big[\delta_{gi}\delta(1-z)(1+f_S(\tau_a,\mu_{S^{\rm meas}})) + f^{gi}_{\mathcal{J}}(\tau_a,z,\mu_{J_{n_3}})\Big] \bullet \frac{D_{i\to J/\psi}(z,\mu_{J_{n_3}})}{2(2\pi)^3}$$

$$\times \Pi(\mu,\mu_H,\mu_\Lambda,\mu_{J_{n_1}},\mu_{J_{n_2}},\mu_{J_{n_3}},\mu_{S^{\rm meas}}) \Bigg\}_+ , \tag{3.32}$$

where $\Omega \equiv \Omega(\mu_{J_{n_3}},\mu_{S^{\rm meas}}) = \omega_{J_n}(\mu,\mu_{J_{n_3}}) + \omega_{S^{\rm meas}}(\mu,\mu_{S^{\rm meas}})$, the b-quark initiated jets $J^{(b)}_{n_1}$ and $J^{(\bar{b})}_{n_2}$ are unmeasured, the expression for f_S is the same as Eq. (5.79) with C_F replaced by C_A, and our expressions for $f^{ij}_{\mathcal{J}}$ are given in terms of the coefficients c_0^{ij}, c_1^{ij} and c_2 given in Eq. (3.18). Here σ_0 is the LO cross section for $e^+e^- \to b\bar{b}g$. We will focus on the Mercedes Benz configuration in which all three jets have (approximately) the same energy, and consider jets with energies large enough that the mass of b-quark can be neglected. Here, $H_3(\mu)$ is $1 + O(\alpha_s)$ where the $O(\alpha_s)$ comes from the NLO virtual corrections to $e^+e^- \to b\bar{b}g$. We do not include this correction. The primary effect of its omission will be on the normalization of the cross section, which is not important for our discussion of the distributions we show below, and to increase the scale uncertainty associated with varying μ_H; however this is not a very important source of uncertainty in our calculations.

While the calculation for B mesons requires a phenomenological FF, the FFs for J/ψ production can be calculated in NRQCD [49]. Refs. [83–86] showed that a J/ψ FF can be calculated in terms of analytically calculable functions of $\alpha_s(2m_c)$ and z multiplied by nonperturbative NRQCD long-distance matrix-elements (LDMEs). As

discussed in Chapter 1 for J/ψ production, the most important gluon fragmentation mechanisms are the color-singlet mechanism, in which the $c\bar{c}$ is produced perturbatively in a ${}^3S_1^{(1)}$ state, and the color-octet mechanisms, in which the $c\bar{c}$ is produced perturbatively in a ${}^1S_0^{(8)}$, ${}^3S_1^{(8)}$, or ${}^3P_J^{(8)}$ state. Here ${}^{2S+1}L_J^{(1,8)}$ refers to the angular momentum and color quantum numbers of the $c\bar{c}$. The numerical values for the corresponding LDMEs are taken to be the central values from the global fits performed in Refs. [2, 3], and are shown in Table 1.2.

The color-singlet LDME scales as v^3, where v is the typical relative velocity of the $c\bar{c}$ in the J/ψ, while the color-octet LDMEs scale as v^7 [49]. This v^4 suppression is clearly seen in the numerical values of the LDMEs in Table 1.2. In the calculation of the gluon FF, this v suppression is compensated by powers of α_s since the leading color-octet contributions are $O(\alpha_s^2)$ in the ${}^1S_0^{(8)}$ and ${}^3P_J^{(8)}$ channels and $O(\alpha_s)$ in the ${}^3S_1^{(8)}$ channel, while the color-singlet contribution is $O(\alpha_s^3)$. In this work we focus on the gluon FJF, $\mathcal{G}_g^{J/\psi}$, and separately compute each of the four NRQCD contributions to $\mathcal{G}_g^{J/\psi}$. To calculate $\mathcal{G}_g^{J/\psi}$, we evolve each FF from the scale $\mu = 2m_c$ to the characteristic scale of the measured jet $\mu_{J_{n_3}}(\tau_a) = \omega\tau_a^{1/(2-a)}$ using the DGLAP evolution equations. For most values of z considered in this section, we do not expect that using a z dependent scale will result in significant improvement in the scale variation. In addition, using a z dependent scale in the ${}^3P_J^{(8)}$ channel yields unphysical results, such as negative values for the FF. After evolution, we perform the convolution $[D \bullet f_{\mathcal{J}}](z)$ in z with the matching coefficients derived in Section 3.4.

Before discussing the comparison of our results with monte carlo, we briefly review how the Madgraph + PYTHIA monte carlo handles color-singlet and color-octet quarkonium production. We produce quarkonia states in Madgraph from the following processes: $e^+e^- \to b\bar{b}gg c\bar{c}[{}^3S_1^{(1)}]$, $e^+e^- \to b\bar{b}gc\bar{c}[{}^1S_0^{(8)}]$, and $e^+e^- \to b\bar{b}c\bar{c}[{}^3S_1^{(8)}]$. The quantum numbers ${}^{2S+1}L_J^{(1,8)}$ are for the $c\bar{c}$ produced in the event. We only in-

clude diagrams in which the virtual photon couples to the $b\bar{b}$ so in all cases the $c\bar{c}$ plus any additional gluons come from the decay of a virtual gluon. We did not simulate production in the ${}^3P_J^{(8)}$ channel in $e^+e^- \to b\bar{b}g \to b\bar{b}c\bar{c}g$ because IR divergences in the matrix elements require much longer running times to get the same number of events. We then perform showering and hadronization on these hard processes using PYTHIA. Analysis is done using RIVET [87]. During PYTHIA's showering phase, color-singlet J/ψ do not radiate gluons. Thus if these J/ψ are produced within a jet, all surrounding radiation is due to the other colored particles in the event [88, 89]. We require that after showering there are only three jets in the event, two from the b-quarks and one from a gluon that contains the J/ψ. We simulate three-jet events at $E_{cm} = 250$ GeV in the Mercedes-Benz configuration by requiring the jets each have energies $E_{jet} > (E_{cm} - \Lambda)/3$ with $\Lambda = 30$ GeV, analagous to what was done in Sec. 3.4.

For $c\bar{c}$ produced in a color-octet state PYTHIA allows the color-octet $c\bar{c}$ to emit gluons with a splitting function $2P_{qq}(z)$. Since $P_{qq}(z)$ is peaked at $z = 1$, the color-octet $c\bar{c}$ pair typically retains most of its energy after these emissions. This model of the production mechanism is very different than the physical process implied by the NLL' calculation. In the NLL' calculation, the FF is calculated at the scale $2m_c$, then evolved up to the jet energy scale using Altarelli-Parisi evolution equations. Since this is a gluon FF, the most important splitting kernel in this evolution is $P_{gg}(z)$. We find that the FFs obtained at the jet energy scale are not significantly changed if we use only this evolution kernel and ignore mixing with quarks. Thus the production process implied by the NLL' calculation is that of a highly energetic gluon produced in the hard process with virtuallity of order the jet energy scale, which then showers by emitting gluons until one of the gluons with virtuality of order $2m_c$ hadronizes into the J/ψ. Because $P_{gg}(z)$ is peaked at $z = 0$ and $z = 1$ the resulting J/ψ distribution in z is much softer than the model employed by PYTHIA.

PYTHIA does not allow one to change the actual splitting function, only to modify the color-factor. Therefore, in order to get a softer z distribution we changed the coefficient of PYTHIA's splitting kernel for a gluon radiating off a color-octet $c\bar{c}$ pair from $2P_{qq}$ to $C_A P_{qq} = 3P_{qq}$. This results in a slighter softer z distribution than default PYTHIA, but is still inconsistent with the NLL' calculation. This change does not have significant impact on the τ_a distributions. The τ_a distributions are generally in better agreement. The variable τ_a depends on all of the hadrons in the jet and is therefore less sensitive to the behavior of the J/ψ, especially when the J/ψ carries a small fraction of the jet energy. In that case, τ_a distributions in the NLL' calculation look similar for all color-octet mechanisms.

In an attempt to see if PYTHIA can be modified to reproduce the z distributions obtained in our NLL' calculations, and confirm the physical picture of the NLL' calculation described above, we generate $e^+e^- \to b\bar{b}g$ events in Madgraph and allow PYTHIA to shower but not hadronize the events. If we allow the shower to evolve to a scale where the typical invariant mass of a gluon is $2m_c$ and then convolve the gluon distribution with the NRQCD FFs at this scale, we expect that the resulting z distributions should mimic our NLL' calculation. The lower cutoff scale in PYTHIA's parton shower is set by the parameter TimeShower:pTmin, which is related to the minimal virtuality of the particles in the shower, and whose default value is 0.4 GeV. We change this parameter to 1.6 GeV, which corresponds to a virtuality of $\sim 2m_c$, then obtain a z distribution for the gluons by randomly choosing a gluon from the gluon initiated jet. We then numerically convolve this z distribution with the analytic expression for the NRQCD FF. This procedure, which we will refer to as Gluon Fragmentation Improved PYTHIA (GFIP), yields z distributions that are consistent with our NLL' result, as we will see below. We tested an analogous procedure for two-jet events with B mesons by showering $e^+e^- \to b\bar{b}$ with PYTHIA with hadronization turned off. We then convolved the resulting b quark distribution with the b-quark FF

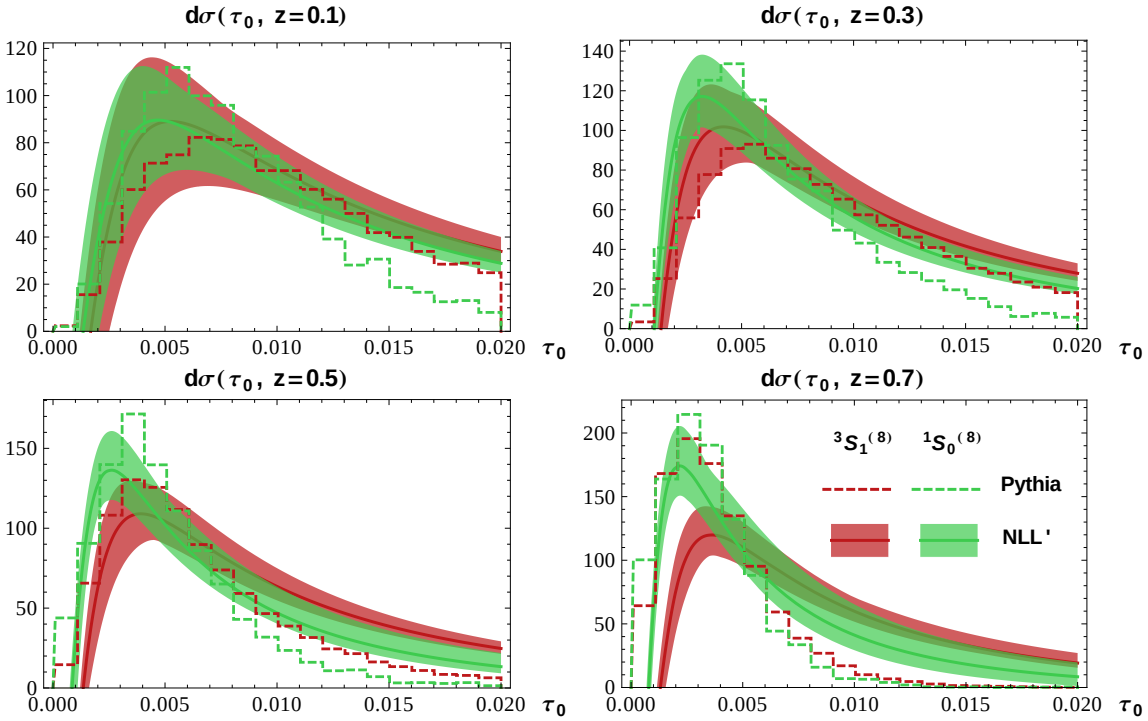

FIGURE 3.4: Angularity distributions of $d\sigma(\tau_a, z)$ for $a = 0$ at $z = 0, 1,\ 0.3,\ 0.5,\ 0.7$. Analytic calculations are shown as red (green) bands for the ${}^3S_1^{(8)}$ (${}^1S_0^{(8)}$) production mechanisms. Results from Madgraph + PYTHIA are shown as red (green) dashed lines for the same mechanisms.

at the scale $2m_b$, and found results for B mesons that are consistent with our NLL' calculations. Note that PYTHIA treats the radiation coming from the octet $c\bar{c}$ pair the same regardless of the angular momentum quantum numbers. In contrast, GFIP like the NLL' calculation gives different results for all three channels by applying different FFs at the end of the parton shower phase. Also GFIP can be applied to all four NRQCD production mechanisms, since convergence issues for the ${}^3P_J^{(8)}$ channels are absent.

Fig. 3.4 shows our NLL' calculation and Madgraph + PYTHIA results for the distribution of τ_0 for various fixed values of z for the ${}^3S_1^{(8)}$ (red) and ${}^1S_0^{(8)}$ (green) channels. We see fairly good agreement between analytic and Monte Carlo results in the peak regions for smaller values of z and notice some qualitative differences

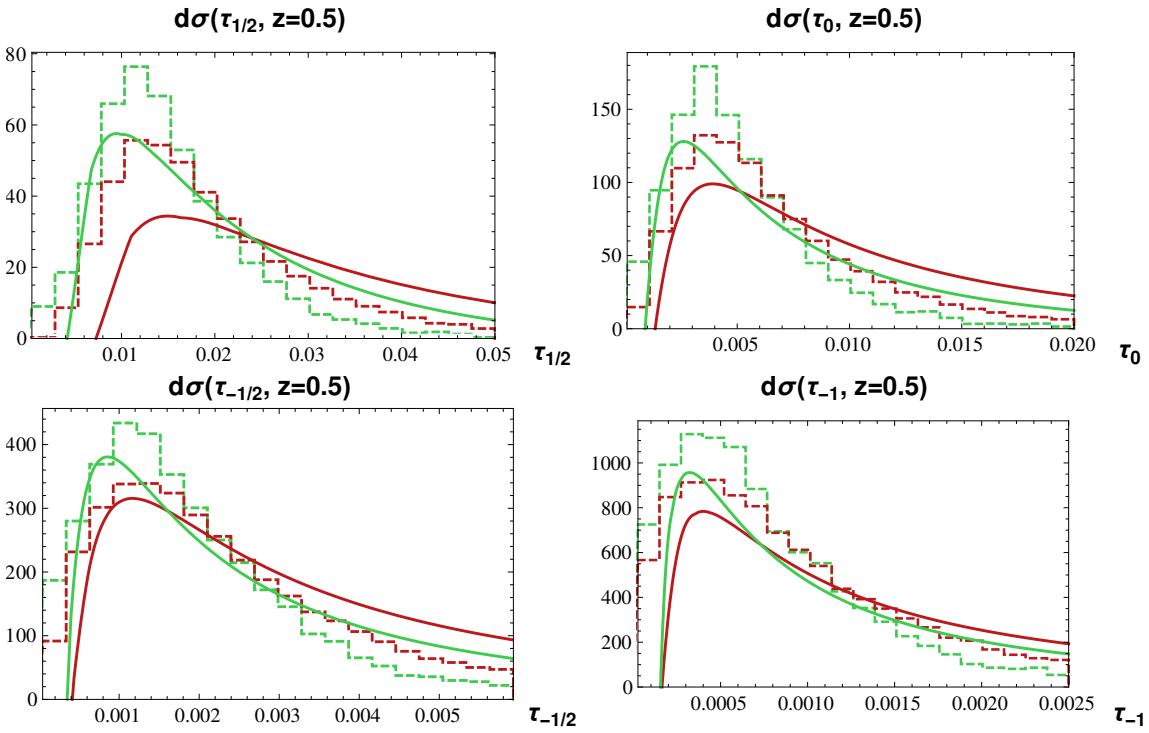

FIGURE 3.5: Angularity distributions of $d\sigma(\tau_a, z)$ for $a = +1/2,\ 0,\ -1/2,\ -1$ at $z = 0.5$. Analytic calculations are shown as red (green) solid lines for the ${}^3S_1^{(8)}$ (${}^1S_0^{(8)}$) production mechanisms. Results from Madgraph + PYTHIA are shown as red (green) dashed lines for the same mechanisms.

in the tail regions, especially for the ${}^1S_0^{(8)}$ channel. At higher values of z where the number of final state particles is small, differences in the τ_0 distributions could be attributed to the increasing influence of Pythia's unrealistic model of quarkonium production. As $z \to 0$, we also see similar τ_0 dependence for the two color-octet channels in our analytic results. This suggests that in the small z region, the jet substructure is independent of the production mechanism. Thus, attempts to use angularity distributions to extract the various LDMEs should focus on the range $0.3 < z < 0.7$.

In Fig. 3.5, we show the angularity distributions (without uncertainties) for the ${}^1S_0^{(8)}$ and ${}^3S_1^{(8)}$ mechanisms for $a = +1/2,\ 0,\ -1/2,\ -1$. These are computed analytically and using monte carlo and we again see reasonable agreement. As a is

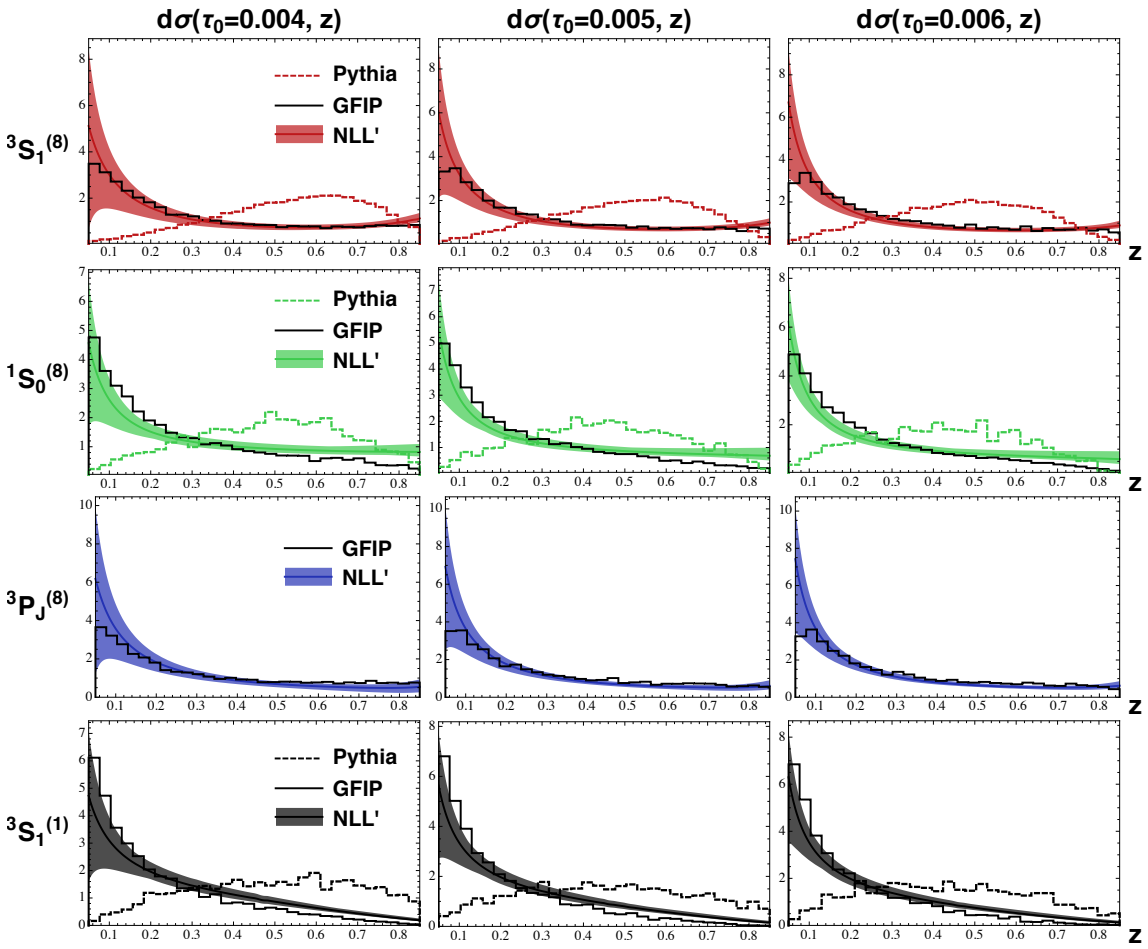

FIGURE 3.6: z distributions of $d\sigma(\tau_a, z)$ for NLL' analytic calculations (bands), PYTHIA (dashed lines), and GFIP (solid lines) for fixed values of $\tau_0 = (4,\ 5,\ 6) \times 10^{-3}$.

decreased, we see less discrimination between the two production mechanisms. Thus extraction of LDMEs should ideally be done with larger values of a, for $a < 1$ where factorization in SCET$_I$ holds, with the caveat that there is a trade-off since the predictability of the analytical results is limited for a too close to 1 since power corrections grow as $1/(1-a)$ [90].

In contrast to the angularity distributions, Fig. 3.6 shows that analytic and monte carlo calculations of the z distributions using Madgraph + PYTHIA yield strikingly different results, with Madgraph+PYTHIA yielding a much harder z-distribution.

Fig. 3.6 also shows the z distributions using GFIP. The GFIP modification yields significantly different results for the z distributions that align more closely with NLL' calculation. While this is far from a proper modification of PYTHIA, it shows us that implementing the missing $g \to J/\psi$ fragmentation yields encouraging similarities to our analytical calculations using the FJF formalism with NRQCD FFs. This also suggests that if monte carlo is modified to properly include NRQCD FFs at the scale $2m_c$ it will yield results that are consistent with FJFs combined with NLL' resummation. Correct monte carlo implementation of the NRQCD FFs is important because the GFIP modification can only be used to calculate the z distribution. There are many other jet shape observables, such as N-subjettiness or ΔR (where ΔR is the angle between the J/ψ and the jet axis), that should be able to discriminate between NRQCD production mechanisms, and many of these are most easily predicted using monte carlo.

3.6 Semi-analytic calculations for $pp \to jet(J/\psi) + X$

In this section we perform the corresponding calculation for the LHCb experiment already discussed in Chapter 1. We do not use a factorization theorem analogous to Eq. (3.23) for pp collisions, which would have the added complication that it would need to include convolution over incoming parton densities and beam functions. We instead perform the calculation in two different ways. Our first method is analogous to the GFIP calculation discussed in the previous section. We start by generating events corresponding to hard production of c quarks and gluons in pp collisions at $\sqrt{s} = 13$ GeV using MadGraph [91].[3] In the LHCb data, all jets have pseudorapidity $2.5 < y < 4.0$, $R = 0.5$, and the jets are required to have $p_T > 20$ GeV. The hard partons generated by MadGraph satisfy the jet constraints of LHCb. PYTHIA is

[3] Note that the contribution from quarks from the hard collision other than c give contributions to J/ψ production that are suppressed, either due to the soft gluon emission or by α_s evaluated at a large energy scale, and are therefore we neglect their contribution.

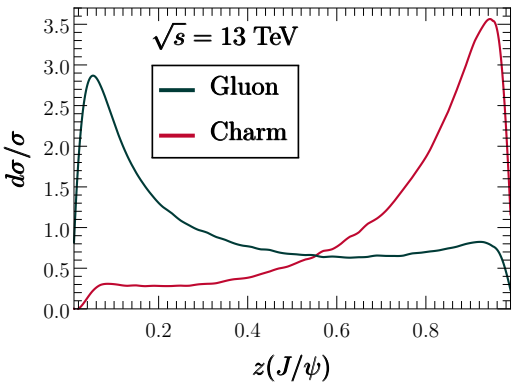

FIGURE 3.7: PYTHIA predictions for c and g z distributions (where z is the fraction of the energy of the parton initiating the jet) after showering to the scale $2m_c$.

then used to shower the event down to a scale of $\sim 2m_c$. Jet algorithms are applied to the output of the PYTHIA shower and the c quarks and gluons must be within jets of radius $R = 0.5$ satisfying the criteria of the LHCb data described above. The resulting c and gluon distributions are shown in Fig. 3.7. Note that the c quark distribution is peaked near $z = 1$ while the gluon z distribution is much softer and peaked near $z = 0$. The p_T and y distributions for the c quarks and gluons are then convolved manually with the NRQCD fragmentation functions evaluated at leading order (LO) in perturbation theory to obtain p_T and y distributions for J/ψ. We consider contributions only from the five production mechanisms included in Table 1.3.

At the LHCb the J/ψ is identified through the di-muon decay where is required that both muons have $2.0 < y < 4.5$, energy > 5 GeV, and $p_T > 0.5$ GeV. The energy cut clearly suppresses contributions from partons with low z and hence enhances the contribution from c quark initiated jets. We implement the muon cuts by assuming the J/ψ are unpolarized and therefore decays to $\mu^+\mu^-$ isotropically in its rest frame, and the LHCb cuts on the muons are applied to the muons after they are boosted back to the lab frame. From this a normalized distribution in $z(J/\psi)$ is constructed for each production mechanism. Each mechanism is characterized by an initial parton

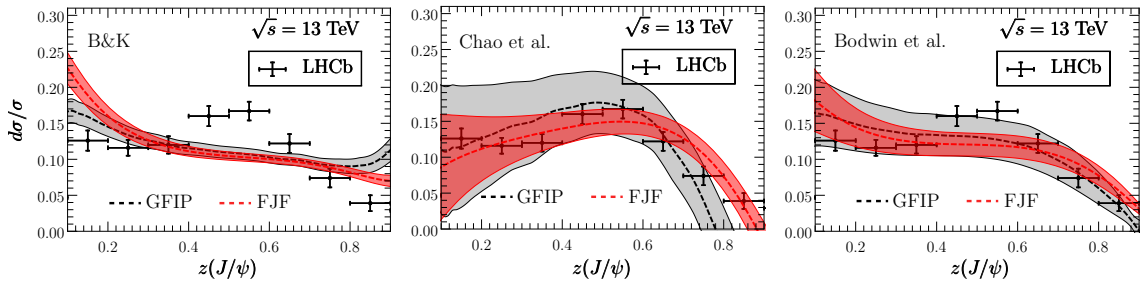

FIGURE 3.8: Predicted $z(J/\psi)$ distribution using GFIP (gray) and FJF (red) for the three choices of LDME in Table 1 and the LHCb measurements of $z(J/\psi)$.

i and quantum numbers n, and is multiplied by a weight

$$r(i,n) = \frac{d\hat{\sigma}(pp \to i + X) \int_0^1 dz D^n_{i\to J/\psi}(z)}{d\hat{\sigma}(pp \to c + X) \int_0^1 dz D^{^3S_1^{[1]}}_{c\to J/\psi}(z)} \,. \tag{3.33}$$

The weight in Eq. (3.33) ensures that the total number of J/ψ coming from each mechanism are in the proper ratio. This is where the fitted LDMEs enter the calculation as $D^n_{i\to J/\psi}(z) \propto \langle \mathcal{O}^{J/\psi}(n) \rangle$. Because of possible large corrections near $z \to 0$ and $z \to 1$, we only compare with LHCb data in the range $0.1 < z < 0.9$. Finally, the overall normalization is adjusted to agree with the normalization of the LHCb data in this range.

Our second method, which we will refer to as the FJF method, employs FJFs evaluated at the jet energy scale, E_J, combined with hard events generated by Madgraph. While this calculation does not include soft and other jet functions in Eq. (3.23), these functions are independent of $z(J/\psi)$, so the $z(J/\psi)$ dependence of the cross section is controlled by the FJF. The energy distribution of hard partons is combined with the FJFs for anti-k_T jets with $R = 0.5$ to produce a $z(J/\psi)$ distribution for each of the five mechanisms. To account for the muon cuts we apply a correction that is obtained from the GFIP calculations of $z(J/\psi)$. The $z(J/\psi)$ distributions from each mechanism are weighted by the factors in Eq. (3.33) as before.

Fig. 3.8 shows the predicted $z(J/\psi)$ distributions for the three choices of LDME's

Table 3.2: NRQCD LDMEs for J/ψ production mechanisms used in this paper in units of GeV^3.

	$\langle\mathcal{O}(^3S_1^{[1]})\rangle$ $\times$ GeV^3	$\langle\mathcal{O}(^3S_1^{[8]})\rangle$ $\times 10^{-2}$ GeV^3	$\langle\mathcal{O}(^1S_0^{[8]})\rangle$ $\times 10^{-2}\mathrm{GeV}^3$	$\langle\mathcal{O}(^3P_0^{[8]})\rangle/m_c^2$ $\times 10^{-2}\mathrm{GeV}^3$
B & K [2, 3]	1.32 ± 0.20	0.224 ± 0.59	4.97 ± 0.44	-0.72 ± 0.88
Chao, et al. [92]	1.16 ± 0.20	8.9 ± 0.98	0.30 ± 0.12	0.56 ± 0.21
Bodwin et al. [46]	1.32 ± 0.20	1.1 ± 1.0	9.9 ± 2.2	0.49 ± 0.44

in Table 3.2 using the GFIP (gray) and FJF (red) methods, which are in good agreement. Uncertainties are due to LDMEs only. In the case of Ref. [46], the errors in Table 3.2 are supplemented with an error correlation matrix provided by the authors through private communication. In Ref. [92] a fixed relationship between the $^3S_1^{[8]}$ and $^3P_J^{[8]}$ LDMEs is required to obtain unpolarized J/ψ. This constraint is taken into account when computing the uncertainty due to the LDMEs. These constraints significantly reduce the uncertainty in the predictions relative to naively adding uncertainties in Table 3.2 in quadrature. Other sources of uncertainty such as scale variation have not been included. Estimating theory uncertainties reliably in the absence of a complete factorization theorem is difficult. For example, using the FJF method, the μ dependence of the FJF should be cancelled by μ dependence in hard and soft functions that have not been computed. Note that since the normalization of theoretical curves is fixed to the LHCb data, any scale variation that affects normalization but not the shapes of the $z(J/\psi)$ distribution will not contribute to the uncertainty.

All three choices of LDMEs give better agreement to the LHCb data than default PYTHIA shown in Ref. [13]. This gives support to the picture of quarkonium production in the previous and this section. The LDMEs from global fits [2, 3] give

worse agreement than the fits from Refs. [46, 92]. The LHCb data is a decreasing function of $z(J/\psi)$ as $z(J/\psi) \to 1$. This is a property of the ${}^3S_1^{[1]}$ and ${}^1S_0^{[8]}$ FJFs, but not the ${}^3S_1^{[8]}$ and ${}^3P_J^{[8]}$ FJFs, which actually diverge as $z \to 1$. In order to obtain negligible polarization at high p_T, the ${}^3S_1^{[8]}$ and ${}^3P_J^{[8]}$ LDMEs of Refs. [46, 92] have relative signs such that they roughly cancel, so the ${}^1S_0^{[8]}$ dominates production and J/ψ are unpolarized. The same cancellation here allows the $z(J/\psi)$ distribution go to zero as $z(J/\psi) \to 1$. Such a cancellation does not occur for the LDMEs from the global fits so the $z(J/\psi)$ distribution starts to turn up at large $z(J/\psi)$.

3.7 Conclusion

The study of hadrons within jets provides new tests of perturbative QCD dynamics. The distribution in z (the fraction of jet energy carried by the identified hadron) can be calculated as a convolution of the well-known fragmentation functions (FFs) for that hadron with perturbative matching coefficients that are calculable at the jet energy scale, which is typically well above $\Lambda_{\rm QCD}$. At hadron colliders this provides a new way to extract FFs and will be especially important for pinning down gluon FFs, which are of subleading importance in e^+e^- colliders where FFs are usually measured. The production of heavy quarkonia within high energy jets in collider experiments also provides new tests of NRQCD.

In this chapter, we studied cross sections for jets with heavy mesons as a function of z and the substructure variable angularity, τ_a. We provided for the first time the NLO matching coefficients for jets with measured τ_a, and used these along with the known RGE for the hard, jet, and soft functions to obtain NLL' accuracy calculations of cross sections for jets with heavy mesons. We considered the production of B mesons in two-jet events in e^+e^- collisions at $E_{\rm cm} = 250$ GeV as well as J/ψ production in three-jet events at the same energies. Though not relevant to any ex-

periment, this is useful for comparing NLL' calculations with monte carlo simulations of fragmenting jets whose energy is comparable to those measured at the LHC. In the simulations of quarkonia production, the underlying hard process was generated using Madgraph and then PYTHIA was used to shower and hadronize the events. In the simulations involving B meson production we also used HERWIG.

For B mesons, we find that the z and τ_a distributions computed using monte carlo and NLL' are in excellent agreement, giving us confidence in our analytic approach. In the case of J/ψ, we considered three-jet events in which the jets all had the same energy and the J/ψ in both simulation and NLL' calculations was required to come from the gluon jet. This allowed us to study J/ψ production via the fragmentation of high energy gluon initiated jets, which we expect to be an important mechanism at the LHC. Earlier studies of gluon FJFs in Ref. [73] indicated that the z and E dependence of these jets could discriminate between various NRQCD production mechanisms. The analytic NLL' studies of this chapter are consistent with Ref. [73]; we also find that the τ_a and z distributions can discriminate between different various NRQCD production mechanisms.

For monte carlo simulations, we used Madgraph to calculate $e^+e^- \to b\bar{b}g$ followed by the gluon fragmenting into a a $c\bar{c}$ pair in either a ${}^3S_1^{(8)}$, ${}^1S_0^{(8)}$, or ${}^3S_1^{(1)}$ state. As explained earlier we do not simulate events in the ${}^3P_J^{(8)}$ channel. The events were then showered and hadronized using PYTHIA. While the τ_a distributions are similar to analytical calculations, the z distributions are much harder and their shape looks nothing like the NLL' calculation. We attribute this to a naive model that PYTHIA uses for simulating the radiation of gluons from color-octet $c\bar{c}$ pairs.

We then considered an alternative simulation approach where $e^+e^- \to b\bar{b}g$ events are generated using Madgraph, then PYTHIA is used to shower the event to a low scale near $2m_c$ without hadronization. The resulting gluon distribution is then

convolved with the analytically calculated NRQCD FFs calculated at the scale $2m_c$. This procedure yields z distributions that are in much better agreement with our NLL' calculations.

We have analyzed the recent LHCb data on J/ψ production within jets. We used a combination of Madgraph, PYTHIA, and LO NRQCD fragmentation functions first introduced in Ref. [56] as well as an approach based on monte carlo evaluation of the hard process combined with J/ψ FJFs evolved to the jet energy scale. Both methods yield $z(J/\psi)$ distributions that agree much better with data than default PYTHIA simulations. The $z(J/\psi)$ distributions are very well described by LDMEs from fits to large p_T data, and less well described by LDMEs from global fits. It would be interesting to perform a combined fit to the LHCb data and the large p_T data used in Refs. [46, 92] to see if consistent LDMEs with smaller errors can be obtained. Experimental measurement of jets at central rapidity and the polarization of J/ψ as a function of $z(J/\psi)$ [93] would also be of interest. Finally it would be especially interesting to find ways of discriminating charm and gluon initiated jets [94], as a sample containing only gluon initiated jets will have greater sensitivity to color-octet LDMEs.

Future work will focus on extending the NLL' calculations to hadron colliders, where the unmeasured jet and soft function calculated in 5 (also cf. Ref. [58]) must be combined with the FJFs calculated in this chapter. It would be of great interest to compare the results of these calculations with data from the LHC on high energy jets with heavy mesons and quarkonia. Finally, there needs to be more work on improving the understanding of the differences between NLL' and monte carlo simulations. Monte carlo simulations that can properly simulate the production of quarkonia within jets will be essential for calculating other jet observables for which NLL' calculations are either unavailable or impractical.

4

Transverse Momentum Dependent Fragmenting Jet Functions with Applications to Quarkonium Production

4.1 Outline

In this chapter we extend FJFs to transverse momentum dependent distributions (TMDs). Recently, TMDs have been studied extensively within and outside the framework of SCET [95–103]. TMDs offer a new technology for the study of hadron substructure in hadron colliders (TMD parton distribution functions (TMDPDFs)) and hadron production (TMD fragmentation functions (TMDFFs)). TMDPDFs have been used in SCET for studies of Higgs production in the small transverse momentum limit at the LHC [103–108]. TMD fragmenting jet functions (TMDFJF) depend on three kinematic variables: the jet energy, $\omega/2$, the fraction of this energy carried by the identified hadron, z, and the hadron transverse momentum with respect to the axis of direction of the original parton, $\mathbf{p}_\perp^h$. The modes that give

important contributions to the transverse momentum are

$$\begin{aligned} \text{collinear-soft:} \quad & p_{cs}^{\mu} \sim \omega(\lambda r, \lambda/r, \lambda), \quad \lambda = p_{\perp}/\omega \\ \text{collinear:} \quad & p_{n}^{\mu} \sim \omega(\lambda^2, 1, \lambda), \end{aligned} \tag{4.1}$$

where collinear-soft modes are soft modes collinear to the direction of the jet axis first introduced in Ref. [60] and $r \equiv \tan(R/2)$ for jet cone size R. Similar modes are also studied in [5]. To incorporate contributions from soft-collinear modes, we make use of the SCET$_+$ formalism. SCET$_+$ and other similar extensions of SCET have been used to study processes with multiple well-separated scales and distinct phase space regions (e.g. [5, 60, 101, 109]).

In Section 4.2, we give a definition of the TMDFJF and show how it emerges from definitions of TMDFFs in the literature. We then perform a matching calculation at next-to-leading order (NLO) onto SCET$_+$ and derive a result that is completely factorized into hard, collinear, collinear-soft, and ultra-soft modes. We present a calculation of the matching coefficients $\mathcal{J}_{ij}$ between the TMDFJF and the more traditionally studied FFs. Additionally, we present a perturbative calculation of the corresponding collinear-soft function at NLO. In Section 4.3, we use renormalization group (RG) and rapidity renormalization group (RRG) techniques to resum logarithms to next-to-leading-log-prime (NLL') accuracy. The TMDFJF formalism is applied to the production of J/ψ in gluon jets where the FFs are calculated to LO in NRQCD. We find that distributions in $p_\perp$ and z as well as the average angle of J/ψ relative to the axis of the jet can discriminate between the various NRQCD production mechanisms. The material of this chapter was published in Ref. [57].

4.2 Transverse momentum dependent fragmenting jet function

In this section we will present the definition of the TMDFJF, connecting it with definitions of TMDFFs from the literature. We first show the matching calculation of

the TMDFJF onto SCET$_+$ and its factorization into pure collinear, soft-collinear, and hard pieces. We then present perturbative calculations of the matching coefficients, $\mathcal{J}_{i/j}$, from matching the pure collinear function onto the FF as well as the one-loop expression for the soft-collinear function.

4.2.1 Definition and factorization

The operator definition of the quark FF is given by [48]:

$$D_{q/h}(z,\mu) = \frac{1}{z}\sum_X \frac{1}{2N_c}\delta(\omega - p_X^- - p_h^-)\ \mathrm{Tr}\left[\frac{\bar{\not{n}}}{2}\langle 0|\psi(0)|Xh\rangle\langle Xh|\bar{\psi}(0)|0\rangle\right]\Big|_{\mathbf{p}_\perp^X = -\mathbf{p}_\perp^h}, \quad (4.2)$$

where $\psi(x)$ is the quark field in QCD. The TMDFF is given by a similar expression but is unintegrated in the transverse components of the hadron momentum. It is defined by [110]

$$D_{q/h}(\mathbf{p}_\perp^h, z, \mu) = \frac{1}{z}\int \frac{d^2x_\perp}{(2\pi)^2}\sum_X \frac{1}{2N_c}\delta(\omega - p_X^- - p_h^-) \times \mathrm{Tr}\left[\frac{\bar{\not{n}}}{2}\langle 0|\psi(0,0,x_\perp)|Xh\rangle\langle Xh|\bar{\psi}(0)|0\rangle\right], \quad (4.3)$$

such that,

$$\int d^2\mathbf{p}_\perp^h\ D_{q/h}(\mathbf{p}_\perp^h, z, \mu) = D_{q/h}(z,\mu). \quad (4.4)$$

Here, $\mathbf{p}_\perp^h$ is the transverse momentum of the hadron h with respect to the direction of the original fragmenting quark. In order to identify the experimentally measured jet axis with the direction of the parton initiating the jet, there needs to be a constraint that only ultrasoft radiation is outside the jet. Alternative definitions of the TMDFF often involve the transverse momentum measured with respect to different axes (e.g., the beam axis). In order to extend this concept to identified hadrons within jets we consider the collinear limit of Eq.(4.3) by matching onto SCET where now $z \equiv$

E_h/E_J. This yields the operator definition of the TMDFJF

$$\mathcal{G}_{q/h}(\mathbf{p}_\perp, z, \mu) = \frac{1}{z}\sum_X \frac{1}{2N_c}\delta(p^-_{Xh;r})\delta^{(2)}(\mathbf{p}_\perp + \mathbf{p}^X_\perp)$$
$$\times \mathrm{Tr}\left[\frac{\bar{\not{n}}}{2}\langle 0|\delta_{\omega,\overline{\mathcal{P}}}\chi^{(0)}_n(0)|Xh\rangle\langle Xh|\bar{\chi}^{(0)}_n(0)|0\rangle\right], \quad (4.5)$$

where in the equation above the states $|Xh\rangle$ corresponds to the a final state of collinear particles within a jet, in contrast with the the state $|Xh\rangle$ in Eqs. (4.2) and (4.3) which correspond to the inclusive case. The index (0) indicates that the field has been decoupled from the ultra-soft gluons via BPS field redefinitions

$$\chi^{(0)}_{n,\omega}(x) = Y^\dagger_n(x)\chi_n(x) \quad \text{and} \quad A^{(0)}_n(x) = Y^\dagger_n(x)A_n(x)Y_n(x), \quad (4.6)$$

and $\chi_n \equiv W^\dagger_n\xi_n$ is defined in terms of the collinear quark fields of SCET and the ultrasoft and collinear Wilson lines are

$$Y^\dagger_n(x) = \mathbb{P}\exp\left(ig\int_0^\infty ds\, n\cdot A_{us}(x+sn)\right) \quad \text{and} \quad W_n(x) = \sum_{\text{perms}}\exp\left(\frac{-g}{\bar{n}\cdot\mathcal{P}}\bar{n}\cdot A_n x\right). \quad (4.7)$$

As we show in Appendix C.1, the expression for the TMDFJF given in Eq.(4.5) is closely related to the FJF introduced in Ref. [55].

As discussed in the introduction, the TMDFJF receives contributions from two different modes, collinear and colllinear-soft or csoft . In order to make the contribution of the csoft modes explicit, we now match our expression onto SCET_+,

$$\mathcal{G}_{q/h}(\mathbf{p}_\perp, z, \mu) = C^\dagger_+(\mu)C_+(\mu)\frac{1}{z}\sum_X \frac{1}{2N_c}\delta(p^-_{Xh;r})\delta^{(2)}(\mathbf{p}_\perp + \mathbf{p}^X_\perp)$$
$$\times \mathrm{Tr}\left[\frac{\bar{\not{n}}}{2}\langle 0|\delta_{\omega,\overline{\mathcal{P}}}V^{\dagger\,(0)}_n(0)\chi^{(0)}_n(0)|Xh\rangle\langle Xh|\bar{\chi}^{(0)}_n(0)V^{(0)}_n(0)|0\rangle\right], \quad (4.8)$$

where

$$V^{(0)}_n(x) = \sum_{\text{perm}}\exp\left(\frac{-g}{\bar{n}\cdot\mathcal{P}}\bar{n}\cdot A^{(0)}_{n,cs}(x)\right), \quad (4.9)$$

are Wilson lines of csoft fields (the csoft analogue of W_n) and $C_+(\mu)$ are SCET$_+$ matching coefficients. In order to decouple the collinear fields $A_n^{(0)}$ and $\chi_n^{(0)}$ from the csoft gluons, we now perform field redefintions similar to those of the BPS procdure [60]

$$\mathcal{G}_{q/h}(\mathbf{p}_\perp, z, \mu) = C_+^\dagger(\mu) C_+(\mu) \frac{1}{z} \sum_X \frac{1}{2N_c} \delta(p^-_{Xh;r}) \delta^{(2)}(\mathbf{p}_\perp + \mathbf{p}_\perp^X)$$
$$\times \mathrm{Tr}\left[\frac{\bar{\not{n}}}{2} \langle 0 | \delta_{\omega,\overline{\mathcal{P}}} V_n^{\dagger\,(0)}(0) U_n^{(0)}(0) \chi_n^{(0,0)}(0) | Xh \rangle \right.$$
$$\left. \times \langle Xh | \bar{\chi}_n^{(0,0)}(0) U_n^{\dagger\,(0)}(0) V_n^{(0)}(0) | 0 \rangle \right], \quad (4.10)$$

where

$$U_n^{\dagger\,(0)}(x) = \mathbb{P} \exp\left(ig \int_0^\infty ds\, n \cdot A^{(0)}_{n,\,cs}(ns + x) \right), \quad (4.11)$$

and the superscript $(0,0)$ denotes that the corresponding fields are decoupled from both ultra-soft and collinear-soft modes. Having factorized our operators, we now factorize the phase-space into collinear and collinear-soft Hilbert states.

$$|Xh\rangle \;\to\; |X_n h\rangle |X_{cs}\rangle, \quad (4.12)$$

$$\sum_X \;\to\; \sum_{X_n} \sum_{X_{cs}}, \quad (4.13)$$

$$\delta^{(2)}(\mathbf{p}_\perp + \mathbf{p}_\perp^X) \;\to\; \delta^{(2)}(\mathbf{p}_\perp + \mathbf{p}_\perp^{X_n} + \mathbf{p}_\perp^{X_{cs}}). \quad (4.14)$$

This allows us to factorize the TMDFJF into three pieces

$$\mathcal{G}_{q/h}(\mathbf{p}_\perp, z, \mu) = H_+(\mu) \times \Big[\mathcal{D}_{q/h} \otimes_\perp S_C \Big](\mathbf{p}_\perp, z, \mu)\,, \quad (4.15)$$

where H_+ is proportional to the square of the matching coefficient from $\mathcal{G}_{q/h}$ in SCET$_I$ to SCET$_+$, and $\mathcal{D}_{q/h}$ and S_C are the contributions collinear and the collinear-soft modes of SCET$_+$ to the TMDFJF, respectively. These are defined by

$$H_+(\mu) = (2\pi)^2 N_c\, C_+^\dagger(\mu) C_+(\mu)\,, \quad (4.16)$$

$$\mathcal{D}_{q/h}(\mathbf{p}_\perp^{\mathcal{D}}, z) \equiv \frac{1}{z}\sum_{X_n}\frac{1}{2N_c}\delta(p^-_{Xh;r})\delta^{(2)}(p^\perp_{Xh;r})\,\mathrm{Tr}\left[\frac{\bar{\not{n}}}{2}\langle 0|\delta_{\omega,\overline{\mathcal{P}}}\chi_n(0)\delta^{(2)}(\mathcal{P}_\perp^{X_n}+\mathbf{p}_\perp^{\mathcal{D}})|X_n h\rangle \right.$$
$$\left. \times \langle X_n h|\bar{\chi}_n(0)|0\rangle\right], \quad (4.17)$$

$$S_C(\mathbf{p}_\perp^S) \equiv \frac{1}{N_c}\sum_{X_{cs}}\mathrm{Tr}\left[\langle 0|V_n^\dagger(0)U_n(0)\delta^{(2)}(\mathcal{P}_\perp+\mathbf{p}_\perp^S)|X_{cs}\rangle\langle X_{cs}|U_n^\dagger(0)V_n(0)|0\rangle\right], \quad (4.18)$$

where the Tr is over Dirac and color indices in $\mathcal{D}_{q/h}$ and color indices in S_C. From now on, we drop the (0) and $(0,0)$ superscripts since the different collinear, soft-collinear, and ultra-soft modes are now factorized. We also employ the following shorthand for the convolution in the $\perp$ components

$$\mathcal{D}_{q/h}\otimes_\perp S_C(\mathbf{p}_\perp) = \int\frac{d^2\mathbf{p}'_\perp}{(2\pi)^2}\;\mathcal{D}_{q/h}(\mathbf{p}_\perp-\mathbf{p}'_\perp)S_C(\mathbf{p}'_\perp). \quad (4.19)$$

Analogously for gluon fragmentation we have

$$\mathcal{D}_{g/h}(\mathbf{p}_\perp, z, \mu) = -g_{\mu\nu}\frac{1}{z}\sum_X\frac{\omega}{(d-2)(N_c^2-1)}\delta(p^-_{Xh;r})\delta^{(2)}(\mathbf{p}_\perp+\mathbf{p}_\perp^X)$$
$$\times\langle 0|\delta_{\omega,\overline{\mathcal{P}}}\mathcal{B}^{\nu,a}_{n,\perp}(0)\delta^{(2)}(\mathcal{P}_\perp^{X_n}+\mathbf{p}_\perp^{\mathcal{D}})|Xh\rangle\langle Xh|\mathcal{B}^{\mu,a}_{n,\perp}(0)|0\rangle, \quad (4.20)$$

where the collinear gluon field is

$$B^\mu_{n,\perp}(y) = \frac{1}{g}\left[W_n^\dagger(y)iD_{n\perp}W_n(y)\right], \quad (4.21)$$

and $iD_{n\perp} = \mathcal{P}^\mu_{n\perp} + gA^\mu_{n\perp}$ is the standard $\perp$-collinear covariant derivative in SCET.

At this point, only the purely collinear term $\mathcal{D}_{i/h}$ contains information about the hadron h. The collinear-soft function (S_C) and the hard function (H_+) are universal functions dependent on the fragmenting parton i but not on the hadron h. Additionally, in the limit that $|\mathbf{p}_\perp| \gg \Lambda_{\mathrm{QCD}}$, we may use the operator product expansion to factorize $\mathcal{D}_{i/h}$ into short distance coefficients and the more commonly

studied FFs, $D_{j/h}$, via,

$$\mathcal{D}_{i/h}(\mathbf{p}_\perp, z, \mu, \nu) = \int_z^1 \frac{dx}{x}\, \mathcal{J}_{i/j}(\mathbf{p}_\perp, x, \mu, \nu) D_{j/h}\left(\frac{z}{x}, \mu\right) \;+\; \mathcal{O}\left(\frac{\Lambda^2_{QCD}}{|\mathbf{p}_\perp|^2}\right), \qquad (4.22)$$

where $\mathcal{J}_{i/j}$ are the short distance coefficients that do not depend on the final hadron and can be calculated order by order in perturbation theory.

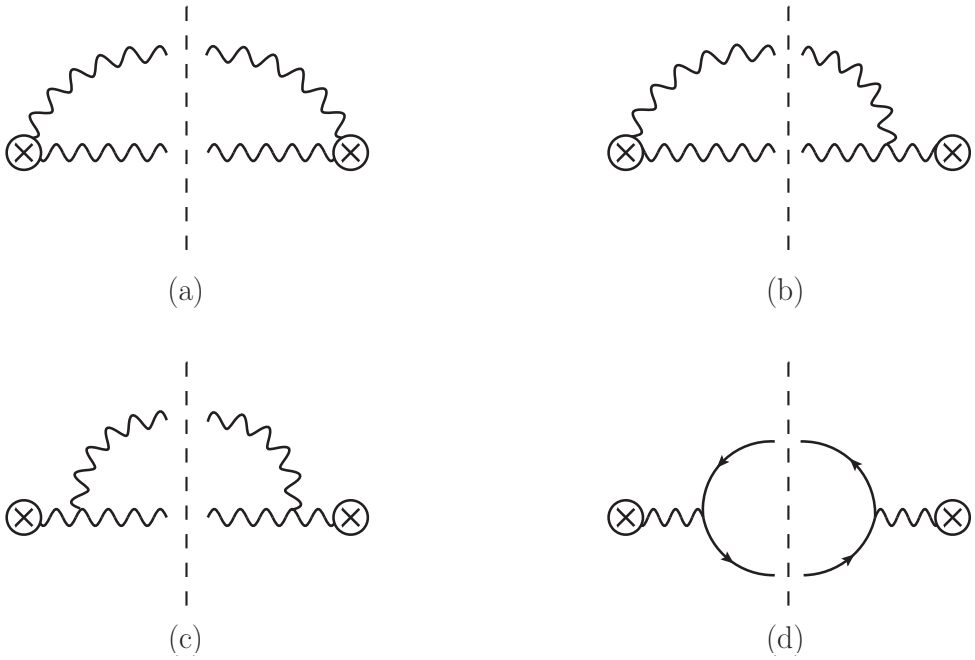

FIGURE 4.1: Feynman diagrams that give non-scaleless contributions to the gluon TMDFJF at NLO in α_s. Diagram (b) also has a mirror image that is not explicitly shown.

4.2.2 Perturbative results

The $O(\alpha_s)$ diagrams contributing to the gluon and quark TMDFJFs are shown in Figs. 4.1 and 4.2, respectively. At NLO, the matching coefficients $\mathcal{J}_{i/j}$ are directly related to the matching coefficients $\mathcal{I}_{i/j}$ between TMDPDFs and the more commonly

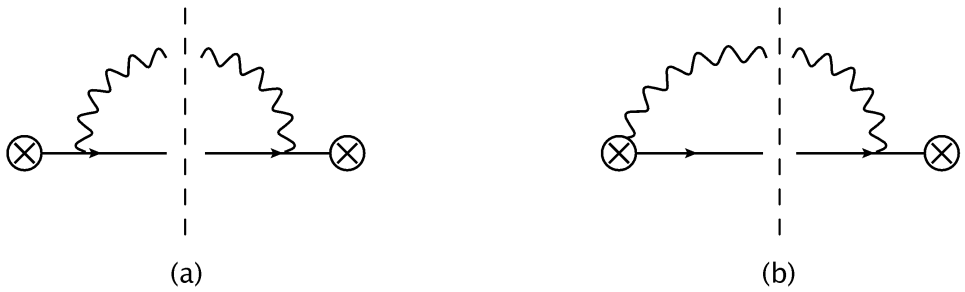

FIGURE 4.2: Associated non-scaleless diagrams that contribute to the quark TMD-FJF at NLO. Again, Diagram (b) has a mirror image that is not explicitely drawn above.

studied PDFs calculated in Refs. [101, 103] by the substitution $\mathcal{I}_{i/j} \to \mathcal{J}_{j/i}$. See Appendix C.2 for additional details of the matching calculation. Following Ref. [103], a rapidity regulator is used to regulate rapidity divergences in the perturbative calculation. This is implemented by first modifying the form of the collinear and collinear-soft Wilson lines

$$\begin{aligned} W_n &= \sum_{\text{perms}} \exp\left(-\frac{g\, w^2}{\bar{n}\cdot\mathcal{P}} \frac{|\bar{n}\cdot\mathcal{P}_g|^{-\eta}}{\nu^{-\eta}} \bar{n}\cdot A_n\right) \\ V_n &= \sum_{\text{perms}} \exp\left(-\frac{g\, w}{\bar{n}\cdot\mathcal{P}} \frac{|\bar{n}\cdot\mathcal{P}_g|^{-\eta/2}}{\nu^{-\eta/2}} \bar{n}\cdot A_{n,cs}\right), \end{aligned} \tag{4.23}$$

with similar modifications to U_n. This introduces a regulator η, a bookkeeping parameter w, and a new dimensionful parameter ν. The dependence of our results on ν should of course cancel amongst the terms in our factorization theorem. The renormalized results for the $\mathcal{J}_{i/j}$ in the $\overline{\text{MS}}$ scheme can be written,

$$\begin{aligned} \mathcal{J}_{i/j}(\mathbf{p}_\perp, z, \mu, \nu) &= \delta_{ij}\delta(1-z)\delta^{(2)}(\mathbf{p}_\perp) \\ &+ \frac{\alpha_s T_{ij}}{\pi}\Big\{ \left(\delta_{ij}\delta(1-z)\ln\left(\frac{\omega^2}{\nu^2}\right) + \bar{P}_{ji}(z)\right)\mathcal{L}_0(\mathbf{p}_\perp^2, \mu^2) + c_{ij}(z)\delta^{(2)}(\mathbf{p}_\perp),\Big\}, \end{aligned} \tag{4.24}$$

with

$$\bar{P}_{qq}(z) = P_{qq}(z) - \bar{\gamma}_q \delta(1-z) = (1+z^2)\mathcal{L}_0(1-z),$$

$$\bar{P}_{gq}(z) = P_{gq}(z) = \frac{1+(1-z)^2}{z},$$

$$\bar{P}_{qg}(z) = P_{qg}(z) = z^2 + (1-z)^2,$$

$$\bar{P}_{gg}(z) = P_{gg}(z) - \bar{\gamma}_g \delta(1-z) = 2\frac{(1-z+z^2)^2}{z}\mathcal{L}_0(1-z), \tag{4.25}$$

and

$$c_{qq}(z) = \frac{1-z}{2}, \;\; c_{qg}(z) = \frac{z}{2}, \;\; c_{gg}(z) = 0, \;\; c_{gq}(z) = z(1-z), \tag{4.26}$$

where $T_{qq} = T_{qg} = C_F$, $T_{gg} = C_A$, $T_{gq} = T_F$, $\bar{\gamma}_q = 3/2$ and $\bar{\gamma}_g = \beta_0/(2C_A)$. For convenience we use the following shorthand notation for the vector plus-distributions,

$$\mathcal{L}_n(\mathbf{p}_\perp^2, \mu^2) = \frac{1}{2\pi\mu^2}\mathcal{L}_n\left(\frac{\mathbf{p}_\perp^2}{\mu^2}\right) = \frac{1}{2\pi\mu^2}\left(\frac{\mu^2}{\mathbf{p}_\perp^2}\ln^n(\mu^2/\mathbf{p}_\perp^2)\right)_+ . \tag{4.27}$$

Performing the convolutions in the energy ratio parameter z we get,

$$\mathcal{D}_{i/h}(\mathbf{p}_\perp^2, z, \mu, \nu) = D_{i/h}(z,\mu)\delta^{(2)}(\mathbf{p}_\perp) + \frac{\alpha_s}{\pi}\Big\{\Big[T_{ii}D_{i/h}(z,\mu)\ln\left(\frac{\omega^2(1-z)^2}{\nu^2}\right) + f^{i/h}_{P\otimes D}(z,\mu)\Big]\mathcal{L}_0(\mathbf{p}_\perp^2,\mu^2) + f^{i/h}_{c\otimes D}(z,\mu)\delta^{(2)}(\mathbf{p}_\perp)\Big\}, \tag{4.28}$$

where

$$f^{i/h}_{P\otimes D}(z,\mu) = \sum_j \Big\{\delta_{ij}T_{ii}\int_z^1 \frac{dx}{1-x}\left[p_i(x)D_{i/h}\left(\frac{z}{x},\mu\right) - 2D_{i/h}\left(z,\mu\right)\right] + (1-\delta_{ij})T_{ij}\int_z^1 \frac{dx}{x}\, P_{ji}(x)D_{j/h}\left(\frac{z}{x},\mu\right)\Big\}, \tag{4.29}$$

with $p_q(x) = (1+x^2)/x$, $p_g(x) = 2(1-x+x^2)^2/x^2$ and

$$f^{i/h}_{c\otimes D}(z,\mu) = \sum_j T_{ij}\int_z^1 \frac{dx}{x}\, c_{ij}(x)D_{j/h}\left(\frac{z}{x},\mu\right), \tag{4.30}$$

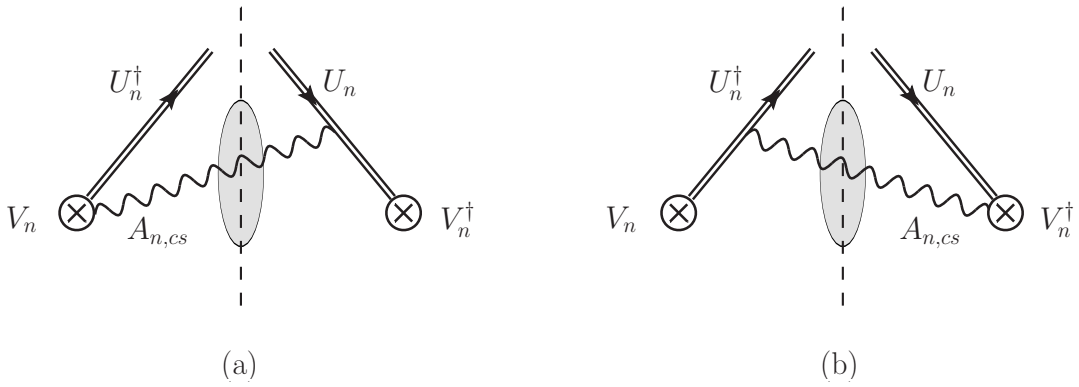

FIGURE 4.3: Real gloun emission diagrams that contribute to the collinear-soft function $S_C^i(\mathbf{p}_\perp, z, \mu, \nu)$ at $\mathcal{O}(\alpha_s)$. The gluons passing through the shaded oval indicate they are contained within the phase-space of the jet.

At NLO, the collinear-soft function, defined by Eq. (4.18), receives contributions from the two diagrams shown in Fig. 4.3. The real gluon is contained within a jet defined by a cone or k_T-type jet algorithm with cone size parameter R. A global soft funciton of similar form has been calculated at NLO in Ref. [103] and at NNLO in Ref. [105] in studies of Higgs p_T spectrum. The two diagrams in Fig. 4.3 yield identical contributions and thier sum is given by,

$$S_C^{i,B(1)}(\mathbf{p}_\perp) = g^2 w^2 \left(\frac{e^{\gamma_E}\mu^2}{4\pi}\right)^\epsilon \nu^\eta \, C_i \int \frac{dk^+ dk^- d^{d-2}k_\perp}{2(2\pi)^{d-1}} \, \frac{2\,\delta(k^2)}{k^+(k^-)^{1+\eta}} \delta^{(2)}(\mathbf{k}_\perp + \mathbf{p}_\perp)\, \Theta_{\rm alg}$$

$$= \frac{\alpha_s w^2 C_i}{\pi} \frac{e^{\gamma_E \epsilon}}{\Gamma(1-\epsilon)} \left(\frac{\nu r}{\mu}\right)^\eta \frac{1}{\eta} \frac{1}{2\pi\mu^2} \left(\frac{\mu^2}{\mathbf{p}_\perp^2}\right)^{1+\epsilon+\eta/2}, \tag{4.31}$$

where $\Theta_{\rm alg}$ defines the jet algorithm, $r \equiv \tan(\mathrm{R}/2)$, and $C_q = C_F,\ C_g = C_A$. After an expansion in η followed by an expansion in ϵ and summing both diagrams we get,

$$S_C^{i,B}(\mathbf{p}_\perp,\mu,\nu) = \delta^{(2)}(\mathbf{p}_\perp) + \frac{\alpha_s w^2 C_i}{\pi}\Big\{\frac{2}{\eta}\left(-\frac{1}{2\epsilon}\delta^{(2)}(\mathbf{p}_\perp) + \mathcal{L}_0(\mathbf{p}_\perp^2,\mu^2)\right)$$
$$+ \delta^{(2)}(\mathbf{p}_\perp)\left(\frac{1}{2\epsilon^2} + \frac{1}{2\epsilon}\ln\left(\frac{\mu^2}{r^2\nu^2}\right)\right) - \mathcal{L}_0(\mathbf{p}_\perp^2,\mu^2)\ln\left(\frac{\mu^2}{r^2\nu^2}\right) + \mathcal{L}_1(\mathbf{p}_\perp^2,\mu^2)$$
$$- \frac{\pi^2}{24}\delta^{(2)}(\mathbf{p}_\perp)\Big\}, \tag{4.32}$$

The renormalized result (where we have now set $w \to 1$)in the $\overline{\rm MS}$ scheme is thus

$$S_C^{i,R}(\mathbf{p}_\perp,\mu,\nu) = \delta^{(2)}(\mathbf{p}_\perp) - \frac{\alpha_s C_i}{\pi}\Big\{\mathcal{L}_0(\mathbf{p}_\perp^2,\mu^2)\ln\left(\frac{\mu^2}{r^2\nu^2}\right) - \mathcal{L}_1(\mathbf{p}_\perp^2,\mu^2) + \frac{\pi^2}{24}\delta^{(2)}(\mathbf{p}_\perp)\Big\}. \tag{4.33}$$

While in general this expression receives contributions from virtual gluon emission diagrams at NLO, these diagrams yield scaleless integrals when using this particular set of regulators. Thus virtual diagrams are neglected and all singularities from these real emission diagrams are interpreted as UV divergences. We also verified, using a set of regulators where such virtual gluons give non-zero contributions, that the result is identical.[1] Note if pure dimensional regularization is used for ultraviolet and infrared divergences then $H_+ = (2\pi)^2 N_c$ as discussed in Ref. [101].

4.3 Numerical Results

4.3.1 Renormalization Group (RG) and Rapidity Renormalization Group (RRG)

Individual diagrams for the collinear-soft function S_C and the matching coefficients $\mathcal{J}_{i/j}$ suffer from infra-red (IR), ultra-violet (UV) and rapidity divergences (RD). We use dimensional regularization and a rapidity regulator (as introduced and developed in Ref. [103, 111]) to regulate these divergences. IR divergences in the collinear-soft

[1] In order to verify that all IR divergences do indeed cancel, we used a gluon mass, rapidity regulator, and dimensional regulator where diagrams with virtual gluons give non-scaleless contributions.

function cancel when summing over all diagrams. In the matching coefficients $\mathcal{J}_{i/j}$, IR divergences cancel in the matching of the collinear functions $\mathcal{D}_{i/h}$ onto traditional FFs, $D_{j/h}$. The remaining poles (UV and rapidity), are removed by renormalization. In addition to the scale μ introduced by dimensional regularization our use of a rapidity regulator requires the introduction of an additional scale, ν. With this scale are associated rapidity renormalization group (RRG) equations which can be used to resum large logarithms by evolving each function from its canonical scale to a common scale. Bare and renormalized quantities are related through the following convolution with the renormalization factor Z,

$$F^B(\mathbf{p}_\perp) = Z_F(\mathbf{p}_\perp, \mu, \nu) \otimes_\perp F^R(\mathbf{p}_\perp, \mu, \nu), \tag{4.34}$$

where F can be either $\mathcal{D}_{i/h}$ or S_C^i and satisfies the following RG and RRG equations,

$$\begin{aligned}
\frac{d}{d\ln\mu} F^R(\mathbf{p}_\perp, \mu, \nu) &= \gamma_\mu^F(\mu, \nu) \times F^R(\mathbf{p}_\perp, \mu, \nu) \\
\frac{d}{d\ln\nu} F^R(\mathbf{p}_\perp, \mu, \nu) &= \gamma_\nu^F(\mathbf{p}_\perp, \mu, \nu) \otimes_\perp F^R(\mathbf{p}_\perp, \mu, \nu).
\end{aligned} \tag{4.35}$$

Here γ_μ^F and γ_ν^F are the anomalous dimensions associated to RG and RRG respectively and are defined by,

$$\begin{aligned}
\Big[(2\pi)^2\delta^{(2)}(\mathbf{p}_\perp)\Big] \times \gamma_\mu^F(\mu, \nu) &= -Z_F^{-1}(\mathbf{p}_\perp, \mu, \nu) \otimes_\perp \frac{d}{d\ln\mu} Z_F(\mathbf{p}_\perp, \mu, \nu) \\
\gamma_\nu^F(\mathbf{p}_\perp, \mu, \nu) &= -Z_F^{-1}(\mathbf{p}_\perp, \mu, \nu) \otimes_\perp \frac{d}{d\ln\nu} Z_F(\mathbf{p}_\perp, \mu, \nu).
\end{aligned} \tag{4.36}$$

For the renormalization factors we find,

$$\begin{aligned}
Z^{\mathcal{D}}(\mathbf{p}_\perp, \mu, \nu) =& (2\pi)^2\delta^{(2)}(\mathbf{p}_\perp) + (4\pi)\alpha_s w^2 C_F \Big\{ -\frac{2}{\eta}\left(-\frac{1}{2\epsilon}\delta^{(2)}(\mathbf{p}_\perp) + \mathcal{L}_0(\mathbf{p}_\perp^2, \mu^2)\right) \\
&+ \frac{1}{2\epsilon}\left(\ln\left(\frac{\nu^2}{\omega^2}\right) + \bar{\gamma}_i\right)\delta^{(2)}(\mathbf{p}_\perp)\Big\}
\end{aligned} \tag{4.37}$$

$$Z^{S_C}(\mathbf{p}_\perp,\mu,\nu) =(2\pi)^2\delta^{(2)}(\mathbf{p}_\perp) + (4\pi)\alpha_s w^2 C_F\Big\{ + \frac{2}{\eta}\left(-\frac{1}{2\epsilon}\delta^{(2)}(\mathbf{p}_\perp) + \mathcal{L}_0(\mathbf{p}_\perp^2,\mu^2)\right)$$
$$+ \frac{1}{2\epsilon}\left(\ln\left(\frac{\mu^2}{r^2\nu^2}\right) + \frac{1}{\epsilon}\right)\delta^{(2)}(\mathbf{p}_\perp),\Big\} \tag{4.38}$$

The μ anomalous dimensions are found using Eq. (4.36),

$$\gamma_\mu^{\mathcal{D}}(\nu) = \frac{\alpha_s C_i}{\pi}\left(\ln\left(\frac{\nu^2}{\omega^2}\right) + \bar{\gamma}_i\right) \tag{4.39}$$

$$\gamma_\mu^{S_C}(\nu) = \frac{\alpha_s C_i}{\pi}\ln\left(\frac{\mu^2}{r^2\nu^2}\right), \tag{4.40}$$

For the ν anomalous dimensions, our bookkeeping parameter w plays an analogous role to the coupling g for the case of the μ anomalous dimension, although w itself is not a coupling, such that,

$$\nu\frac{\partial}{\partial\nu}w = -\frac{\eta}{2}w, \tag{4.41}$$

thus yielding

$$\gamma_\nu^{\mathcal{D}}(p_\perp,\mu) = -(8\pi)\alpha_s C_i\ \mathcal{L}_0(\mathbf{p}_\perp,\mu^2) \tag{4.42}$$

$$\gamma_\nu^{S_C}(p_\perp,\mu) = +(8\pi)\alpha_s C_i\ \mathcal{L}_0(\mathbf{p}_\perp,\mu^2). \tag{4.43}$$

The anomalous dimensions satisfy

$$\gamma_\mu^{\mathcal{D}}(\nu) + \gamma_\mu^{S_C}(\nu) = \gamma_\mu^J = \frac{\alpha_s C_i}{\pi}\left(\ln\left(\frac{\mu^2}{r^2\omega^2}\right) + \bar{\gamma}_i\right), \tag{4.44}$$

where γ_J is the anomalous dimension of the unmeasured quark jet function [65] and

$$\gamma_\nu^{\mathcal{D}}(\mathbf{p}_\perp,\mu) + \gamma_\nu^{S}(\mathbf{p}_\perp,\mu) = 0. \tag{4.45}$$

In order to resum our results to NLL' accuracy we evolve the purely collinear function and the collinear-soft function from their characteristic scales where logarithms are minimized to common scales in μ and ν using the RG and RRG respectively. To

perform the evolution, we first solve the Fourier transforms of both the RRG and RG equations. We then perform the evolution using the RG and RRG before finally performing the inverse Fourier transform. The simplest resummation procedure is, in this case, to first evolve our collinear-soft function in RRG space and choose the common scale to be $\nu = \nu_{\mathcal{D}}$. We then evolve both functions in RG space to the common scale $\mu = \omega r$. Notice that S_C and $\mathcal{D}$ have the same characteristic renormalization scale $\mu_{S_C} = \mu_{\mathcal{D}} \equiv \mu_C$. The equivalence of the virtualities of the soft and collinear modes is a defining feature of SCET_{II}.

To make the interpretation of our plots easier, we study the quantity $\mathcal{G}_{i/h}(p_\perp, z, \mu)$ which is related to the TMDFJF by the change of variables from vector transverse momenta ($\mathbf{p}_\perp$) to the amplitude ($p_\perp = |\mathbf{p}_\perp|$). Performing the evolutions described above we find,

$$\mathcal{G}_{i/h}(p_\perp, z, \mu) = (2\pi)^2\, p_\perp \int_0^\infty db\, bJ_0(bp_\perp)\mathcal{U}_{S_C}(\mu, \mu_{S_C}, m_{S_C})\mathcal{U}_{\mathcal{D}}(\mu, \mu_{\mathcal{D}}, 1)$$
$$\times\, \mathcal{V}_{S_C}(b, \mu_{S_C}, \nu_{\mathcal{D}}, \nu_{S_C})\mathcal{FT}\Big[\mathcal{D}_{i/h}(\mathbf{p}_\perp, z, \mu_{\mathcal{D}}, \nu_{\mathcal{D}}) \otimes_\perp S_C^i(\mathbf{p}_\perp, \mu_{S_C}, \nu_{S_C})\Big], \quad (4.46)$$

where $\boldsymbol{b}$ is the Fourier conjugate variable of $\mathbf{p}_\perp$, J_0 is a Bessel function of the first kind,

$$\mathcal{U}_F(\mu, \mu_0, m_F) = \exp\left(K_F(\mu, \mu_0)\right)\left(\frac{\mu_0}{m_F}\right)^{\omega_F(\mu,\mu_0)}, \quad (4.47)$$

$$\text{and}\;\; \mathcal{V}_F(b, \mu, \nu, \nu_0) = \left(\frac{\mu}{\mu_C(b)}\right)^{\eta_F(\mu,\nu,\nu_0)} \quad \text{where} \quad \mu_C(b) = 2\exp(-\gamma_E)/b, \quad (4.48)$$

are the evolution kernels resulting from solving the RG and RRG equations respectively. The pure collinear term $\mathcal{D}_{i/h}$ in Eq.(4.46) involves the convolution of the perturbatively calculated short distance coefficients and the standard fragmentation functions evolved from their canonical scale to the canonical scale of the collinear term in momentum space, $\mu = p_\perp$. The form of the fragmentation functions is fixed

during the Fourier transforms in Eq.(4.46). The scales μ_F, ν_F and m_F for each of the functions are given in Table 4.1 and more details of the RG and RRG evolution are provided in Appendix A.

Table 4.1: Characteristic scales of the different functions in the factorization theorem.

Function (F)	RG scale (μ_F)	RRG scale (ν_F)	m_F
$\mathcal{D}_{i/h}$	$\mu_C(b)$	ω	n.a.
S_C^i	$\mu_C(b)$	$\mu_C(b)/r$	νr

4.3.2 Applications to quarkonium production

In this section we apply our TMDFJF formalism to the production of quarkonium in jets. We will focus on J/ψ production within jets initiated by gluons, though our results can be easily generalized to Υ or other quarkonia and jets initiated by quarks. Our goal is to see if the z and $p_\perp$ dependence of the TMDFJF can discriminate between these competing mechanisms.

The TMDFJF as a function of $p_\perp$ for fixed z, for $z = 0.3, 0.5, 0.7$, and 0.9, are shown Figs. 4.4 and 4.5, for jet energies of 100 GeV and 500 GeV, respectively. In order to make it easier to view all distributions simultaneously, we have rescaled the ${}^3S_1^{[8]}$, ${}^1S_0^{[8]}$, ${}^3P_J^{[8]}$,and ${}^3S_1^{[1]}$ distributions, by factors of 10^6, 10^6, $3.0\,10^5$ and $4.0\,10^5$, respectively. The same rescaling factor is used in all eight plots in Figs. 4.4 and 4.5, and theoretical uncertainties are calculated by varying the RRG and RG scales ν_{S_C}, $\nu_{\mathcal{D}}$, and μ by a factor of 2 and 1/2. The central dashed lines in the figures correspond to the scale choices $\nu = \nu_{\mathcal{D}} = \omega$ and $\mu = \omega r$. Though we plot our distributions in the range $0 < p_\perp < 20$ GeV, it is important that to keep in mind that our calculations are only reliable for $p_\perp \geqslant 2m_c = 3$ GeV.

These plots show that the TMDFJF does in fact provide discriminating power

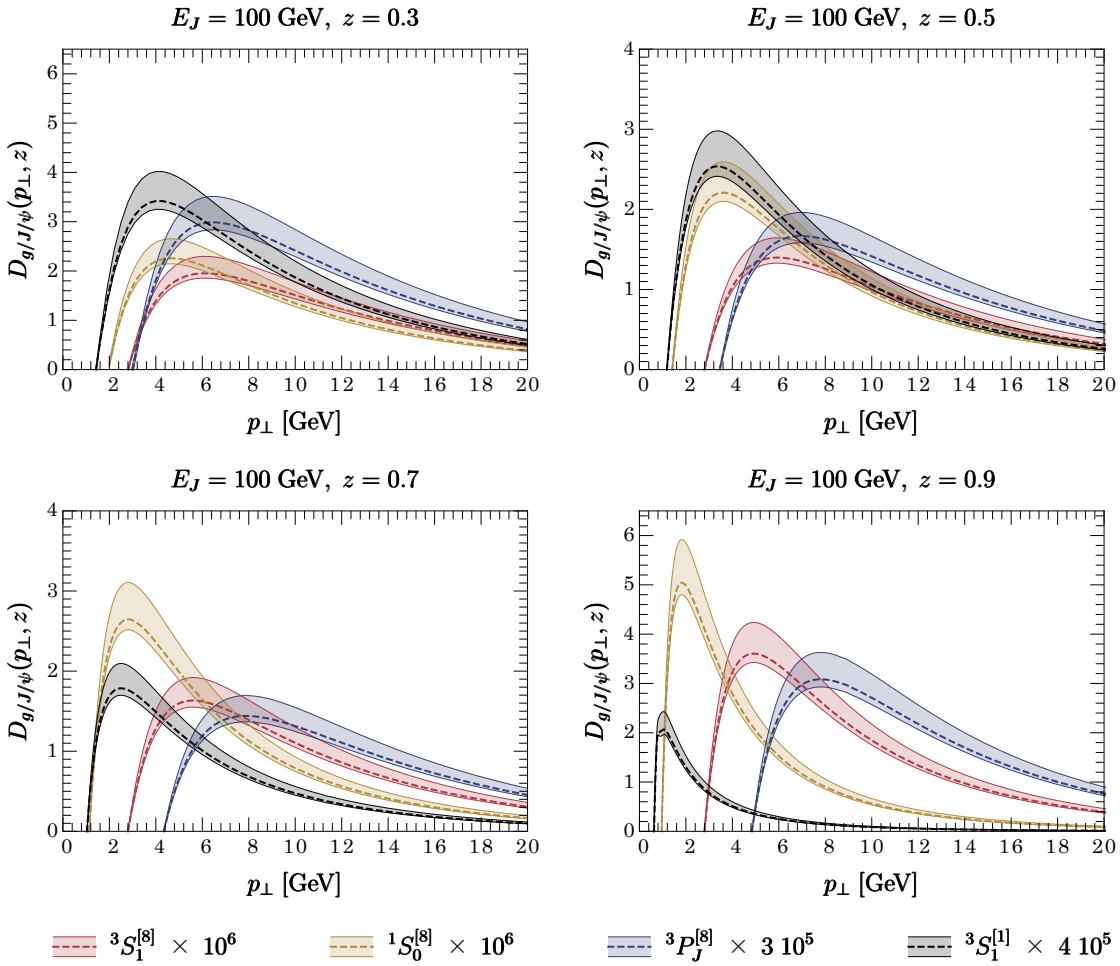

FIGURE 4.4: The TMDFJF as a function of the $p_\perp$ of the J/ψ for the $^3S_1^{[1]}, ^3S_1^{[8]}, ^1S_0^{[8]}, ^3P_J^{[8]}$ production mechanisms where the for jet energies $E_J = 100$ GeV. Theoretical uncertainties are calculated by varying the renormalization scales by factors of 1/2 and 2.

amongst the four mechanisms. For $z = 0.3$, all four distributions look similar for both $E_J = 100$ GeV and 500 GeV. The distributions peak at roughly the same location and they have same slope for large $p_\perp$. For $z \geqslant 0.5$, the color-singlet $^3S_1^{[1]}$ mechanism and the color-octet $^1S_0^{[8]}$ mechanism peak at lower values of $p_\perp$ and fall more steeply with $p_\perp$ than the $^3S_1^{[8]}$ and $^3P_J^{[8]}$ color-octet mechanisms. The $^3P_J^{[8]}$ mechanism has the peculiar feature that in order to obtain a positive FF we need to have a negative LDME, as is found in the fits of Refs. [2, 3]. The peaks in the $p_\perp$ distribution for

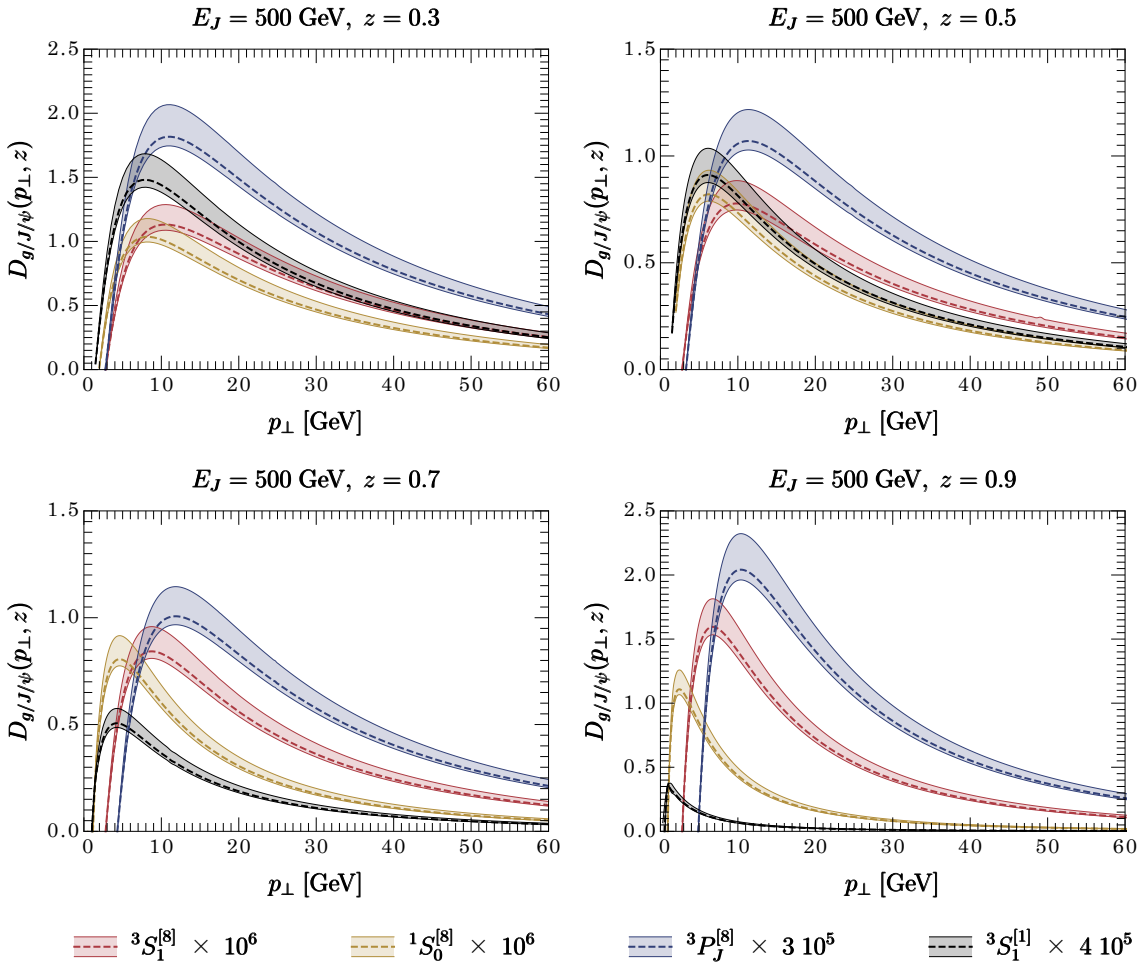

FIGURE 4.5: The TMDFJF as a function of the $p_\perp$ of the J/ψ for the $^3S_1^{[1]}, ^3S_1^{[8]}, ^1S_0^{[8]}, ^3P_J^{[8]}$ production mechanisms where the for jet energies $E_J = 500\,\text{GeV}$. Theoretical uncertainties are calculated by varying the renormalization scales by factors of 1/2 and 2.

the $^3S_1^{[1]}$ and $^1S_0^{[8]}$ mechanisms are at very low $p_\perp$ where perturbation theory is not reliable. On the other hand, the peaks of the $^3S_1^{[8]}$ and $^3P_J^{[8]}$ distributions are at larger values of $p_\perp \sim 6 - 8$ GeV where perturbation theory can be trusted. The $^3P_J^{[8]}$ gives a slightly harder $p_\perp$ distribution than $^3S_1^{[8]}$ mechanism, and both are significantly harder than the other mechanisms.

It is interesting to study the dependence of the TMDFJF as a function of z with $p_\perp$ fixed to be a perturbative scale. In Fig. 4.6 we plot the TMDFJF as a function

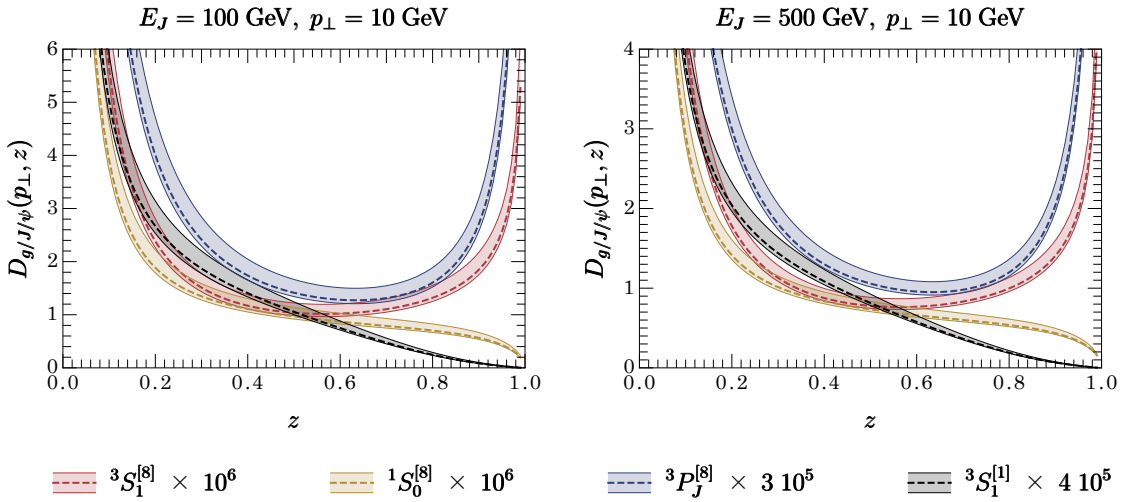

FIGURE 4.6: The TMDFJF as a function of the z of the J/ψ for the ${}^3S_1^{[1]}, {}^3S_1^{[8]}, {}^1S_0^{[8]}, {}^3P_J^{[8]}$ production mechanisms, with $p_\perp = 10$ GeV for $E_J = 100$ and 500 GeV. Theoretical uncertainties are calculated by varying the renormalization scales by factors of 1/2 and 2.

of z for $p_\perp = 10$ GeV for jets with energy $E_J = 100$ and 500 GeV. Large logarithms and shape function effects will affect these distributions in both the $z \to 0$ and $z \to 1$ limits, but our calculations should be reliable for intermediate values of z. While for $z < 0.5$ the distributions have similar shapes, in the range $0.5 < z < 0.9$, the shapes of all four mechanisms are different. The z dependence of the TMDFJF for fixed $p_\perp$ can be used to differentiate between the NRQCD production mechanisms.

The TMDFJF formalism also allows us to calculate the angle at which J/ψ are produced relative to the jet axis. The average production angle for the J/ψ is given by

$$\langle\theta\rangle(z) = \frac{\int \theta d\theta (d\sigma/d\theta dz)}{\int d\theta (d\sigma/d\theta dz)}. \tag{4.49}$$

Using the small angle approximation the differential cross section can be written as

$$\frac{d\sigma}{d\theta dz} = \int dp_\perp \, \delta\left(\theta - \frac{2p_\perp}{z\omega}\right) \frac{d\sigma}{dp_\perp dz}. \tag{4.50}$$

Substituting this into Eq. 4.49 yields

$$\langle\theta\rangle(z) = \frac{2\int dp_\perp p_\perp (d\sigma/dp_\perp dz)}{z\omega\int dp_\perp (d\sigma/dp_\perp dz)}. \tag{4.51}$$

As discussed in Appendix C.1, the cross section $d\sigma/d\theta dz$ can be factorized into hard, soft and collinear terms in SCET. In general the hard and soft contributions will not cancel because there is a sum over partonic channels in both the numerator and denominator of Eq. 4.51. However, they will if gluon fragmentation dominates production, then the expression above can be written as

$$\langle\theta\rangle(z) \sim \frac{2\int dp_\perp\ p_\perp \mathcal{G}_{g/h}(p_\perp, z, \mu)}{z\omega\int dp_\perp\ \mathcal{G}_{g/h}(p_\perp, z, \mu)} \equiv f_\omega^h(z), \tag{4.52}$$

where $\mathcal{G}_{g/h}(p_\perp, z, \mu)$ is the gluon TMDFJF. Fig. 4.7 the function $f_\omega^{J/\psi}(z)$ is plotted at points $z = 0.3, 0.5, 0.7$, and 0.9 for $\omega = 2E_J = 200\,\text{GeV}$ and $1\,\text{TeV}$ for J/ψ with $p_\perp \in [5, 20]$ GeV and $p_\perp \in [5, 60]$ GeV, respectively. As was done earlier we have fixed the scale $\mu = \omega r$. Note the typical angles are small enough that the small angle approximation is justified. The dashed lines in figure show the results of a fit to the functional form, $C_0 \exp(-z\, C_1)$, the values of C_0 and C_1 for each mechanism at each energy are shown in Table 4.2. Again we see that differences between the various NRQCD mechanisms become more pronounced as z increases. This shows that the average angle does in fact yield some discriminating power between the octet mechanisms. In particular the slope on the semilog plot, which is determined by the parameter C_1 in Table 4.2, differs by as much as 20% between the various NRQCD mechansims for $E_J = 100$ GeV and and as much as 40% for $E_J = 500$ GeV. Note however that ${}^1S_0^{[8]}$ and ${}^3S_1^{[1]}$ give very similar predictions for this observable.

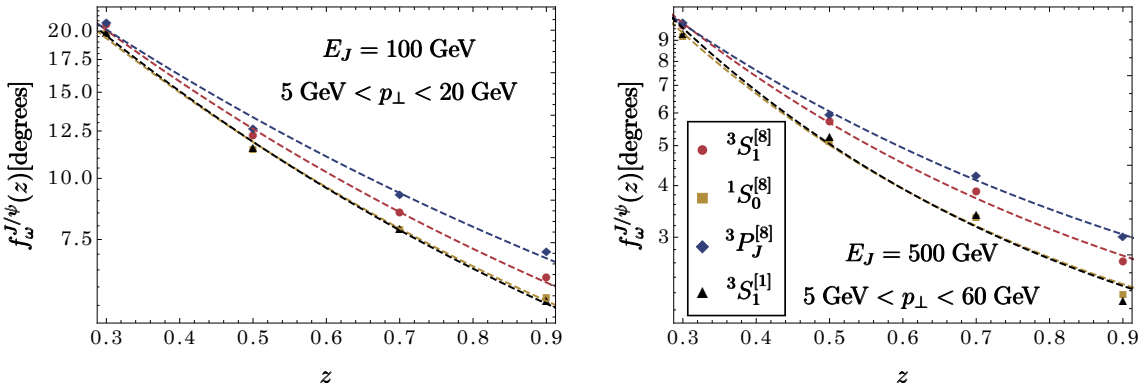

FIGURE 4.7: The function $f_\omega^{J/\psi}(z)$ (as defined in the text) as a function of z relative to the jet axis for each NRQCD production mechanism where the jet has $E_J = \omega/2 =$ 100 GeV(left) and 500 GeV (right). The J/ψ is restricted to have $p_\perp \in [5, 20]$ GeV in the 100 GeV jet and $p_\perp \in [5, 60]$ GeV in the 500 GeV jet.

Table 4.2: Results of fits of $\ln(f_\omega(z))$ shown in Fig. 4.7 to the function $C_0 \exp(-z\, C_1)$.

$E_J = 100$ GeV		
$^{2S+1}L_J^{[1,8]}$	C_0	C_1
$^3S_1^{[1]}$	3.92	0.92
$^3S_1^{[8]}$	3.86	0.84
$^1S_0^{[8]}$	3.88	0.90
$^3P_J^{[8]}$	3.75	0.74

$E_J = 500$ GeV		
$^{2S+1}L_J^{[1,8]}$	C_0	C_1
$^3S_1^{[1]}$	3.75	1.68
$^3S_1^{[8]}$	3.48	1.39
$^1S_0^{[8]}$	3.66	1.64
$^3P_J^{[8]}$	3.28	1.20

4.4 Conclusions

In this chapter we introduce the transverse momentum dependent fragmenting jet function (TMDFJF) in the framework of SCET and show how it is related to the previously introduced TMDFFs and fragmenting jet functions (FJFs). TMDFJFs describe the transverse as well as longitudinal momentum distribution of an identified hadron within a jet. TMDFJFs evolve with the renormalization group (RG) scale μ and obey RG equations similar to jet functions. Using SCET$_+$ we show that this new distribution can be further factorized into soft and purely collinear terms. The purely

collinear factor can be written as a convolution of perturbatively calculable short distance coefficients and the standard FFs, where the soft factor is given by a vacuum matrix element of product of Wilson lines. This factorization introduces rapidity divergences that are regulated with the rapidity regulator. We check that at NLO the regulator dependence vanishes in the final product. Associated with rapidity divergences are rapidity renormalization group (RRG) equations. By evolving the collinear and soft terms separately using the RG and RRG equations all orders resummation of large logarithms in the TMDFJF can be performed.

As an example we implement this formalism for the case of quarkonium production. In the case of quarkonia the TMDFJF can be calculated in terms of the NRQCD FFs which are perturbatively calculable at the scale $2m_Q$. For the gluon TMDFJF for J/ψ, we study the $p_\perp$ and z dependence predicted by the four production mechanisms: ${}^3S_1^{[1]}$, ${}^3S_1^{[8]}$, ${}^1S_0^{[8]}$, and ${}^3P_J^{[8]}$. We use the leading order (in α_S) NRQCD FF for each of these mechanisms, and the RG and RRG equations are used to calculate the TMDFJFs to next-to-leading-logarithmic-prime (NLL') accuracy. We find that the z dependence (for fixed $p_\perp$) is different for all four mechanisms. We also find that the dependence on $p_\perp$ and the average angle of the J/ψ relative to the jet axis can discriminate between the various NRQCD production mechanisms.

5

Jet Shapes in Dijet Events at the LHC in SCET

5.1 Outline

Jet measurements at hadron colliders typically involve identifying jets of size $\mathcal{R}$ with the use of a jet algorithm, imposing a veto on the out-of-jet transverse momentum $p_T^{\rm cut}$ for all radiation[1] with (pseudo-)rapidity y in the range $|y| < y_{\rm cut}$ measured with respect to the beam axis. Such measurements are sensitive to hard scales (such as the Mandelstam variables s, t, u in the case of dijet production) in addition to scales induced by the parameters $\mathcal{R}$, $y_{\rm cut}$, and $p_T^{\rm cut}$. When the substructure of jets is probed in the context of a jet measurement, additional scales such as Qe and Qe^α for jet shapes are induced. Thus, there are not only scales associated with the substructure itself but also those associated with the more global context with which the probed jet was produced, and the large set of scales involved can span a wide range of energies.

Many of the ratios of these scales can be resummed using well known techniques such as SCET in similar ways to those described above for e^+e^-. In addition to

[1] As discussed below, to the order we work this is the same as putting a veto on the third hardest jet.

the ingredients used in e^+e^- collisions, factorization formulae for hadronic collisions involve beam functions B which account for initial-state radiation [112, 113], and we schematically have

$$d\sigma^{pp} \sim H \times B \otimes \bar{B} \otimes J_{n_1} \otimes \cdots \otimes J_{n_N} \otimes S_{B\bar{B}n_1n_2\cdots} \,. \tag{5.1}$$

While RGE of the functions appearing in Eq. (5.1) resums a large set of logarithms, others, such as logarithms of $\mathcal{R}$ [114–116] and non-global logarithms (NGLs) [117–120], can present more of a challenge. Importantly, resummation of the jet size $\mathcal{R}$ has recently been explored in the context of subjets in [121] and in jet rates in the context of e^+e^- collisions in [5,122], and in addition there has been progress in understanding NGLs both at fixed-order [123–126] and more recently a few novel approaches to understanding their all-orders resummation have been proposed [122, 127, 128].

In this chapter we consider the case where the kinematics are such that NGLs are not enhanced and instead focus on resummation of logarithms of ratios of the dynamical scales associated with substructure (such as Qe/Q and Qe^α/Q) with fixed p_T^{cut}, y_{cut}, $\mathcal{R}$, and jet p_T^J. To this end, we restrict ourselves to the kinematic region

$$\begin{aligned} e^{-y_{\text{cut}}} &\ll 1 \\ p_T^J \sim \sqrt{\hat{s}} &\sim \sqrt{\hat{t}} \sim \sqrt{\hat{u}} \\ p_T^{\text{cut}}\mathcal{R}^2/p_T^J \sim e &\ll \mathcal{R}^2 \ll 1 \,. \end{aligned} \tag{5.2}$$

Our approximations are valid to the order we work within about a decade of the value(s) of these parameters for which the NGLs are minimized. In the example we present, we have $e \sim \mathcal{O}(10^{-3})$ in the peak region of the distribution and $\mathcal{R}^2 \sim \mathcal{O}(10^{-1})$, which means the leading NGLs, which are of the form $\alpha_s^n \ln^n(p_T^{\text{cut}}\,\mathcal{R}^2/p_T^J\, e)$ (and first appear for $n \geqslant 2$), are not enhanced for $p_T^{\text{cut}}/p_T^J \sim \mathcal{O}(10^{-2})$.

One class of event shapes that has been studied extensively in the literature and is the focus of the present work is that of angularities τ_a, parameterized by a continuous

variable a (with $a < 2$ for IR safety). The choice $a = 0$ corresponds to the classic event shape thrust and $a = 1$ corresponds to jet broadening. Angularities were originally defined in [77, 129] and studied in the context of SCET in [130–132]. In Ref. [65], "jet shapes"[2] were defined by restricting the angularities to the constituents of a jet as defined by a jet algorithm (as opposed to all particles in the event) and were resummed to next-to-leading logarithmic (NLL) accuracy. In this work we consider a modified definition of angularities that is designed to be boost invariant about the colliding hadrons' axis, i.e., the beam axis.

We also note that the definition of the angularities we consider (which differs from that defined for e^+e^- colliders by a rescaling in the small τ_a limit) is such that the choice $a = 0$ is closely related to the jet mass,

$$\tau_0 = m_J^2/(p_T^J)^2 + \mathcal{O}(\tau_0^2)\,. \tag{5.3}$$

Jet mass resummation has been studied indirectly by looking at the 1-jettiness global event shape [137] for single jet events in Ref. [138], by using pQCD methods that neglect color interference effects in Ref. [139], and in the threshold limit in Refs. [140, 141], but to our knowledge has not been studied with the cuts described above, with full NLL' color interference effects[3], and in a manner that is valid away from the threshold limit. In addition, our results for $a = 0$ can be straightforwardly extended to NNLL using the known anomalous dimensions together with the recently deduced two-loop unmeasured jet function anomalous dimension [5], which controls the evolution of both unmeasured jet and beam functions. In addition, we apply the refactorization procedure described in Ref. [5] which allows the resummation of logarithms of $\mathcal{R}$ in the region described by Eq. (5.2).

While we choose to study angularities as the choice of substructure observable,

[2] This is distinct from *the jet shape* as defined in [133,134] and studied more recently in Ref. [135, 136].

[3] For an explanation of which terms are included in our cross section by working to this order, see for example Ref. [66].

our basic setup is much more general. Indeed, we obtain many of the results specific to our choice of angularities by using identities that relate the jet functions and the observable-dependent part of our soft function to analogous calculations in e^+e^- collisions. The part of the soft function that requires an entirely new calculation simply imposes the experimental p_T^{cut} cut on radiation outside of the jets and the beams. This universal part of the soft function, labeled $\mathbf{S}^{\text{unmeas}}$, encapulates all the interjet cross-talk, and hence contains all perturbative information associated with real emission about the directions n_i and the color flow. For each jet which has the angularity probed, which here and below we refer to (using the terminology of Ref. [65]) as a "measured jet," we add a jet function and a soft function contribution that are both angularity dependent but color- and direction-trivial. Thus, other substructure measurements can be straightforwardly incorporated by substituting for their appropriate contributions at this step. If no measurement is performed on a jet (that is, the jet is identified but otherwise unprobed), which we refer to as an "unmeasured jet," only an unmeasured jet function (which we also present to $\mathcal{O}(\alpha_s)$) and $\mathbf{S}^{\text{unmeas}}$ are required. For dijet production, which is the focus of the current work, all four Wilson lines (those of the beams and the two jets) are confined to a plane, and the calculation of $\mathbf{S}^{\text{unmeas}}$ to $\mathcal{O}(\alpha_s)$ is tractable. In addition, the effect of different experimentally used vetoes, such as putting a p_T^{cut} only on the third hardest jet (as opposed to all out-of-jet radiation) will only result in a difference in $\mathbf{S}^{\text{unmeas}}$ at $\mathcal{O}(\alpha_s^2)$ so our calculations apply there as well.

We also point out that while for unmeasured jets, the jet size $\mathcal{R}$ must scale with the SCET power counting parameter λ and hence the requirement $\mathcal{R} \ll 1$ is essential, for measured jets this is not strictly needed since $\tau_a \ll 1$ is sufficient to ensure SCET kinematics. However, as we will see, both the jet algorithms and measurements simplify significantly in this limit up to power corrections of the form $\mathcal{R}^2$ and $\tau_a/\mathcal{R}^2$, respectively, although we emphasize that the exact results can be obtained

numerically using subtractions such as those of Ref. [142]. Finally, we note that because there is no measurement on any radiation with $|y| < y_{\rm cut}$, our factorization formulae will include "'unmeasured beam functions," which to our knowledge have not appeared in the literature.

The chapter is organized as follows. In Sec. 5.2, we define the classes of jet algorithms and angularity definitions suitable for hadron colliders and relate them to the corresponding e^+e^- algorithms and angularities in the small $\mathcal{R}$ limit. In Sec. 5.3 we outline the $2 \to 2$ kinematic relations needed for dijet production and discuss how both the Born cross section and the fully factorized and resummed SCET cross section are related to the basic building blocks that we then calculate to fixed order in Sec. 5.4, namely the hard, jet, soft, and beam functions. We then use these results in Sec. 5.5 to arrive at the NLL' resummed cross section for a generic $2 \to 2$ scattering channel both for when the jets are identified but otherwise left unmeasured (i.e., we are inclusive in the substructure properties) and for when the angularity of either (or both) jets is measured. From our calculations, one can obtain results for the case where the angularities of both jets τ_a^1 and τ_a^2 are separately measured (and by integrating, the case where $\tau_a^1 + \tau_a^2$ is measured) as well as the cases where only one or neither are measured. For illustrative purposes, in our plots we focus on the case where both τ_a^1 and τ_a^2 are measured and $\tau_a^1 = \tau_a^2$. Furthermore, we present explicit results for the simple channel $qq' \to qq'$ with different values of $\mathcal{R}$ and $p_T^{\rm cut}$ and for several choices of the angularity parameter a, and demonstrate the reduction in scale uncertainty resulting from the refactorization techniques of [5]. We conclude in Sec. 5.6. The material of this chapteris collaborative work with Andrew Horning and Thomas Mehen and was published in Ref. [58].

5.2 Jet Algorithms and Shapes at Hadron Colliders

The main difference between jet cross section measurements at e^+e^- colliders and hadron colliders is that the latter prefer observables that are invariant under boosts along the beam direction. The k_T-type algorithms used at the LHC (described in more detail in, for example, Ref. [143]) merge particles successively using a pairwise metric

$$\rho_{ij} = \min\{(p_T^i)^{2p}, (p_T^j)^{2p}\}\frac{\Delta\mathcal{R}_{ij}^2}{\mathcal{R}^2}\,, \tag{5.4}$$

where $p = +1, 0$, and -1 for the k_T, C/A, and anti-k_T algorithms, respectively, p_T^i is the transverse momentum (with respect to the beam) of particle i, $\mathcal{R}$ is a parameter characterizing the jet size, and

$$\Delta\mathcal{R}_{ij} \equiv \sqrt{(\Delta y_{ij})^2 + (\Delta\phi_{ij})^2}\,, \tag{5.5}$$

where Δy_{ij} and $\Delta\phi_{ij}$ are the pseudo-rapidity and azimuthal angle differences of the particles measured with respect to the beam axis. Since pseudo-rapidities simply shift under boosts and azimuthal angles are invariant, $\Delta\mathcal{R}_{ij}$ is invariant under boosts along the beam direction. This pairwise metric is compared to the single particle metric of each particle, defined as

$$\rho_i = (p_T^i)^{2p}\,. \tag{5.6}$$

Two particles are merged if their pairwise metric is the smallest for the (ij) pair over all particle pairs and is less than both of the single particle metrics, i.e., $\rho_{ij} < \min\{\rho_i, \rho_j\}$. This latter constraint amounts to

$$\Delta\mathcal{R}_{ij} < \mathcal{R}\,. \tag{5.7}$$

In the following, we will work under the assumption that all particles in the jet are close to a jet axis at polar angle θ_J with respect to the beam axis such that $\Delta\mathcal{R}_{ij}$

can be expanded as

$$\Delta\mathcal{R}_{ij} = \frac{1}{\sin\theta_J}\sqrt{(\Delta\theta_{ij})^2 + \sin^2\theta_J(\Delta\phi_{ij})^2} + \mathcal{O}((\Delta\theta_{ij})^2, (\Delta\phi_{ij})^2)$$
$$= \frac{\theta_{ij}}{\sin\theta_J} + \mathcal{O}(\theta_{ij}^2)\,, \tag{5.8}$$

where in the first equality $\Delta\theta_{ij}$ and $\Delta\phi_{ij}$ are the angle differences in a spherical coordinate system with $\hat{z}$ in the beam axis direction, and θ_{ij} in the second equality is simply the angle between particles i and j. This implies we can impose an e^+e^--type polar angle restriction that particles are within a jet of size R and rescale the results by

$$R \to \mathcal{R}\sin\theta_J = \frac{\mathcal{R}}{\cosh y_J}\,, \tag{5.9}$$

where y_J is the jet pseudo-rapidity, up to $\mathcal{O}(\mathcal{R}^2)$ corrections. This allows us to recycle many of the results of Ref. [65]. The difference between our results and those obtained from the exact expression Eq. (5.5) can be obtained numerically, e.g., with the methods of Ref. [142], although the details are beyond the scope of the present work.

It is helpful to re-write the angularity definition used in Ref. [65] in the context of e^+e^- collisions in terms of ingredients that are boost invariant, such as p_T and the right-hand side of Eq. (5.8). To do so, first recall the definition used in terms of the pseudo-rapidities y_{iJ} and transverse momenta $p_\perp^{iJ}$ of particles *with respect to the jet axis*,

$$\tau_a^{e^+e^-} = \frac{1}{2E_J}\sum_{i\in\text{jet}} |p_\perp^{iJ}| e^{-(1-a)|y_{iJ}|}\,. \tag{5.10}$$

In the small angle approximation, we can write this as

$$\tau_a^{e^+e^-} = (2E_J)^{-(2-a)}(p_T)^{1-a}\sum_{i\in\text{jet}} |p_T^i|\left(\frac{\theta_{iJ}}{\sin\theta_J}\right)^{2-a}\left(1+\mathcal{O}(\theta_{iJ}^2)\right). \tag{5.11}$$

From the discussion above, all terms in the sum over particles are boost invariant. The one term that is not boost invariant is just the overall factor of $(2E_J)^{2-a}$. Therefore, we can arrive at a boost invariant version of τ_a suitable for hadron colliders with a simple rescaling by a dimensionless factor,

$$\begin{aligned}\tau_a \equiv \tau_a^{pp} &\equiv \frac{1}{p_T} \sum_{i \in \text{jet}} |p_T^i| (\Delta \mathcal{R}_{iJ})^{2-a} \\ &= \left(\frac{2E_J}{p_T}\right)^{2-a} \tau_a^{e^+e^-} + \mathcal{O}(\tau_a^2)\,. \end{aligned} \tag{5.12}$$

We emphasize again that the quantities on the right-hand side of the first line of Eq. (5.12) are manifestly invariant under boosts along the beam axis, and that the second line allows us to recycle many of the results of Ref. [65].

The one main difference between measurements done at e^+e^- colliders and hadron colliders that requires a novel calculation is the out-of-jet energy veto. In e^+e^- colliders, this is typically a cut on energy, whereas in hadron colliders it is typically a veto on transverse momentum: $p_T = E \sin\theta < p_T^{\text{cut}}$. This will require an entirely new soft function, which we present below.

5.3 Factorized Dijet Cross Section

For dijet production at tree-level, momentum conservation implies that there are just three non-trivial variables to describe the final state at tree level, which we can take to be the jet (pseudo-) rapidities $y^{1,2}$ and the jet $p_T = |\mathbf{p}_T^1| = |\mathbf{p}_T^2|$. The momentum fractions of the incoming partons are related to these variables via

$$x_{1,2} = \frac{2p_T}{\mathrm{E_{cm}}} \cosh\frac{\Delta y}{2} e^{\pm Y}\,, \tag{5.13}$$

where $\Delta y = y_1 - y_2$ is the rapidity difference of the two jets and $Y = (y_1 + y_2)/2$. The (partonic) Mandelstam variables can be written as

$$\begin{aligned} s &= 4p_T^2 \cosh^2 \frac{\Delta y}{2} \\ t &= -2p_T^2 e^{\Delta y/2} \cosh \frac{\Delta y}{2} \\ u &= -2p_T^2 e^{-\Delta y/2} \cosh \frac{\Delta y}{2} = -s - t \,. \end{aligned} \tag{5.14}$$

The tree-level matrix element squared can be written as

$$|\mathcal{M}_{\text{tree}}|^2 = \text{Tr}\{\mathbf{H}_0 \mathbf{S}_0\} \,, \tag{5.15}$$

where $\mathbf{H}_0$ and $\mathbf{S}_0$ are the tree-level hard and soft functions, respectively, so the Born cross section takes form

$$\frac{d\sigma_{\text{born}}}{dy_1 dy_2 dp_T} = \frac{p_T}{8\pi x_1 x_2 E_{\text{cm}}^4} \frac{1}{N} f_1(x_1, \mu) f_2(x_2, \mu) \, \text{Tr}\{\mathbf{H}_0 \mathbf{S}_0\} \tag{5.16}$$

where N is the normalization associated with averaging over initial particle quantum numbers (e.g., $N = 4N_c^2$ for quark scattering) and $f_i(x_i, \mu)$ is a PDF for parton i with momentum fraction x_i.

The effect of radiative corrections to Eq. (5.16) is described in the soft and collinear limits by higher-order hard, soft, beam, and jet functions. We consider the cases when both jets are unmeasured and when both jets are measured. When both jets are unmeasured the all-orders cross section takes the form

$$d\sigma \equiv \frac{d\sigma}{dy_1 dy_2 dp_T} \tag{5.17}$$

$$\begin{aligned} &= \frac{p_T}{8\pi x_1 x_2 E_{\text{cm}}^4} \frac{1}{N} B(x_1, \mu) \bar{B}(x_2, \mu) \, \text{Tr}\{\mathbf{H}(\mu) \mathbf{S}^{\text{unmeas}}(\mu)\} J_1(\mu) J_2(\mu) \\ &\quad + \mathcal{O}(\alpha_s \mathcal{R}^2, \alpha_s e^{-2y_{\text{cut}}}) \,, \end{aligned} \tag{5.18}$$

where the $J_i(\mu)$ are unmeasured jet functions and S^{unmeas} is the unmeasured soft

function. When both jets are measured, the cross section takes the form

$$\begin{aligned} d\sigma(\tau_a^1, \tau_a^2) &\equiv \frac{d\sigma}{dy_1 dy_2 dp_T d\tau_a^1 d\tau_a^2} \\ &= \frac{p_T}{8\pi x_1 x_2 E_{\rm cm}^4} \frac{1}{N} B(x_1,\mu)\bar{B}(x_2,\mu) \\ &\quad \times \mathrm{Tr}\{\mathbf{H}(\mu)\mathbf{S}(\tau_a^1,\tau_a^2,\mu)\} \otimes [J_1(\tau_a^1,\mu)J_2(\tau_a^2,\mu)] \\ &\quad + \mathcal{O}(\alpha_s \tau_a^i/\mathcal{R}^2, \alpha_s e^{-2y_{\rm cut}}) \,, \end{aligned} \tag{5.19}$$

where $\otimes$ represents the two convolutions over the $\tau_a^{1,2}$. The case of a single measured jet, with the other jet unmeasured, is the obvious generalization of Eqs. (5.17) and (5.19). The power corrections to Eqs. (5.17) and (5.19) can be included via matching to fixed order QCD. Resummation of logs of τ_a is achieved by RG evolution of each factorized component from its canonical scale (cf. Table 5.2) to the common scale μ. Both the hard and soft function are in general matrices (which here and below we will refer to with bold face) which are hermitian and of rank R equal to the number of linearly independent color operators associated with the hard process (e.g., $R = 2$ for $qq \to qq$, 3 for $qq \to gg$, and 8 for $gg \to gg$). These operators mix under RG evolution which is accounted for with matrix RG equations. The fixed order calculation of the components in Eqs. (5.17) and (5.19) and their RG evolution is the subject of the next sections.

5.4 Fixed-Order $\mathcal{O}(\alpha_s)$ Calculation of Factorized Components

5.4.1 Jet Functions

In Ref. [65], there are both "measured" and "unmeasured" jet functions, corresponding to jets whose angularity was measured as opposed to those that were identified but otherwise unprobed. The latter can be obtained using the hadron collider algo-

rithms with the rescaling in Eq. (5.9). We obtain

$$J_i = 1 + \frac{\alpha_s}{2\pi}\left[\left(\frac{C_i}{\epsilon^2} + \frac{\gamma_i}{\epsilon}\right)\left(\frac{\mu}{p_T \mathcal{R}}\right)^{2\epsilon} + d_J^{i,\mathrm{alg}}\right] \tag{5.20}$$

where $i = q, g$ for quark and gluon jets (and C_i is the Casimir invariant, $C_q = C_F$ and $C_g = C_A$), respectively, and

$$\gamma_q = \frac{3C_F}{2}\,, \quad \gamma_g = \frac{\beta_0}{2}\,. \tag{5.21}$$

(with β_0 given in Eq.(A.11)) and the finite corrections $d_J^{i,\mathrm{alg}}$ are given in Eqs. A.19 and A.30 of [65],

$$d_J^{i,\mathrm{cone}} = 2\gamma_i \ln 2 - C_i \frac{5\pi^2}{12} + \begin{cases} C_F \frac{7}{2} & \text{if } i = q \\ C_A \frac{137}{36} - T_R N_f \frac{23}{18} & \text{if } i = g \end{cases} \tag{5.22}$$

$$d_J^{i,k_T} = -C_i \frac{3\pi^2}{4} + \begin{cases} C_F \frac{13}{2} & \text{if } i = q \\ C_A \frac{67}{9} - T_R N_f \frac{23}{9} & \text{if } i = g \end{cases} \tag{5.23}$$

where d_J^{i,k_T} is the same constant for all k_T-type algorithms (k_T, anti-k_T, and C/A).

For measured jet functions, we need to apply the rescaling Eq. (5.12). The identity

$$A^{-1}\delta\big(A^{-1}\tau - \hat{\tau}\big) = \delta\big(\tau - A\hat{\tau}\big)\,, \tag{5.24}$$

implies that this rescaling can be accomplished to all orders via the transformation

$$J_i(\tau_a) = \left(\frac{p_T}{2E_J}\right)^{2-a} J_i^{e^+e^-}\left(\left(\frac{p_T}{2E_J}\right)^{2-a}\tau_a\right), \tag{5.25}$$

where $J_i^{e^+e^-}(\tau_a)$ is the jet function of [65]. This gives

$$J_i(\tau_a) = J_i^{e^+e^-}(\tau_a)\big|_{2E_J \to p_T}\,, \tag{5.26}$$

i.e., it is simply obtained from $J_i^{e^+e^-}(\tau_a)$ by making the replacement $2E_J \to p_T$. These can be obtained for the quark case from Ref. [132] and for the gluon case by

performing the integral in Eq. (4.22) of Ref. [65] after setting $\Theta_{\rm alg}(x) \to 0$ which is valid to $\mathcal{O}(\tau_a/\mathcal{R}^2)$. We record the results here as

$$J_i(\tau_a) = \delta(\tau_a) - \frac{\alpha_s}{2\pi}\left[\left(\frac{\mu}{p_T}\right)^{2\epsilon}\left(\frac{1}{\tau_a}\right)^{1+\frac{2\epsilon}{2-a}}\left(\frac{1}{\epsilon}\frac{2C_i}{1-a} + \frac{\gamma_i}{1-a/2}\right) - \delta(\tau_a) f_i(a)\right], \quad (5.27)$$

where

$$\begin{aligned} f_q(a) = \frac{2C_F}{1-a/2}\Bigg[&\frac{7-13a/2}{4} - \frac{\pi^2}{12}\frac{3-5a+9a^2/4}{1-a} \\ &- \int_0^1 dx\, \frac{1-x+x^2/2}{x}\ln[x^{1-a}+(1-x)^{1-a}]\Bigg] \end{aligned} \quad (5.28)$$

$$\begin{aligned} f_g(a) = \frac{1}{1-a/2}\Bigg[&C_A\Bigg((1-a)\left(\frac{67}{18}-\frac{\pi^2}{3}\right) + \frac{\pi^2}{6}\frac{(1-a/2)^2}{1-a} \\ &- \int_0^1 dx\, \frac{(1-x(1-x))^2}{x(1-x)}\ln[x^{1-a}+(1-x)^{1-a}]\Bigg) \\ &- T_R N_f\left(\frac{20-23a}{18} - \int_0^1 dx\, \big(2x(1-x)-1\big)\ln[x^{1-a}+(1-x)^{1-a}]\right)\Bigg]. \end{aligned}$$

Finally, we note that the integral over τ_a of the measured jet function is not simply related to the unmeasured jet function and refer the reader to Ref. [5] for a detailed explanation.

5.4.2 Unmeasured Beam Functions

While the unmeasured beam function has not to our knowledge appeared in the literature, it is directly related to the unmeasured fragmenting jet function of [70]. The unmeasured fragmenting jet function for a jet of energy E and (e^+e^-) cone radius R can be written as

$$\mathcal{G}(E, R, z, \mu) = \sum_i \int \frac{dz'}{z'} \mathcal{J}_{ij}(E, R, z', \mu) D_j^h(z/z', \mu) + \mathcal{O}(\Lambda^2_{\rm QCD}/E^2)\,, \quad (5.29)$$

where $D_i^h(x,\mu)$ is a fragmentation function for parton i in hadron h and the $\mathcal{J}_{ij}$ are matching coefficients which are given in Eq. (5) of Ref. [70]. The dependence on E

and R in $\mathcal{J}_{ij}$ (at least to $\mathcal{O}(\alpha_s)$) is such that we can write

$$\mathcal{J}_{ij}(E, R, z', \mu) \equiv \mathcal{J}_{ij}(2E \tan \frac{R}{2}, z', \mu)\,, \tag{5.30}$$

i.e., E and R always appear in the combination $E \tan \frac{R}{2}$. Using the crossing relations of Sec. IIIC of Ref. [144], it can be shown that an unmeasured beam function in a collider with center-of-mass energy $\mathrm{E_{cm}}$ and a rapidity cut of y_{cut} can be written as

$$\begin{aligned} B_i(x_i, \mu) &\equiv B_i(\mathrm{E_{cm}}, y_{\mathrm{cut}}, x_i, \mu) \\ &= \sum_j \int \frac{dz}{z} \mathcal{J}_{ij}(x_i \mathrm{E_{cm}} e^{-y_{\mathrm{cut}}}, z, \mu) f_j(x_i/z, \mu) + \mathcal{O}(\Lambda^2_{\mathrm{QCD}}/E^2) \end{aligned} \tag{5.31}$$

where $\mathcal{J}_{ij}$ are *the same* matching coefficients as in Eq. (5.29), at least to $\mathcal{O}(\alpha_s)$,[4] and we used the correspondence between an e^+e^- jet and a beam with label momentum $x_i \mathrm{E_{cm}}$ and rapidity cut y_{cut}

$$E \tan \frac{R}{2} \to x_i \mathrm{E_{cm}} e^{-y_{\mathrm{cut}}}\,, \tag{5.32}$$

which is valid up to $\mathcal{O}(e^{-2y_{\mathrm{cut}}})$ corrections. For the dijet cross section we consider, the x_i are fixed via Eq. (5.13).

5.4.3 Soft Function

In general, we can write the bare soft function at $\mathcal{O}(\alpha_s)$ for dijet production when both jets have τ_a measured as

$$\mathbf{S}(\tau_a^1, \tau_a^2) = \mathbf{S}^{\mathrm{unmeas}} \delta(\tau_a^1)\delta(\tau_a^2) + [\mathbf{S}_0 S^{\mathrm{meas}}(\tau_a^1)\delta(\tau_a^2) + (1 \leftrightarrow 2)] + \mathcal{O}(\alpha_s^2)\,, \tag{5.33}$$

where $\mathbf{S}^{\mathrm{unmeas}} = \mathbf{S}_0 + \mathcal{O}(\alpha_s)$ is the part of the soft function that is always present (both when the jets are measured and unmeasured). The bare soft function is μ

[4] It is argued in [55] that measured beam and jet functions have the same anomalous dimension to all orders (at least for the measured case), but since the PDFs and fragmentation functions differ perturbatively at $\mathcal{O}(\alpha_s^2)$ [145] the matching coefficients must differ for the beam and jet functions starting at this order.

independent, and we will distinguish the corresponding renormalized function with an explicit argument μ. In the cases that neither of the jets or only one jet is measured, the corresponding $S^{\rm meas}$ pieces on the right-hand are simply not included, while $\mathbf{S}^{\rm unmeas}$ is always included. For more jets, the result can be extended straightforwardly, although our explicit results only apply to planar jet configurations (as is necessarily the case for dijet production).

Calculation of the One-Loop Ingredients

The part of the soft function corresponding to the measurement of τ_a^i on jet i, $S^{\rm meas}(\tau_a^i)$, is obtained from summing over the interference of jet i with all other jets and the beams. Contributions from radiation arising from the interference of jets/beams j and k with $j,k \neq i$ give power corrections in $\mathcal{R}$. The calculation of $S^{\rm meas}(\tau_a^i)$ can be obtained from the results for $S_{ij}^{\rm meas}(\tau_a^i)$ given in Eq. (5.18) of Ref. [65] through the rescaling in Eq. (5.12). We find

$$\begin{aligned} S^{\rm meas}(\tau_a^i) &= 2\sum_{i<j}\left(\frac{p_T}{2E_J}\right)^{2-a} S_{ij}^{\rm meas}\left(\left(\frac{p_T}{2E_J}\right)^{2-a}\tau_a^i\right) \\ &= \frac{1}{\epsilon}\frac{\alpha_s C_i}{\pi}\frac{e^{\gamma_E\epsilon}}{\Gamma(1-\epsilon)}\frac{1}{1-a}\left(\frac{1}{\tau_a^i}\right)^{1+2\epsilon}\left(\frac{\mu}{p_T}\right)^{2\epsilon}\mathcal{R}^{2\epsilon(1-a)}\,, \end{aligned} \tag{5.34}$$

which clearly has the desired boost-invariant properties.

The additional part of the soft function we require, $\mathbf{S}^{\rm unmeas}$, can be written as a sum of contributions in the same manner as Ref. [65],

$$\mathbf{S}^{\rm unmeas} = \mathbf{S}_0 + \left[\mathbf{S}_0\sum_{i<j}\mathbf{T}_i\cdot\mathbf{T}_j\Big(S_{ij}^{\rm incl} + \sum_{k=1}^{N} S_{ij}^k\Big) + \text{h.c.}\right], \tag{5.35}$$

where h.c. denotes the hermitian conjugate. Here, we use the color space formalism as described in Refs. [146, 147]. The $4!/(2!)^2 = 6$ matrices $\mathbf{T}_i\cdot\mathbf{T}_j$ are of rank R, the same as that of $\mathbf{S}_0$, and account for the mixing of color operators in a given basis into each other at $\mathcal{O}(\alpha_s)$. The difference from Ref. [65] is that now each contribution

involves a p_T veto instead of an energy veto as well as a different jet algorithm. In particular, defining

$$\Theta_{p_T} \equiv \Theta(k^0 \sin\theta_{kB} < p_T^{\rm cut})$$
$$\Theta_{\mathcal{R}}^k \equiv \Theta(\mathcal{R}_{kJ} < \mathcal{R})\,, \tag{5.36}$$

we now have

$$S_{ij}^{\rm incl} \equiv \frac{1}{\epsilon}\frac{\alpha_s}{2\pi}\left(\frac{\mu}{p_T^{\rm cut}}\right)^{2\epsilon}\mathcal{I}_{ij}^{\rm incl} = -g^2\mu^{2\epsilon}\int\frac{d^dk}{(2\pi)^{d-1}}\frac{n_i\cdot n_j}{(n_i\cdot k)(n_j\cdot k)}\delta(k^2)\Theta(k^0)\Theta_{p_T}\,, \tag{5.37}$$

and

$$S_{ij}^{k} \equiv \frac{1}{\epsilon}\frac{\alpha_s}{2\pi}\left(\frac{\mu}{p_T^{\rm cut}}\right)^{2\epsilon}\mathcal{I}_{ij}^{k} = g^2\mu^{2\epsilon}\int\frac{d^dk}{(2\pi)^{d-1}}\frac{n_i\cdot n_j}{(n_i\cdot k)(n_j\cdot k)}\delta(k^2)\Theta(k^0)\,\Theta_{p_T}\Theta_{\mathcal{R}}^k\,, \tag{5.38}$$

where i, j, and k can each be either of the beams or one of the jets (with $i \neq j$).

We first perform the energy and trivial parts of the angular integration of Eq. (5.37) for generic i, j (either jet or beam). To do this, we align the 1-direction (or "$\hat{z}$") with direction $\vec{n}_i$ and put the $\vec{n}_j$ vector in the 12-plane, and the beam direction $\vec{n}_B$ in the 123-spatial part of d-dimensional space. Using the shorthands $c_{ij} \equiv 1 - n_i\cdot n_j$, $s_{ij} \equiv (1-c_{ij}^2)^{1/2}$, $c_i \equiv \cos\theta_i$, and $s_i \equiv \sin\theta_i$, the dot products of the gluon's 3-momentum, $\vec{k}$, with these unit vectors take the form

$$\vec{n}_i\cdot\vec{k} = c_1$$
$$\vec{n}_j\cdot\vec{k} = c_{ij}c_1 + s_{ij}s_1c_2$$
$$\vec{n}_B\cdot\vec{k} = n_{B1}c_1 + n_{B2}s_1c_2 + n_{B3}s_1s_2c_3\,, \tag{5.39}$$

for the i, j, and beam directions, respectively. In this frame, $\mathcal{I}_{ij}^{\rm incl}$ takes the form (in $\overline{\rm MS}$)

$$\mathcal{I}_{ij}^{\rm incl} = \frac{(1-c_{ij})e^{\gamma_E\epsilon}}{2\sqrt{\pi}\Gamma(1/2-\epsilon)}\int_0^\pi d\theta_1\,\sin^{1-2\epsilon}\theta_1\int_0^\pi d\theta_2\,\sin^{-2\epsilon}\theta_2\frac{1}{1-c_1}\frac{1}{1-c_{ij}c_1-s_{ij}s_1c_2}$$
$$\times\left[\frac{\Gamma(1/2-\epsilon)}{\sqrt{\pi}\Gamma(-\epsilon)}\int_0^\pi d\theta_3\,\sin^{-1-2\epsilon}\theta_3\big(1-(n_{B1}c_1+n_{B3}s_1c_2+n_{B3}s_1s_2c_3)^2\big)^\epsilon\right]. \tag{5.40}$$

The quantity in parenthesis to the ϵ^1 power in the second line is the square of the sine of the gluon-beam angle and comes from doing the k^0 (energy) integral over the p_T veto, Θ_{p_T}. For planar events (such as dijet events at hadron colliders), $n_{B3} = 0$ (since the beam is in the ij-plane for all i, j) and the integration over θ_3 can be easily performed. The entire second line (the quantity in brackets) then becomes simply

$$\left[\cdots \right] \xrightarrow{\text{planar}} \left(1 - (n_{B1}c_1 + n_{B2}s_1c_2)^2\right)^\epsilon , \tag{5.41}$$

with $n_{B2}^2 = 1 - n_{B1}^2$. We also note that when i is equal to the beam direction (so $n_{B1} = 1$ and $n_{B2} = 0$), this quantity reduces to

$$\left[\cdots \right] \xrightarrow{n_i = n_B} \sin^{2\epsilon}\theta_1 . \tag{5.42}$$

In this case, the ϵ dependence in the overall power of $\sin\theta_1$ cancels and we are left with a divergence unregulated by dimensional regularization. This is the well-known rapidity divergence that is present for a p_T veto. This can be treated within the context of SCET_{II} as was done for example in Ref. [111]. Here, we will opt instead to veto on radiation only below a rapidity cut y_{cut} which is consistent with what is done at the LHC since radiation going down the beam pipes is not measured. We compute the soft function components $\mathcal{I}_{ij}^i$ and $\mathcal{I}_{ij}^{\text{incl}}$ for the case i and j can each either be beams or jets in Appendix D and record the results in Table 5.1. For the case that either i or j is a beam, we only compute the full out-of-beam contribution, e.g. $\mathcal{I}_{JB}^{\text{incl}} + \mathcal{I}_{JB}^B$ (or $\mathcal{I}_{B\bar{B}}^{\text{incl}} + \mathcal{I}_{B\bar{B}}^B + \mathcal{I}_{B\bar{B}}^{\bar{B}}$ for the case both i and j are beams) to avoid having to regulate the rapidity divergences in individual components.

For several of the components, we use the fact that the result is boost invariant along the beam direction to boost to the frame where the jets are back-to-back. The relation between the back-to-back frame beam-jet angle θ_J and the jet rapidities in the lab frame is

$$\cos\theta_J = \tanh\frac{\Delta y}{2} , \tag{5.43}$$

Table 5.1: A summary of results for the "unmeasured" part of the soft function, S^{unmeas}, up to $\mathcal{O}(e^{-y_{\text{cut}}}, \mathcal{R}^2)$. Here, the subscript J refers to the two jets, $J = 1, 2$, and B and $\bar{B}$ refer to the two beams, and $\Delta y = y_1 - y_2$. Each component is explicitly boost invariant about the beam direction (with $2y_{\text{cut}}$ in the B-$\bar{B}$ interference terms in general given by the rapidity difference of the forward and backward beam cuts).

Contribution	Result
$\mathcal{I}^{\text{incl}}_{B\bar{B}} + \mathcal{I}^{B}_{B\bar{B}} + \mathcal{I}^{\bar{B}}_{B\bar{B}}$	$2y_{\text{cut}}$
$\mathcal{I}^{1}_{B\bar{B}} + \mathcal{I}^{2}_{B\bar{B}}$	$\mathcal{O}(\mathcal{R}^2)$
$\mathcal{I}^{\text{incl}}_{BJ} + \mathcal{I}^{B}_{BJ} + \mathcal{I}^{\bar{B}}_{BJ}$	$-\frac{1}{2\epsilon} + y_{\text{cut}} - y_J + \epsilon\frac{\pi^2}{24}$
$\mathcal{I}^{J}_{BJ}$	$\frac{1}{2\epsilon}\mathcal{R}^{-2\epsilon}\big(1 - \epsilon^2\frac{\pi^2}{12}\big)$
$\mathcal{I}^{k\neq J,B}_{BJ}$	$\mathcal{O}(e^{-y_{\text{cut}}}, \mathcal{R}^2)$
$\mathcal{I}^{\text{incl}}_{12}$	$(2\cosh\frac{\Delta y}{2})^{-2\epsilon}(-\frac{1}{\epsilon} + \frac{\epsilon}{2}(\Delta y)^2 + \epsilon\frac{\pi^2}{12})$
$\mathcal{I}^{1}_{12} + \mathcal{I}^{2}_{12}$	$\frac{1}{\epsilon}\mathcal{R}^{-2\epsilon}\big(1 - \epsilon^2\frac{\pi^2}{12}\big)$
$\mathcal{I}^{B,\bar{B}}_{12}$	$\mathcal{O}(e^{-y_{\text{cut}}})$

where $\Delta y = y_1 - y_2$ is the rapidity difference of the two jets. This also means that when putting a polar angle restriction on the emitted gluon in the back-to-back frame, one has to apply the correspondence Eq. (5.43) in using Eq. (5.9), which amounts to the replacement

$$\tan\frac{R}{2} \to \frac{\mathcal{R}}{2\cosh\Delta y/2}\,, \tag{5.44}$$

where dependence on the left-hand side arises from enforcing a restriction on the polar angle of the gluon about a jet ($\theta < R$) in the back-to-back frame.

Using the color algebra identity $\sum_i \mathbf{T}_i = 0$ and the kinematic relations

$$\begin{aligned}\ln\frac{n_J\cdot n_B}{2} &= -y_J - \ln(2\cosh y_J)\\ \ln\frac{n_J\cdot \bar{n}_B}{2} &= y_J - \ln(2\cosh y_J)\,,\end{aligned} \tag{5.45}$$

for jets $J = 1, 2$, and

$$\ln \frac{n_1 \cdot n_2}{2} = \ln \frac{(2\cosh \Delta y/2)^2}{(2\cosh y_1)(2\cosh y_2)}\,, \tag{5.46}$$

we find

$$\begin{aligned}\mathbf{S}^{\rm unmeas} = \mathbf{S}_0 + \frac{\alpha_s}{\pi}\Bigg\{\mathbf{S}_0\Bigg[\left(\frac{1}{2\epsilon} + \ln\frac{\mu}{p_T^{\rm cut}}\right)\Big(\mathbf{S}^{\rm div} + \sum_{i=1,2} C_i \ln \mathcal{R}\Big) - \frac{1}{2}\sum_{i=1,2} C_i \ln^2 \mathcal{R} \\ - \mathbf{T}_1\cdot\mathbf{T}_2 \ln\left(1+e^{\Delta y}\right)\ln\left(1+e^{-\Delta y}\right)\Bigg] + \text{h.c.}\Bigg\} + \mathcal{O}(\alpha_s^2)\,.\end{aligned} \tag{5.47}$$

In this equation,

$$\begin{aligned}\mathbf{S}^{\rm div} &= \sum_{i<j} \mathbf{T}_i\cdot\mathbf{T}_j \ln\frac{n_i\cdot n_j}{2} - y_{\rm cut}\big(C_B + C_{\bar B}\big) - \sum_{i=1,2} C_i \ln(2\cosh y_i) \\ &= \Delta\gamma_{ss}(m_i) - \mathbf{M}'(m_i)\,,\end{aligned} \tag{5.48}$$

where in the second line we wrote the result in terms two functions defined by

$$\begin{aligned}\Delta\gamma_{ss}(m_i) &= \sum_{i=B,\bar B} C_i \ln\frac{x_i \mathrm{E}_{\rm cm} e^{-y_{\rm cut}}}{m_i} + \sum_{i=1,2} C_i \ln\frac{p_T}{m_i} \\ \mathbf{M}'(m_i) &\equiv -\sum_{i<j} \mathbf{T}_i\cdot\mathbf{T}_j \ln\frac{s_{ij}}{m_i m_j}\,,\end{aligned} \tag{5.49}$$

where $s_{ij} \equiv 2p_i\cdot p_j > 0$ (and where $p_i = x_i \mathrm{E}_{\rm cm}$ for the beams $i = B, \bar B$). Note that for later convenience we have defined these functions so that each separately depends on a set of parameters m_i. The dependence on m_i cancels in the sum in the second line of Eq. (5.48).

Refactorization

We note here that one can also construct the ingredients needed for the refactorized cross section as was done in Ref. [5] for the resummation of (global) logs of $\mathcal{R}$ from

the ingredients in Table 5.1. In particular, the conclusions of Ref. [5] suggest that $\mathbf{S}^{\text{unmeas}}$ should be factorized as

$$\begin{aligned}\mathbf{S}^{\text{unmeas}} &= \frac{1}{2}\mathbf{S}_0 \int_0^{p_T^{\text{cut}}} dE \left[\mathbf{s}_s(E) \otimes s_{sc}^1(E\mathcal{R}) \otimes s_{sc}^2(E\mathcal{R})\right] + \text{h.c.} \\ &= \mathbf{S}_0 + \frac{\alpha_s}{4\pi}\frac{1}{2}\Big[\mathbf{S}_0\Big(\mathbf{S}_s^{(1)}(p_T^{\text{cut}}) + \sum_{k=1,2} S_{sc}^{k(1)}(p_T^{\text{cut}}\mathcal{R})\Big) + \text{h.c.}\Big] + \mathcal{O}(\alpha_s^2)\,, \end{aligned} \tag{5.50}$$

where $\otimes$ is a convolution over the variable E and the functions $\mathbf{S}_s$ and S_{sc}^k are the global soft (with radiation anywhere except for the beams) and soft-collinear (with radiation within jet k) functions, respectively, and where

$$\begin{aligned}\mathbf{s}_s(p_T^{\text{cut}}) &\equiv \frac{d}{dp_T^{\text{cut}}}\mathbf{S}_s(p_T^{\text{cut}}) \\ s_{sc}^k(p_T^{\text{cut}}\mathcal{R}) &\equiv \frac{d}{dp_T^{\text{cut}}} S_{sc}^k(p_T^{\text{cut}}\mathcal{R}) \end{aligned} \tag{5.51}$$

with both functions $f = \mathbf{S}_s, S_{sc}^k$ normalized as $f(x) = \theta(x) + \sum_{i=1}(\frac{\alpha_s}{4\pi})^n f^{(n)}(x)$. Note that all of the non-trivial color mixing occurs in $\mathbf{S}_s$. This is due to the fact that the soft-collinear modes of Refs. [5, 122] are confined to a single jet and is expected to hold to all orders.

In terms of the ingredients in Table 5.1, we have

$$\begin{aligned}\mathbf{S}_s^{(1)}(p_T^{\text{cut}}) &= \frac{4}{\epsilon}\left(\frac{\mu}{p_T^{\text{cut}}}\right)^{2\epsilon} \sum_{i<j} \mathbf{T}_i \cdot \mathbf{T}_j \Big[\mathcal{I}_{ij}^{\text{incl}} + (\delta_{iB} + \delta_{i\bar{B}})(\delta_{jJ_1} + \delta_{jJ_2})\mathcal{I}_{ij}^i \\ &\quad + \delta_{iB}\delta_{i\bar{B}}(\mathcal{I}_{ij}^i + \mathcal{I}_{ij}^j)\Big] \\ &= \frac{4}{\epsilon}\left(\frac{\mu}{p_T^{\text{cut}}}\right)^{2\epsilon}\Big[\sum_{i=1,2}\frac{C_i}{2\epsilon}\Big(1 - \epsilon^2\frac{\pi^2}{12}\Big) \\ &\quad + \mathbf{S}^{\text{div}} - 2\epsilon\,\mathbf{T}_1\cdot\mathbf{T}_2 \ln\left(1 + e^{\Delta y}\right)\ln\left(1 + e^{-\Delta y}\right)\Big] \end{aligned} \tag{5.52}$$

and

$$S_{sc}^{k(1)}(p_T^{\rm cut}\mathcal{R}) = \frac{4}{\epsilon}\left(\frac{\mu}{p_T^{\rm cut}}\right)^{2\epsilon}\sum_{i<j}\mathbf{T}_i\cdot\mathbf{T}_j\Big[\delta_{ik}\mathcal{I}_{ij}^i\Big] = \frac{4}{\epsilon}\left(\frac{\mu}{p_T^{\rm cut}\mathcal{R}}\right)^{2\epsilon}\Big[-\frac{C_k}{2\epsilon}\Big(1-\epsilon^2\frac{\pi^2}{12}\Big)\Big]\,. \tag{5.53}$$

5.5 RG Evolution and the Total NLL' Cross Section

In this section, we apply Renormalization Group (RG) methods to the functions calculated in this chapter and arrive at the result for the total NLL' resummed cross section. These functions can be divided into those which are multiplicatively renormalized and those that renormalize via a convolution. The former include the hard function and unmeasured jet functions and the unmeasured part of the soft function, and the latter includes measured jet and soft functions.

5.5.1 Hard Function

The hard function $\mathbf{H}$ for $N-2$ jet production in hadron collisions is a matrix in color space with rank R (the same as that of the soft function). It can be written in terms of Wilson coefficients C_i as $(\mathbf{H})_{ij} = C_i C_j^*$, each of which mix into each other under renormalization, i.e, $C_i^{\rm bare} = \sum_j (\mathbf{Z}_H(\mu))_{ij} C_j$ which implies that

$$\mathbf{H}^{\rm bare} = \mathbf{Z}_H(\mu)\mathbf{H}(\mu)\mathbf{Z}_H^\dagger(\mu)\,. \tag{5.54}$$

The μ-independence of the left-hand side of Eq. (5.54) implies that $\mathbf{H}\equiv\mathbf{H}(\mu)$ obeys the RGE

$$\frac{d\,\mathbf{H}}{d\ln\mu} = \mathbf{\Gamma}_H\,\mathbf{H} + \mathbf{H}\,\mathbf{\Gamma}_H^\dagger\,, \tag{5.55}$$

where

$$\mathbf{\Gamma}_H \equiv -\mathbf{Z}_H^{-1}\frac{d}{d\ln\mu}\mathbf{Z}_H \tag{5.56}$$

This RGE preserves the hermiticity of $\mathbf{H}$ under RG evolution. $\mathbf{\Gamma}_H$ in Eq. (5.55) is given (to $\mathcal{O}(\alpha_s^2)$) by [148, 149]

$$\mathbf{\Gamma}_H = \frac{1}{2}\sum_{i=1}^{N}\left[C_i\,\Gamma_c(\alpha_s)\ln\frac{m_i^2}{\mu^2} - \frac{\alpha_s}{\pi}\gamma_i\right] + \Gamma_c(\alpha_s)\,\mathbf{M}(m_i)\,, \tag{5.57}$$

where γ_i is given in Eq. (5.21), $\Gamma_c(\alpha_s)$ is the cusp anomalous dimension (given in Eq.(A.3)), and m_i is an arbitrary parameter(s) which can be chosen for convenience and can be shown to cancel between the first term and $\mathbf{M}(m_i)$. The first term is (implicitly) proportional to an identity matrix and $\mathbf{M}$ in the second term involvers a non-trivial matrix of rank R, which can be written as

$$\begin{aligned}\mathbf{M}(m_i) &\equiv -\sum_{i<j}\mathbf{T}_i\cdot\mathbf{T}_j\left[\ln\left((-1)^{\Delta_{ij}}\frac{s_{ij}}{m_i m_j} - i0^+\right)\right] \\ &= \mathbf{M}'(m_i) + i\pi\mathbf{T}\,,\end{aligned} \tag{5.58}$$

where Δ_{ij} is 0 for beam-jet interference and 1 for beam-beam and jet-jet interference, $s_{ij} = 2p_i\cdot p_j > 0$, and in the second line we explicitly separated the terms of the form $\Delta_{ij}\ln(-1)$ into the matrix $i\pi\mathbf{T}$, where

$$\mathbf{T} \equiv \sum_{i<j}\Delta_{ij}\,\mathbf{T}_i\cdot\mathbf{T}_j\,. \tag{5.59}$$

and $\mathbf{M}'(m_i)$ is defined in Eq. (5.49). The matrix $\mathbf{M}$ is worked out for a set of choices of color bases for all $2\to 2$ channels in Ref. [4] with the choice $m_i^2 = -t > 0$ (the Mandelstam variable) in the $qq'\to qq'$ channel (and the choice for other channels obtained by crossing relations). Importantly, for any μ-independent choice for m_i, $\mathbf{M}$ is independent of μ.

The effect of the color-trivial component of Eq. (5.55) (i.e., the contribution from the term in brackets in Eq. (5.57)) can be obtained using the results in Appendix A and gives rise to a factor Π_H as in Eq. (A.7) with the parameters needed for K_H and ω_H at NLL' given in Table 5.2. We can straightforwardly include the effect of

$\Gamma_c(\alpha_s)\,\mathbf{M}(m_i)$ via matrix exponentiation and record the solution as

$$\mathbf{H}(\mu,\mu_H) = \Pi_H(\mu,\mu_H)\,\mathbf{\Pi}_H(\mu,\mu_H)\mathbf{H}(\mu_H)\mathbf{\Pi}_H^\dagger(\mu,\mu_H)\,, \tag{5.60}$$

where

$$\mathbf{\Pi}_H(\mu,\mu_H) \equiv \exp\Big\{\mathbf{M}\int_{\alpha_s(\mu_H)}^{\alpha_s(\mu)}\frac{d\alpha}{\beta[\alpha]}\Gamma_c(\alpha)\Big\} = \exp\Big\{\mathbf{M}\Big(\frac{2}{\beta_0}\ln\frac{\alpha_s(\mu_H)}{\alpha_s(\mu)}+\cdots\Big)\Big\}\,, \tag{5.61}$$

where in the second equality we expanded to NLL' accuracy. This matrix exponential can be defined by first constructing the matrix $\mathbf{R}$ of eigenvectors of $\mathbf{M}$ such that $\mathbf{R}^{-1}\mathbf{M}\mathbf{R} = \mathbf{\Lambda}_H$ is the diagonal matrix of eigenvalues of $\mathbf{M}$, and then defining $\exp(\mathbf{M}) \equiv \mathbf{R}\exp(\mathbf{\Lambda}_H)\mathbf{R}^{-1}$.

5.5.2 Jet Functions and Unmeasured Beam Functions

Since the jet functions can be obtained directly from rescalings of those in Ref. [65] as described in Sec. 5.4.1, the renormalization is similarly related to the results in Ref. [65]. For measured (renormalized) jet functions we have

$$\gamma_{J_i}(\tau_a^i,\mu) = \left[2\Gamma_c(\alpha_s)C_i\frac{2-a}{1-a}\ln\frac{\mu}{p_T}+\frac{\alpha_s}{\pi}\gamma_i\right]\delta(\tau_a^i) - 2\Gamma_c(\alpha_s)C_i\frac{1}{1-a}\left(\frac{1}{\tau_a^i}\right)_+\,, \tag{5.62}$$

which is of the general form Eq.(A.13) with cusp ($\Gamma_F[\alpha_s]$) and non-cusp ($\gamma_F[\alpha_s]$) pieces given in Table 5.2. Here and below, the '+' distribution is defined for example in Eq. (A.2) of Ref. [65].

To RG evolve the jet function, we perform the integral in Eq. (A.15) for the case $F = J$. Integrals of this form are most easily performed by convolving the right-hand side against $1 = Z^{-1}\otimes Z$ and first performing the convolution of U_F with the bare function, i.e., $Z\otimes F$, then expanding in ϵ, and finally performing the Z^{-1} convolution (which just removes the $1/\epsilon$ poles in a minimal subtraction scheme). For

the jet function, we obtain

$$
\begin{aligned}
J^{\rm meas}(\tau_a^i,\mu) &= Z_J^{-1}(\tau_a^i,\mu_J)\otimes\Big[J^{\rm meas}(\tau_a^i)\otimes U_J(\tau_a^i,\mu,\mu_J)\Big] \\
&= Z_J^{-1}(\tau_a^i,\mu_J)\otimes\Bigg\{U_J(\tau_a^i,\mu,\mu_J)\Bigg(1-\frac{\alpha_s(\mu_J)}{2\pi}\Bigg[-f_i(a)+ \\
&\qquad\left(\frac{1}{\epsilon}\frac{2C_i}{1-a}+\frac{\gamma_i}{1-a/2}\right)\frac{\Gamma(-2\epsilon/(2-a))\Gamma(-\omega_J^i)}{\Gamma(-2\epsilon/(2-a)-\omega_J^i)}\left(\frac{\mu_J}{p_T(\tau_a^i)^{1/(2-a)}}\right)^{2\epsilon}\Bigg]\Bigg)\Bigg\}_+ \\
&= \Big\{U_J(\tau_a^i,\mu,\mu_J)\Big(1+f_J^i(\tau_a^i;\omega_J^i,\mu_J)\Big)\Big\}_+ \,, \qquad (5.63)
\end{aligned}
$$

where $f_J(\tau,\Omega,\mu)$ is the one loop part of the renormalized jet function after RG evolution,

$$
\begin{aligned}
f_J^i(\tau,\Omega,\mu) = \frac{\alpha_s}{\pi(2-a)}\Bigg\{&\frac{2-a}{2}f_i(a)+\gamma_i\Bigg[H(-1-\Omega)+(2-a)\ln\frac{\mu}{p_T\,\tau^{1/(2-a)}}\Bigg] \qquad (5.64)\\
&+\frac{C_i}{1-a}\Bigg[\left(H(-1-\Omega)+(2-a)\ln\frac{\mu}{p_T\,\tau^{1/(2-a)}}\right)^2-\psi^{(1)}(-\Omega)+\frac{\pi^2}{6}\Bigg]\Bigg\},
\end{aligned}
$$

and $H(x)$ is the harmonic number function and $\psi^{(1)}(x)$ is the polygamma function of order 1 and $f_i(a)$ is given in Eq. (5.28). The natural scale for the jet function suggested by Eq. (5.64) is

$$
\mu_J^{\rm meas} \equiv p_T(\tau_a^i)^{1/(2-a)}\,. \qquad (5.65)
$$

From the discussion in Sec. 5.4.2 and the results of Sec. 5.4.1, we have for both unmeasured jet functions and unmeasured beam functions the anomalous dimensions

$$
\gamma_{J_i} = 2\Gamma_c(\alpha_s)C_i\ln\frac{\mu}{p_T\mathcal{R}}+\frac{\alpha_s}{\pi}\gamma_i\,, \qquad (5.66)
$$

and

$$
\gamma_{B_i} = 2\Gamma_c(\alpha_s)C_i\ln\frac{\mu}{x_i\mathrm{E}_{\rm cm}e^{-y_{\rm cut}}}+\frac{\alpha_s}{\pi}\gamma_i\,, \qquad (5.67)
$$

which have the form of Eq.(A.2). We have summarized the cusp and non-cusp parts in Table 5.2 and γ_i is given in Eq. (5.21) for quark and gluon jets. Eqs. (5.66) and (5.67) (together with Eq. (5.20)) suggests the canonical scale choices

$$\mu_J^{\text{unmeas}} = p_T \mathcal{R} \qquad \text{and} \qquad \mu_B = x_i \mathrm{E}_{\text{cm}} e^{-y_{\text{cut}}}\,, \tag{5.68}$$

with x_i fixed via Eq. (5.13).

5.5.3 Soft Function

The total measured soft function, which includes both the $\mathbf{S}^{\text{unmeas}}$ and a S^{meas} contribution for each measured jet as in Eq. (5.33), can be evolved by using a multiplicative-type RGE (cf. Eq.(A.1)) for $\mathbf{S}^{\text{unmeas}}$ and a convolution-type RGE (cf. Eq.(A.12)) for S^{meas}, and each can be evolved from a separate scale (an unmeasured soft scale and a measured soft scale, respectively). This corresponds an early version of "refactorization" originally suggested in Ref. [65]. A more complete refactorization procedure was recently introduced in [5] which involves further refactorizing $\mathbf{S}^{\text{unmeas}}$ into a global soft contribution and a soft-collinear contribution, as in Eq. (5.50). In this section, we demonstrate how both approaches are achieved so that they can be compared numerically in Sec. 5.5.5.

Unmeasured Evolution

The unmeasured component of the soft function $\mathbf{S}^{\text{unmeas}}$ is renormalized much like the hard function[5]

$$\mathbf{S}^{\text{unmeas, bare}} = \mathbf{Z}_S^\dagger(\mu)\, \mathbf{S}^{\text{unmeas}}(\mu)\, \mathbf{Z}_S(\mu) \tag{5.69}$$

which gives rise to an RGE of the form

$$\frac{d}{d\ln\mu}\mathbf{S}^{\text{unmeas}} = \mathbf{S}^{\text{unmeas}}\boldsymbol{\Gamma}_S^{\text{unmeas}} + \text{h.c.}\,, \tag{5.70}$$

[5] Note that Eq. (5.69) takes the form of Eq. (5.54) but with $\mathbf{Z}_H \leftrightarrow \mathbf{Z}_S^\dagger$. This gives rise to the RGE Eq. (5.70) which is of the form Eq. (5.55) but with $\boldsymbol{\Gamma}_S^{\text{unmeas}} \leftrightarrow \boldsymbol{\Gamma}_H^\dagger$. RGE invariance then requires $\boldsymbol{\Gamma}_H = -\boldsymbol{\Gamma}_S^{\text{unmeas}} + \cdots$ where the ellipses denote color-trivial contributions.

with

$$\begin{aligned}\mathbf{\Gamma}_S^{\text{unmeas}} &\equiv \frac{\alpha_s}{\pi}(\mathbf{S}^{\text{div}} - i\pi\mathbf{T} + \sum_{i=1,2} C_i \ln \mathcal{R}) \\ &= \frac{\alpha_s}{\pi}\Big(\Delta\gamma_{ss}(m_i) - \mathbf{M}(m_i) + \sum_{i=1,2} C_i \ln \mathcal{R}\Big)\,, \end{aligned} \tag{5.71}$$

where $\mathbf{S}^{\text{div}}$ and $\Delta\gamma_{ss}$ are defined in Eqs. (5.48) and (5.49), and $\mathbf{M}$ and $\mathbf{T}$ are defined in Eqs. (5.58) and (5.59). In Eq. (5.71), we have inserted the factor $i\pi\mathbf{T}$ to comply with matrix-level consistency of the anomalous dimensions, which is consistent with the one loop bare soft function calculation Eq. (5.47) since $\mathbf{S}_0\mathbf{T} = \mathbf{T}^\dagger\mathbf{S}_0$.

The solution to this RGE is completely analogous to that of the hard RGE Eq. (5.55). The result is

$$\mathbf{S}^{\text{unmeas}}(\mu, \mu_S) = \Pi_S^{\text{unmeas}}(\mu, \mu_S)\big[\mathbf{\Pi}_S^\dagger(\mu, \mu_S)\mathbf{S}^{\text{unmeas}}(\mu_S)\mathbf{\Pi}_S(\mu, \mu_S)\big] \tag{5.72}$$

where Π_S^{unmeas} is of the form Eq. (A.7) with NLL' parameters given in Table 5.2 and

$$\mathbf{\Pi}_S(\mu, \mu_S) \equiv \exp\Big\{ -\mathbf{M}\int_{\alpha_s(\mu_S)}^{\alpha_s(\mu)} \frac{d\alpha}{\beta[\alpha]}\Gamma_c(\alpha)\Big\} = \exp\Big\{ -\mathbf{M}\Big[\frac{2}{\beta_0}\ln\frac{\alpha_s(\mu_S)}{\alpha_s(\mu)} + \cdots\Big]\Big\} \tag{5.73}$$

where in the second equality we expanded to NLL' accuracy. Inspection of the unmeasured soft function Eq. (5.47) suggests the canonical unmeasured soft scale choice

$$\mu_S^{\text{unmeas}} \equiv p_T^{\text{cut}}\,. \tag{5.74}$$

Measured Evolution

When the jets are measured, RGE takes the form

$$\frac{d}{d\ln\mu}\mathbf{S}(\tau_a^1, \tau_a^2, \mu) = \int d\tau' d\tau''[\mathbf{S}(\tau', \tau'', \mu)\,\mathbf{\Gamma}_S(\tau_a^1 - \tau', \tau_a^2 - \tau'', \mu) + \text{h.c.}]\,, \tag{5.75}$$

with the soft anomalous dimension given to NLL accuracy by

$$\mathbf{\Gamma}_S(\tau_a^1, \tau_a^2, \mu) = \mathbf{\Gamma}_S^{\text{unmeas}}\delta(\tau_a^1)\delta(\tau_a^2) + \Big[\frac{1}{2}\gamma_S^{\text{meas}}(\tau_a^1, \mu)\delta(\tau_a^2) + (1 \leftrightarrow 2)\Big]\,, \tag{5.76}$$

where $\gamma^{\rm meas}$ is given by

$$\gamma_S^{\rm meas}(\tau_a^i,\mu) = -\Gamma_c(\alpha_s)C_i\frac{1}{1-a}\left\{2\ln\frac{\mu\mathcal{R}^{1-a}}{p_T}\delta(\tau_a^i) - 2\left(\frac{1}{\tau_a^i}\right)_+\right\} \tag{5.77}$$

which has the form of Eq.(A.13). The τ_a dependence of measured jets requires the inclusion of the evolution kernels $U_S^i(\tau_a,\mu,\mu_0)$ as in Eq. (A.16) with NLL' parameters given in Table 5.2. To evaluate the effect of convolving these kernels, we use the same method as in Eqs. (5.63) and (5.64). This gives for the RG evolved measured part of the soft function

$$\begin{aligned} S^{\rm meas}(\tau_a^i;\mu) &= Z_S^{-1}(\tau_a^i,\mu_S)\otimes\left[U_S^i(\tau_a^i,\mu,\mu_S)\left(1+\frac{1}{\epsilon}\frac{\alpha_s(\mu_S)C_i}{\pi(1-a)}\frac{e^{\gamma_E\epsilon}}{\Gamma(1-\epsilon)}\right.\right.\\ &\qquad\left.\left.\times\frac{\Gamma(-2\epsilon)\Gamma(-\omega_S^i)}{\Gamma(-2\epsilon-\omega_S^i)}\left(\frac{\mu_S\mathcal{R}^{1-a}}{p_T\,\tau_a^i}\right)^{2\epsilon}\right)\right]_+\\ &= U_S^i(\tau_a^i,\mu,\mu_S)\Big(1+f_S^i(\tau_a^i;\omega_S^i,\mu_S)\Big)\,, \end{aligned} \tag{5.78}$$

$$f_S^i(\tau;\Omega,\mu) = \frac{\alpha_s C_i}{\pi(1-a)}\left[\psi^{(1)}(-\Omega) - \left(H(-1-\Omega)+\ln\frac{\mu\mathcal{R}^{1-a}}{p_T\,\tau}\right)^2 - \frac{\pi^2}{8}\right], \tag{5.79}$$

which suggests the canonical scale choice

$$\mu_S^{\rm meas} \equiv \frac{p_T\tau_a^i}{\mathcal{R}^{1-a}}\,. \tag{5.80}$$

Taking the scales from which the two measured components and the unmeasured component are evolved from to be $\mu_S^{1,2}$ and $\bar\mu_S$, respectively, we record the final result as

$$\begin{aligned} \mathbf{S}(\tau_a^1,\tau_a^2,\mu,\mu_S^1,\mu_S^2,\bar\mu_S) &= U_S^1(\tau_a^1,\mu,\mu_S^1)U_S^1(\tau_a^2,\mu,\mu_S^2)\big[1+(f_S^1(\tau_a^1;\omega_S^1,\mu_S^1)\\ &+ f_S^2(\tau_a^2;\omega_S^2,\mu_S^2))\big]\Pi_S^{\rm unmeas}(\mu,\bar\mu_S)\big[\mathbf{\Pi}_S^\dagger(\mu,\bar\mu_S)\mathbf{S}^{\rm unmeas}(\bar\mu_S)\mathbf{\Pi}_S(\mu,\bar\mu_S)\big]\,. \end{aligned} \tag{5.81}$$

Refactorized Evolution

The components of the refactorized $\mathbf{S}^{\rm unmeas}$ (cf. Eq. (5.50)), $\mathbf{s}_s$ and s_{cs}^k for $k=1,2$ evolve as

$$\frac{d}{d\ln\mu}\mathbf{s}_s(E) = \int dE'\,\mathbf{s}_s(E')\,\mathbf{\Gamma}_{ss}(E-E')\,, \tag{5.82}$$

and

$$\frac{d}{d\ln\mu} s_{sc}^k(E\mathcal{R}) = \int dE'\, s_{sc}^k(E'\mathcal{R})\, \Gamma_{sc}^k((E-E')\mathcal{R})\,, \tag{5.83}$$

respectively. The anomalous dimensions take the form Eq.(A.13) and satisfy the relations

$$\frac{1}{2}\int_0^{p_T^{\rm cut}} dE\, \Gamma_{sc}^k(E) = -C_k \Gamma_c[\alpha_s] \ln\frac{\mu}{p_T^{\rm cut}\mathcal{R}} + \gamma_{\rm hemi}^k[\alpha_s]\,, \tag{5.84}$$

and

$$\frac{1}{2}\int_0^{p_T^{\rm cut}} dE\, \mathbf{\Gamma}_{ss}(E) = \sum_{i=1,2} \left(C_i \Gamma_c[\alpha_s] \ln\frac{\mu}{p_T^{\rm cut}} - \gamma_{\rm hemi}^i[\alpha_s]\right) + \frac{\alpha_s}{\pi}(\Delta\gamma_{ss}(m_i) - \mathbf{M}(m_i))\,, \tag{5.85}$$

where we used that to all-orders, the non-cusp part of the anomalous dimension for γ_{sc} is the same as that of the hemisphere thrust distribution [5] (of the color-representation of jet k). At $\mathcal{O}(\alpha_s)$, $\gamma_{\rm hemi}^i = 0$. The additional non-cusp parts of Eq. (5.85) (which do not appear in the analogous e^+e^- calculation [5]) are needed for this measurement to ensure the consistency of refactorization at $\mathcal{O}(\alpha_s)$,

$$\frac{1}{2}\int_0^{p_T^{\rm cut}} dE \left(\mathbf{\Gamma}_{ss}(E) + \sum_k \Gamma_{sc}^k(E)\right) = \mathbf{\Gamma}_S^{\rm unmeas}\,. \tag{5.86}$$

To RG evolve the refactorized soft function, we write

$$\begin{aligned} \mathbf{S}_{ss}^{(1)} &= \frac{1}{\epsilon}\left(\frac{\mu}{p_T^{\rm cut}}\right)^{2\epsilon} \mathbf{f}_s \\ \sum_{k=1,2} S_{sc}^{k(1)} &= \frac{1}{\epsilon}\left(\frac{\mu}{p_T^{\rm cut}\mathcal{R}}\right)^{2\epsilon} f_c \end{aligned} \tag{5.87}$$

where $f_{s,c} = \sum_{\{i=0,1,2\}} \epsilon^{i-1} f_{s,c}^i$ can be read off from the $\mathcal{O}(\alpha_s)$ results Eqs. (5.52) and (5.53) and are given by

$$\begin{aligned} f_c^0 &= -2(C_1+C_2) & \mathbf{f}_s^0 &= -f_c^0 \\ f_c^1 &= 0 & \mathbf{f}_s^1 &= 4\mathbf{S}^{\rm div} \\ f_c^2 &= \frac{\pi^2}{6}(C_1+C_2) & \mathbf{f}_s^2 &= -8\mathbf{T}_1\cdot\mathbf{T}_2 \ln(1+e^{\Delta y})\ln(1+e^{-\Delta y}) - f_c^2\,. \end{aligned} \tag{5.88}$$

This allows us to write the RG evolved bare functions (using a similar argument as that described above Eq. (5.63)) as

$$\begin{aligned}
&\int_0^{p_T^{\rm cut}} dE \left[\mathbf{s}_s(E) \otimes U_{ss}(E/\mu_{ss}, \mu, \mu_{ss})\right] \otimes_{i=1,2} \left[s^i_{sc}(E\mathcal{R}) \otimes U^i_{sc}(E\mathcal{R}/\mu_{sc}, \mu, \mu_{sc})\right] \\
&= \int_0^{p_T^{\rm cut}} dE \left[\mathbf{s}_s(E) \otimes_{i=1,2} s^i_{sc}(E\mathcal{R})\right] \otimes \left[U_{ss}(E/\mu_{ss}, \mu, \mu_{ss}) \otimes_{i=1,2} U^i_{sc}(E\mathcal{R}/\mu_{sc}, \mu, \mu_{sc})\right] \\
&= \int_0^{p_T^{\rm cut}} dE \left[1 - 2\frac{\Gamma(-2\epsilon)\Gamma(-\Omega_S)}{\Gamma(-2\epsilon-\Omega_S)}\left(\frac{\alpha_s(\mu_{ss})}{4\pi}\left(\frac{\mu_{ss}}{E}\right)^{2\epsilon}\mathbf{f}_s \right.\right. \\
&\qquad\qquad \left.\left. + \frac{\alpha_s(\mu_{sc})}{4\pi}\left(\frac{\mu_{sc}}{E\mathcal{R}}\right)^{2\epsilon} f_c\right)\right] U_S(E, \mu, \mu_{ss}, \mu_{sc}) \,,
\end{aligned} \tag{5.89}$$

where in the 3rd line we truncated the series in parenthesis to $\mathcal{O}(\alpha_s)$ and we defined

$$\Omega_S \equiv \omega_{ss}(\mu, \mu_{ss}) + \sum_{i=1,2} \omega^i_{sc}(\mu, \mu_{sc}) \tag{5.90}$$

and

$$U_S(E, \Omega_S, \mu_{ss}, \mu_{sc}) \equiv \left[U_{ss}(E/\mu_{ss}, \mu, \mu_{ss}) \otimes_{i=1,2} U^i_{sc}(E\mathcal{R}/\mu_{sc}, \mu, \mu_{sc})\right] \tag{5.91}$$

and used that U_S scales as

$$U_S \propto \frac{1}{\Gamma(-\Omega_S)} E^{-1-\Omega_S} \,. \tag{5.92}$$

Expanding in ϵ and dropping the $1/\epsilon$ poles gives the renormalized, refactorized and RG evolved $\mathbf{S}^{\rm unmeas}(\mu)$,

$$\mathbf{S}^{\rm unmeas}(\mu) \to \mathbf{S}^{\rm unmeas}(\Omega_S, \mu_{ss}, \mu_{sc}) \int_0^{p_T^{\rm cut}} dE\, U_S(E, \Omega_S, \mu_{ss}, \mu_{sc}) \tag{5.93}$$

where

$$\mathbf{S}^{\rm unmeas}(\Omega,\mu_{sc},\mu_{ss}) \equiv \mathbf{S}_0 + \Bigg\{\mathbf{S}_0\Bigg[\frac{\alpha_s(\mu_{ss})}{4\pi}\Bigg(\frac{1}{2}\mathbf{f}_s^2 + \mathbf{f}_s^1\Big(\ln\frac{\mu_{ss}}{p_T^{\rm cut}} + H(-\Omega)\Big) \tag{5.94}$$

$$+ \mathbf{f}_s^0\Big(\frac{\pi^2}{6} - \psi^{(1)}(1-\Omega) + \Big(\ln\frac{\mu_{ss}}{p_T^{\rm cut}} + H(-\Omega)\Big)^2\Big)\Bigg)$$

$$+ \frac{\alpha_s(\mu_{sc})}{4\pi}\Bigg(\frac{1}{2}f_c^2 + f_c^1\Big(\ln\frac{\mu_{sc}}{p_T^{\rm cut}\mathcal{R}} + H(-\Omega)\Big)$$

$$+ f_c^0\Big(\frac{\pi^2}{6} - \psi^{(1)}(1-\Omega) + \Big(\ln\frac{\mu_{sc}}{p_T^{\rm cut}\mathcal{R}} + H(-\Omega)\Big)^2\Big)\Bigg)\Bigg] + \text{h.c.}\Bigg\}.$$

We note that when combined into the full cross section in Sec. 5.5.4, the μ dependence can be cancelled to all orders between Eq. (5.93) and the remainder of the cross section (using consistency and Eq. (5.86)) at the expense of running all factorized components from μ_{ss} to the scale of the component. This means for example that we have

$$\Omega_S \to \sum_{i=1,2}\omega_{sc}^i(\mu_{ss},\mu_{sc}) \equiv \omega_{sc}\,. \tag{5.95}$$

This means in particular we can make the replacement

$$\mathbf{S}^{\rm unmeas}(\mu) \to \mathbf{S}^{\rm unmeas}(\omega_{sc},\mu_{ss},\mu_{sc})\,U_{sc}(\omega_{sc},\mu_{ss},\mu_{sc}) \tag{5.96}$$

where

$$U_{sc}(\omega_{sc},\mu_{ss},\mu_{sc}) \equiv \int_0^{p_T^{\rm cut}} dE\,U_S(E,\omega_{sc},\mu_{ss},\mu_{sc}) = \frac{e^{K_{sc}+\gamma_E\omega_{sc}}}{\Gamma(1-\omega_{sc})}\Big(\frac{\mu_{sc}}{p_T^{\rm cut}\mathcal{R}}\Big)^{\omega_{sc}}, \tag{5.97}$$

where $K_{sc} \equiv \sum_{i=1,2} K_{sc}(\mu_{ss},\mu_{sc})$. The parameters needed for K_{sc} and ω_{sc} at NLL' (which can be expanded as in Eq.(A.10)) can be read off from Eqs. (5.84) and (5.85) and are given in Table 5.2.

Table 5.2: Ingredients for anomalous dimensions of the color-trivial parts components to the factorization formula and the corresponding canonical scale choices μ_F, which take the form of Eq.(A.2) and (A.13). The hard and (unmeasured) soft components require an additional color-nontrivial factor derived explicitly in the text. Here, C_i is the quadratic Casimir (C_F or C_A for quarks and gluons, respectively), γ_i is given in Eq. (5.21), $\Gamma \equiv \Gamma_c(\alpha_s)$ is the cusp (given in Eq.(A.3)), x_i are the momentum fractions of the partons in the beams (fixed via Eq. (5.13)), and $\Delta\gamma_{ss}$ is given in Eq. (5.49) (and m_i is an arbitrary parameter that cancels both within $\mathbf{\Gamma}_H$ and within $\mathbf{\Gamma}_S$ and can for example be chosen based on the partonic channel to coincide with the conventions of Ref. [4] as described in the text). For refactorizing the soft function as in [5], the last two rows are used in place of $\gamma_S^{\rm unmeas}$.

	$\Gamma_F[\alpha_s]$	$\gamma_F[\alpha_s]$	j_F	m_F	μ_F
γ_H	$-\Gamma \sum_i C_i$	$-\sum_i \frac{\alpha_s}{\pi}\gamma_i$	1	$\prod_i m_i^{C_i/\sum_j C_j}$	m_i
$\gamma_{J_i}(\tau_a^i)$	$\Gamma C_i \frac{2-a}{1-a}$	$\frac{\alpha_s}{\pi}\gamma_i$	$2-a$	p_T	$p_T(\tau_a^i)^{1/(2-a)}$
$\gamma_S^{\rm meas}(\tau_a^i)$	$-\Gamma C_i \frac{1}{1-a}$	0	1	$p_T/\mathcal{R}^{1-a}$	$p_T\,\tau_a^i/\mathcal{R}^{1-a}$
γ_{J_i}	ΓC_i	$\frac{\alpha_s}{\pi}\gamma_i$	1	$p_T\mathcal{R}$	$p_T\mathcal{R}$
γ_{B_i}	ΓC_i	$\frac{\alpha_s}{\pi}\gamma_i$	1	$x_i \mathrm{E}_{\rm cm} e^{-y_{\rm cut}}$	$x_i \mathrm{E}_{\rm cm} e^{-y_{\rm cut}}$
$\gamma_S^{\rm unmeas}$	0	$\frac{2\alpha_s}{\pi}\Delta\gamma_{ss}(m_i)$ $+\frac{2\alpha_s}{\pi}(C_1+C_2)\ln\mathcal{R}$	1	—	$p_T^{\rm cut}$
γ_{ss}	$\Gamma(C_1+C_2)$	$\frac{2\alpha_s}{\pi}\Delta\gamma_{ss}(m_i)$	1	$p_T^{\rm cut}$	$p_T^{\rm cut}$
γ_{sc}^i	$-\Gamma C_i$	0	1	$p_T^{\rm cut}\mathcal{R}$	$p_T^{\rm cut}\mathcal{R}$

5.5.4 Total NLL' Resummed Cross Section

For the case of unmeasured jets, we can now readily assemble the ingredients in Eq. (5.17) to obtain

$$d\sigma = \frac{p_T}{8\pi x_1 x_2 E_{\rm cm}^4}\frac{1}{N} B(x_1,\mu_B^1)\bar{B}(x_2,\mu_B^2) J_1(\bar{\mu}_J^1) J_2(\bar{\mu}_J^2)\,\Pi^{\rm unmeas}(\bar{\mu}_S,\bar{\mu}_J^{1,2},\mu_B^{1,2},\mu_H)$$
$$\times \mathrm{Tr}\{\mathbf{H}(\mu_H)\mathbf{\Pi}^\dagger(\bar{\mu}_S,\mu_H)\mathbf{S}^{\rm unmeas}(\bar{\mu}_S)\mathbf{\Pi}(\bar{\mu}_S,\mu_H)\} \tag{5.98}$$

where here and below we use a bar over a parameter to denote that it is an unmeasured quantity (so for example $\bar{\mu}_S$ denotes the unmeasured soft scale while μ_S denotes the measured soft scale), and $x_{1,2}$ are fixed to the values in Eq. (5.13). The function Π in Eq. (5.98) is defined as

$$\begin{aligned}\mathbf{\Pi}(\bar{\mu}_S, \mu_H) = \mathbf{\Pi}_S(\mu, \bar{\mu}_S)\mathbf{\Pi}_H(\mu, \mu_H) &= \exp\left\{\mathbf{M}\int_{\alpha_s(\mu_H)}^{\alpha_s(\bar{\mu}_S)} \frac{d\alpha}{\beta[\alpha]}\Gamma_c(\alpha)\right\} \\ &= \exp\left\{\mathbf{M}\left[\frac{2}{\beta_0}\ln\frac{\alpha_s(\mu_H)}{\alpha_s(\bar{\mu}_S)} + \cdots\right]\right\} \qquad (5.99)\end{aligned}$$

with $\mathbf{\Pi}_H$ and $\mathbf{\Pi}_S$ defined in Eqs. (5.61) and (5.73), respectively, where in the second equality we canceled the μ dependence (to all orders) and in the third equality we expanded to NLL' accuracy. We also used the definition of the overall multiplicative RG kernel as

$$\begin{aligned}\Pi^{\text{unmeas}}(\bar{\mu}_S, \bar{\mu}_J^{1,2}, \mu_B^{1,2}, \mu_H) &\equiv \Pi_H(\mu, \mu_H)\Pi_S^{\text{unmeas}}(\mu, \bar{\mu}_S)\prod_{i=1,2}\Pi_B^i(\mu, \mu_B^i)\prod_{i=1,2}\bar{\Pi}_J^i(\mu, \bar{\mu}_J^i) \\ &= \prod_{F=H,B_1,B_2,J_1,J_2} e^{K_F(\bar{\mu}_S,\mu_F)}\left(\frac{\mu_F}{m_F}\right)^{\omega_F(\bar{\mu}_S,\mu_F)}, \qquad (5.100)\end{aligned}$$

where m_F, K_F^i, ω_F^i for $F = J_i, B_i, H$ are given to NLL' in Eq.(A.8) and (A.9) in terms of the parameters of Table 5.2. To arrive at Eq. (5.100), we used the consistency of the anomalous dimensions to explicitly cancel the μ dependence to all orders. Here and below, we denote unmeasured quantities with bars to distinguish them from the corresponding measured quantities below.

When the angularity of one or more jets is measured, we need to include $S^{\text{meas}}(\tau_a^i)$ (and its corresponding anomalous dimension $\gamma_S^{\text{meas}}(\tau_a^i)$) for each measured jet, and we need to replace the unmeasured jet functions J_i with measured ones $J(\tau_a^i)$ (and replace $\bar{\Pi}_J^i \to U_J(\tau_a^i)$). To perform the convolutions for measured jet functions with the measured part of the soft functions, it is easier to first do the convolutions of the evolution factors with each other, and then convolve the resulting full kernel with

the renormalized functions. For the case of two measured jets, this yields

$$d\sigma(\tau_a^1,\tau_a^2) = \frac{p_T}{8\pi x_1 x_2 E_{\rm cm}^4}\frac{1}{N}B(x_1,\mu_B^1)\bar{B}(x_2,\mu_B^2)\Bigg[\Pi^{\rm meas}(\tau_a^{1,2},\mu_S^{1,2},\bar{\mu}_S,\mu_J^{1,2},\mu_B^{1,2},\mu_H)$$
$$\times\left[1+\left(f_S^1(\tau_a^1;\omega_S^1,\mu_S^1)+f_J^1(\tau_a^1;\omega_S^1,\mu_J^1)+(1\leftrightarrow 2)\right)\right]\Bigg]_+$$
$$\times\,{\rm Tr}\left\{\mathbf{H}(\mu_H)\mathbf{\Pi}^\dagger(\bar{\mu}_S,\mu_H)\mathbf{S}^{\rm unmeas}(\bar{\mu}_S)\mathbf{\Pi}(\bar{\mu}_S,\mu_H)\right\}, \tag{5.101}$$

where $f_J^i(\tau,\Omega,\mu)$ and $f_S^i(\tau,\Omega,\mu)$ are given in Eqs. (5.64) and (5.79), respectively, and we defined

$$\Pi^{\rm meas}(\tau_a^{1,2},\mu_S^{1,2},\bar{\mu}_S,\mu_J^{1,2},\mu_B^{1,2},\mu_H)$$
$$\equiv\frac{\Pi^{\rm unmeas}(\bar{\mu}_S,\mu_J^{1,2},\mu_B^{1,2},\mu_H)}{\prod_{i=1,2}\bar{\Pi}_J^i(\mu,\mu_J^i)}\prod_{i=1,2}U_J^i(\tau_a^i,\mu,\mu_J^i)\otimes U_S^i(\tau_a^i,\mu,\mu_S^i)$$
$$=\Pi^{\rm unmeas}(\bar{\mu}_S,\mu_J^{1,2},\mu_B^{1,2},\mu_H)\prod_{i=1,2}\frac{e^{K_S^i+\gamma_E\,\omega_S^i}}{\Gamma(-\omega_S^i)}\left(\frac{\mu_S^i}{m_S^i}\right)^{\omega_S^i}\frac{\Theta(\tau_a^i)}{(\tau_a^i)^{1+\omega_S^i}}, \tag{5.102}$$

where γ_E is the Euler constant. The K_S^i and ω_S^i appearing in these Eqs. (5.101) and (5.102) are expanded to NLL' in Eq.(A.8) and (A.9) in terms of the parameters in Table 5.2 and are evaluated at the scales

$$\omega_S^i\equiv\omega_S^i(\mu_J^i,\mu_S^i)$$
$$K_S^i\equiv K_S^i(\mu_J^i,\mu_S^i)\,. \tag{5.103}$$

To arrive at Eq. (5.102), we used that

$$\gamma_{J_i}(\tau_a^i,\mu)+\gamma_S^{\rm meas}(\tau_a^i,\mu)-\gamma_{J_i}(\mu)\,\delta(\tau_a^i)=0 \tag{5.104}$$

to explicitly cancel the μ dependence of the measured jet and soft functions and the subtracted out unmeasured jet functions (evaluated at the measured jet scale μ_J).

In particular, Eq. (5.104) implies that

$$e^{K_S^i(\mu_J,\mu_S)}\left(\frac{\mu_S}{m_S}\right)^{j_S\omega_S^i(\mu_J,\mu_S)} = e^{K_J^i(\mu,\mu_J)+K_S^i(\mu,\mu_S)-\bar{K}_J^i(\mu,\mu_J)} \times \left(\frac{\mu_J}{m_J}\right)^{j_J\omega_J^i(\mu,\mu_J)}\left(\frac{\mu_S}{m_S}\right)^{j_S\omega_S^i(\mu,\mu_S)}\left(\frac{\mu_J}{\bar{m}_J}\right)^{-\bar{\omega}_J^i(\mu,\mu_J)}, \tag{5.105}$$

and that

$$\omega_S^i(\mu_J,\mu_S) = \omega_S^i(\mu,\mu_S) + \omega_J^i(\mu,\mu_J)\,. \tag{5.106}$$

Finally, we note that to refactorize the cross section and resum logarithms of $\mathcal{R}$ as in Ref. [5], we simply need to make the replacement Eq. (5.96) for both the case of unmeasured and of measured jet formula, Eqs. (5.98) and (5.101), respectively, and interpret $\bar{\mu}_S \to \mu_{ss}$. We discuss the numerical impact of this effect in the next Section.

5.5.5 A Simple Example

We consider the simple partonic channel $qq' \to qq'$. Of course to compute a physically observable cross section we will need to sum over all partonic channels, however, this is beyond the scope of this work. Our aim is to consider the scale variation of the cross section and investigate the impact of refactorization of the soft function on the differential cross section. We find the main effect of refactorization is to reduce the normalization of the cross section and to lower the scale uncertainty, which is qualitatively similar to what is found in the study of refactorization in e^+e^- collisions recently completed in Ref. [5]. We also study the dependence of the cross section on the parameters $\mathcal{R}$, p_T^{cut}, and a, and comment on the physics responsible for this dependence.

From the results of Ref. [4] we have the ($\overline{\text{MS}}$ renormalized) hard function to $\mathcal{O}(\alpha_s)$ in the color basis that corresponds to the t-channel $\mathbb{8}\otimes\mathbb{8}$ and $\mathbb{1}\otimes\mathbb{1}$ operators,

$$\mathbf{H}(\mu) = 8g^4\big(\mathbf{H}_0 + \frac{\alpha_s}{4\pi}\mathbf{H}_1(\mu) + \mathcal{O}(\alpha_s^2)\big)\,, \tag{5.107}$$

where

$$\mathbf{H}_0 = \frac{s^2+u^2}{t^2}\begin{pmatrix} 1 & 0 \\ 0 & 0 \end{pmatrix}, \tag{5.108}$$

and

$$\begin{aligned}
[\mathbf{H}_1(\mu)]_{11} &= \frac{s^2+u^2}{t^2}\bigg(-4C_F \ln^2\frac{-t}{\mu^2} + 2\,\mathrm{Re}[X_1(s,t,u)]\ln\frac{-t}{\mu^2} + 2Y\bigg) \\
&\quad + \frac{s^2}{t^2}\Big(C_A - 4C_F\Big)\,\mathrm{Re}[Z(s,t,u)] + \frac{u^2}{t^2}(4C_F - 2C_A)\,\mathrm{Re}[Z(u,t,s)] \\
[\mathbf{H}_1(\mu)]_{21} &= \frac{s^2+u^2}{t^2}X_2(s,t,u)\ln\frac{-t}{\mu^2} - \frac{s^2}{t^2}\frac{C_F}{2C_A}Z(s,t,u) + \frac{u^2}{t^2}\frac{C_F}{2C_A}Z(u,t,s) \\
[\mathbf{H}_1(\mu)]_{12} &= [\mathbf{H}_1(\mu)]^*_{21} \\
[\mathbf{H}_1(\mu)]_{22} &= 0\,,
\end{aligned} \tag{5.109}$$

where $X_{1,2}$, Z, and Y are defined in Eqs. (33)-(36) of [4] and s, t, and u are given in terms of the jet rapidities and p_T in Eq. (5.14).

To use the convention of [4], we set $m_i = \sqrt{-t}$ for this channel and have

$$\mathbf{M}'(\sqrt{-t}) = \begin{pmatrix} 4C_F \ln\frac{-u}{s} - C_A \ln\frac{tu}{s^2} & 2\ln\frac{-u}{s} \\ \frac{C_F}{C_A}\ln\frac{-u}{s} & 0 \end{pmatrix} \tag{5.110}$$

and

$$\mathbf{M}(\sqrt{-t}) = \mathbf{M}'(\sqrt{-t}) + i\pi\mathbf{T}\,, \tag{5.111}$$

where

$$\mathbf{T} = \begin{pmatrix} -2/C_A & 2 \\ C_F/C_A & 0 \end{pmatrix}. \tag{5.112}$$

Computing the eigenvalues of $\mathbf{M}$ gives

$$\begin{aligned}
\lambda^H_{1,2} &= -\frac{C_A}{2}\Big(\ln\frac{ut}{s^2} + 2i\pi\Big) + 2C_F\Big(\ln\frac{-u}{s} + i\pi\Big) \\
&\quad \pm\sqrt{\frac{C_A^2}{4}\Big(\ln\frac{ut}{s^2} + 2i\pi\Big)^2 - 2C_FC_A\Big(\ln\frac{-u}{s} + i\pi\Big)\Big(\ln\frac{-t}{s} + i\pi\Big)}\,,
\end{aligned} \tag{5.113}$$

and for the eigenvectors we find

$$\mathbf{R} = \begin{pmatrix} \lambda_1^H & \lambda_2^H \\ \frac{C_F}{C_A}\Big(\ln\frac{-u}{s} + i\pi\Big) & \frac{C_F}{C_A}\Big(\ln\frac{-u}{s} + i\pi\Big) \end{pmatrix} . \tag{5.114}$$

The $\overline{\text{MS}}$ renormalized soft function for the naive factorization is given by

$$\mathbf{S}^{\text{unmeas}}(\mu) = \mathbf{S}_0 + \frac{\alpha_s}{\pi}\Bigg\{\mathbf{S}_0\Bigg[(\mathbf{S}^{\text{div}} + 2C_F \ln\mathcal{R})\ln\frac{\mu}{p_T^{\text{cut}}} - C_F \ln^2\mathcal{R} \\ - \mathbf{T}_1\cdot\mathbf{T}_2 \ln\left(1+e^{\Delta y}\right)\ln\left(1+e^{-\Delta y}\right)\Bigg] + \text{h.c.}\Bigg\}, \tag{5.115}$$

whereas the refactorized result is obtained with the replacement Eq. (5.96). The tree level soft function in this basis is given by

$$\mathbf{S}_0 = \begin{pmatrix} \frac{1}{2}C_F C_A & 0 \\ 0 & C_A^2 \end{pmatrix} \tag{5.116}$$

In addition to S_0 and the matrix component $\mathbf{M}'(m_i)$ of $\mathbf{S}^{\text{div}}$ given above, we need the matrix $\mathbf{T}_1\cdot\mathbf{T}_2$, which for a general $2 \to 2$ scattering is given by

$$\mathbf{T}_1\cdot\mathbf{T}_2 = \mathbf{T}_B\cdot\mathbf{T}_{\bar{B}} + \frac{1}{2}(C_B + C_{\bar{B}} - C_1 - C_2)\,. \tag{5.117}$$

For $qq \to qq$, $C_i = C_F$ for all i so the C_i cancel and we have

$$\mathbf{T} = \frac{1}{2}\Big[2\mathbf{T}_B\cdot\mathbf{T}_{\bar{B}} + 2\mathbf{T}_1\cdot\mathbf{T}_2\Big] = 2\mathbf{T}_1\cdot\mathbf{T}_2\,. \tag{5.118}$$

To estimate uncertainty from higher orders in perturbation theory, we vary the hard scale μ_H and the unmeasured jet and soft scales, $\bar{\mu}_J$ and $\bar{\mu}_S$, separately by $\pm 50\%$ around their central values, which we take to be the canonical scales μ_F given in Table 5.2. For the refactorized case, we vary the soft scales μ_{ss} and μ_{sc} simultaneously. However, to avoid varying the measured jet and soft scales for $\mu_{J,S} \sim \Lambda_{\text{QCD}}$, we vary them around profile functions [81, 82]. This is done by defining $\mu_{J,S}$ as

$$\mu_S^i(\tau_a^i) = (1 + e_S g(\tau))\mu(\tau_a^i) \\ \mu_J^i(\tau_a^i) = (1 + e_J g(\tau))\big(p_T\mathcal{R}\big)^{\frac{1-a}{2-a}}\big(\mu(\tau_a^i)\big)^{\frac{1}{2-a}}\,. \tag{5.119}$$

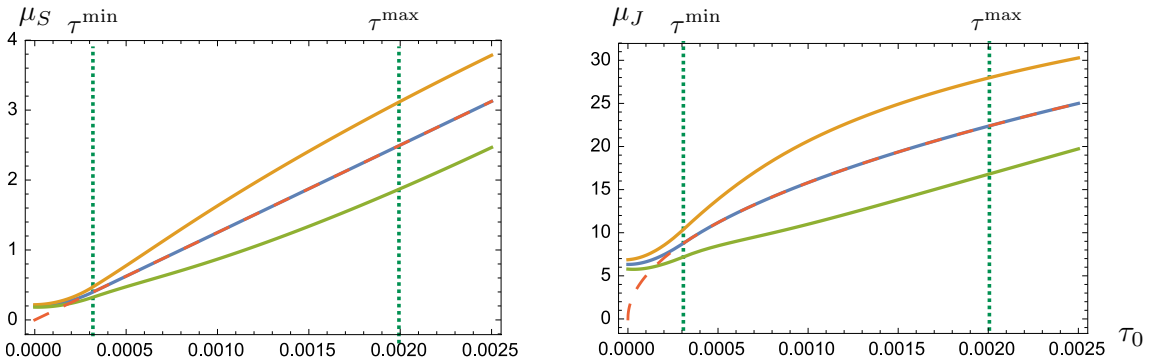

FIGURE 5.1: Profile functions for μ_S and μ_J. These functions are defined in Eq. (5.119) and below.

with $e_{J,S} \in (-1/2, 1/2)$. The total uncertainty bands are defined to be the envelope of all of the above variations.

In terms of the function

$$\theta_\epsilon(x) \equiv \frac{1}{1 + \exp\left(-x/\epsilon\right)}\,, \tag{5.120}$$

which becomes a Heaviside step function in the limit $\epsilon \to 0$,

$$\lim_{\epsilon \to 0} \theta_\epsilon(x) = \theta(x)\,, \tag{5.121}$$

the function $g(\tau)$ is chosen to be

$$g(\tau) = \theta_{\epsilon_1}(\tau - \tau^{\min})\, \theta_{\epsilon_2}(\tau^{\max} - \tau)\,, \tag{5.122}$$

and $\mu(\tau)$ is chosen to be

$$\mu(\tau) = \begin{cases} \mu_0 + \alpha \tau^\beta \sqrt{-t}, & \tau < \tau^{\min} \\ \dfrac{p_T\, \tau}{\mathcal{R}^{1-a}}, & \tau > \tau^{\min} \end{cases}\,, \tag{5.123}$$

where α and β are fixed by the continuity of $\mu(\tau)$ and its first derivative to be

$$\begin{aligned} \alpha &= \frac{p_T}{\beta (\tau^{\min})^{\beta-1} \mathcal{R}^{1-a} \sqrt{-t}} \\ \beta &= \left(1 - \frac{\mu_0 R^{1-a}}{p_T \tau^{\min}}\right)^{-1}\,, \end{aligned} \tag{5.124}$$

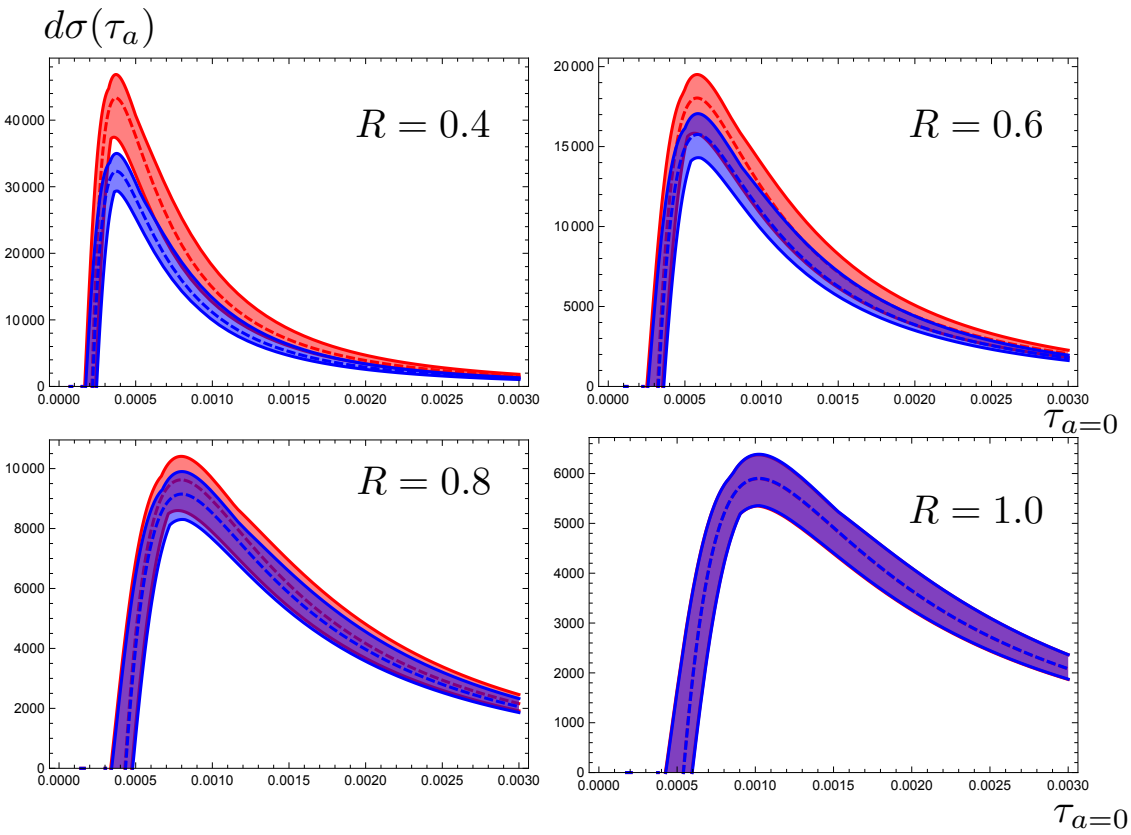

FIGURE 5.2: Differential cross section for four different values of R with soft function refactorized (blue) and without (red). Central values are dotted lines and band includes scale variation.

respectively. The continuity conditions also require that β is greater than unity which implies we need $\tau^{\min} > \mu_0 \mathcal{R}^{1-a}/p_T$.

The profile functions for μ_S and μ_J, for $a = 0$, are shown in Fig. 5.1. Eqs. (5.122) and (5.123) together ensure that for sufficiently small τ, the scale choice becomes frozen to be μ_0 (and non-perturbative physics dominates), above some scale $\tau^{\min}$ we recover the canonical choices (cf. $m_{J,S}$ of table Table 5.2), and above a third scale $\tau^{\max}$ individual H, J, S scale variation begins to dampen (as that should be handled by the traditional μ variation of fixed-order QCD using a tail-region matching scheme). This is expected to give reasonable scale variation for the range of validity, roughly $\tau^{\min} < \tau < \tau^{\max}$.

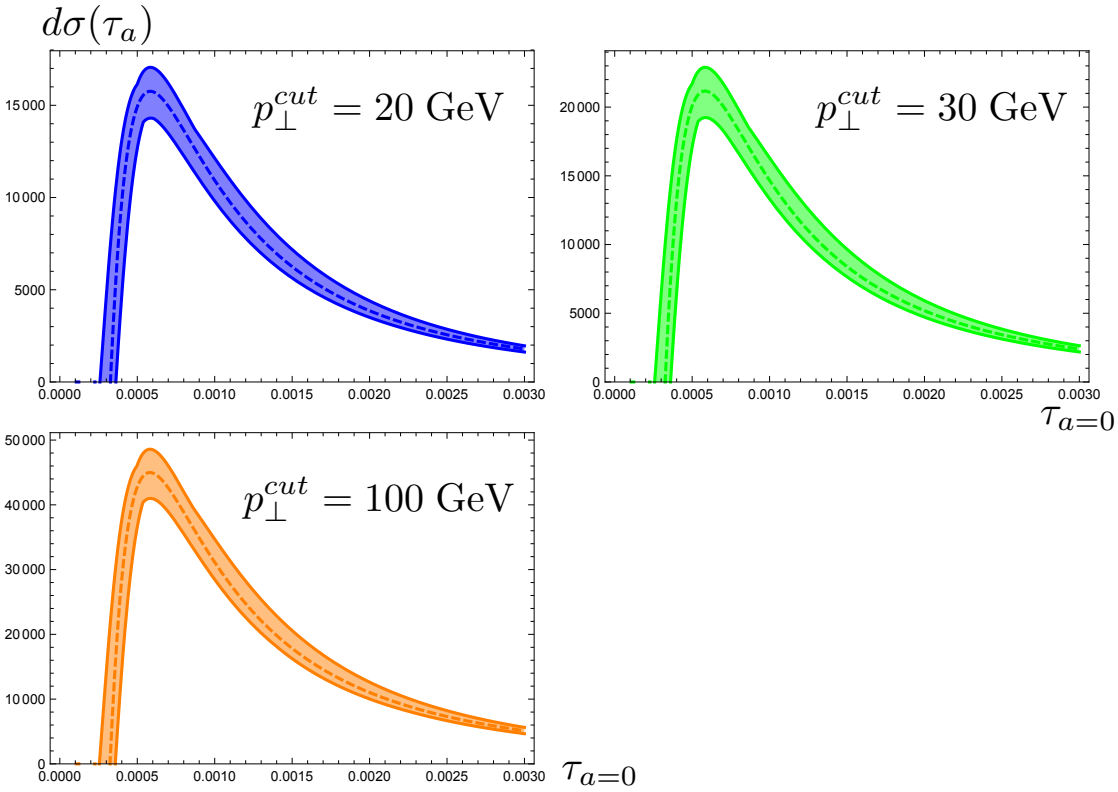

FIGURE 5.3: Differential cross sections for three different values of $p_T^{\rm cut}$.

For the sake of illustration, we plot the "normalized cross section" (which neglects the PDFs and effects of the fixed order beam function corrections, the latter of which can be found in [70] following the discussion in Sec. 5.4.2), defined as

$$d\tilde{\sigma}(\tau_a) \equiv \frac{B(x_1,\mu=\mu_H)\bar{B}(x_2,\mu=\mu_H)}{B(x_1,\mu=\mu_B^1)\bar{B}(x_2,\mu=\mu_B^2)} \frac{d\sigma(\tau_a^1,\tau_a^2)}{\sigma^{\rm LO}(\mu=\mu_H)}\bigg|_{\tau_a^1=\tau_a^2=\tau_a} . \tag{5.125}$$

For the kinematic and algorithm/observable parameters, we choose for a set of default parameters (fixed to these values unless explicitly varying them in the figures)

$$\begin{array}{llll} \mathrm{E_{cm}} = 10 \text{ TeV} & y_1 = 1.0 & p_T = 500 \text{ GeV} & \mathcal{R} = 0.6 \\ a = 0 & y_2 = 1.4 & p_T^{\rm cut} = 20 \text{ GeV} & y_{\rm cut} = 1.7 \end{array} , \tag{5.126}$$

which corresponds to (via Eqs. (5.13) and (5.14))

$$\begin{array}{l} t/s = -0.401 \\ u/s = -0.599 \\ \sqrt{s}/\mathrm{E_{cm}} = 0.051 \end{array} \quad \text{and} \quad \begin{array}{l} x_1 = 0.169 \\ x_2 = 0.015 \end{array}, \tag{5.127}$$

and for the profile functions parameters, we choose

$$\begin{array}{l} \tau^{\min} = 2(1-a)\mu_0 \mathcal{R}^{1-a}/p_T = .00032(1-a) \\ \tau^{\max} = .002 \end{array} \quad \text{and} \quad \begin{array}{l} \dfrac{\epsilon_1}{\tau^{\min}} = \dfrac{\epsilon_2}{\tau^{\max}} = 10^{-0.1} \\ \mu_0 = 200\,\mathrm{MeV} \end{array}. \tag{5.128}$$

In Fig. 5.2 we show the NLL' calculations for four different values of $\mathcal{R}$, with all other parameters set to their default values in Eq. (5.126). In these plots the blue bands are the predictions with a refactorized soft function and the red bands are the predictions without refactorization. In the limit $\mathcal{R} \to 1$ the scales μ_{ss} and μ_{sc} coincide and the two calculations must give the same result, as seen in the figure. For the smallest value of $\mathcal{R} = 0.4$, refactorization lowers the normalization of the cross sections by a factor of roughly two, without changing the shape of the distribution or the location of the peak. Refactorization gives a small reduction in the scale uncertainty for $\mathcal{R} < 1$. Note that as $\mathcal{R}$ decreases the peak in the τ_0 distribution shifts to smaller values of τ_0 because the jets are narrower.

Fig. 5.3 shows the refactorized NLL' resummed cross section for three different values of p_T^{cut} with all other parameters set to their defaults in Eq. (5.126). Interestingly the shape of the distribution and the location of the peak in the cross section are completely independent of p_T^{cut}, only the normalization of the cross section is affected. As expected, the cross section is larger for larger values of p_T^{cut}. As discussed in the Introduction, the NGLs, which are of the form $\alpha_s^n \ln^n(p_T^{\mathrm{cut}}\,\mathcal{R}^2/p_T^J\,\tau_a)$, for $n \geqslant 2$, combine p_T^{cut} and τ_a in a nontrivial way. It is possible that when the NGLs are included in the calulcation, the location of the peak of the τ_a distribution may

no longer be p_T^{cut} independent. Therefore, the dependence of the peak on p_T^{cut} might be an observable that is sensitive to the NGLs.

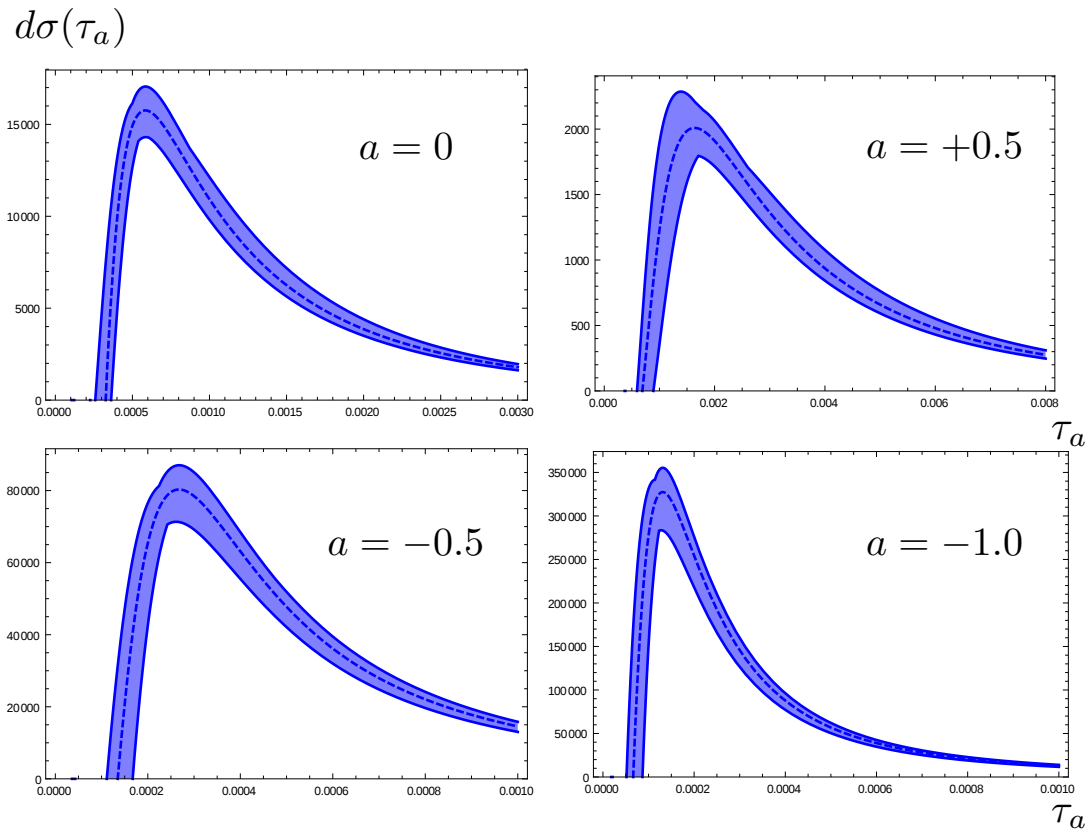

FIGURE 5.4: Differential cross sections for four different values of a.

Fig. 5.4 shows the refactorized NLL' resummed cross section for four different values of a with other parameters set to the default values. As a is made large and negative, the contribution to the angularity from particles collinear to the jet axis is suppressed by large powers of the angle with the jet axis. Correspondingly the distribution is peaked at smaller values of τ_a, a behavior also seen in calculations of jet angularities in e^+e^- collisions [65]. It is important for obtaining sensible scale variation for all values of a that the parameter τ^{min} defined in Eq. (5.128) is proportional $(1-a)$. Both perturbative and power corrections grow with $1/(1-a)$ and factorization breaks down completely for $a = 1$ in SCET_I (although an SCET_II

approach can be used for $a = 1$ [103]). Thus, one expects increasing uncertainty as $a \to 1$ from below, and we see from Fig. 5.3 that the uncertainties in the predictions are substantially larger for $a = 0.5$ than for $a \leqslant 0$.

5.6 Conclusion

In this work, we presented the factorization formulae valid for jet production in hadron colliders with rapidity cuts about the beams, an out-of-jet p_T^{cut} veto, and the jets identified with either a k_T-type (including k_T, C/A, and anti-k_T) or cone-type algorithm. We considered the cases that the jets can either be identified but otherwise unprobed ("unmeasured" jets) or are further probed with angularities ("measured" jets). The ingredients of these formulae involved jet functions, unmeasured beam functions, and an observable dependent soft function. This soft function was further written in terms of a universal piece, $\mathbf{S}^{\text{unmeas}}$, which encodes the out-of-jet energy veto p_T^{cut} and angularity independent (but color and direction dependent) pieces.

We were able to relate all of the ingredients of the factorization formula except for $\mathbf{S}^{\text{unmeas}}$ to analogous quantities that have previously been calculated in the context of e^+e^- collisions to NLL' accuracy. $\mathbf{S}^{\text{unmeas}}$ was explicitly computed for the case of dijet production (for which all Wilson lines are coplanar) in terms of color operators $\mathbf{T}_i \cdot \mathbf{T}_j$ that encode the color correlations at this order. We in turn explicitly presented results for these color operators (which become matrices in color space) for the $qq' \to qq'$ channel, and plotted the corresponding distribution for the illustrative example where both jets are measured with τ_a for $a = 0$ in the $\tau_a^1 = \tau_a^2$ bin. We also generalized the refactorization of Ref. [5] to include color-mixing effects and found that, as was already seen in e^+e^-, the normalization of the cross section and the corresponding scale uncertainty were reduced. Using the results of Ref. [5], our results can now be straightforwardly extended to NNLL for any combination of measured (at least for $a = 0$) and unmeasured jets. The non-global logarithms which we do not include

and would appear in a fixed order calculation of the soft function beginning at $\mathcal{O}(\alpha_s^2)$ have arguments of order $p_T^{\text{cut}}\mathcal{R}^2/p_T^J\tau_a$ which for the peak region of the distribution (where we trust our calculation) is $\mathcal{O}(1)$ to within a decade.

Armed with this foundation, we can now (after including all the partonic channels) make meaningful comparisons with Monte Carlo event generators and directly with data. It will be of particular interest to study the sensitivity of the proposed, factorized cross section to effects like multiple parton interactions. Other observables that are sensitive to radiation near the beam pipes like beam thrust [150] have been noted to receive $\mathcal{O}(1)$ corrections from these effects. We expect that our observables will be less sensitive to this effect because the jets are isolated and the unmeasured beam functions should not be sensitive to radiation near the beam pipe. We also hope to be able to incorporate other effects with the recent developments for NGLs as discussed in the Introduction. In addition, we are interested in extending the results of this chapter to cross sections for jets in which there is an identified heavy quarkonia, especially J/ψ and Υ. The cross sections will take essentially the same form as the cross sections in this chapter, with an additional convolution of the cross section with the heavy quark or quarkonium fragmentation as well as a modified f_J factor that depends on the matching coefficients in the fragmenting jet function. We expect to compare these predictions to Monte Carlo event generators and LHC measurements [151].

6

Conclusions

In this thesis the development of a complete framework for studies of quarkonium production within jets is presented. The methodology used is based on the factorization theorems of Soft-Collinear Effective Theory and Non-Relativistic Quantum Chromodynamics. In Chapter 3 we show how this formalism can be extended to various jet observables and particularly we studied a family of jet-shape observables referred to as angularities. We calculated the cross section at NLL accuracy for the production of B mesons and J/ψ through b-quark and gluon fragmentation, respectively. For the case of J/ψ we considered four NRQCD production mechanisms, in particular: ${}^3S_1^{[1]}$, ${}^1S_0^{[8]}$, ${}^3S_1^{[8]}$, and ${}^3P_J^{[8]}$. We compare our results against monte carlo simulations using Pythia and Herwig simulation packages. While our analytic calculations are in very good agreement with the results from simulations for the case of B mesons, they differ significantly for J/ψ. The problem was traced to the unrealistic showering of color-octet $c\bar{c}$ pair in the simulations. By modifying the simulations in order to implement a more realistic showering process, we found consistency with our analytic calculations. Furthermore our results showed some discriminating power between the various production mechanisms of J/ψ.

As an extension of the work on FJFs, in Chapter 4 we introduced the Transverse Momentum Dependent FJF (TMDFJF). Similar to the standard FJFs, the TMDFJFs describe a hadron produced within a jet and in addition the transverse momentum of the hadron is measured with respect to the jet axis. Using the framework of TMDFJF, we derive expressions for the angular distributions of hadrons with respect to the jet axis. We implement our results for the case of J/ψ production for the four mechanisms mentioned earlier. The mean angle, as a function of the energy fraction, was found to have significant discriminating power between the production mechanisms.

As a step towards applying this formalism to similar cross sections in hadron colliders, we completed the calculations of all the necessary parts for evaluating the dijet cross section at LHC. For this purpose we constructed the universal part of the soft function and introduced the unmeasured beam functions that describe the initial state jets. We also presented the implementation of a recently-developed factorization approach for resumation of the global logarithms of the jet cone size parameter.

We also performed a semi-analytic calculation for proton-proton collisions at $\sqrt{s} = 13$ GeV and compared against recent measurements from the LHCb collaboration. Our formalism showed that the energy ratio parameter z is sensitive to the values of LDMEs and that various extractions of the LDMEs give significantly different distributions. LDMEs extracted from high $p_\perp$ hadron collider data show much better agreement with the experimental data.

The work presented in this thesis consists of a complete formalism that can be used to study quarkonium production in jets at hadron colliders that will give a further insight into quarkonium production mechanisms.

Appendix A

Renormalization Group and Resummation

A.1 Evolution of Measured and Unmeasured Functions

The RGEs satisfied by the elements of the factorization theorem are separated into two categories; terms that do depend on the variable τ_a and terms that do not. The latter satisfy the following RGE

$$\mu \frac{d}{d\mu} f(\mu) = \gamma_f(\mu) f(\mu)\,, \tag{A.1}$$

where $\gamma_F(\mu)$ is the anomalous dimension

$$\gamma_F(\mu) = -\frac{1}{Z_F(\mu)} \mu \frac{d}{d\mu} Z_F(\mu) = \Gamma_F(\alpha_s) \ln\left(\frac{\mu^2}{m_F^2}\right) + \gamma_F(\alpha_s)\,, \tag{A.2}$$

where m_F is related to the characteristic scale for the particular function, and $Z_F(\mu)$ is the renormalization function for $F(\mu)$. The coefficient $\Gamma_F(\alpha_s)$ is proportional to the cusp anomalous dimension, $\Gamma_{\rm cusp}(\alpha_s)$, which can be expanded in α_s

$$\Gamma_{\rm cusp}(\alpha_s) = \sum_{n=0}^{\infty} \left(\frac{\alpha_s}{4\pi}\right)^{1+n} \Gamma_c^n, \tag{A.3}$$

and $\Gamma_F = (\Gamma_F^0/\Gamma_c^0)\Gamma_{\rm cusp}$. The non-cusp part, $\gamma_F(\alpha_s)$, has a similar expansion

$$\gamma_F(\alpha_s) = \sum_{i=0}^{\infty} \left(\frac{\alpha_s}{4\pi}\right)^{1+i} \gamma_F^i. \tag{A.4}$$

The solution to RGE is given by

$$F(\mu) = \exp\left(K_F(\mu,\mu_0)\right) \left(\frac{\mu_0}{m_F}\right)^{\omega_F(\mu,\mu_0)} F(\mu_0)\,, \tag{A.5}$$

or equivalently

$$F(\mu) = \Pi_F(\mu,\mu_0) F(\mu_0)\,, \tag{A.6}$$

where the evolution kernel Π_F is given by

$$\Pi_F(\mu,\mu_0) = e^{K_F(\mu,\mu_0)} \left(\frac{\mu_0}{m_F}\right)^{\omega_F(\mu,\mu_0)}, \tag{A.7}$$

where the exponents K_F and ω_F are given in terms of the anomalous dimension,

$$K_F(\mu,\mu_0) = 2\int_{\alpha(\mu)}^{\alpha(\mu_0)} \frac{d\alpha}{\beta(\alpha)} \Gamma_F(\alpha) \int_{\alpha(\mu_0)}^{\alpha} \frac{d\alpha'}{\beta(\alpha')} + \int_{\alpha(\mu)}^{\alpha(\mu_0)} \frac{d\alpha}{\beta(\alpha)} \gamma_F(\alpha), \tag{A.8}$$

$$\omega_F(\mu,\mu_0) = 2\int_{\alpha(\mu)}^{\alpha(\mu_0)} \frac{d\alpha}{\beta(\alpha)} \Gamma_F(\alpha), \tag{A.9}$$

and for up to NLL and NLL' accuracy are given by

$$\begin{aligned} K_F(\mu,\mu_0) &= -\frac{\gamma_F^0}{2\beta_0} \ln r - \frac{2\pi\Gamma_F^0}{(\beta_0)^2}\Big[\frac{r-1+r\ln r}{\alpha_s(\mu)} + \left(\frac{\Gamma_c^1}{\Gamma_c^0} - \frac{\beta_1}{\beta_0}\right)\frac{1-r+\ln r}{4\pi} \\ &\quad + \frac{\beta_1}{8\pi\beta_0}\ln^2 r\Big], \\ \omega_F(\mu,\mu_0) &= -\frac{\Gamma_F^0}{j_F\beta_0}\Big[\ln r + \left(\frac{\Gamma_c^1}{\Gamma_c^0} - \frac{\beta_1}{\beta_0}\right)\frac{\alpha_s(\mu_0)}{4\pi}(r-1)\Big], \end{aligned} \tag{A.10}$$

where $r = \alpha(\mu)/\alpha(\mu_0)$ and β_n are the coefficients of the QCD β-function,

$$\beta(\alpha_s) = \mu\frac{d\alpha_s}{d\mu} = -2\alpha_s \sum_{n=0}^{\infty} \left(\frac{\alpha_s}{4\pi}\right)^{1+n} \beta_n\,. \tag{A.11}$$

The RGEs for functions that depend on the variable τ_a are of the form

$$\mu\frac{d}{d\mu}F(\tau_a,\mu) = \Big[\gamma_F(\mu)\otimes F(\mu)\Big](\tau_a)\,, \tag{A.12}$$

where

$$\begin{aligned}\gamma_F(\tau_a,\mu) &= -\Big[Z_F^{-1}(\mu)\otimes\mu\frac{d}{d\mu}Z_F(\mu)\Big](\tau_a)\\ &= \Gamma_F(\alpha_s)\left(\ln\frac{\mu^2}{m_F^2}-\frac{2}{j_F}\left(\frac{\Theta(\tau_a)}{\tau_a}\right)_+\right)+\gamma_F(\alpha_s)\delta(\tau_a)\,,\end{aligned} \tag{A.13}$$

and the solution to this equation is given by

$$F(\tau_a,\mu) = \exp\left(K_F+\gamma_E\omega_F\right)\frac{1}{\Gamma(-\omega_F)}\left(\frac{\mu_0}{m_F}\right)^{j_F\omega_F}\left[\left(\frac{\Theta(\tau_a)}{(\tau_a)^{1+\omega_F}}\right)_+\otimes F(\tau_a,\mu_0)\right]. \tag{A.14}$$

or equivalently

$$F(\tau_a,\mu) = \int d\tau'\,U_F(\tau_a-\tau_a',\mu,\mu_0)F(\tau_a',\mu_0)\,, \tag{A.15}$$

where to all orders in α_s the evolution kernel U_F is given by [152–156]

$$U_F(\tau_a,\mu,\mu_0) = \frac{e^{K_F+\gamma_E\omega_F}}{\Gamma(-\omega_F)}\left(\frac{\mu_0}{m_F}\right)^{j_F\omega_F}\left[\frac{\Theta(\tau_a)}{(\tau_a)^{1+\omega_F}}\right]_+\,, \tag{A.16}$$

where γ_E is the Euler constant.

A.1.1 Plus-distribution identities

We begin with the equation

$$\int d\tau''\Big[\frac{\Theta(\tau-\tau'')}{(\tau-\tau'')^{1+\omega_1}}\Big]_+\Big[\frac{\Theta(\tau''-\tau')}{(\tau''-\tau')^{1+\omega_2}}\Big]_+ = \frac{\Gamma(-\omega_1)\Gamma(-\omega_2)}{\Gamma(-\omega_1-\omega_2)}\Big[\frac{\Theta(\tau-\tau')}{(\tau-\tau')^{1+\omega_1+\omega_2}}\Big]_+\,, \tag{A.17}$$

which can be easily proven using Laplace transforms and the defining equation of the plus distribution,

$$[f(\tau)]_+ \equiv \lim_{\beta\to 0}\frac{d}{d\tau}\left[\theta(\tau-\beta)F(\tau)\right], \tag{A.18}$$

where $F(\tau)$ is defined as

$$F(\tau) \equiv \int_1^\tau d\tau' f(\tau'), \tag{A.19}$$

which yields

$$\mathcal{L}\Big\{\left(\frac{1}{\tau^{1+\omega}}\right)_+\Big\} = s^\omega\Gamma(-\omega). \tag{A.20}$$

The following equations can be derived by setting $\tau'\to 0$ in Eq. (A.17), expanding in ω_2 both sides and matching powers:

$$\int d\tau'\Big[\frac{\Theta(\tau-\tau')}{(\tau-\tau')^{1+\omega}}\Big]_+\mathcal{L}_{-1}(\tau') = \Big[\frac{\Theta(\tau)}{\tau^{1+\omega}}\Big]_+, \tag{A.21}$$

$$\int d\tau'\Big[\frac{\Theta(\tau-\tau')}{(\tau-\tau')^{1+\omega}}\Big]_+\mathcal{L}_0(\tau') = \Big[\frac{\Theta(\tau)}{\tau^{1+\omega}}\Big]_+\left(\ln\tau - H(-1-\omega)\right),$$

$$\int d\tau'\Big[\frac{\Theta(\tau-\tau')}{(\tau-\tau')^{1+\omega}}\Big]_+\mathcal{L}_1(\tau') = \Big[\frac{\Theta(\tau)}{\tau^{1+\omega}}\Big]_+\frac{\left(\ln\tau - H(-1-\omega)\right)^2 + \pi^2/2 - \psi^{(1)}(-\omega)}{2},$$

where we used [65]

$$\Big[\frac{\Theta(\tau)}{\tau^{1+\omega}}\Big]_+ = \sum_{n=-1}^{\infty}(-\omega)^n\mathcal{L}_n(\tau'), \tag{A.22}$$

where

$$\mathcal{L}_{-1}(\tau) = \delta(\tau) \quad \text{and} \quad \mathcal{L}_{n>-1}(\tau') = \Big[\frac{\Theta(\tau)\ln^n(\tau)}{\tau}\Big]_+. \tag{A.23}$$

A.2 Reorganization of logarithms of $(1-z)$

The convolutions in the variable z need to be performed numerically since they involve the evolved FFs, which are evaluated by solving the DGLAP equation using Mellin transformations. For this reason we expand the plus-distributions using the following relations

$$\int_z^1 \frac{dx}{x}\Big(\frac{1}{1-x}\Big)_+ f\left(\frac{z}{x}\right) = \int_z^1 dx\ \frac{1}{1-x}\Big(\frac{1}{x}f\left(\frac{z}{x}\right) - f(z)\Big) + f(z)\ln(1-z), \quad \text{(A.24)}$$

$$\int_z^1 \frac{dx}{x}\Big(\frac{\ln(1-x)}{1-x}\Big)_+ f\left(\frac{z}{x}\right) = \int_z^1 dx\ \frac{\ln(1-x)}{1-x}\Big(\frac{1}{x}f\left(\frac{z}{x}\right) - f(z)\Big) + f(z)\frac{1}{2}\ln^2(1-z). \quad \text{(A.25)}$$

Thus for every function $D(z)$ the convolution with $f_{\mathcal{J}}^{ij}(\tau,z,\mu)$ gives

$$\frac{1}{T_{ij}}\frac{2\pi}{\alpha_s(\mu)} f_{\mathcal{J}}^{ij}(\tau,z,\mu) \bullet D(z) = \delta_{ij}\ f_1(\tau,z,\mu)\ D(z) - g_1(\tau,z,\mu) + g_2(\tau,z,\mu), \quad \text{(A.26)}$$

where

$$\begin{aligned}
f_1(\tau,z,\mu) &= \frac{1-a/2}{1-a}\Big(f_2(\tau,z,\mu)\Big)^2 + \frac{a(1-a/4)}{(1-a)(1-a/2)}\frac{\pi^2}{6} - \frac{\psi^{(1)}(-\Omega)}{(1-a)(1-a/2)},\\
f_2(\tau,z,\mu) &= 2\ln\left(\frac{\mu}{\mu_J(\tau,z)}\right) + \frac{1}{1-a/2}H(-1-\Omega),\\
g_1(\tau,z,\mu) &= \int_z^1 dx\ \ f_2(\tau,x,\mu)\Big(\frac{\bar{P}_{ji}(x)}{x}\circ D\left(\frac{z}{x}\right)\Big),\\
g_2(\tau,z,\mu) &= \int_z^1 dx\ \ \Big[c_{ij}(x) - \frac{1}{1-a/2}\ln\left(1+\left(\frac{1-x}{x}\right)^{1-a}\right)\frac{\bar{P}_{ji}(x)}{x}\Big]\circ D\left(\frac{z}{x}\right),
\end{aligned} \quad \text{(A.27)}$$

with

$$\mu_J(\tau,z) = \omega\tau^{1/(2-a)}(1-z)^{(1-a)/(2-a)},$$

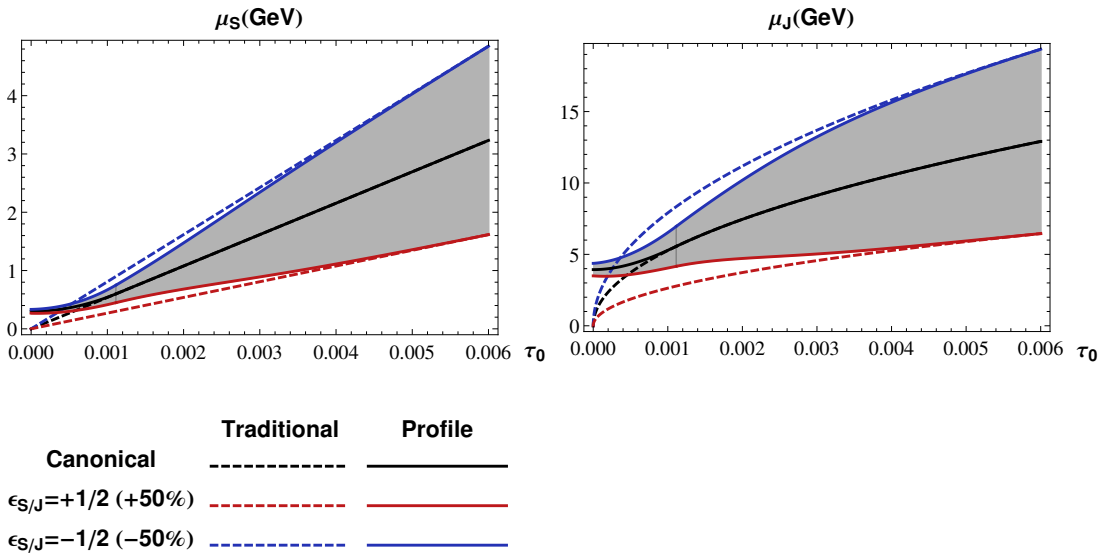

FIGURE A.1: Profile functions for $\mu_S^{PF}(\tau_0)$ and $\mu_J^{PF}(\tau_0)$, the τ_0-dependent renormalization scales that we use in the scale variations of our measured soft function and measured jet function. Also shown are traditional scale variations done by varying μ by $\pm 50\%$.

$$
\begin{aligned}
c_{qq}(z) &= \frac{1-z}{z}, \\
c_{gg}(z) &= 0, \\
c_{gq}(z) &= 2(1-z), \\
c_{qg}(z) &= 1,
\end{aligned}
$$

and

$$
\begin{aligned}
f(x) \circ g(x) &= f(x)g(x)\,, \\
[f(x)(h(x))_+] \circ g(x) &= h(x)[f(x)g(x) - f(1)g(1)]\,.
\end{aligned}
$$

A.3 Profile Functions

Here, we write down the profile functions used to perform scale variations for our measured soft and measured jet functions. We use profile functions to introduce a

τ_a-dependent scale variation that freezes at the characteristic scale for high values of τ_a where the factorization theorem breaks down and at a fixed scale for small values of τ_a where we reach the non-perturbative regime. The profile function for the measured soft function, $\mu_S^{PF}(\tau_0)$, and the profile function for the measured jet function, $\mu_J^{PF}(\tau_0)$, are plotted in Fig. A.1 (for the case $a = 0$). The analytic formulae for these functions are

$$\mu_S^{PF}(\tau_a) = \left[1 + \epsilon_S \frac{g(\tau_a)}{g(1)}\right] \times \begin{cases} \mu_{min} + \alpha\tau_a^\beta & 0 < \tau_a < \tau_{min} \\ \omega\tau_a / r^{(1-a)} & \tau_{min} \leqslant \tau_a \end{cases},$$

$$\mu_J^{PF}(\tau_a) = \left[1 + \epsilon_J \frac{g(\tau_a)}{g(1)}\right] \times \begin{cases} (\omega r)^{(1-a)/(2-a)} (\mu_{min} + \alpha\tau_a^\beta)^{1/(2-a)} & 0 < \tau_a < \tau_{min} \\ \omega\tau_a^{1/(2-a)} & \tau_{min} \leqslant \tau_a \end{cases}, \tag{A.28}$$

where we have defined

$$g(\tau) = \frac{1}{\exp\left(1.26(\tau_{min} - \tau)/\tau_{min}\right) + 1}, \tag{A.29}$$

and where α and β are defined to be

$$\beta = \frac{\tau_{min}}{\tau_{min} - \mu_{min} r^{(1-a)}/\omega} \quad \text{and} \quad \alpha = \frac{\omega}{\beta \tau_{min}^{\beta-1} r^{(1-a)}}. \tag{A.30}$$

These choices for α and β ensure that the profile functions and their first derivatives are continuous. We use the following values for the parameters

$$\begin{aligned} \tau_{min} &= 2\mu_{min} r^{1-a}/\omega \\ \mu_{min} &= 0.3\,\text{GeV}. \end{aligned} \tag{A.31}$$

We define our scale variations via

$$\begin{aligned} \epsilon_{S/J} = 1/2 \quad &\rightarrow \quad +50\% \text{ variation}, \\ \epsilon_{S/J} = -1/2 \quad &\rightarrow \quad -50\% \text{ variation}, \\ \epsilon_{S/J} = 0 \quad &\rightarrow \quad \text{Canonical scale}, \end{aligned}$$

and take the final scale variation bands as the envelope of the set of bands from the individual variations.

A.4 Rapidity RG Evolution

The RRG equation in momentum space for a renormalized function F^R is given by

$$\nu\frac{d}{d\nu}F^R(\mathbf{p}_\perp,\mu,\mu/\nu)=\gamma_\nu^F(\mathbf{p}_\perp,\mu,\nu)\otimes_\perp F^R(\mathbf{p}_\perp,\mu,\mu/\nu), \tag{A.32}$$

where the anomalous dimension can be written in the following generic form,

$$\gamma_\nu^F(\mathbf{p}_\perp,\mu,\nu)=\Gamma_\nu^F[\alpha_s]\mathcal{L}_0(\mathbf{p}_\perp^2,\mu^2)+\gamma_\nu^F[\alpha_s]\delta^{(2)}(\mathbf{p}_\perp), \tag{A.33}$$

where

$$\delta^{(2)}(\mathbf{p}_\perp)=\frac{1}{\pi}\delta(\mathbf{p}_\perp^2). \tag{A.34}$$

The cusp and non-cusp parts of the anomalous dimension are listed in Table A.1. Taking the Fourier transform of Eq. (A.32) yields,

$$\frac{d}{d\ln\nu}\tilde{F}(b,\mu,\nu)=\tilde{\gamma}_\nu^F(b,\mu,\nu)\tilde{F}(b,\mu,\nu), \tag{A.35}$$

where the Fourier conjugate of $\mathbf{p}_\perp$ is $\boldsymbol{b}$ where $|\boldsymbol{b}|=b$ and using the form of the anomalous dimensions in Eq. (4.42,4.43) gives that,

$$\tilde{\gamma}_\nu^F(b,\mu,\nu)=-\frac{\Gamma_\nu^F[\alpha_s]}{(2\pi)^2}\ln\left(\frac{\mu}{\mu_C(b)}\right)+\frac{\gamma_\nu^F[\alpha_s]}{(2\pi)^2}, \tag{A.36}$$

where $\mu_C(b)=2e^{-\gamma_E}/b$. Integrating Eq. (A.35) yields

$$\tilde{F}(b,\mu,\nu)=\tilde{F}(b,\mu,\nu_0)\mathcal{V}_F(b,\mu,\nu,\nu_0), \tag{A.37}$$

where

$$\mathcal{V}_F(b,\mu,\nu,\nu_0)=\exp\Big[G_F(\mu,\nu,\nu_0)\Big]\left(\frac{\mu}{\mu_C}\right)^{\eta_F(\mu,\nu,\nu_0)}, \tag{A.38}$$

with

$$G_F(\mu,\nu,\nu_0) = \frac{\gamma_\nu^F[\alpha_s]}{(2\pi)^2}\ln\left(\frac{\nu}{\nu_0}\right) \qquad \text{and} \qquad \eta_F(\mu,\nu,\nu_0) = -\frac{\Gamma_\nu^F[\alpha_s]}{(2\pi)^2}\ln\left(\frac{\nu}{\nu_0}\right). \quad \text{(A.39)}$$

Table A.1: Values of the cusp and non-cup parts of the anomalous dimensions for the collinear and collinear-soft functions.

Function (F)	Γ_ν^F	γ_ν^F	Γ_F^0	γ_F^0
$\mathcal{D}_{i/h}$	$-(8\pi)\alpha_s C_i + \mathcal{O}(\alpha_s^2)$	$\mathcal{O}(\alpha_s^2)$	0	$4C_i(\ln(\nu^2/\omega^2) + \bar{\gamma}_i)$
S_C^i	$(8\pi)\alpha_s C_i + \mathcal{O}(\alpha_s^2)$	$\mathcal{O}(\alpha_s^2)$	$4C_i$	0

Appendix B

FJFs matching Coefficients and Consistency Checks

B.1 Evaluation of matching coefficients

In pure dimensional regularization all diagrams contributing to the FFs vanish, and the only diagrams that contribute to the angularity FJF for quarks are Figs. 3a) and 3b) of Ref. [68]. For Fig. 3a) we get

$$\frac{C_F\alpha_s}{2\pi}\frac{(4\pi\mu^2)^\epsilon(1-\epsilon)}{\Gamma[1-\epsilon]}\frac{1-z}{1-a/2}\,\omega^{2a\epsilon/(2-a)}(1-z)^{-2(1-a)\epsilon/(2-a)} \times\left(1+\frac{(1-z)^{1-a}}{z^{1-a}}\right)^{2\epsilon/(2-a)}\frac{1}{s_a^{1+2\epsilon/(2-a)}}\,, \quad \text{(B.1)}$$

and for Fig. 3b) we get

$$\frac{C_F\alpha_s}{2\pi}\frac{2z}{1-a/2}\frac{(4\pi\mu^2)^\epsilon}{\Gamma[1-\epsilon]}\omega^{2a\epsilon/(2-a)}\frac{1}{(1-z)^{1+2(1-a)\epsilon/(2-a)}} \times\left(1+\frac{(1-z)^{1-a}}{z^{1-a}}\right)^{2\epsilon/(2-a)}\frac{1}{s_a^{1+2\epsilon/(2-a)}}\,, \quad \text{(B.2)}$$

where $s_a = \omega^2\tau_a$. The first expression is singular as $\tau_a \to 0$ the second is singular as $z \to 1$ and $\tau_a \to 0$, but the singularities are regulated by dimensional regularization.

Employing the distributional identity

$$\frac{1}{(1-z)^{1+\epsilon}} = -\frac{1}{\epsilon}\delta(1-z) + \left(\frac{1}{1-z}\right)_+ - \epsilon\left(\frac{\ln(1-z)}{1-z}\right)_+ + \dots, \tag{B.3}$$

and similarly for τ_a we find for the divergent terms

$$\frac{C_F\alpha_s}{2\pi}\Bigg(\delta(s_a)\delta(1-z)\left[\frac{2-a}{1-a}\frac{1}{\epsilon^2} + \frac{2-a}{1-a}\frac{1}{\epsilon}\ln\left(\frac{\mu^2}{\omega^2}\right) + \frac{3}{2\epsilon}\right] \\ - \frac{1}{1-a}\frac{2}{\epsilon}\delta(1-z)\frac{1}{\omega^2}\left[\frac{1}{\tau_a}\right]_+ - \delta(s_a)\frac{1}{\epsilon}P_{qq}(z)\Bigg), \tag{B.4}$$

where P_{qq} is defined in Eq. (3.20). The first four terms in this expression are the expected UV poles for the angularity jet function (multiplied by $\delta(1-z)$), see Eq. (3.37) of Ref. [132]. In order to simplify this expression we have redefined $4\pi e^{-\gamma_E}\mu^2 \to \mu^2$, i.e., we are working in the $\overline{MS}$ scheme. The last term is the expected UV pole in the perturbative evaluation of the QCD fragmentation function. Since $\mathcal{G}_i(\tau_a, z, \mu)$ is expected to evolve like the angularity jet function, this is the correct structure of UV divergences implied by Eq. (3.10). The finite pieces are given by

$$\frac{1}{\omega^2}\frac{\mathcal{J}_{qq}(\tau_a, z, \mu)}{2(2\pi)^3} = \frac{C_F\alpha_s}{2\pi}\frac{1}{\omega^2}\Bigg\{\delta(\tau_a)\delta(1-z)\frac{2-a}{1-a}\left(-\frac{\pi^2}{12} + \frac{1}{2}\ln^2\left(\frac{\mu^2}{\omega^2}\right)\right) \\ + \delta(\tau_a)\left(1 - z - \left[\ln\left(\frac{\mu^2}{\omega^2}\right) + \frac{1}{1-a/2}\ln\left(1 + \frac{(1-z)^{1-a}}{z^{1-a}}\right)\right]\frac{1+z^2}{(1-z)_+} \\ + \frac{1-a}{1-a/2}(1+z^2)\left(\frac{\ln(1-z)}{1-z}\right)_+\right) \\ + \left[\frac{1}{\tau_a}\right]_+\left(\frac{1}{1-a/2}\frac{1+z^2}{(1-z)_+} - \delta(1-z)\frac{2}{1-a}\ln\left(\frac{\mu^2}{\omega^2}\right)\right) \\ + \frac{2\delta(1-z)}{(1-a)(1-a/2)}\left[\frac{\ln\tau_a}{\tau_a}\right]_+\Bigg\}. \tag{B.5}$$

In the limit $a \to 0$ this becomes

$$\frac{1}{\omega^2}\frac{\mathcal{J}_{qq}(\tau_0, z, \mu)}{2(2\pi)^3} = \frac{C_F\alpha_s}{2\pi}\left\{\delta(s)\delta(1-z)\left(-\frac{\pi^2}{6} + \ln^2\left(\frac{\mu^2}{\omega^2}\right)\right)\right.$$
$$+ \delta(s)\left(1 - z - \ln\left(\frac{\mu^2}{\omega^2}\right)\frac{1+z^2}{(1-z)_+} + \ln z\, P_{qq}(z) + (1+z^2)\left(\frac{\ln(1-z)}{1-z}\right)_+\right) \quad \text{(B.6)}$$
$$\left. + \frac{1}{\omega^2}\left[\frac{1}{\tau_0}\right]_+\left(\frac{1+z^2}{(1-z)_+} - 2\delta(1-z)\ln\left(\frac{\mu^2}{\omega^2}\right)\right) + 2\delta(1-z)\frac{1}{\omega^2}\left[\frac{\ln\tau_0}{\tau_0}\right]_+\right\},$$

where we have used $\delta(\tau_0)/\omega^2 = \delta(s)$. Using the following distributional identities

$$\frac{1}{\omega^2}\left[\frac{1}{\tau_0}\right]_+ = \frac{1}{\omega^2}\left[\frac{\omega^2}{s}\right]_+ = \frac{1}{\mu^2}\left[\frac{\mu^2}{s}\right]_+ + \ln\left(\frac{\mu^2}{\omega^2}\right)\delta(s)\,,$$
$$\frac{1}{\omega^2}\left[\frac{\ln\tau_0}{\tau_0}\right]_+ = \frac{1}{\omega^2}\left[\frac{\ln(s/\omega^2)}{s/\omega^2}\right]_+ = \frac{1}{\mu^2}\left[\frac{\ln(s/\mu^2)}{s/\mu^2}\right]_+ + \frac{\ln(\mu^2/\omega^2)}{\mu^2}\left[\frac{\mu^2}{s}\right]_+$$
$$+ \frac{1}{2}\ln\left(\frac{\mu^2}{\omega^2}\right)\delta(s)\,, \quad \text{(B.7)}$$

which are readily verified by integrating both sides over s, one finds that in the $a \to 0$ limit the finite piece is given by

$$\frac{\mathcal{J}_{qq}(s, z, \mu)}{2(2\pi)^3)} = \frac{C_F\alpha_s}{2\pi}\left\{\delta(s)\left(1 - z + \ln z\, P_{qq}(z) + (1+z^2)\left(\frac{\ln(1-z)}{1-z}\right)_+\right.\right.$$
$$\left.\left. - \frac{\pi^2}{6}\delta(1-z)\right) + \frac{1}{\mu^2}\left[\frac{\mu^2}{s}\right]_+\frac{1+z^2}{(1-z)_+} + 2\delta(1-z)\frac{1}{\mu^2}\left[\frac{\ln(s/\mu^2)}{s/\mu^2}\right]_+\right\}, \quad \text{(B.8)}$$

which agrees with the matching coefficient found in Eq. (2.32) of Ref. [68].

Next we calculate $\mathcal{J}_{qg}(\tau_a, z, \mu)$. Naively this is related to $\mathcal{J}_{qq}(\tau_a, z, \mu)$ by the replacement $z \to 1 - z$. However, because in the convolution integral of Eq. (3.10) the argument of $\mathcal{J}_{ij}(\tau_a, z/z', \mu)$ is never zero, there is no need to regulate poles of z. Therefore, a divergent factor of $(1-z)^{-1-\epsilon}$ in $\mathcal{J}_{qq}(\tau_a, z, \mu)$ becomes in $\mathcal{J}_{qg}(\tau_a, z, \mu)$

$$\frac{1}{z^{1+\epsilon}} = \frac{1}{z} - \epsilon\frac{\ln z}{z} + O(\epsilon^2)\,. \quad \text{(B.9)}$$

Thus, $\mathcal{J}_{qg}(\tau_a, z, \mu)$ is obtained by making the substitution $z \to 1 - z$ and then dropping all $\delta(z)$ and plus prescriptions. This is true for the $\mathcal{J}_{qg}(s, z, \mu)$ calculated in Ref. [68] and remains true for $\mathcal{J}_{qg}(\tau_a, z, \mu)$. We thus find for the divergent terms

$$\frac{1}{\omega^2}\frac{\mathcal{J}_{qg}^{div}(\tau_a, z, \mu)}{2(2\pi)^3} = -\frac{1}{\omega^2}\frac{C_F\alpha_s}{2\pi}\frac{1}{\epsilon}\delta(\tau_a)P_{gq}(z)\,, \tag{B.10}$$

where P_{gq} is given in Eq. (3.20). For the finite pieces we get

$$\begin{aligned}\frac{1}{\omega^2}\frac{\mathcal{J}_{qg}(\tau_a, z, \mu)}{2(2\pi)^3} = \frac{C_F\alpha_s}{2\pi}\frac{1}{\omega^2}\Bigg\{\delta(\tau_a)\Bigg(z + \Bigg[\frac{1}{1-a/2}\ln\left(\frac{z^{1-a}(1-z)^{1-a}}{z^{1-a}+(1-z)^{1-a}}\right) \\ - \ln\left(\frac{\mu^2}{\omega^2}\right)\Bigg]P_{gq}(z)\Bigg) + \frac{1}{1-a/2}\left[\frac{1}{\tau_a}\right]_+ P_{gq}(z)\Bigg\}\,.\end{aligned} \tag{B.11}$$

Again, these reproduce the matching coefficients of Ref. [68] in the $a \to 0$ limit.

For the divergent contributions to $\mathcal{J}_{gg}(\tau_a, z, \mu)$ we get (from the diagrams in Fig. 4 of Ref. [68])

$$\begin{aligned}\frac{1}{\omega^2}\frac{\mathcal{J}_{gg}^{div}(\tau_a, z, \mu)}{2(2\pi)^3} = \frac{C_A\alpha_s}{2\pi}\frac{1}{\omega^2}\Bigg(\delta(\tau_a)\delta(1-z)\left[\frac{2-a}{1-a}\frac{1}{\epsilon^2} + \frac{2-a}{1-a}\frac{1}{\epsilon}\ln\left(\frac{\mu^2}{\omega^2}\right) + \frac{\beta_0}{2C_A}\frac{1}{\epsilon}\right] \\ - \frac{1}{1-a}\frac{2}{\epsilon}\delta(1-z)\left[\frac{1}{\tau_a}\right]_+\Bigg) - \frac{\alpha_s}{2\pi}\frac{1}{\omega^2}\delta(\tau_a)\frac{1}{\epsilon}\tilde{P}_{gg}(z)\,,\end{aligned} \tag{B.12}$$

where the $\tilde{P}_{gg}(z)$ is the **full** QCD splitting function that includes the term propor-

tional to $\beta_0\delta(1-z)$. For the finite parts of $\mathcal{J}_{gg}(\tau_a,z,\mu)$ we find

$$\begin{aligned}\frac{1}{\omega^2}\frac{\mathcal{J}_{gg}(\tau_a,z,\mu)}{2(2\pi)^3} &= \frac{C_A\alpha_s}{2\pi}\frac{1}{\omega^2}\left\{\delta(\tau_a)\delta(1-z)\frac{2-a}{1-a}\left(-\frac{\pi^2}{12}+\frac{1}{2}\ln^2\left(\frac{\mu^2}{\omega^2}\right)\right)\right.\\ &+\delta(\tau_a)\left(-P_{gg}(z)\left[\ln\left(\frac{\mu^2}{\omega^2}\right)+\frac{1}{1-a/2}\ln\left(1+\frac{(1-z)^{1-a}}{z^{1-a}}\right)\right]\right.\\ &+\left.\frac{1-a}{1-a/2}\frac{2(1-z+z^2)^2}{z}\left(\frac{\ln(1-z)}{1-z}\right)_+\right)\\ &+\left[\frac{1}{\tau_a}\right]_+\left(\frac{1}{1-a/2}P_{gg}(z)-\delta(1-z)\frac{2}{1-a}\ln\left(\frac{\mu^2}{\omega^2}\right)\right)\\ &+\left.\frac{2\delta(1-z)}{(1-a)(1-a/2)}\left[\frac{\ln\tau_a}{\tau_a}\right]_+\right\}, \end{aligned} \tag{B.13}$$

where P_{gg} is given in Eq. (3.20). In the limit $a\to 0$, this expression reduces to $\mathcal{J}_{gg}(s,z,\mu)/(16\pi^3)$ found in Eq. (2.33) of Ref. [68].

For the divergent contributions to $\mathcal{J}_{gq}(\tau_a,z,\mu)$ we find

$$\frac{1}{\omega^2}\frac{\mathcal{J}_{gq}^{div}(\tau_a,z,\mu)}{2(2\pi)^3} = -\frac{1}{\omega^2}\frac{\alpha_s T_R}{2\pi}\frac{1}{\epsilon}\delta(\tau_a)P_{qg}(z)\,. \tag{B.14}$$

For the finite parts we get

$$\begin{aligned}\frac{1}{\omega^2}\frac{\mathcal{J}_{gq}(\tau_a,z,\mu)}{2(2\pi)^3} &= \frac{\alpha_s T_R}{2\pi}\frac{1}{\omega^2}\left\{\frac{1}{1-a/2}\left[\frac{1}{\tau_a}\right]_+P_{qg}(z)+\delta(\tau_a)2z(1-z)\right.\\ &+\left.\delta(\tau_a)P_{qg}(z)\left[\frac{1}{1-a/2}\ln\left(\frac{z^{1-a}(1-z)^{1-a}}{z^{1-a}+(1-z)^{1-a}}\right)-\ln\left(\frac{\mu^2}{\omega^2}\right)\right]\right\}, \end{aligned} \tag{B.15}$$

where P_{qg} is again given in Eq. (3.20). In the limit $a\to 0$, this expression reduces to $\mathcal{J}_{gq}(s,z,\mu)/(16\pi^3)$ in Eq. (2.33) of Ref. [68].

B.2 Sum Rules

The sum rules,

$$J_i(\tau_a) = \frac{1}{2(2\pi)^3} \sum_j \int_0^1 dz\, z\, \mathcal{J}_{ij}(\tau_a, z)\,, \tag{B.16}$$

can be checked for $i = q$ by performing the integral

$$J_q(\tau_a) = \frac{1}{2(2\pi)^3} \sum_j \int_0^1 dz\, z\, \mathcal{J}_{qj}(\tau_a, z) \tag{B.17}$$

$$= \frac{1}{2(2\pi)^3} \int_0^1 dz\, z\, \left(\mathcal{J}_{qq}(\tau_a, z) + \mathcal{J}_{qg}(\tau_a, z)\right) \tag{B.18}$$

$$= \frac{1}{2(2\pi)^3} \int_0^1 dz\, z\, \left(\mathcal{J}_{qq}(\tau_a, z) + \mathcal{J}_{qq}(\tau_a, 1-z)\right) \tag{B.19}$$

$$= \frac{1}{2(2\pi)^3} \int_0^1 dz\, \mathcal{J}_{qq}(\tau_a, z), \tag{B.20}$$

where in the last line we changed variables to $z \to 1 - z$ in the 2nd term. Inserting the expression in Eq. (B.5) into this integral yields the $J_q(\tau_a)$ found in Eq. (3.35) of Ref. [132].

In the case of the $i = g$ we have

$$J_g(\tau_a) = \frac{1}{2(2\pi)^3} \int_0^1 dz\, z\, \left(\mathcal{J}_{gg}(\tau_a, z) + \mathcal{J}_{gq}(\tau_a, z)\right)$$

$$= \frac{1}{2(2\pi)^3} \int_0^1 dz\, \frac{\mathcal{J}_{gg}(\tau_a, z) + \mathcal{J}_{gq}(\tau_a, z)}{2}\,, \tag{B.21}$$

because both $\mathcal{J}_{gg}(\tau_a, z)$ and $\mathcal{J}_{gq}(\tau_a, z)$ are symmetric under $z \to 1 - z$. The sum rule is easiest to verify by writing the d-dimensional expressions for $\mathcal{J}_{gg}(\tau_a, z)$ and $\mathcal{J}_{gq}(\tau_a, z)$ before expanding in $\epsilon = (4 - d)/2$. We find

$$\frac{1}{\omega^2}\frac{\mathcal{J}_{gg}(\tau_a, z, \mu)}{2(2\pi)^3} = \frac{1}{\omega^2}\left(\frac{4\pi\mu^2}{\omega^2}\right)^{\epsilon} \frac{C_A \alpha_s}{2\pi} \frac{1}{\Gamma[1-\epsilon]} \frac{1}{1 - a/2} (z^{a-1} + (1-z)^{a-1})^{\frac{2\epsilon}{2-a}}$$

$$\times \left(\frac{1}{\tau_a}\right)^{1+\frac{2\epsilon}{1-a}} \left(\frac{2z}{1-z} + \frac{2(1-z)}{z} + 2z(1-z)\right), \tag{B.22}$$

$$\frac{1}{\omega^2}\frac{\mathcal{J}_{gq}(\tau_a,z,\mu)}{2(2\pi)^3} = \frac{1}{\omega^2}\left(\frac{4\pi\mu^2}{\omega^2}\right)^{\epsilon}\frac{T_R\alpha_s}{2\pi}\frac{1}{\Gamma[1-\epsilon]}\frac{1}{1-a/2}(z^{a-1}+(1-z)^{a-1})^{\frac{2\epsilon}{2-a}}$$
$$\times\left(\frac{1}{\tau_a}\right)^{1+\frac{2\epsilon}{1-a}}\left(1-\frac{2}{1-\epsilon}z(1-z)\right). \tag{B.23}$$

Inserting these two expressions into Eq. (B.21) one obtains exactly the integral expression for the d-dimensional $J_g(\tau_a)$ found in Eq. (4.22) of Ref. [65].

Appendix C

TMDFJFs in Factorization Theorems

C.1 Definition and relation to jet functions

Much like the standard FJFs, TMDFJFs appear in factorization theorems for cross-sections that are differential in z, the fraction of a jet initiating parton's energy carried by an identified hadron, and $\mathbf{p}_\perp$, the transverse momenta of the hadron measured from the parton's momentum. It is shown in Ref. [65] that the cross-section for the production of two jets in electron-positron annihilation can be written as,

$$d\sigma = d\sigma^{(0)} H_2(\mu) \times S_\Lambda(\mu) \times J_n^q(\omega, \mu) \times J_{\bar{n}}^{\bar{q}}(\omega, \mu)\,, \tag{C.1}$$

where $d\sigma^{(0)}$ is the Born cross section, $H_2(\mu)$ is the hard function resulting from matching a 2-jet operator in full QCD onto the corresponding SCET operators, $S_\Lambda(\mu)$ is a soft function that describes soft scale cross-talk between the jets and the soft out-of-jet radiation is constrained via $E_{\rm out} < \Lambda$, and $J_n(\omega, \mu)$ is a jet function that describes collinear radiation within a jet in the $\hat{n}$ direction that has energy $E_J = \omega/2$ (here $\omega = E_{\rm cm}$). The jet function can be defined in SCET as

$$J_n^q(\omega, \mu) = \int \frac{dk^+}{2\pi} \int d^4x \, \exp(ik^+x^-/2) \frac{1}{N_C} \mathrm{Tr}\left[\frac{\bar{\not{n}}}{2} \langle 0|\delta_{\omega,\overline{\mathcal{P}}}\, \delta_{0,\mathcal{P}_\perp} \chi_n(x) \bar{\chi}_n(0)|0\rangle\right]. \tag{C.2}$$

To study jets with identified hadrons, we insert the following expression for the identity

$$\mathbf{1} = \sum_X |X\rangle\langle X| = \sum_X \sum_{h\in\mathcal{H}_i} \int \frac{dz d^2\mathbf{p}_\perp^h}{2(2\pi)^3} |Xh(z,\mathbf{p}_\perp^h)\rangle\langle Xh(z,\mathbf{p}_\perp^h)| \tag{C.3}$$

$$J_n^q(\omega,\mu) = \sum_{h\in\mathcal{H}_i} \int \frac{dz d^2\mathbf{p}_\perp}{2(2\pi)^3} \int \frac{dk^+}{2\pi} \int d^4x \ \exp(ik^+x^-/2) \frac{1}{N_C}$$
$$\times \sum_X \mathrm{Tr}\Big[\frac{\bar{\not{n}}}{2}\langle 0|\delta_{\omega,\overline{\mathcal{P}}}\ \delta_{0,\mathcal{P}_\perp}\chi_n(x)|Xh(z,\mathbf{p}_\perp)\rangle\langle Xh(z,\mathbf{p}_\perp)|\bar{\chi}_n(0)|0\rangle\Big]. \tag{C.4}$$

where h is an identified hadron within the jet. Performing the integration over x, which is the Fourier conjugate of the residual momenta, and the residual k^+ yields

$$J_n^q(\omega,\mu) = \sum_{h\in\mathcal{H}_i} \int z dz d^2\mathbf{p}_\perp\ \mathcal{G}_{q/h}(\mathbf{p}_\perp,z,\mu). \tag{C.5}$$

Insetrting this back to Eq.(C.1) we have

$$d\sigma = \sum_{h\in\mathcal{H}_i} \int z dz d^2\mathbf{p}_\perp\ d\sigma^{(0)} H_2(\mu) \times S_\Lambda(\mu) \times \mathcal{G}_{q/h}(\mathbf{p}_\perp,z,\mu) \times J_{\bar{n}}^{\bar{q}}(\omega,\mu). \tag{C.6}$$

which directly implies

$$\frac{d\sigma^{i/h}}{dz d^2\mathbf{p}_\perp} = d\sigma^{(0)} H_2(\mu) \times S_\Lambda(\mu) \times \mathcal{G}_{q/h}(\mathbf{p}_\perp,z,\mu) \times J_{\bar{n}}^{\bar{q}}(\omega,\mu) + \mathcal{O}\left(\frac{\Lambda}{E_J}, \frac{\Lambda_{\mathrm{QCD}}^2}{p_\perp^2}\right). \tag{C.7}$$

This suggests a rather powerful rule (already known to be true for the standard FJFs) for constructing the factorization theorem in SCET with identified hadron with measured transverse momenta :

$$\frac{d\sigma^{i/h}}{dz d^2\mathbf{p}_\perp} = d\sigma\Big[J^i(\omega,\mu) \to \mathcal{G}_{i/h}(\mathbf{p}_\perp,z,\mu)\Big] \tag{C.8}$$

C.2 Matching calculation

In this Appendix we provide details for the evaluation of the matching coefficients, $\mathcal{J}_{i/j}$. From the sum of diagrams in Figs. 4.2a) and 4.2b) we get:

$$\begin{aligned}
\mathcal{D}_{q/q}^{B(1)}(\mathbf{p}_\perp, z, \mu, \nu) =& \frac{\alpha_s w^2 C_F}{\pi} \frac{e^{\gamma_E \epsilon}}{\Gamma(1-\epsilon)} \left(\frac{\nu}{\omega}\right)^\eta \frac{1}{2\pi\mu^2} \left(\frac{\mu^2}{\mathbf{p}_\perp^2}\right)^{1+\epsilon} \\
& \times \left\{ 2z \left(\frac{1}{1-z}\right)^{1+\eta} + (1-\epsilon)(1-z) \right\} \\
=& \frac{\alpha_s w^2 C_F}{\pi} \Big\{ \Big[-\frac{2}{\eta} \left(-\frac{1}{2\epsilon} \delta^{(2)}(\mathbf{p}_\perp) + \mathcal{L}_0(\mathbf{p}_\perp^2, \mu^2) \right) \\
& + \frac{1}{2\epsilon} \left(\ln\left(\frac{\nu^2}{\omega^2}\right) + \frac{3}{2} \right) \delta^{(2)}(\mathbf{p}_\perp) \Big] \delta(1-z) - \frac{1}{2\epsilon} P_{qq}(z) \delta^{(2)}(\mathbf{p}_\perp) \\
& + \left(-\delta(1-z) \ln\left(\frac{\nu^2}{\omega^2}\right) + \bar{P}_{qq}(z) \right) \mathcal{L}_0(\mathbf{p}_\perp^2, \mu^2) + c_{qq}(z) \delta^{(2)}(\mathbf{p}_\perp) \Big\} \\
& + \mathcal{O}(\eta, \epsilon),
\end{aligned} \tag{C.9}$$

where we define $c_{qq}(z) = (1-z)/2$. The superscripts B and R denote bare and renormalized quantities, respectively, and the superscript (1) indicates that this is the $O(\alpha_S)$ contribution. The NLO matching coefficient is given by

$$\mathcal{J}_{q/q}^{R(1)}(\mathbf{p}_\perp, z, \mu) = \mathcal{D}_{q/q}^{R(1)}(\mathbf{p}_\perp, z, \mu) - D_{q/q}^{R(1)}(z, \mu) \delta^{(2)}(\mathbf{p}_\perp), \tag{C.10}$$

where

$$D_{q/q}^{R(1)}(z) = -\frac{\alpha_s C_F}{\pi} P_{qq}(z) \frac{1}{2\epsilon}. \tag{C.11}$$

The $1/\epsilon$ pole appearing in the FF is interpreted as an infrared divergence. Although for extracting the renormalized matching coefficients $\mathcal{J}_{i/j}$ we can ignore scaleless integrals and interpret the finite terms as the renormalized result to that particular order, here we are interested in the origin of the poles since this will allow us to

extract the anomalous dimensions. Performing the matching we get:

$$\mathcal{J}^R_{q/q}(\mathbf{p}_\perp, z, \mu, \nu) = \delta^{(2)}(\mathbf{p}_\perp)\delta(1-z)$$
$$+ \frac{\alpha_s C_F}{\pi}\Big\{ \left(\delta(1-z)\ln\left(\frac{\omega^2}{\nu^2}\right) + \bar{P}_{qq}(z)\right)\mathcal{L}_0(\mathbf{p}_\perp^2, \mu^2) + c_{qq}(z)\delta^{(2)}(\mathbf{p}_\perp)\Big\}. \tag{C.12}$$

For the coefficient $\mathcal{J}_{q/g}$ we simply perform the replacement $z \to (1-z)$ and drop $\delta(z)$ and plus-distributions since these functions are always integrated for values of z greater than zero. Thus

$$\mathcal{J}^R_{q/g}(\mathbf{p}_\perp, z, \mu, \nu) = \frac{\alpha_s C_F}{\pi}\Big\{\bar{P}_{gq}(z)\mathcal{L}_0(\mathbf{p}_\perp^2, \mu^2) + c_{qg}(z)\delta^{(2)}(\mathbf{p}_\perp)\Big\}, \tag{C.13}$$

where $c_{qg}(z) = c_{qq}(1-z) = z/2$. For the gluon splitting we get

$$\mathcal{D}^{B(1)}_{g/g}(\mathbf{p}_\perp, z, \mu, \nu) = \frac{\alpha_s C_A w^2}{\pi}\frac{\mathrm{e}^{\epsilon\gamma_E}}{\Gamma(1-\epsilon)}\left(\frac{\nu}{\omega}\right)^\eta \frac{1}{2\pi\mu^2}\left(\frac{\mu^2}{\mathbf{p}_\perp^2}\right)^{1+\epsilon}$$
$$\times\, 2\left[\frac{z}{(1-z)^{1+\eta}} + \frac{(1-z)}{z} + z(1-z)\right]. \tag{C.14}$$

Expanding in η and ϵ we have

$$\mathcal{D}^{B(1)}_{g/g}(\mathbf{p}_\perp, z, \mu, \nu) = \frac{\alpha_s C_A w^2}{\pi}\Big[-\frac{1}{2\epsilon}\delta^{(2)}(\mathbf{p}_\perp) + \mathcal{L}_0(\mathbf{p}_\perp^2, \mu^2)\Big]$$
$$\times\Big[-\frac{2}{\eta}\delta(1-z) - \ln\left(\frac{\nu^2}{\omega^2}\right)\delta(1-z) + \bar{P}_{gg}(z)\Big]$$
$$= \frac{\alpha_s C_A w^2}{\pi}\Big\{\Big[-\frac{2}{\eta}\left(-\frac{1}{2\epsilon}\delta^{(2)}(\mathbf{p}_\perp) + \mathcal{L}_0(\mathbf{p}_\perp^2, \mu^2)\right)$$
$$+ \frac{1}{2\epsilon}\left(\ln\left(\frac{\nu^2}{\omega^2}\right) + \frac{1}{2}\beta_0\right)\delta^{(2)}(\mathbf{p}_\perp)\Big]\delta(1-z) - \frac{1}{2\epsilon}P_{gg}(z)\delta^{(2)}(\mathbf{p}_\perp)$$
$$+ \left(-\delta(1-z)\ln\left(\frac{\nu^2}{\omega^2}\right) + \bar{P}_{gg}(z)\right)\mathcal{L}_0(\mathbf{p}_\perp^2, \mu^2)\Big\}, \tag{C.15}$$

and since the corresponding FF is given by:

$$D^R_{g/g}(z) = \delta(1-z) - \frac{\alpha_s C_A}{\pi}P_{gg}(z)\frac{1}{2\epsilon} + \mathcal{O}(\alpha_s^2), \tag{C.16}$$

where the $1/\epsilon$ pole is an infrared divergence, we have

$$\mathcal{J}^R_{g/g}(\mathbf{p}_\perp, z, \mu, \nu) = \delta^{(2)}(\mathbf{p}_\perp)\delta(1-z) + \frac{\alpha_s C_A}{\pi}\left(\delta(1-z)\ln\left(\frac{\omega^2}{\nu^2}\right) + \bar{P}_{gg}(z)\right)\mathcal{L}_0(\mathbf{p}_\perp^2, \mu^2). \tag{C.17}$$

A similar calculation yields the kernel $\mathcal{J}_{g/q}$,

$$\begin{aligned}\mathcal{D}^{B(1)}_{g/q}(\mathbf{p}_\perp, z, \mu, \nu) &= \frac{\alpha_s T_F w^2}{\pi}\frac{\mathrm{e}^{\epsilon\gamma_E}}{\Gamma(2-\epsilon)}\frac{1}{2\pi\mu^2}\left(\frac{\mu^2}{\mathbf{p}_\perp^2}\right)^{1+\epsilon} \times \left(\bar{P}_{qg}(z) - \epsilon\right) \\ &= \frac{\alpha_s T_F w^2}{\pi}\Big\{(c_{gq}(z) - \frac{1}{2\epsilon}\bar{P}_{qg}(z))\delta^{(2)}(\mathbf{p}_\perp) + \mathcal{L}_0(\mathbf{p}_\perp^2, \mu^2)\bar{P}_{qg}(z)\Big\},\end{aligned} \tag{C.18}$$

where $c_{gq}(z) = z(1-z)$. Performing the matching and since the corresponding FF is

$$D^R_{g/q}(z) = -\frac{\alpha_s T_F}{\pi}P_{qg}(z)\frac{1}{2\epsilon} + \mathcal{O}(\alpha_s^2), \tag{C.19}$$

where again the $1/\epsilon$ pole is an infrared divergence, we get

$$\mathcal{J}^R_{g/q}(\mathbf{p}_\perp, z, \mu, \nu) = \delta^{(2)}(\mathbf{p}_\perp)\delta(1-z) + \frac{\alpha_s T_F}{\pi}\Big\{\mathcal{L}_0(\mathbf{p}_\perp^2, \mu^2)\bar{P}_{qg}(z) + c_{gq}(z)\delta^{(2)}(\mathbf{p}_\perp)\Big\}. \tag{C.20}$$

Appendix D

Calculations of Soft Function Components

In this Appendix, we calculate the various components needed for S^{unmeas}. As explained in the main body of the text, we only calculate combinations of terms that explicitly remove radiation out of the beams, i.e., with $y > y_{\text{cut}}$ or $y < -y_{\text{cut}}$. We use the definitions $c_J \equiv \vec{n}_J \cdot \vec{n}_B$, $s_J \equiv (1 - c_J^2)^{1/2}$, $c_i \equiv \cos\theta_i$, and $s_i \equiv \sin\theta_i$. All the expressions are special cases of the general form Eq. (5.40) in the planar limit, given by the substitution in Eq. (5.41). For subtraction terms S_{ij}^k defined in Eq. (5.38) there is an additional factor of $-\Theta_{\mathcal{R}}^k$ given in Eq. (5.36).

D.1 Beam-Beam Interference Terms

We first calculate the beam-beam interference with the gluon out of the beams

$$\begin{aligned}
\mathcal{I}^{\text{out}}_{B\bar{B}} &\equiv \mathcal{I}^{\text{incl}}_{B\bar{B}} + \mathcal{I}^{B}_{B\bar{B}} + \mathcal{I}^{\bar{B}}_{B\bar{B}} \\
&= \frac{e^{\gamma_E \epsilon}}{\sqrt{\pi}\Gamma(1/2-\epsilon)} \int_0^\pi d\theta_1 \sin\theta_1 \frac{1}{1-c_1} \frac{1}{1+c_1} \int_0^\pi d\theta_2 \sin^{-2\epsilon}\theta_2 \\
&= \frac{e^{\gamma_E \epsilon}}{\Gamma(1-\epsilon)} \int_{-\tanh y_{\text{cut}}}^{\tanh y_{\text{cut}}} \frac{dc_1}{1-c_1^2} \\
&= \ln \frac{1+\tanh y_{\text{cut}}}{1-\tanh y_{\text{cut}}} \\
&= 2 y_{\text{cut}} \,. \qquad \text{(D.1)}
\end{aligned}$$

The region that must be added to remove radiation in the jets goes as $\mathcal{R}^2$ and so is power suppressed for small jets, but we record it here for completeness. In a frame where the jet is perpendicular to the beam,

$$I^{J}_{B\bar{B}} = \frac{e^{\gamma_E \epsilon}}{\sqrt{\pi}\Gamma(1/2-\epsilon)} \int_0^R d\theta_1 \sin^{1-2\epsilon}\theta_1 \int_0^\pi d\theta_2 \sin^{-2\epsilon}\theta_2 \big[1-(s_1 c_2)^2\big]^{-1+\epsilon} \,. \qquad \text{(D.2)}$$

In this frame ($\theta_J = \pi/2$), we can make the substitution $R \to \mathcal{R}\sin\pi/2 = \mathcal{R}$ to get a frame invariant result. This gives

$$\mathcal{I}^{J}_{B\bar{B}} = \frac{1}{2}\ln(1-\mathcal{R}^2) - \epsilon\left(\frac{\pi^2}{12} - \frac{1}{2}\,\text{Li}_2(1-\mathcal{R}^2)\right) = \mathcal{O}(\mathcal{R}^2) \,. \qquad \text{(D.3)}$$

D.2 Beam-Jet Interference Terms

The beam-jet interference term with the gluon out of both beams is simplest to compute in the polar coordinates about the beam axis. Defining $\cos\theta_c \equiv t_c \equiv$

$\tanh y_{\rm cut}$, it can be written as

$$\begin{aligned}\mathcal{I}_{BJ}^{\rm out} &\equiv \mathcal{I}_{BJ}^{\rm incl} + \mathcal{I}_{BJ}^{B} + \mathcal{I}_{BJ}^{\bar{B}} \\ &= \frac{(1-c_J)e^{\gamma_E\epsilon}}{2\sqrt{\pi}\Gamma(1/2-\epsilon)}\int_{\theta_c}^{\pi-\theta_c} d\theta_1\, \sin\theta_1 \int_0^{\pi} d\theta_2\, \sin^{-2\epsilon}\theta_2 \frac{1}{1-c_1}\frac{1}{1-c_Jc_1-s_Js_1c_2} \\ &= \frac{e^{\gamma_E\epsilon}}{2}\int_{-t_c}^{t_c}\frac{dc_1}{1-c_1^2}\frac{1-c_1}{1-c_1c_J}\,{}_2\tilde{F}_1(1/2,1;1-\epsilon;z)\,, \end{aligned} \tag{D.4}$$

where $z = (1-c_1^2)(1-c_J^2)/(1-c_1c_J)^2$. We can proceed by extracting the $c_J = c_1$ singular via the identity

$$\begin{aligned}{}_2\tilde{F}_1\big(\frac{1}{2},1;1-\epsilon;z\big) = \frac{\sqrt{\pi}}{\Gamma(1/2-\epsilon)\cos\pi\epsilon}\bigg[z^{\epsilon}\bigg(\frac{1-c_1c_J}{|c_1-c_J|}\bigg)^{1+2\epsilon} \\ + \frac{\epsilon\sqrt{\pi}}{\Gamma(1-\epsilon)}\,{}_2\tilde{F}_1\big(\frac{3}{2},1;\frac{3}{2}+\epsilon;1-z\big)\bigg]. \end{aligned} \tag{D.5}$$

The singularities are regulated by the $|c_1-c_J|^{-1-2\epsilon}$ in the first term in brackets on the right hand side of Eq. (D.5) (and the second term is finite and $\mathcal{O}(\epsilon)$). After adding and subtracting the rest of the functional dependence on c_1, $f(c_1)$, at the point $c_1 = c_J$ (so that $|c_1-c_J|^{-1-2\epsilon}\,(f(c_1)-f(c_J))$ can safely be expanded in ϵ) and performing some algebra, we arrive at the result

$$\begin{aligned}\mathcal{I}_{BJ}^{\rm out} &= \frac{e^{\gamma_E\epsilon}}{\Gamma(1-\epsilon)}\bigg\{-\frac{1}{2\epsilon}+\frac{1}{2}\bigg[\ln\left(e^{2(y_{\rm cut}-y_J)}-1\right)+\ln\left(1-e^{-2(y_{\rm cut}+y_J)}\right)\bigg] \\ &\quad -\epsilon\bigg[\frac{1}{2}\ln^2\left(1-e^{-2(y_{\rm cut}-y_J)}\right)+\mathrm{Li}_2\left(e^{-2(y_{\rm cut}-y_J)}\right)+\frac{1}{2}\ln^2\left(1-e^{-2(y_{\rm cut}+y_J)}\right)\bigg]\bigg\} \\ &= \frac{e^{\gamma_E\epsilon}}{\Gamma(1-\epsilon)}\bigg[-\frac{1}{2\epsilon}+y_{\rm cut}-y_J+\mathcal{O}(e^{-y_{\rm cut}})\bigg]. \end{aligned} \tag{D.6}$$

For the jet region subtraction term S_{JB}^{J}, in coordinates about the jet axis, we

have

$$\mathcal{I}^J_{BJ} = \frac{(1-c_J)e^{\gamma_E\epsilon}}{2\sqrt{\pi}\Gamma(1/2-\epsilon)}\int_0^R d\theta_1\,\sin^{1-2\epsilon}\theta_1\int_0^\pi d\theta_2\,\sin^{-2\epsilon}\theta_2$$
$$\times\,\frac{1}{1-c_1}\frac{1}{1-c_Jc_1-s_Js_1c_2}\Big[1-(c_Jc_1+s_Js_1c_2)^2\Big]^\epsilon$$
$$= \frac{(1-c_J)e^{\gamma_E\epsilon}}{2\sqrt{\pi}\Gamma(1/2-\epsilon)}\int_{\cos R}^1 dc_1(1-c_1)^{-1-\epsilon}f(c_1)\,, \tag{D.7}$$

where we defined

$$f(c) = (1+c)^{-\epsilon}\int_0^\pi d\theta_2\sin^{-2\epsilon}\theta_2\frac{\big[1-(c_Jc+s_J(1-c^2)^{1/2}c_2)^2\big]^\epsilon}{1-c_Jc-s_J(1-c^2)^{1/2}c_2}\,. \tag{D.8}$$

Up to corrections that scale as $\mathcal{O}(\mathcal{R}^2)$, we can set $f(c) = f(1)$ which is just

$$f(1) = \frac{2^{-\epsilon}}{1-c_J}s_J^{2\epsilon}\frac{\sqrt{\pi}\Gamma(1/2-\epsilon)}{\Gamma(1-\epsilon)}\,. \tag{D.9}$$

Using the substitution Eq. (5.9), we find

$$\mathcal{I}^J_{BJ} = \frac{e^{\gamma_E\epsilon}}{\Gamma(1-\epsilon)}\frac{1}{2\epsilon}\mathcal{R}^{-2\epsilon} + \mathcal{O}(\mathcal{R}^2)\,. \tag{D.10}$$

D.3 Jet-Jet Interference Terms

For the jet-jet interference terms, we work in coordinates about the jet axes in the frame where they are back-to-back, and then convert to lab frame variables. For the term with the gluon allowed anywhere, labeling the jets as 1 and 2, we have in the frame of back-to-back jets,

$$\mathcal{I}^J_{BJ} = \frac{e^{\gamma_E\epsilon}}{\sqrt{\pi}\Gamma(1/2-\epsilon)}\int_0^R d\theta_1\,\sin^{1-2\epsilon}\theta_1\int_0^\pi d\theta_2\,\sin^{-2\epsilon}\theta_2$$
$$\times\,\frac{1}{1-c_1}\frac{1}{1+c_1}\Big[1-(c_Jc_1+s_Js_1c_2)^2\Big]^\epsilon$$
$$= \frac{e^{\gamma_E\epsilon}}{\sqrt{\pi}\Gamma(1/2-\epsilon)}\,2\int_0^1 dc_1(1-c_1)^{-1-\epsilon}g(c_1)\,, \tag{D.11}$$

where we defined

$$g(c) = (1+c)^{-1-\epsilon} \int_0^\pi d\theta_2 \sin^{-2\epsilon}\theta_2 \big[1 - (c_J c + s_J(1-c^2)^{1/2} c_2)^2\big]^\epsilon \,. \tag{D.12}$$

As before, we can add and subtract $g(1)$, with

$$g(1) = \frac{2^{-1-\epsilon}}{1-c_J} s_J^{2\epsilon} \frac{\sqrt{\pi}\Gamma(1/2-\epsilon)}{\Gamma(1-\epsilon)} \,, \tag{D.13}$$

and expand the part of the integrand with $(1-u)^{-1-\epsilon}(f(u)-f(1))$ in ϵ. To evaluate the result, note that

$$\begin{aligned} h(c_J, c_1) &\equiv \frac{1}{\pi}\int_0^\pi d\theta \ln \frac{1-(c_1 c_J + (1-c_1^2)^{1/2}(1-c_J^2)^{1/2}\cos\theta)^2}{1-c_J^2} \\ &= \begin{cases} \ln\left[\frac{1-c_1^2}{1-c_J^2}\left(\frac{1+|c_J|}{2}\right)^2\right] & \text{for } |c_1| < |c_J| \\ 2\ln\frac{1+|c_1|}{2} & \text{for } |c_1| > |c_J| \end{cases} , \end{aligned} \tag{D.14}$$

and that

$$\int_0^1 \frac{dc_1}{1-c_1^2} f(c_J, c_1) = -\frac{\pi^2}{6} + \frac{1}{2}\ln^2\frac{1-c_J}{1+c_J} \,, \tag{D.15}$$

to finally obtain

$$\mathcal{I}_{12}^{\text{incl}} = \frac{e^{\gamma_E \epsilon}}{\Gamma(1-\epsilon)} \left(\frac{1-\cos^2\theta_J}{4}\right)^\epsilon \left[-\frac{1}{\epsilon} + \frac{\epsilon}{2}\ln^2\frac{1-c_J}{1+c_J}\right] . \tag{D.16}$$

Noting that $c_J \equiv \cos\theta_J$ in the back-to-back frame is related to the jet rapidities in the lab frame via $\cos\theta_J = \tanh\Delta y/2$ (cf. Eq. (5.43)), we find

$$\begin{aligned} \mathcal{I}_{12}^{\text{incl}} &= -\frac{e^{\gamma_E\epsilon}}{\Gamma(1-\epsilon)} \big(2\cosh(\Delta y/2)\big)^{-2\epsilon} \left[\frac{1}{\epsilon} - \frac{\epsilon}{2}(\Delta y)^2\right] \\ &= -\big(2\cosh(\Delta y/2)\big)^{-2\epsilon} \left[\frac{1}{\epsilon} - \frac{\epsilon}{2}(\Delta y)^2 - \frac{\pi^2}{12}\right] . \end{aligned} \tag{D.17}$$

For the jet region subtraction terms, we have

$$\mathcal{I}_{12}^1 = \frac{e^{\gamma_E\epsilon}}{\sqrt{\pi}\Gamma(1/2-\epsilon)} \, 2\int_{\cos R}^1 dc_1 (1-c_1)^{-1-\epsilon} g(c_1) \,, \tag{D.18}$$

which now involves the integral of $h(c_J, c_1)$ (cf. Eq. (D.14)) over the range $c_1 \in (\cos R, 1)$ with $c_J < \cos R$ (so only the case $|c_1| > |c_J|$ is needed). After some algebra and using the substitution $\tan R/2 \to \mathcal{R}/(2\cosh \Delta y/2)$, we arrive at the result

$$\mathcal{I}_{12}^1 = \frac{e^{\gamma_E \epsilon}}{\Gamma(1-\epsilon)} \frac{1}{2\epsilon} \mathcal{R}^{-2\epsilon} \,. \tag{D.19}$$

Bibliography

[1] G. P. Lepage, L. Magnea, C. Nakhleh, U. Magnea and K. Hornbostel, *Improved nonrelativistic QCD for heavy quark physics*, *Phys. Rev.* **D46** (1992) 4052–4067, [hep-lat/9205007].

[2] M. Butenschoen and B. A. Kniehl, *World data of J/psi production consolidate NRQCD at NLO*, *Phys. Rev.* **D84** (2011) 051501, [1105.0820].

[3] M. Butenschoen and B. A. Kniehl, *Next-to-leading-order tests of NRQCD factorization with J/ψ yield and polarization*, *Mod. Phys. Lett.* **A28** (2013) 1350027, [1212.2037].

[4] R. Kelley and M. D. Schwartz, *1-loop matching and NNLL resummation for all partonic 2 to 2 processes in QCD*, *Phys.Rev.* **D83** (2011) 045022, [1008.2759].

[5] Y.-T. Chien, A. Hornig and C. Lee, *Soft-collinear mode for jet cross sections in soft collinear effective theory*, *Phys. Rev.* **D93** (2016) 014033, [1509.04287].

[6] Particle Data Group collaboration, C. Patrignani et al., *Review of Particle Physics*, *Chin. Phys.* **C40** (2016) 100001.

[7] ATLAS collaboration, G. Aad et al., *Measurement of the differential cross-sections of inclusive, prompt and non-prompt J/ψ production in proton-proton collisions at $\sqrt{s} = 7$ TeV*, *Nucl. Phys.* **B850** (2011) 387–444, [1104.3038].

[8] M. Butenschoen and B. A. Kniehl, *J/psi polarization at Tevatron and LHC: Nonrelativistic-QCD factorization at the crossroads*, *Phys. Rev. Lett.* **108** (2012) 172002, [1201.1872].

[9] B. Gong, L.-P. Wan, J.-X. Wang and H.-F. Zhang, *Polarization for Prompt J/ψ and $(2S)$ Production at the Tevatron and LHC*, *Phys. Rev. Lett.* **110** (2013) 042002, [1205.6682].

[10] H.-S. Shao and K.-T. Chao, *Spin correlations in polarizations of P-wave charmonia χ_{cJ} and impact on J/ψ polarization*, *Phys. Rev.* **D90** (2014) 014002, [1209.4610].

[11] LHCb collaboration, R. Aaij et al., *Measurement of J/ψ polarization in pp collisions at $\sqrt{s} = 7$ TeV*, *Eur. Phys. J.* **C73** (2013) 2631, [1307.6379].

[12] P. Faccioli, C. Lourenco, J. Seixas and H. K. Wohri, *Towards the experimental clarification of quarkonium polarization*, *Eur. Phys. J.* **C69** (2010) 657–673, [1006.2738].

[13] LHCb collaboration, R. Aaij et al., *Study of J/ψ production in jets*, 1701.05116.

[14] SLAC-SP-017 collaboration, J. E. Augustin et al., *Discovery of a Narrow Resonance in e+ e- Annihilation*, *Phys. Rev. Lett.* **33** (1974) 1406–1408.

[15] E598 collaboration, J. J. Aubert et al., *Experimental Observation of a Heavy Particle J*, *Phys. Rev. Lett.* **33** (1974) 1404–1406.

[16] J. D. Bjorken and S. L. Glashow, *Elementary Particles and SU(4)*, *Phys. Lett.* **11** (1964) 255–257.

[17] S. L. Glashow, J. Iliopoulos and L. Maiani, *Weak Interactions with Lepton-Hadron Symmetry*, *Phys. Rev.* **D2** (1970) 1285–1292.

[18] S. W. Herb et al., *Observation of a Dimuon Resonance at 9.5-GeV in 400-GeV Proton-Nucleus Collisions*, *Phys. Rev. Lett.* **39** (1977) 252–255.

[19] S. Okubo, *Phi meson and unitary symmetry model*, *Phys. Lett.* **5** (1963) 165–168.

[20] G. Zweig, *An SU(3) model for strong interaction symmetry and its breaking. Version 2*, in *DEVELOPMENTS IN THE QUARK THEORY OF HADRONS. VOL. 1. 1964 - 1978* (D. Lichtenberg and S. P. Rosen, eds.), pp. 22–101. 1964.

[21] C. Quigg and J. L. Rosner, *Quantum Mechanics with Applications to Quarkonium*, *Phys. Rept.* **56** (1979) 167–235.

[22] D. Ebert, R. N. Faustov and V. O. Galkin, *Properties of heavy quarkonia and B_c mesons in the relativistic quark model*, *Phys. Rev.* **D67** (2003) 014027, [hep-ph/0210381].

[23] S. Godfrey and N. Isgur, *Mesons in a Relativized Quark Model with Chromodynamics*, *Phys. Rev.* **D32** (1985) 189–231.

[24] J. L. Richardson, *The Heavy Quark Potential and the Upsilon, J/psi Systems*, *Phys. Lett.* **B82** (1979) 272–274.

[25] S. J. Brodsky, P. Hoyer, N. Marchal, S. Peigne and F. Sannino, *Structure functions are not parton probabilities*, *Phys. Rev.* **D65** (2002) 114025, [hep-ph/0104291].

[26] V. N. Gribov and L. N. Lipatov, *Deep inelastic e p scattering in perturbation theory*, *Sov. J. Nucl. Phys.* **15** (1972) 438–450.

[27] G. Altarelli and G. Parisi, *Asymptotic Freedom in Parton Language*, *Nucl. Phys.* **B126** (1977) 298–318.

[28] Y. L. Dokshitzer, *Calculation of the Structure Functions for Deep Inelastic Scattering and e+ e- Annihilation by Perturbation Theory in Quantum Chromodynamics.*, *Sov. Phys. JETP* **46** (1977) 641–653.

[29] H. Fritzsch, *Producing Heavy Quark Flavors in Hadronic Collisions: A Test of Quantum Chromodynamics*, *Phys. Lett.* **67B** (1977) 217–221.

[30] F. Halzen, *Cvc for Gluons and Hadroproduction of Quark Flavors*, *Phys. Lett.* **B69** (1977) 105–108.

[31] M. Gluck, J. F. Owens and E. Reya, *Gluon Contribution to Hadronic J/psi Production*, *Phys. Rev.* **D17** (1978) 2324.

[32] Quarkonium Working Group collaboration, N. Brambilla et al., *Heavy quarkonium physics*, hep-ph/0412158.

[33] M. B. Einhorn and S. D. Ellis, *Hadronic Production of the New Resonances: Probing Gluon Distributions*, *Phys. Rev.* **D12** (1975) 2007.

[34] S. D. Ellis, M. B. Einhorn and C. Quigg, *Comment on Hadronic Production of Psions*, *Phys. Rev. Lett.* **36** (1976) 1263.

[35] C. E. Carlson and R. Suaya, *Hadronic Production of psi/J Mesons*, *Phys. Rev.* **D14** (1976) 3115.

[36] J. H. Kuhn, *Hadronic Production of P Wave Charmonium States*, *Phys. Lett.* **B89** (1980) 385–390.

[37] T. A. DeGrand and D. Toussaint, *The Decay of b Quarks Into ψs*, *Phys. Lett.* **B89** (1980) 256–258.

[38] M. B. Wise, *An Estimate of J/ψ Production in B Decays*, *Phys. Lett.* **B89** (1980) 229–231.

[39] W. E. Caswell and G. P. Lepage, *Effective Lagrangians for Bound State Problems in QED, QCD, and Other Field Theories*, *Phys. Lett.* **B167** (1986) 437–442.

[40] CDF collaboration, F. Abe et al., *Production of J/ψ mesons from χ_c meson decays in $p\bar{p}$ collisions at $\sqrt{s} = 1.8$ TeV*, *Phys. Rev. Lett.* **79** (1997) 578–583.

[41] P. Faccioli, C. Lourenco, J. Seixas and H. K. Woehri, *Study of ψ' and χ_c decays as feed-down sources of J/ψ hadro-production*, *JHEP* **10** (2008) 004, [0809.2153].

[42] M. Butenschoen and B. A. Kniehl, *Reconciling J/ψ production at HERA, RHIC, Tevatron, and LHC with NRQCD factorization at next-to-leading order*, *Phys. Rev. Lett.* **106** (2011) 022003, [1009.5662].

[43] CMS collaboration, S. Chatrchyan et al., *Measurement of the prompt J/ψ and $\psi(2S)$ polarizations in pp collisions at $\sqrt{s} = 7$ TeV*, *Phys. Lett.* **B727** (2013) 381–402, [1307.6070].

[44] ALICE collaboration, B. Abelev et al., *J/ψ polarization in pp collisions at $\sqrt{s} = 7$ TeV*, *Phys. Rev. Lett.* **108** (2012) 082001, [1111.1630].

[45] CDF collaboration, A. Abulencia et al., *Polarization of J/ψ and ψ_{2S} mesons produced in $p\bar{p}$ collisions at $\sqrt{s} = 1.96$-TeV*, *Phys. Rev. Lett.* **99** (2007) 132001, [0704.0638].

[46] G. T. Bodwin, H. S. Chung, U.-R. Kim and J. Lee, *Fragmentation contributions to J/ψ production at the Tevatron and the LHC*, *Phys. Rev. Lett.* **113** (2014) 022001, [1403.3612].

[47] G. T. Bodwin, K.-T. Chao, H. S. Chung, U.-R. Kim, J. Lee and Y.-Q. Ma, *Fragmentation contributions to hadroproduction of prompt J/ψ , χ_{cJ} , and $\psi(2S)$ states*, *Phys. Rev.* **D93** (2016) 034041, [1509.07904].

[48] J. C. Collins and D. E. Soper, *Parton Distribution and Decay Functions*, *Nucl. Phys.* **B194** (1982) 445–492.

[49] G. T. Bodwin, E. Braaten and G. P. Lepage, *Rigorous QCD analysis of inclusive annihilation and production of heavy quarkonium*, *Phys. Rev.* **D51** (1995) 1125–1171, [hep-ph/9407339].

[50] K. Gottfried and J. D. Jackson, *On the Connection between production mechanism and decay of resonances at high-energies*, *Nuovo Cim.* **33** (1964) 309–330.

[51] J. C. Collins and D. E. Soper, *Angular Distribution of Dileptons in High-Energy Hadron Collisions*, *Phys. Rev.* **D16** (1977) 2219.

[52] C. W. Bauer, S. Fleming and M. E. Luke, *Summing Sudakov logarithms in $B \to X_s\gamma$ in effective field theory*, *Phys. Rev.* **D63** (2000) 014006, [hep-ph/0005275].

[53] C. W. Bauer, S. Fleming, D. Pirjol and I. W. Stewart, *An Effective field theory for collinear and soft gluons: Heavy to light decays*, *Phys. Rev.* **D63** (2001) 114020, [hep-ph/0011336].

[54] C. W. Bauer and I. W. Stewart, *Invariant operators in collinear effective theory*, *Phys. Lett.* **B516** (2001) 134–142, [hep-ph/0107001].

[55] M. Procura and I. W. Stewart, *Quark Fragmentation within an Identified Jet*, *Phys.Rev.* **D81** (2010) 074009, [0911.4980].

[56] R. Bain, L. Dai, A. Hornig, A. K. Leibovich, Y. Makris and T. Mehen, *Analytic and Monte Carlo Studies of Jets with Heavy Mesons and Quarkonia*, *JHEP* **06** (2016) 121, [1603.06981].

[57] R. Bain, Y. Makris and T. Mehen, *Transverse Momentum Dependent Fragmenting Jet Functions with Applications to Quarkonium Production*, *JHEP* **11** (2016) 144, [1610.06508].

[58] A. Hornig, Y. Makris and T. Mehen, *Jet Shapes in Dijet Events at the LHC in SCET*, 1601.01319.

[59] G. Sterman and S. Weinberg, *Jets from quantum chromodynamics*, *Phys. Rev. Lett.* **39** (Dec, 1977) 1436–1439.

[60] C. W. Bauer, F. J. Tackmann, J. R. Walsh and S. Zuberi, *Factorization and Resummation for Dijet Invariant Mass Spectra*, *Phys. Rev.* **D85** (2012) 074006, [1106.6047].

[61] I. Z. Rothstein and I. W. Stewart, *An Effective Field Theory for Forward Scattering and Factorization Violation*, *JHEP* **08** (2016) 025, [1601.04695].

[62] I. W. Stewart, *Lectures on the Soft-Collinear Effective Theory*, .

[63] A. V. Manohar and M. B. Wise, *Heavy quark physics*, *Camb. Monogr. Part. Phys. Nucl. Phys. Cosmol.* **10** (2000) 1–191.

[64] A. V. Manohar, T. Mehen, D. Pirjol and I. W. Stewart, *Reparameterization invariance for collinear operators*, *Phys. Lett.* **B539** (2002) 59–66, [hep-ph/0204229].

[65] S. D. Ellis, C. K. Vermilion, J. R. Walsh, A. Hornig and C. Lee, *Jet Shapes and Jet Algorithms in SCET*, *JHEP* **11** (2010) 101, [1001.0014].

[66] L. G. Almeida, S. D. Ellis, C. Lee, G. Sterman, I. Sung and J. R. Walsh, *Comparing and counting logs in direct and effective methods of QCD resummation*, *JHEP* **04** (2014) 174, [1401.4460].

[67] X. Liu, *SCET approach to top quark decay*, *Phys.Lett.* **B699** (2011) 87–92, [1011.3872].

[68] A. Jain, M. Procura and W. J. Waalewijn, *Parton Fragmentation within an Identified Jet at NNLL*, *JHEP* **1105** (2011) 035, [1101.4953].

[69] A. Jain, M. Procura and W. J. Waalewijn, *Fully-Unintegrated Parton Distribution and Fragmentation Functions at Perturbative k_T*, *JHEP* **1204** (2012) 132, [1110.0839].

[70] M. Procura and W. J. Waalewijn, *Fragmentation in Jets: Cone and Threshold Effects*, *Phys.Rev.* **D85** (2012) 114041, [1111.6605].

[71] A. Jain, M. Procura, B. Shotwell and W. J. Waalewijn, *Fragmentation with a Cut on Thrust: Predictions for B-factories*, *Phys. Rev.* **D87** (2013) 074013, [1207.4788].

[72] C. W. Bauer and E. Mereghetti, *Heavy Quark Fragmenting Jet Functions*, *JHEP* **04** (2014) 051, [1312.5605].

[73] M. Baumgart, A. K. Leibovich, T. Mehen and I. Z. Rothstein, *Probing Quarkonium Production Mechanisms with Jet Substructure*, *JHEP* **11** (2014) 003, [1406.2295].

[74] T. Kaufmann, A. Mukherjee and W. Vogelsang, *Hadron Fragmentation Inside Jets in Hadronic Collisions*, *Phys. Rev.* **D92** (2015) 054015, [1506.01415].

[75] Y.-T. Chien, Z.-B. Kang, F. Ringer, I. Vitev and H. Xing, *Jet fragmentation functions in proton-proton collisions using soft-collinear effective theory*, *JHEP* **05** (2016) 125, [1512.06851].

[76] R. Bain, L. Dai, A. Leibovich, Y. Makris and T. Mehen, *NRQCD Confronts LHCb Data on Quarkonium Production within Jets*, 1702.05525.

[77] C. F. Berger, T. Kucs and G. F. Sterman, *Event shape / energy flow correlations*, *Phys. Rev.* **D68** (2003) 014012, [hep-ph/0303051].

[78] V. G. Kartvelishvili and A. K. Likhoded, *Heavy Quark Fragmentation Into Mesons and Baryons*, *Sov. J. Nucl. Phys.* **29** (1979) 390.

[79] B. A. Kniehl, G. Kramer, I. Schienbein and H. Spiesberger, *Finite-mass effects on inclusive B meson hadroproduction*, *Phys. Rev.* **D77** (2008) 014011, [0705.4392].

[80] M. Cacciari, G. P. Salam and G. Soyez, *FastJet User Manual*, *Eur. Phys. J.* **C72** (2012) 1896, [1111.6097].

[81] Z. Ligeti, I. W. Stewart and F. J. Tackmann, *Treating the b quark distribution function with reliable uncertainties*, *Phys. Rev.* **D78** (2008) 114014, [0807.1926].

[82] R. Abbate, M. Fickinger, A. H. Hoang, V. Mateu and I. W. Stewart, *Thrust at N^3LL with Power Corrections and a Precision Global Fit for alphas(mZ)*, *Phys.Rev.* **D83** (2011) 074021, [1006.3080].

[83] E. Braaten, K.-m. Cheung and T. C. Yuan, *Z0 decay into charmonium via charm quark fragmentation*, *Phys. Rev.* **D48** (1993) 4230–4235, [hep-ph/9302307].

[84] E. Braaten and T. C. Yuan, *Gluon fragmentation into heavy quarkonium*, *Phys. Rev. Lett.* **71** (1993) 1673–1676, [hep-ph/9303205].

[85] E. Braaten and S. Fleming, *Color octet fragmentation and the psi-prime surplus at the Tevatron*, *Phys. Rev. Lett.* **74** (1995) 3327–3330, [hep-ph/9411365].

[86] E. Braaten and Y.-Q. Chen, *Helicity decomposition for inclusive J / psi production*, *Phys. Rev.* **D54** (1996) 3216–3227, [hep-ph/9604237].

[87] A. Buckley, J. Butterworth, L. Lonnblad, D. Grellscheid, H. Hoeth, J. Monk et al., *Rivet user manual*, *Comput. Phys. Commun.* **184** (2013) 2803–2819, [1003.0694].

[88] T. Sjostrand, S. Mrenna and P. Z. Skands, *PYTHIA 6.4 Physics and Manual*, *JHEP* **05** (2006) 026, [hep-ph/0603175].

[89] *An Introduction to PYTHIA 8.2*, *Comput. Phys. Commun.* **191** (2015) 159–177, [1410.3012].

[90] C. Lee and G. Sterman, *Momentum flow correlations from event shapes: Factorized soft gluons and Soft-Collinear Effective Theory*, *Phys. Rev.* **D75** (2007) 014022, [hep-ph/0611061].

[91] J. Alwall, M. Herquet, F. Maltoni, O. Mattelaer and T. Stelzer, *MadGraph 5 : Going Beyond*, *JHEP* **06** (2011) 128, [1106.0522].

[92] K.-T. Chao, Y.-Q. Ma, H.-S. Shao, K. Wang and Y.-J. Zhang, *J/ψ Polarization at Hadron Colliders in Nonrelativistic QCD*, *Phys. Rev. Lett.* **108** (2012) 242004, [1201.2675].

[93] Z.-B. Kang, J.-W. Qiu, F. Ringer, H. Xing and H. Zhang, *J/ψ production and polarization within a jet*, 1702.03287.

[94] P. Ilten, N. L. Rodd, J. Thaler and M. Williams, *Disentangling Heavy Flavor at Colliders*, 1702.02947.

[95] M. G. Echevarria, A. Idilbi and I. Scimemi, *Factorization Theorem For Drell-Yan At Low q_T And Transverse Momentum Distributions On-The-Light-Cone*, *JHEP* **07** (2012) 002, [1111.4996].

[96] M. G. Echevarria, A. Idilbi, A. Schfer and I. Scimemi, *Model-Independent Evolution of Transverse Momentum Dependent Distribution Functions (TMDs) at NNLL*, *Eur. Phys. J.* **C73** (2013) 2636, [1208.1281].

[97] M. G. Echevarria, A. Idilbi and I. Scimemi, *Unified treatment of the QCD evolution of all (un-)polarized transverse momentum dependent functions: Collins function as a study case*, *Phys. Rev.* **D90** (2014) 014003, [1402.0869].

[98] M. G. Echevarria, I. Scimemi and A. Vladimirov, *Transverse momentum dependent fragmentation function at next-to-next-to-leading order*, *Phys. Rev.* **D93** (2016) 011502, [1509.06392].

[99] M. G. Echevarria, I. Scimemi and A. Vladimirov, *Unpolarized Transverse Momentum Dependent Parton Distribution and Fragmentation Functions at next-to-next-to-leading order*, 1604.07869.

[100] M. Anselmino, M. Boglione, J. O. Gonzalez Hernandez, S. Melis and A. Prokudin, *Unpolarised Transverse Momentum Dependent Distribution and Fragmentation Functions from SIDIS Multiplicities*, *JHEP* **04** (2014) 005, [1312.6261].

[101] M. Procura, W. J. Waalewijn and L. Zeune, *Resummation of Double-Differential Cross Sections and Fully-Unintegrated Parton Distribution Functions*, *JHEP* **02** (2015) 117, [1410.6483].

[102] B. U. Musch, P. Hagler, J. W. Negele and A. Schafer, *Exploring quark transverse momentum distributions with lattice QCD*, *Phys. Rev.* **D83** (2011) 094507, [1011.1213].

[103] J.-Y. Chiu, A. Jain, D. Neill and I. Z. Rothstein, *A Formalism for the Systematic Treatment of Rapidity Logarithms in Quantum Field Theory*, *JHEP* **1205** (2012) 084, [1202.0814].

[104] D. Neill, I. Z. Rothstein and V. Vaidya, *The Higgs Transverse Momentum Distribution at NNLL and its Theoretical Errors*, *JHEP* **12** (2015) 097, [1503.00005].

[105] T. Lbbert, J. Oredsson and M. Stahlhofen, *Rapidity renormalized TMD soft and beam functions at two loops*, *JHEP* **03** (2016) 168, [1602.01829].

[106] T. Becher, M. Neubert and D. Wilhelm, *Higgs-Boson Production at Small Transverse Momentum*, *JHEP* **05** (2013) 110, [1212.2621].

[107] T. Becher, M. Neubert and D. Wilhelm, *Electroweak gauge-boson and Higgs production at Small q_T: Infrared safety from the collinear anomaly*, in *Proceedings, 20th International Workshop on Deep-Inelastic Scattering and Related Subjects (DIS 2012): Bonn, Germany, March 26-30, 2012*, pp. 721–724, 2012. DOI.

[108] V. Ahrens, T. Becher, M. Neubert and L. L. Yang, *Renormalization-Group Improved Prediction for Higgs Production at Hadron Colliders*, *Eur. Phys. J.* **C62** (2009) 333–353, [0809.4283].

[109] P. Pietrulewicz, F. J. Tackmann and W. J. Waalewijn, *Factorization and Resummation for Generic Hierarchies between Jets*, 1601.05088.

[110] S. M. Aybat and T. C. Rogers, *TMD Parton Distribution and Fragmentation Functions with QCD Evolution*, *Phys. Rev.* **D83** (2011) 114042, [1101.5057].

[111] J.-y. Chiu, A. Jain, D. Neill and I. Z. Rothstein, *The Rapidity Renormalization Group*, *Phys. Rev. Lett.* **108** (2012) 151601, [1104.0881].

[112] S. Fleming, A. K. Leibovich and T. Mehen, *Resummation of Large Endpoint Corrections to Color-Octet J/ψ Photoproduction*, *Phys. Rev.* **D74** (2006) 114004, [hep-ph/0607121].

[113] I. W. Stewart, F. J. Tackmann and W. J. Waalewijn, *Factorization at the LHC: From PDFs to Initial State Jets*, *Phys. Rev.* **D81** (2010) 094035, [0910.0467].

[114] S. Alioli and J. R. Walsh, *Jet Veto Clustering Logarithms Beyond Leading Order*, *JHEP* **1403** (2014) 119, [1311.5234].

[115] R. Kelley, J. R. Walsh and S. Zuberi, *Disentangling Clustering Effects in Jet Algorithms*, 1203.2923.

[116] R. Kelley, J. R. Walsh and S. Zuberi, *Abelian Non-Global Logarithms from Soft Gluon Clustering*, *JHEP* **1209** (2012) 117, [1202.2361].

[117] M. Dasgupta and G. P. Salam, *Resummation of non-global QCD observables*, *Phys. Lett.* **B512** (2001) 323–330, [hep-ph/0104277].

[118] A. Banfi, G. Marchesini and G. Smye, *Away-from-jet energy flow*, *JHEP* **08** (2002) 006, [hep-ph/0206076].

[119] R. B. Appleby and G. P. Salam, *Theory and phenomenology of non-global logarithms*, hep-ph/0305232.

[120] Y. L. Dokshitzer and G. Marchesini, *On large angle multiple gluon radiation*, *JHEP* **03** (2003) 040, [hep-ph/0303101].

[121] M. Dasgupta, F. Dreyer, G. P. Salam and G. Soyez, *Small-radius jets to all orders in QCD*, 1411.5182.

[122] T. Becher, M. Neubert, L. Rothen and D. Y. Shao, *An Effective Field Theory for Jet Processes*, 1508.06645.

[123] K. Khelifa-Kerfa and Y. Delenda, *Non-global logarithms at finite Nc beyond leading order*, 1501.00475.

[124] A. Hornig, C. Lee, J. R. Walsh and S. Zuberi, *Double Non-Global Logarithms In-N-Out of Jets*, *JHEP* **1201** (2012) 149, [1110.0004].

[125] A. Hornig, C. Lee, I. W. Stewart, J. R. Walsh and S. Zuberi, *Non-global Structure of the $O(\alpha_s^2)$ Dijet Soft Function*, *JHEP* **1108** (2011) 054, [1105.4628].

[126] R. Kelley, M. D. Schwartz, R. M. Schabinger and H. X. Zhu, *Jet Mass with a Jet Veto at Two Loops and the Universality of Non-Global Structure*, *Phys.Rev.* **D86** (2012) 054017, [1112.3343].

[127] A. J. Larkoski, I. Moult and D. Neill, *Non-Global Logarithms, Factorization, and the Soft Substructure of Jets*, 1501.04596.

[128] D. Neill, *The Edge of Jets and Subleading Non-Global Logs*, 1508.07568.

[129] L. G. Almeida et al., *Substructure of high-p_t jets at the LHC*, *Phys. Rev.* **D79** (2009) 074017, [0807.0234].

[130] C. Lee and G. Sterman, *Universality of nonperturbative effects in event shapes*, hep-ph/0603066.

[131] C. W. Bauer, S. Fleming, C. Lee and G. Sterman, *Factorization of e^+e^- event shape distributions with hadronic final states in Soft Collinear Effective Theory*, *Phys. Rev.* **D78** (2008) 034027, [0801.4569].

[132] A. Hornig, C. Lee and G. Ovanesyan, *Effective predictions of event shapes: Factorized, resummed, and gapped angularity distributions*, *JHEP* **05** (2009) 122, [0901.3780].

[133] S. D. Ellis, Z. Kunszt and D. E. Soper, *Jets at hadron colliders at order α_s^3: A look inside*, *Phys. Rev. Lett.* **69** (1992) 3615–3618, [hep-ph/9208249].

[134] S. D. Ellis, Z. Kunszt and D. E. Soper, *Jets in hadron colliders at order α_s^3*, *Conf. Proc.* **C910725V1** (1991) 417–418.

[135] Y.-T. Chien and I. Vitev, *Jet Shape Resummation Using Soft-Collinear Effective Theory*, *JHEP* **1412** (2014) 061, [1405.4293].

[136] Y.-T. Chien and I. Vitev, *Towards the Understanding of Jet Shapes and Cross Sections in Heavy Ion Collisions Using Soft-Collinear Effective Theory*, 1509.07257.

[137] I. W. Stewart, F. J. Tackmann and W. J. Waalewijn, *N-Jettiness: An Inclusive Event Shape to Veto Jets*, *Phys. Rev. Lett.* **105** (2010) 092002, [1004.2489].

[138] T. T. Jouttenus, I. W. Stewart, F. J. Tackmann and W. J. Waalewijn, *Jet mass spectra in Higgs boson plus one jet at next-to-next-to-leading logarithmic order*, *Phys.Rev.* **D88** (2013) 054031, [1302.0846].

[139] M. Dasgupta, A. Fregoso, S. Marzani and G. P. Salam, *Towards an understanding of jet substructure*, *JHEP* **1309** (2013) 029, [1307.0007].

[140] Y.-T. Chien, R. Kelley, M. D. Schwartz and H. X. Zhu, *Resummation of Jet Mass at Hadron Colliders*, *Phys.Rev.* **D87** (2013) 014010, [1208.0010].

[141] Z. L. Liu, C. S. Li, J. Wang and Y. Wang, *Resummation prediction on the jet mass spectrum in one-jet inclusive production at the LHC*, *JHEP* **04** (2015) 005, [1412.1337].

[142] C. W. Bauer, N. D. Dunn and A. Hornig, *Subtractions for SCET Soft Functions*, 1102.4899.

[143] G. P. Salam, *Towards Jetography*, 0906.1833.

[144] M. Ritzmann and W. J. Waalewijn, *Fragmentation in Jets at NNLO*, *Phys.Rev.* **D90** (2014) 054029, [1407.3272].

[145] R. K. Ellis, W. J. Stirling and B. Webber, *QCD and collider physics*, *Camb.Monogr.Part.Phys.Nucl.Phys.Cosmol.* **8** (1996) 1–435.

[146] S. Catani and M. H. Seymour, *The dipole formalism for the calculation of QCD jet cross sections at next-to-leading order*, *Phys. Lett.* **B378** (1996) 287–301, [hep-ph/9602277].

[147] S. Catani and M. H. Seymour, *A general algorithm for calculating jet cross sections in NLO QCD*, *Nucl. Phys.* **B485** (1997) 291–419, [hep-ph/9605323].

[148] J.-y. Chiu, A. Fuhrer, R. Kelley and A. V. Manohar, *Factorization structure of gauge theory amplitudes and application to hard scattering processes at the LHC*, *Phys. Rev.* **D80** (2009) 094013, [0909.0012].

[149] T. Becher and M. Neubert, *On the Structure of Infrared Singularities of Gauge-Theory Amplitudes*, *JHEP* **0906** (2009) 081, [0903.1126].

[150] I. W. Stewart, F. J. Tackmann and W. J. Waalewijn, *The Beam Thrust Cross Section for Drell-Yan at NNLL Order*, *Phys. Rev. Lett.* **106** (2011) 032001, [1005.4060].

[151] R. Bain, L. Dai, A. Hornig, A. K. Leibovich, Y. Makris and T. Mehen, "Fragmenting jet functions with angularities." 2015.

[152] G. P. Korchemsky and G. Marchesini, *Resummation of large infrared corrections using Wilson loops*, *Phys. Lett.* **B313** (1993) 433–440.

[153] T. Becher, M. Neubert and B. D. Pecjak, *Factorization and momentum-space resummation in deep-inelastic scattering*, *JHEP* **01** (2007) 076, [hep-ph/0607228].

[154] C. Balzereit, T. Mannel and W. Kilian, *Evolution of the light-cone distribution function for a heavy quark*, *Phys. Rev.* **D58** (1998) 114029, [hep-ph/9805297].

[155] M. Neubert, *Advanced predictions for moments of the $\bar{B} \to X_s\gamma$ photon spectrum*, *Phys. Rev.* **D72** (2005) 074025, [hep-ph/0506245].

[156] S. Fleming, A. H. Hoang, S. Mantry and I. W. Stewart, *Top jets in the peak region: Factorization analysis with NLL resummation*, *Phys. Rev.* **D77** (2008) 114003, [0711.2079].

Biography

Yiannis Makris was born December 27, 1988 in Nicosia, Cyprus where he started his early studies in fundamentals of physics in Dasoupoli High-school. He continued his studies in University of Cyprus (UCY) from which he graduated in 2012 with the Bachelor of Science. During his undergraduate studies he work with professor Harris Panagopoulos on perturbative calculations on the anomalous dimension of the chromomagnetic operator in Lattice Quantum Chromodynamics. At UCY he received the Excellence in Performance Award from the School of Natural Sciences in 2012. After his graduation from UCY he enrolled the Ph.D. program in the physics department of Duke University (DU) where he completed the work on the thesis presented in this manuscript. Under the supervision of professor Thomas C. Mehen at DU he worked on the subjects of quarkonium production, jet substructure and jet observables. During his graduate studies at DU, in 2015, he was awarded the A.G. Leventis Foundation Scholarship. After the completion of his doctorate degree he will continue his research on jet substructure and other challenging open question in nuclear and particle physics as a postdoctoral associate in Los Alamos National Laboratory in New Mexico.